RAINFALL OBSERVATIONS USING
DUAL-POLARIZATION RADAR
COUPLED WITH A DROP MOTION
AND EVAPORATION MODEL

_____

A Thesis

presented to

the Faculty of the Graduate School

at the University of Missouri-Columbia

_____

In Partial Fulfillment

of the Requirements for the Degree

Master of Science

_____

by

QUINN PALLARDY

Dr. Neil Fox, Thesis Supervisor

DECEMBER 2013

The undersigned, appointed by the dean of the Graduate School, have examined the thesis entitled

RAINFALL OBSERVATIONS USING
DUAL-POLARIZATION RADAR
COUPLED WITH A DROP MOTION
AND EVAPORATION MODEL

presented by Quinn Pallardy,

a candidate for the degree of master of science,

and hereby certify that, in their opinion, it is worthy of acceptance.

_____

Professor Neil Fox

_____

Professor Thomas R. Marrero

_____

Professor Anthony Lupo

ACKNOWLEDGEMENTS

TABLE OF CONTENTS

LIST OF FIGURES

LIST OF TABLES

Chapter 1. Introduction

1.1 Importance of Radar Estimation of Rainfall

Knowledge of rainfall amounts is very useful information for several disciplines. With respect to environment, heavy rainfall can lead to chemical leaching of soils, causing toxic algal blooms and hypoxic conditions in nearby rivers. Agriculturally, Irrigation requirements and expected crop yields are also dependent on rainfall knowledge.

Immediate physical hazards are another area where rainfall information is important. Flash flooding and landslides are very dangerous to those caught unaware. River level forecasting is dependent on rainfall across very large areas. The level, location, and time of the crest can be estimated if enough data is available.

Evaluation of NWP (numerical weather prediction) models is another important function of rainfall information. These NWP model produce QPFs (quantitative precipitation forecasts). To evaluate the effectiveness of these models, a "truth" field is necessary. Surface rainfall estimations serve as this truth field. Model biases for location, intensity, and total rainfall can be quantified in this manner.

Two sources of rainfall data are generally available: rain gauge data and radar estimated rainfall. The in situ source, rain gauge data, is very limited in spatial coverage, especially in rural areas where agriculture is important. Radar estimated rainfall is remote sensing

based, and can fill in gaps where no rain gauges are present. Areas surrounding

Columbia, Missouri, fit this description. Columbia is located in Central Missouri, an area

far from the nearest radar location. This introduces several problems with radar rainfall

estimation; many of these issues are examined in the following section.

1.2 Sources of Uncertainty

In order to improve rainfall estimation with radar, it is necessary to identify the

difficulties associated with it. These challenges were aggregated by Villarini and

Krajewski (Villarini and Krajewski 2010), referred to as VK10.

The first four error sources reviewed by VK10 were radar miscalibration, attenuation,

ground clutter and anomalous propagation, and beam blockage. The first three of these

sources were ignored in this study. They were ignored based on the assumption that

either corrections had already been made by the weather service, or that the error

caused by the problem was insignificant. Due to the relatively flat topography of the

studied location, beam blockage was not expected to be an issue.

The fifth source of uncertainty was variability in the Z-R relation. Reflectivity (Z) and rain

rates (R) are dependent on drop size distribution (DSD), which the Z-R relationship

depends on. In VK10 it was noted that numerous studies have been performed that

match rain types with corresponding Z-R relations. Also noted were papers describing

DSD as a function of geographic location and rainfall intensity (Tokay et al. 2001; Willis

and Tattelman 1989). More than a dozen studies showing storm to storm and same

storm changes in DSD were listed in VK10. Since VK10 dealt with single polarization

radar, the effects of polarimetric parameters were not discussed. A more in-depth discussion of various Z-R relationships is found in section 1.3.

The sixth source of uncertainty was range degradation. Range degradation was described as a significant cause of underestimation of rainfall amounts at locations far from the radar in several studies. Range degradation was split into two categories: overshooting and beam broadening. Overshooting occurs when the lowest radar elevation angle is too high to capture information about the precipitation. The further one gets from the radar, the higher this lowest elevation angle is. Beam broadening is the reason for the lower resolution data generated for locations far from the radar. This low resolution at far ranges has two immediate consequences; small but intense features are averaged over large areas in all three dimensions, and different precipitation types with different reflectivity signatures can be lumped together. VK10 noted that studies have been performed quantifying bias in measured reflectivity due to beam broadening (Sánchez-Diezma et al. 2000). Little can be done about these two sources for uncertainty with current technology. Due to its location far from the nearest radar, Central Missouri is greatly affected by these issues. Deconvolution of overlapping beams provides limited improvement in these situations.

The seventh source was vertical variability of the precipitation system. The focus of this section was the transition of liquid precipitation types to frozen types higher up in the atmosphere. This transition results in changing reflectivity values due to the differences in shape, size, and physical properties of frozen precipitation. The layer just below the

3

zero degree isotherm is known as the "bright band", due to the enhanced reflectivity within the layer. For this project, the events chosen took place in warm enough atmospheres that this problem was not an issue.

Also discussed in the vertical variability section was hail contamination. Due to the dependency of reflectivity on the sixth power of drop diameter, medium and large hailstones can cause extreme increases in reflectivity. When applied to simple Z-R relationships, this causes unrealistically high instantaneous rain rates. VK10 noted that improvements were found when special Z-R formulas optimized for hail were combined with hail detection schemes (Auer 1994). A form of hail detection/adjustment was utilized for this project.

The eighth source for uncertainty was vertical air motion and precipitation drift. Vertical air motion was a factor that went unaccounted for in this project. Vertical air motion has the biggest effect on smaller drops, as they have the smallest terminal velocity. The areas where vertical air motion has the greatest effect would theoretically be updrafts within thunderstorms. This would be a highly localized phenomenon.

Precipitation drift was a factor considered for this project. In VK10 it was noted that proposals have been made to account for horizontal displacement of drops due to wind drift (Dalezios and Kouwen 1990). Dalezios and Kouwen did not find any significant impact of wind drift on hourly time scales. Further discussion of precipitation drift is conducted in section 1.6.

Temporal sampling error was the final source for uncertainty described by VK10. Unfortunately, little can be done about this without technological upgrades to current radar systems. Finding the optimal interpolation method is the best that can be hoped for.

1.3 Z-R Relationships

In their 1948 paper, Marshall and Palmer postulated that the DSDs are exponential in nature (Marshall and Palmer 1948). The exponential DSD was used to derive a relationship between Z and R. The revised Marshall-Palmer Z-R relationship is given by

$$Z = 200R^{1.6} \tag{1.1}$$

For Equation 1.1, Z has units of mm^6/m^3 and R has units of mm/hour.

More recently, the WSR-88D rainfall algorithm was developed (Fulton et al. 1998). The WSR-88D algorithm has several quality control features to account for many of the sources of uncertainty listed earlier. These include corrections for partial beam blockage, ground clutter, and anomalous propagation.

The default formula used for the WSR-88D algorithm is shown in Equation 1.2.

$$Z = 300R^{1.4} \tag{1.2}$$

In some tropical locations the formula used is Equation 1.3 (Rosenfeld et al. 1993).

$$Z = 250R^{1.2} \tag{1.3}$$

For the WSR-88D rainfall algorithms the rain rates are computed on a 1° X 1 km grid, and averaged in pairs along the radials. The WSR-88D rainfall algorithm also utilizes a

hail cap. The maximum reflectivity is capped at a value of 51 to 55 dBZ, changing based on the location. This cap excludes extreme reflectivity values that can only be caused by hail.

1.4 Dual Polarization

Dual polarization utilizes horizontally and vertically polarized radiation to obtain information about the hydrometeors within an atmospheric column that would otherwise be unavailable. The non-spherical shape of raindrops larger than roughly one millimeter causes the drops to interact differently with the horizontally and vertically polarized radiation. This difference in interaction can be used to calculate the differential reflectivity, specific phase differential, and cross-correlation coefficient. These parameters are dependent on the DSD, and knowledge of them allows for estimates of the DSD to be obtained.

The effectiveness of the polarimetric rainfall algorithms has been evaluated in many studies (Ryzhkov et al. 2005), referred to as RGS05, (Ryzhkov and Zrnić 1996). These formulas have been found to be more effective than the simple Z-R formulas. Most of the rainfall relationships tested by RGS05 were also evaluated for this project. In addition, the three evaluation parameters from RGS05, fractional bias, fractional root mean square error, and fractional standard deviation, were calculated for this project.

RGS05 aggregated several drop shape formulas, and utilized them to generate the tested rainfall relations. Drop shape formulas are given as the raindrop axis ratio as a

function of drop diameter. Larger drops tend to have lower axis ratios, meaning they are elongated in the horizontal direction.

The first drop shape formula listed in RGS05 was based on the equilibrium drop shapes from Beard and Chuang (Beard and Chuang 1987). This formula was

$$a/b = 1.0048 + 0.00057 * D - 0.02628 * D^2 + 0.003682 * D^3 - \qquad (1.4)$$
$$0.0001677 * D^4.$$

Here a/b is the axis ratio and D is the equivolume diameter. The second drop shape formula listed accounted for drop oscillations, which in unsteady flow have the potential to disrupt the equilibrium drop shape (Andsager et al. 1999). The formula was given by

$$a/b = 1.012 - 0.01445 * D - 0.01028 * D^2. \qquad (1.5)$$

The third drop shape formula came from (Brandes et al. 2002). This formula was suited for a more tropical environment and was given by

$$a/b = 0.9951 + 0.02510 * D - 0.03644 * D^2 + 0.005303 * D^3 - \qquad (1.6)$$
$$0.0002492 * D^4.$$

The final drop shape formula listed in RGS05 was the Goddard's axis ratio (Goddard et al. 1995).

$$a/b = 1.075 - 0.065 * D - 0.036 * D^2 + 0.0004 * D^3. \qquad (1.7)$$

Over the range of expected raindrop sizes (zero to six millimeters in diameter), the difference in axis ratios between the first three formulas was not significant. The axis ratio variation at its maximum barely exceeded 3%.

Two types of evaluations were done in RGS05, point evaluations and areal evaluations. The point evaluations were made by comparing radar rainfall estimation with gauge results for a 1° X 1 km region centered on the rain gauge. Areas evaluations were done by comparing average total radar rainfall estimation with average total gage accumulation across all of the rain gauges. The time scale where evaluations were made was one hour. The gauge network consisted of 42 rain gauges located between 85 and 50 km to the southwest of the radar.

The polarimetric formulas tested in RGS05 were split into two groups. The first group consisted of formulas derived from statistics of DSD measurements in central Oklahoma, and varying drop shape formulas. The second group was made up of the most recent polarimetric formulas from the literature at the time (Brandes et al. 2002; Bringi and Chandrasekar 2001; Illingworth and Blackman 2002).

Another type of formula was introduced in RGS05: the synthetic formula. The synthetic formula was designed to handle rainfall situations where the intensity of the rain varies significantly. Three separate equations were utilized; the reflectivity value determined which equation was used. It was found in RGS05 that the synthetic formula performed the best out of all the polarimetric formulas, and significantly better than the simple Z-R relations. A version of the synthetic formula was tested for this project, and more details on the implementation are presented in the methodology section.

1.5 Raindrop Terminal Velocity

One fundamental problem with generating rainfall estimations from radar data is that it provides information about the atmospheric concentration of hydrometeors at a level high above the surface. Many things can happen to the drops while they fall through the atmosphere. They can translate horizontally, collide with other drops, and split into smaller drops. Evaporation reduces the size of the drops as they fall through the atmosphere.

High resolution model data provides the possibility of accounting for some of these factors. To quantify some of the factors affecting the trajectory and size of raindrops, knowledge of several atmospheric variables is required. These include horizontal wind, environmental temperature, and environmental humidity.

The terminal velocity of raindrops is a key component for estimating raindrop trajectories. In 1949, Gunn and Kinzer published a paper showing experimental terminal velocities of drops ranging in size from 0.1 millimeters in diameter up to 5.8 millimeters in diameter (Gunn and Kinzer 1949). Also shown were calculated Reynolds Numbers and drag coefficients. Gunn and Kinzer's measurements were made at the surface; subsequent papers dealt with the velocities of drops aloft, where the air is less dense (Foote and Du Toit 1969). Foote and Du Toit describe the correction factor shown in Equation 1.8.

$$V(D) = V_0(D) \left(\frac{\rho_0}{\rho}\right)^{0.4} \tag{1.8}$$

In Equation 1.8, $V_0(D)$ is the terminal velocity at air density ρ_0 and ρ is the air density at the point where $V(D)$ is being calculated. This equation is actually a simpler, slightly less accurate, version of the more complex equation shown in Foote and Du Toit's 1969 study.

Numerous equations fitted to match the empirical fall velocities have been described (Best 1950; Boxel 1997; Gossard et al. 1990; Gossard et al. 1992; Uplinger 1981). These equations generally have an exponential term. The Gossard equation for drops falling faster than 2.75 meters per second (1990) is shown in Equation 1.9.

$$V_0 = 9.65 - 10.3 * \exp(-0.6D) \tag{1.9}$$

Equation 1.9 is relevant for drops falling near the surface. D is the drop diameter in millimeters and V_t is the terminal velocity in meters per second. Boxel makes a slight modification to prevent the smallest drops from having negative terminal velocities in Equation 1.10.

$$V_0 = 9.65 * (1 - \exp(-0.53 * D)) \tag{1.10}$$

Equation 1.10 ended up being chosen for this project due to its simplicity and the problematic implication of allowing negative terminal velocities. Terminal velocity values from Equation 1.10 differ from their empirical counterparts from Gunn and Kinzer by roughly 5% for three millimeter diameter drops, 3% for two millimeter diameter drops, and 1.5% for one millimeter diameter drops.

1.6 Precipitation Drift

Accounting for horizontal hydrometeor movement has been the subject of several studies (Lack 2004; Lauri et al. 2011; Mittermaier et al. 2004). Lack 2004 utilized radar derived velocity data procured from the Sydney 2000 World Weather Research Programme's (WWRP) Forecast Demonstration Project (FDP) (Keenan et al. 2003). Results from Lack indicated that precipitation drift had the greatest potential for effect when using high resolution data and for situations where low-level directional wind shear was present. Using humidity information to account for drop evaporation was one of the items listed for future work within Lack. The other two studies made no mention of evaporation.

Lauri et al. 2011 and Mittermaier et al. 2004 were more focused on the drift of frozen precipitation above the melting layer. Snowflakes generally fall slower than raindrops, and are thus more affected by wind drift. It was noted in Mittermaier that numerically modeled wind speeds were of sufficient accuracy to yield improvements with the drift scheme they devised. A simple hit, miss, and false alarm evaluation method was used to determine effectiveness in Mittermaier.

Lauri's focus was also on the potential for wind drift to affect frozen hydrometeors. Included in Lauri were radar-to-gauge comparisons illustrating a significant improvement when hydrometeor advection was accounted for. Both Lauri and Mittermaier worked at higher latitudes, where the radar beam was more likely to hit frozen precipitation.

1.7 Drop Size Distribution

Any radar-derived rainfall estimation scheme must take into account the varying size and concentration of raindrops. The purely exponential DSD devised by Marshall and Palmer has largely been replaced by the gamma DSD (Ulbrich 1983). The gamma DSD is given by

$$n(D) = n_0 * D^\mu * \exp(-\Lambda D). \tag{1.11}$$

For the gamma distribution, n_0 is the intercept parameter, μ is the shape parameter, and Λ is the slope parameter. $n(D)$ is the number of drops of diameter D. The shape parameter determines the magnitude of deviation from the exponential distribution. A μ value of zero makes the gamma distribution equal to the exponential distribution (Tokay et al. 2001).

A method for using the three radar parameters, Z, Z_{DR}, and K_{DP}, to obtain the necessary constants within the gamma distribution has been developed (Gorgucci et al. 2002). K_{DP} values, however, are extremely noisy. To eliminate dependence on K_{DP}, Brandes et al. introduced a "constrained-gamma method" (Brandes et al. 2004). This constrained-gamma method made use of empirical dependencies of Λ on μ. With only two unknowns to be found, the constrained-gamma method only requires two radar parameters to estimate the expected DSD.

1.8 Evaporation

Literature dealing with raindrop evaporation calculations is relatively limited in nature. In 1951 Gunn and Kinser published a paper detailing an analytic solution to evaporation for a falling drop (Kinzer and Gunn 1951). The rate of mass change per unit time was given by

$$\frac{dm}{dt} = 4\pi r D_v \Delta\rho_v * \left(1 + \frac{Fr}{s'}\right). \tag{1.12}$$

In Equation 1.12, m was the mass of the raindrop, r was the drop radius, D_v was the diffusivity of water vapor in air, $\Delta\rho_v$ was the vapor density difference, and $1 + \frac{Fa}{s'}$ was the ventilation coefficient term.

Recent updates to this formula have been made (Li and Srivastava 2001). The rate of evaporation in the Li and Srivastava study was calculated as

$$\frac{dm}{dt} = 4\pi r D_v \Delta\rho_v f_v. \tag{1.13}$$

The ventilation coefficient, f_v, was calculated as

$$f_v = 0.78 + 0.308 \left(\frac{v}{D_v}\right)^{\frac{1}{3}} (\frac{VD}{v})^{\frac{1}{2}}. \tag{1.14}$$

In these equations, m is the mass of the rain drop, V is the terminal velocity of the drop, v is the kinematic viscosity of air, D_v is the diffusivity of water vapor in air, r is the drop radius, D is the drop diameter, and $\Delta\rho_v$ is the difference in vapor density between the drop surface and the environment.

13

The Li and Srivastava study established a parameter, D^*, that was defined as the

diameter of raindrop that would just completely evaporate after traveling through a

layer of the atmosphere with specified qualities. This parameter essentially

corresponded to the "drying power" of the layer. The study goes on to detail the

relationship between D^* and several other parameters, including evaporation induced

changes in DSDs and evaporation-related errors in rainfall estimation with Z-R and ZDR-

Z-R relations.

A more focused examination of the effect of evaporation on polarimetric radar

parameters was conducted in 2010 (Kumjian and Ryzhkov 2010). The theoretical effects

of evaporation on Z, Z_{DR}, and K_{DP} were discussed in this study. Evaporation was

calculated to cause substantial alterations in each of the three parameters. Z and K_{DP}

were found to be reduced by evaporation, while ZDR was increased. Since conventional

formulas for rainfall estimation are directly proportion to powers of Z and KDP, but

inversely proportional to powers of Z_{DR}, each of these three changes from evaporation

was expected to result in rainfall overestimation. The study noted that the effects of

evaporation were generally reduced as the rainfall rate increased, and that K_{DP} was the

parameter most affected.

1.9 Objectives

There were two primary objectives for this project. The first was to determine the best

method for radar rainfall estimation over Central Missouri. The second objective was to

evaluate whether the introduction of high resolution model data has the potential to improve the radar rainfall estimation process.

A number of different conventional formulas were considered for the first objective. The conventional formulas were simple functions of the Z, Z_{DR}, and K_{DP} parameters.

The "trace" method was introduced as a way for high resolution model data to potentially improve radar rainfall estimation. The trace method relied on tracing all raindrops hitting the surface at a point back to the locations in space and time at which the radar detected them. Evaporation and horizontal drift were both utilized in the tracing process.

Variations on the trace method were used along with the conventional formulas when the determination of best method was in question. These variations consisted of different combinations of evaporation and horizontal drift. Also included in the trace method was a version where raindrops were assumed to instantaneously reach the ground. Testing each of these variations allowed isolation of the effects a particular parameter had on the effectiveness of the method.

To the author's knowledge, all estimation of raindrop evaporation to date has been theoretical in nature. Evaluations of the trace techniques designed for this project provided a physical test of raindrop evaporation theory. This area of study is at the very least extremely limited in nature.

Chapter 2. Methodology

2.1 Objectives

There were two primary objectives for the study. The first was to determine the best method for radar derived rainfall estimation in Central Missouri. The second objective was to evaluate whether high resolution model data could be utilized to improve radar derived rainfall estimation. In order to complete the objectives required for the study, two things were necessary: a place to store data and the ability to perform computations on the data. Visual Basic for Applications (VBA) and Microsoft Excel were chosen to perform these functions. VBA is a powerful tool for data manipulation when combined with spreadsheet software like Excel. The VBA program created for this project was designed with three requirements in mind. The first requirement was speed; the program would have to perform its calculations in a reasonable amount of time. The second requirement was flexibility. To fulfill the flexibility requirement, the program would have to be able to easily switch between rainfall estimation formulas, events, and locations for evaluation. The final requirement fell upon the results generated by the program. The results the program produced needed to be both graphical and numeric, and easy to interpret.

2.2 Data and Interpolation

2.2.1 Dates

Evaluation of the effectiveness of radar-related rainfall estimation techniques first

requires rain gauge and radar data. The dates used for the study were focused on major

rainfall events over the years 2012 and 2013 in Central Missouri. Criteria for selection

included availability of radar data and rain gauge data, as well as storm type. A wide

variety of storm types was necessary to effectively evaluate the estimation methods.

The final dates chosen are listed in Table 2.1.

Table 2.1 Rainfall Events

Event	Start Time	End Time	Duration (hours)	Mean Site Precipitation (mm)	Notes
March 20, 2012	3/20 21 UTC	3/21 21 UTC	24	36.91	-
April 13, 2012	4/13 05 UTC	4/13 13 UTC	8	6.24	-
April 14, 2012	4/14 02 UTC	4/14 10 UTC	8	17.58	-
April 15, 2012	4/15 11 UTC	4/15 19 UTC	8	4.85	-
June 16, 2012	6/16 19 UTC	6/17 03 UTC	8	20.73	-
August 31, 2012	8/31 12 UTC	8/31 22 UTC	10	34.66	Isaac
September 7, 2012	9/7 20 UTC	9/8 01 UTC	5	12.36	Large Hail
October 13, 2012	10/13 19 UTC	10/14 05 UTC	10	25.48	-
March 10, 2013	3/10 02 UTC	3/10 10 UTC	8	11.23	-
April 10, 2013	4/10 20 UTC	4/11 4 UTC	8	27.83	-
April 17, 2013	4/17 20 UTC	4/18 11 UTC	15	36.52	Large Hail
May 30, 2013	5/30 09 UTC	5/31 17 UTC	32	106.81	-

2.2.2 Rain Gauge Data

Rain gauge data was obtained from nine locations around Central Missouri. Figure 2.1
and Figure 2.2 show the spatial distribution of these locations. Table 2.2 shows the
coordinates of these sites as well as their distance from the radar (KLSX). These sites
used tipping bucket rain gauges to measure rainfall at five minute intervals. Rainfall
measurements were recorded in inches and converted to millimeters. Rain gauge data
were assumed to be the "ground truth" for the purpose of this study. The rain gauge
data were obtained from the Commercial Agriculture Automated Weather Station
Network managed by University of Missouri Extension and Interdisciplinary Laboratory.
All rain gauge data was stored within the Excel file where the main program was
executed from.

Table 2.2 Site Locations

Site	Latitude	Longitude	Radar Distance (km)	Elevation (m)
1	39.023633	-92.246017	140.1	225.6
2	38.982733	-92.279300	141.8	213.8
3	38.948183	-92.305350	143.3	195.8
4	38.927750	-92.342444	146.0	186.8
5	38.914117	-92.400183	150.7	171.9
6	38.897236	-92.218070	134.9	268.8
7	38.929237	-92.321297	144.3	186.2
8	38.906992	-92.269976	139.5	251.8
9	38.942301	-92.320395	144.4	235.0
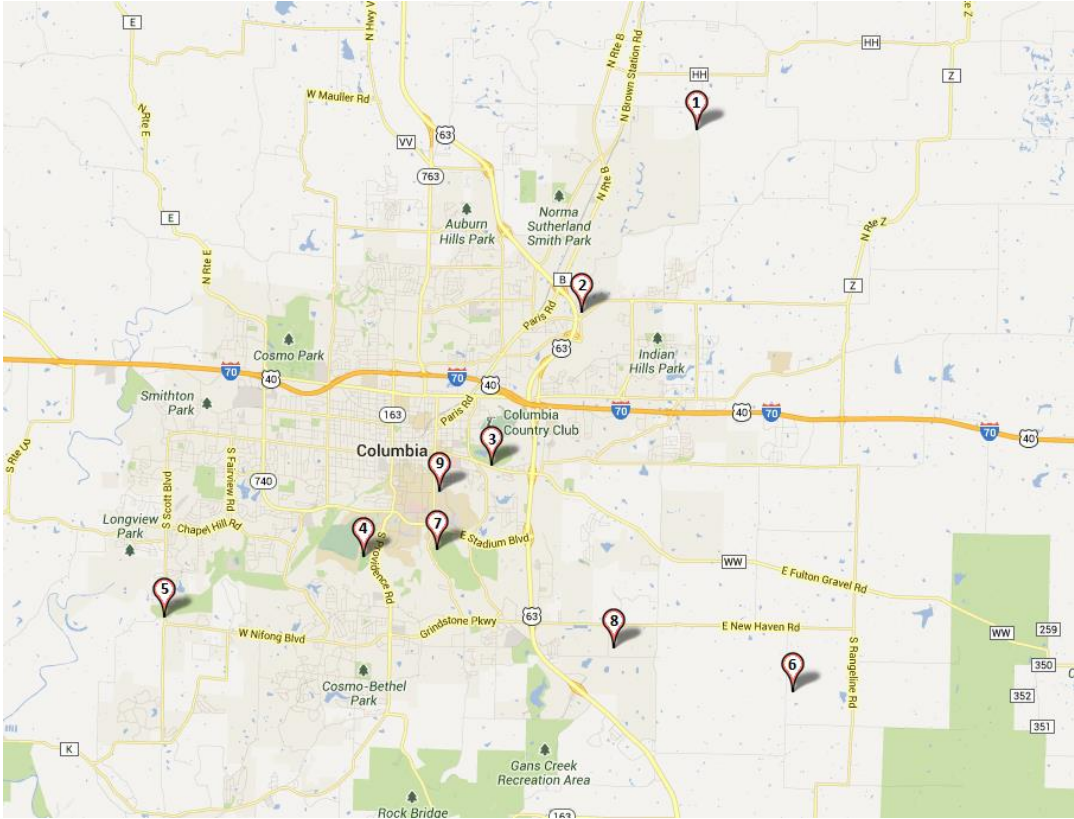
Figure 2.1. Site Locations in and around Columbia, Missouri.
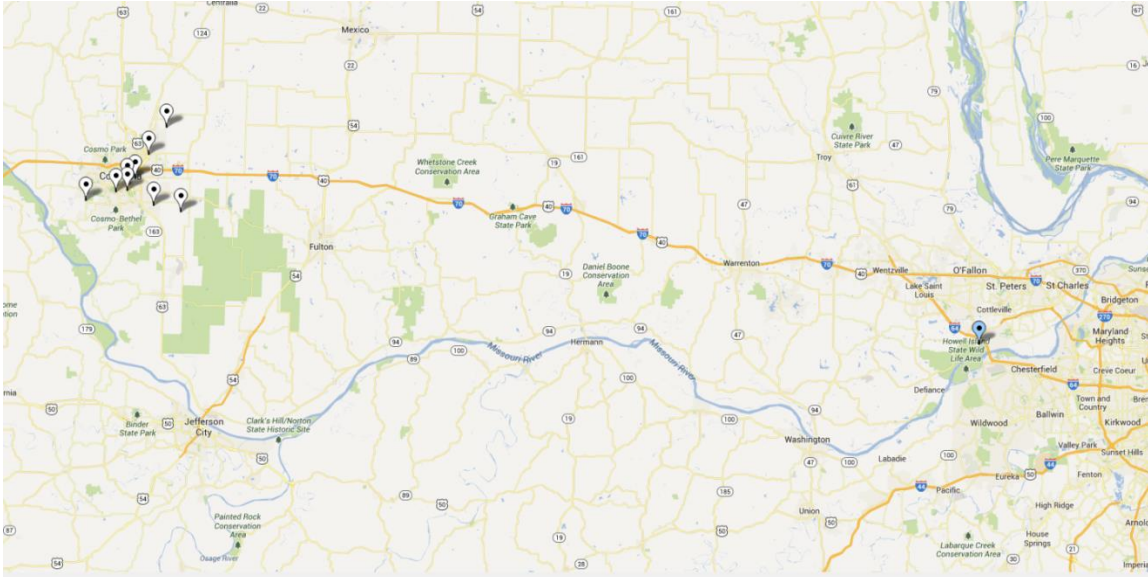
Figure 2.2. Site Locations Relative to KLSX (sky blue marker).

2.2.3 Radar Data

Radar data was Level 2 WRS-88D for KLSX downloaded from NCDC. The data was processed using the Warning Decision Support System (Lakshmanan et al. 2007). The source radar data was converted to a Cartesian CAPPI grid using the w2merger process (Lakshmanan et al. 2006) to produce 1km X 1km grids at nominal five minute intervals (not coincident with scan frequency). Radar files for Z and Z_{DR} were obtained, while K_{DP} was obtained through calculation of the gradient of ϕ_{DP}. This was done using a fixed kernel size resulting in noisy and inconsistent values; the kernel should be adjusted depending on the radar pulse repetition frequency (PRF), which changes with the volume cover pattern (VCP).

The timestamps for these files were unevenly spaced on roughly five minute intervals. For some dates an unequal number of files were generated for the different parameters. For instance, on January 29, 2013, the process produced 133 files for Z, 11 files for Z_{DR}, and 26 files for K_{DP}. This limited the methods available for evaluation on dates where it occurred. The discrepancy was caused by variations in the VCP during the course of the event.

The radar files were zipped NetCDF files. Once unzipped, a regional subsection of the file was written in text format using the ncks tool in the NCO toolbox. Details on how this process was conducted are found in Appendix A. The subsection was chosen to completely encompass the locations of the rain gauges, as well as much of the surrounding area, to enable the trace calculations. The final subsection consisted of 44

grid squares in latitude by 36 grid squares in longitude. Through a VBA script, the data

found in the text files were transported to their final storage location within the Excel

file where the main program was to be executed from.

2.2.4 Timing

All times either originated in UTC or were converted to UTC. Time calculations were all

based on hours since start of event. Hour 0 for each event was assumed to be 00 UTC on

the starting day. For example, hour 0 for the April 13 through April 15, 2012, event

would be equivalent to 00 UTC on April 13. Hour 30.5 for the same event would be

equivalent to 0630 UTC on April 14.

All rainfall estimation techniques were evaluated based on the five minute intervals the

rain gauge data was recorded in. Through simple addition, 10 minute, 20 minute, 30

minute, and 60 minute intervals were also calculated. This made possible an estimation

of effectiveness based on interval length, although only the 60 minute data would be

analyzed in the study.

2.2.5 Conventional Formula Interpolation

Since the radar data were obtained at roughly (uneven) five minute intervals, it was

necessary to interpolate values in between those times. Procedures for rainfall

calculation depended on the technique used. For every technique, each time and site

location was given a rainfall rate. To calculate rainfall for the five minute interval, the

initial and final rainfall rates were averaged. For techniques only dependent on Z and/or

Z_{DR}, or just K_{DP}, rain rates were calculated at the eight surrounding points (the two

horizontal dimensions and time). The rainfall rate at the desired location and time was then found using linear interpolation. Figure 2.3 illustrates this process.

For techniques dependent on combinations of K_{DP} and Z_{DR}, K_{DP} and Z, or K_{DP}, Z, and Z_{DR}, alterations in the calculations were necessary. This was due to the timing differences between the Z and Z_{DR} radar data and the K_{DP} data. For these combinations, Z and/or Z_{DR} values at the eight surrounding points were converted to linear units, and values at the desired time were found via linear interpolation (K_{DP} values were also interpolated this way, although without conversion to linear units). Rainfall rates were then calculated at the resulting four points. Finally, the rainfall rate at the desired location was found through further linear interpolation.

The trace techniques dependent on model data were conducted slightly differently than the conventional methods. A detailed explanation is given in the Trace Method section.
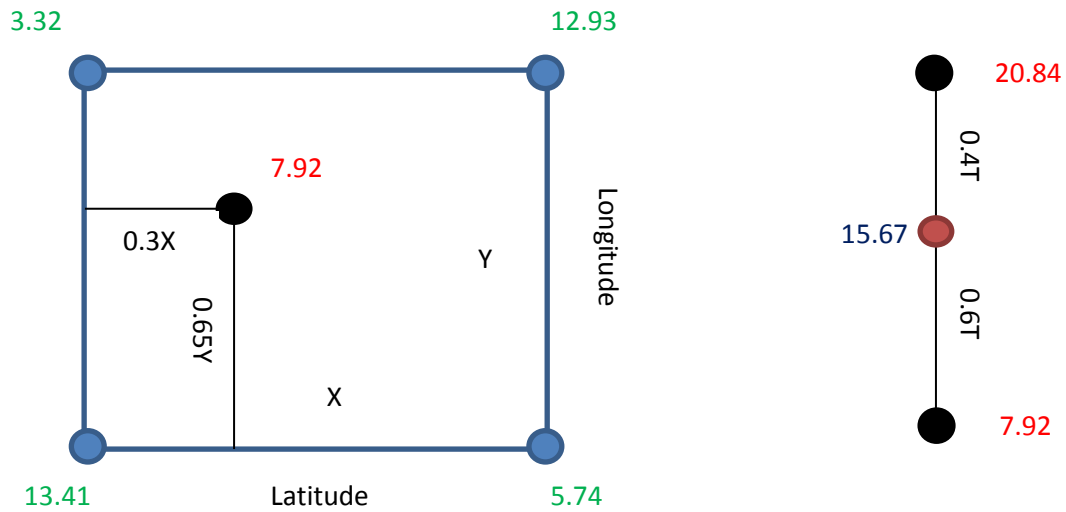
Figure 2.3. Interpolation Process for Formulas not Dependent on KDP and Another Parameter. In the top left image, the blue circles correspond to the surrounding four points where radar data is available. The black circle is the location of the point of interest. The green numbers are the rainfall rate calculations at the surrounding points in millimeters per hour. The red number is the rainfall rate (in mm/hour) at the point of interest, linearly interpolated from the four surrounding points.

The process shown in the top left image is performed twice, once for the radar image preceding the time of interest, and once for the radar image following the time of interest. In the top right image, the two red numbers correspond to these two calculated rainfall rates. The time of interest is marked by the red circle, and the blue number to the left is the linear interpolation of the rainfall rate calculated for the time of interest.

2.3 High Resolution Model Data and the Trace Method

2.3.1 Drift and Evaporation

Traditional techniques for radar rainfall estimation assume the rain drops generating the observed reflectivity are instantly hitting the ground. As the radar beam rises with height, the assumption made in these techniques becomes worse as the point of interest increases in distance from the radar. Central Missouri is one such location, with the nearest radar being KLSX, located in Saint Louis.

Several factors affect where and at what size rain drops hit the surface. Given the necessary information horizontal drift and evaporation can be calculated. This is where high resolution model data becomes useful.

2.3.2 Model Data

The incorporation of high resolution model data into the rainfall estimation program required several steps. The data was obtained from NCDC. 13 kilometer resolution model data were obtained at hourly intervals. Data for the events preceding May of 2012 were from the Rapid Update Cycle (RUC) numerical weather model, which was replaced on May 1, 2012, by the Rapid Refresh (RAP). Both the RUC and the RAP issue hourly forecasts for a multitude of parameters across much of North America. This project used the initialization data for these models (forecast for hour zero). Height, temperature, relative humidity, u wind, and v wind were the necessary fields. Data was obtained at pressure levels ranging from 1000 millibars to 700 millibars (25 millibar intervals).

The model data available from NCDC was in .grb2 format. The wgrib2 tool was used to convert the .grb2 files into csv files (comma separated variables). Detailed information on the use of the wgrib2 tool is available in Appendix A. The csv files were subsequently imported into Excel. The grid the model data came formatted in differed significantly from the grid the radar merging process produced. To map the model grid into a usable grid format several algorithms were employed. The resulting grid contained model data at a resolution of 0.1 degrees longitude by 0.1 degrees latitude.

2.3.3 Trace Method

The theory behind the trace method is that with the right information, a rain drop reaching the surface can be traced backwards in time to its origin. In this case the drop's "origin" refers the time and location at which the drop interacted with the radar beam. Knowledge of atmospheric temperature, relative humidity, wind speed, and wind direction can be used to calculate where the drop's origin is, as well as how much it has evaporated during its time spent in motion.

2.3.4 CAPPI

The CAPPI, or Constant Altitude Plan Position Indicator, was the format used for radar data. With dual polarized radar, the CAPPI provides information about drop size distribution at a constant height in the atmosphere. The CAPPI height used for this project was two kilometers above radar level. The CAPPI was chosen to be at two kilometers due to the relative distance between Central Missouri and the radar in Saint

Louis. Two kilometers above the radar level lies within the lower portion of the 0.5° elevation beam at the KLSX-Columbia distance, which is roughly 140 km.

2.3.5 Calculating Drop Size Distribution

Rain drops reaching the surface range in size from roughly 0 to 6.0 mm in diameter. This is usually given in equivalent spherical drop diameter, as the drops themselves become less spherical as they grow larger. The ratio of vertical diameter to horizontal diameter is called the axis ratio. The axis ratio shrinks as the equivalent spherical drop diameter increases. The axis ratio formula used for this study comes from Beard and Chuang's 1987 study, and is shown in Equation 2.1 (Beard and Chuang 1987).

$$a/b = 1.0048 + 0.00057 * D - 0.02628 * D^2 + 0.003682 * D^3 - \quad (2.1)$$
$$0.0001677 * D^4.$$

In Equation 2.1, D is the drop diameter in millimeters. Other drop shape formulas are available, but as mentioned in Chapter 1 no significant variation is found in the drop diameter range of interest.

Differentially reflectivity, or Z_{DR}, is a value provided by dually polarized radars. The differential reflectivity is defined by

$$Z_{DR} = 10 * \log_{10}\left(\frac{Z_H}{Z_V}\right), \quad (2.2)$$

where Z_H is the horizontal reflectivity and Z_V is the vertical reflectivity.

From Equation 2.1, a drop size distribution resulting in an equivalent differential reflectivity can be estimated. As mentioned in Chapter 1, the gamma drop size

distribution has been shown to correspond best to real world situations. This drop size

distribution is given by

$$n(D) = n_0 * D^\mu * \exp(-\Lambda D), \qquad (2.3)$$

where n(D) is the number of drops of diameter D per meter cubed per drop diameter

interval.

To obtain a drop size distribution from just two parameters, reflectivity and differential

reflectivity, a relationship between μ and Λ must be assumed. In their 2004 paper

Brandes et al. found that the relationship shown in Equation 2.4 worked best (Brandes

et al. 2004).

$$\Lambda = 0.0365 * \mu^2 + 0.735 * \mu + 1.935 \qquad (2.4)$$

Drop concentrations (per m^3) at (discrete) 0.01 mm intervals were calculated based on

the drop size distribution from Equation 2.4, assuming an n_0 value of 1000. From these

concentrations predicted Z and Z_{DR} values were obtained. The Z_{DR} values were

dependent only on μ (and in this case unique); as a consequence corresponding Z_{DR} and

μ values were mapped out. Since adjusting the value of n_0 altered the reflectivity

without changing the differential reflectivity, a value of n_0 and μ could be found to

match up with every possible Z and Z_{DR} combination. Figure 2.4 shows expected rainfall

rate based on different combinations of Z and Z_{DR}, given the assumptions made about μ

and Λ. As a side exercise the coefficients from Equation 2.4 were allowed to vary and

the effects on expected rainfall rate are shown in Figure 2.5, Figure 2.6, and Figure 2.7.

The assumption was made in these calculations that the reflectivity was at a constant 40

dBZ. However, the percent change in rainfall rate was unaffected by the reflectivity

value assumed.
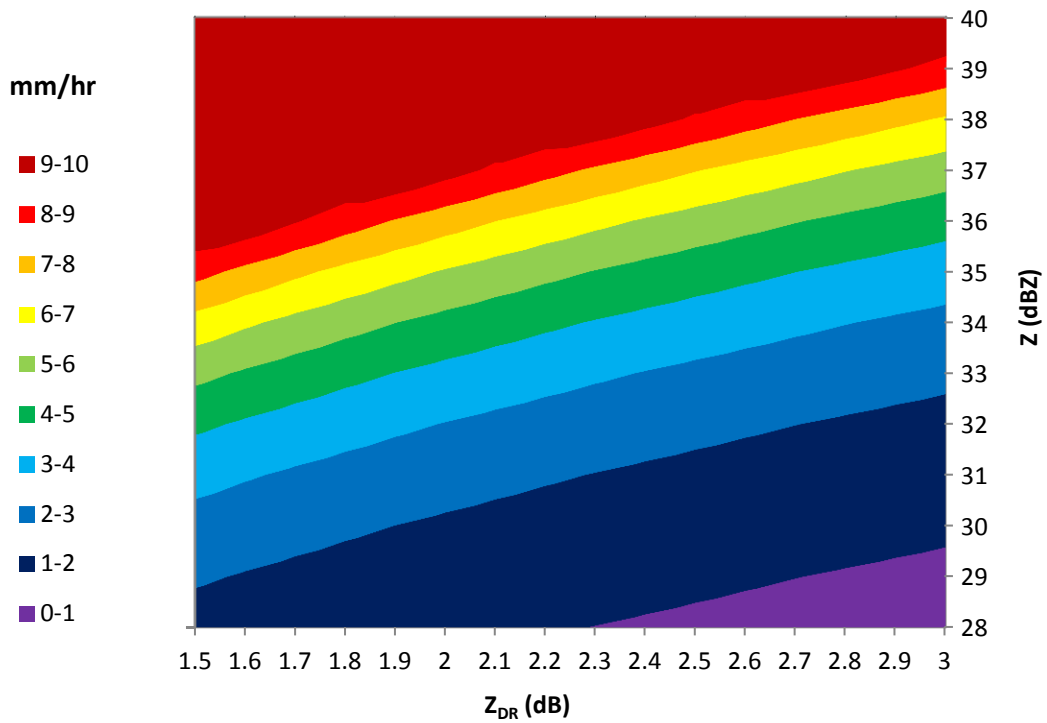
Figure 2.4. Theoretical Rainfall Rates with varying Z and ZDR (mm/hour).
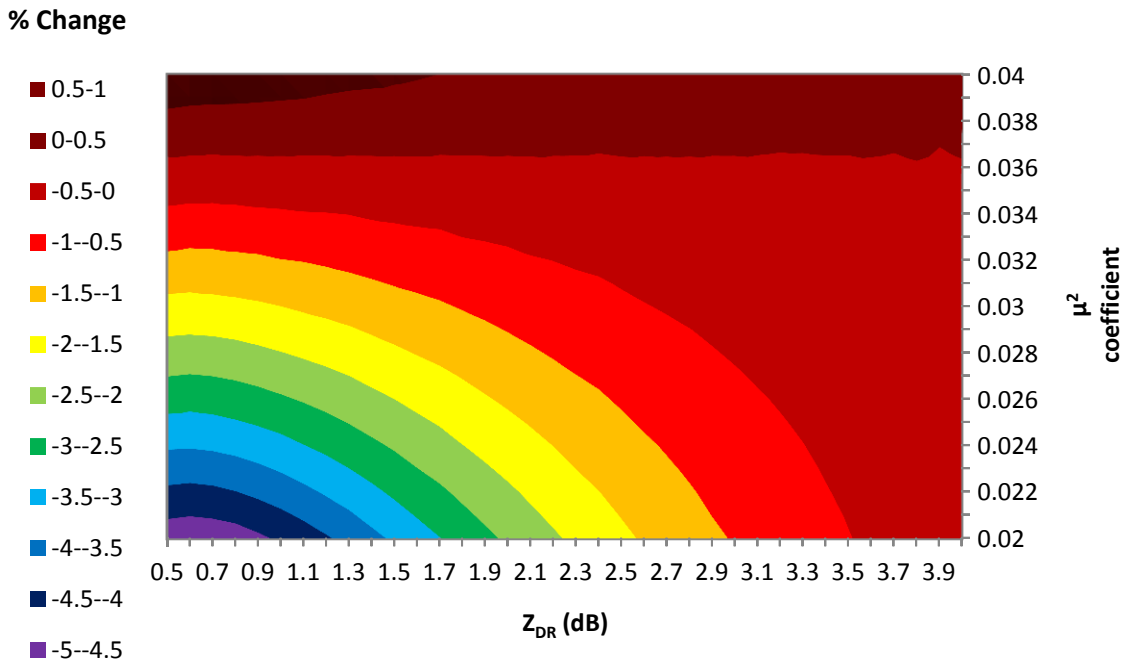
Figure 2.5. Change in Theoretical Rainfall Rate (%) with Varying Z_{DR} and μ^2 Coefficient.
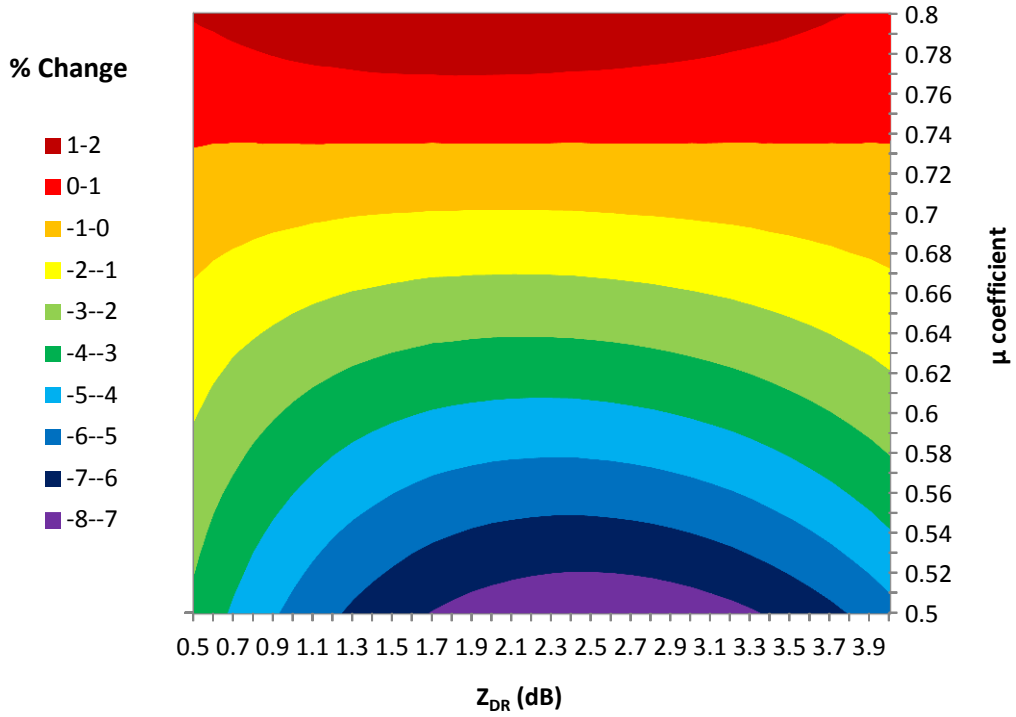
Figure 2.6. Change in Theoretical Rainfall Rate (%) with Varying Z_{DR} and μ Coefficient.
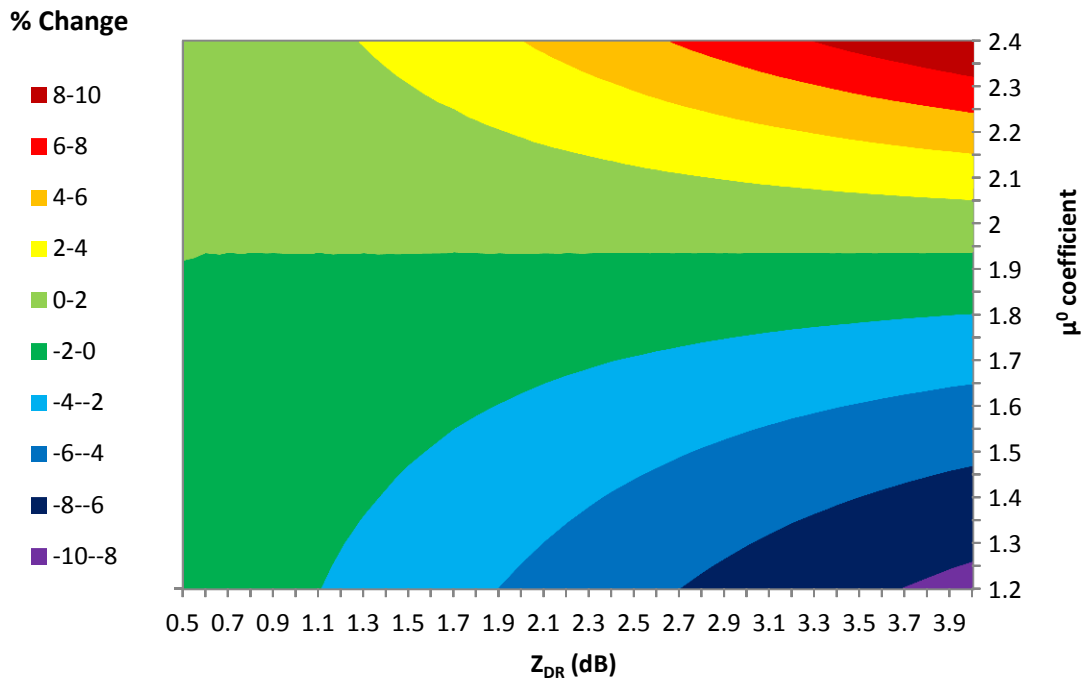
Figure 2.7. Change in Theoretical Rainfall rate (%) with Varying Z_{DR} and μ^0 Coefficient.

2.3.6 Tracing the Drops

At the surface, one might expect a certain concentration of drops of a particular size. To calculate a rainfall rate, a concentration for drops of all sizes is needed. The tracing process therefore attempts to trace drops of all sizes to their respective points of origin. However, at their origins these drops will be different sizes due to the evaporation process. As described in the literature review, drop evaporation is a process dependent on many factors, including drop size, environmental humidity, and environmental temperature. The equation used to calculate drop evaporation comes from Li and Srivastava's 2001 study and is shown in Equation 2.5 (Li and Srivastava 2001).

$$\frac{dm}{dt} = 4\pi r D_v f_v \Delta \rho_v \tag{2.5}$$

The ventilation coefficient, f_v, is calculated as

$$f_v = 0.78 + 0.308 \left(\frac{v}{D_v}\right)^{\frac{1}{3}} (\frac{VD}{v})^{\frac{1}{2}}. \tag{2.6}$$

In these equations, m is the mass of the rain drop, v is the kinematic viscosity of air, V is the terminal velocity, D_v is the diffusivity of water vapor in air, r is the drop radius, D is the drop diameter, and $\Delta \rho_v$ is the difference in vapor density between the drop surface and the environment.

Along with evaporation, calculating drop terminal velocity is also necessary for tracing drops to their origin. Drop terminal velocity is also dependent on many factors, the most important being size and air density. The equation used for drop terminal velocity for this study was from Boxel's 1997 paper and is shown in Equation 2.7 (Boxel 1997).

$$V_t = \left(\frac{\rho_b}{\rho}\right)^{0.4} 9.65 * (1 - \exp(-0.53 * D)) \qquad (2.7)$$

For Equation 2.7 ρ_b is the standard atmosphere air density, ρ is the air density at point

of calculation, and D is the drop diameter in millimeters.

For each site, each day, and each five minute time step, 60 drop sizes were traced to

their origins. The tracing was done in one second intervals. Every second the following

parameters were recalculated for each individual drop.

- Latitude

- Longitude

- Height

- Pressure

- Relative humidity

- Temperature

- U wind

- V wind

- Terminal velocity

- Evaporation rate (mass loss per second)

- Virtual temperature

The three motion vectors given to each drop were used to calculate a position one

second in the past. The evaporation rate was used to calculate a drop size for that

position. New motion vectors and an evaporation rate were then calculated for the new

position; these new values were averaged with the original values and used to calculate the drop's "official" position one second before. Calculation of the evaporation rate required estimation of the wet bulb temperature; this was done using an iterative process. Estimation of the pressure, which was needed for air density calculations, was done using the hypsometric equation and several assumptions about the temperature lapse rate. As described earlier, model data was obtained at 25 millibar intervals. The average virtual temperature of a layer is necessary to estimate its thickness. Given the virtual temperature at the top and bottom of the 25 millibar layer, an average lapse rate can be calculated. However, the average virtual temperature given by this average lapse rate may not necessarily correspond to the thickness of the layer given by the model data. To maintain the model estimated thickness of the layer, as well as the apparent average lapse rate in the model, the virtual temperatures at the top and bottom of the layer were adjusted. These virtual temperature assumptions, the predicted height of the drop, and the hypsometric equation were then used to calculate the pressure. A detailed explanation of this process is found in Appendix C.

A sample tracing was done for six rain drop sizes on August 31, 2012, and May 20, 2013. The drop diameters at the surface were 0.1, 0.4, 1.0, 1.5, 3.0, and 6.0 millimeters. These drops reached the surface at site 1.

On August 31, 2012, each drop was assumed to have reached the surface a few minutes after 12 UTC. Figure 2.8 shows the diameter of the four smallest drops as they are traced back to their points of origin, while Figure 2.9 shows the horizontal trajectories of

all six drops. Figure 2.10 and Figure 2.11 show the same statistics for hypothetical drops

on May 20, 2013.
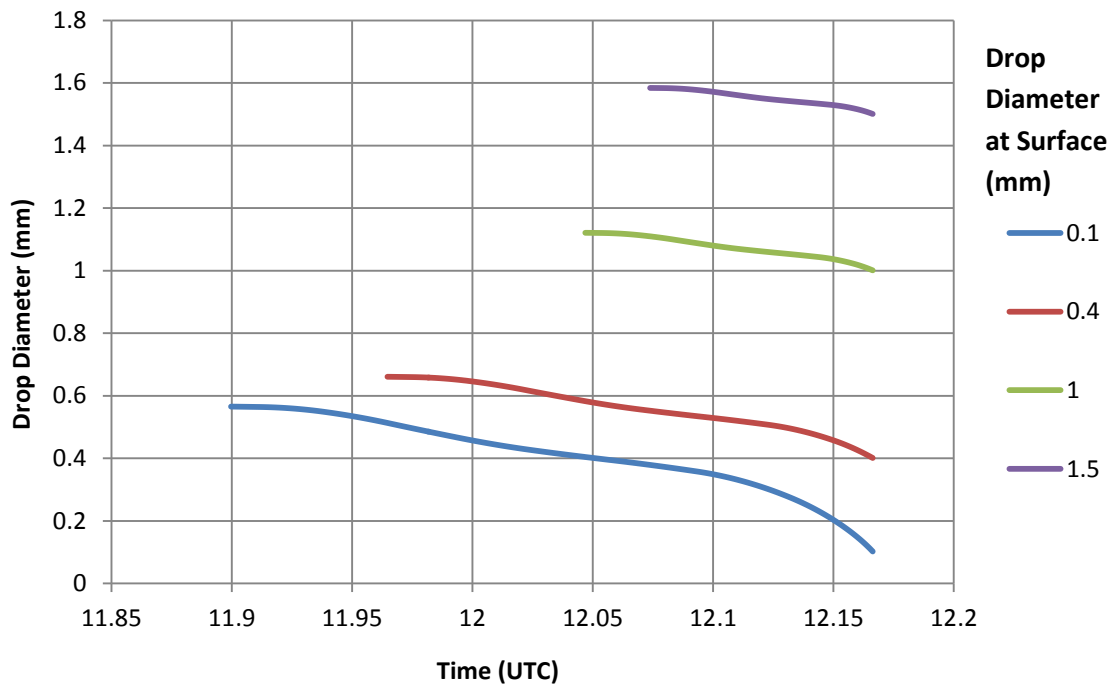
Figure 2.8. Drop Diameter as a Function of Time for August 31, 2012. Drop diameters at the surface are 0.1, 0.4, 1.0, and 1.5 mm. Drops reached the surface at roughly 1210 UTC.
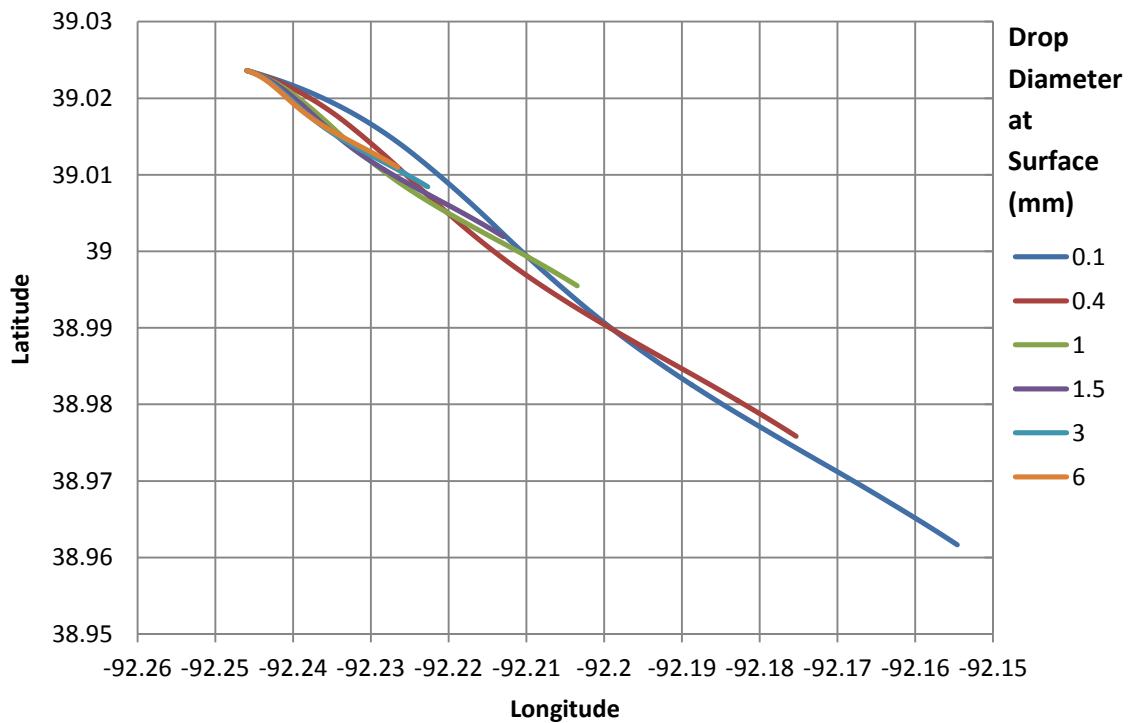
Figure 2.9. Drop Trajectories for August 31, 2012. Drop diameters at the surface are 0.1, 0.4, 1.0, 1.5, 3.0, and 6.0 mm. Drops reached the surface at 39.024^o N, 92.246^o W.

Figure 2.10. Drop Diameter as a Function of Time for May 20, 2013. Drop diameters at the surface are 0.1, 0.4, 1.0, 1.5, and 3.0 mm. Drops reached the surface at roughly 1350 UTC.
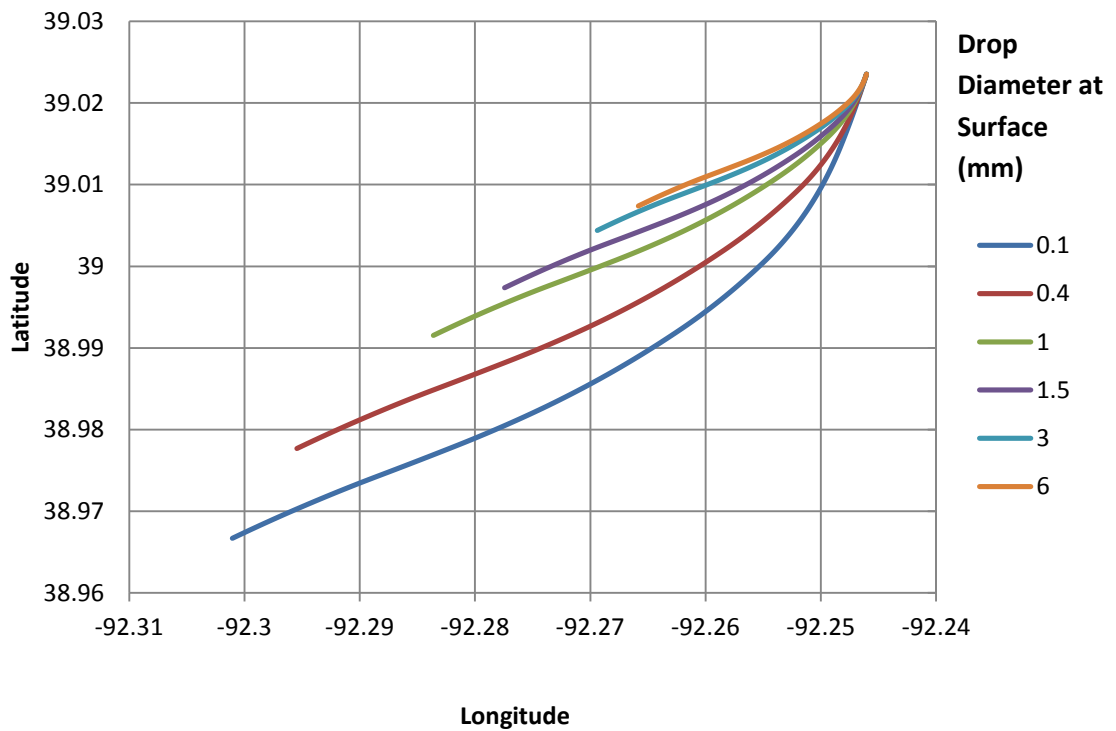
Figure 2.11. Drop Trajectories for May 20, 2013. Drop diameters at the surface are 0.1, 0.4, 1.0, 1.5, 3.0, and 6.0 mm. Drops reached the surface at 39.024° N, 92.246° W.

2.3.7 Types of Tracing

In addition to the tracing done to account for drift *and* evaporation, four other versions of drop tracing were also calculated for control purposes. The first was to simply assume the drops aloft instantly reached the ground with no drift or evaporation. The second was calculated under the assumption that the drops took time to reach the ground, but remained unaffected by drift or evaporation. The third and fourth versions took into account either drift or evaporation, but not both.

2.3.8 Estimating Rainfall with the Trace Method

For each five minute time step, the trace calculations yielded data on the origins of 60 drop sizes ranging from 0.1 mm in diameter to 6.0 mm in diameter (at 0.1 mm intervals). These drops were sorted by their size at the surface, as their size at point of origin varied considerably. Estimated points of origin were defined by three parameters: drop size at point of origin, time, and location.

For calculation of rainfall, a higher resolution of drop size was used. The drop sizes were further split into 591 categories, still ranging from 0.10 mm in diameter to 6.00 mm in diameter, but at 0.01 mm intervals. The points of origin for the drop sizes at 0.01 mm intervals were found through linear interpolation of the lower resolution points of origin. Figure 2.12 illustrates this process.

Once a time, size, size interval, and location of origin for a drop reaching the surface were obtained, the concentration of drops fitting those parameters was estimated using the drop size distribution derived from the corresponding radar data. Similar to the

process shown in Figure 2.4, these concentrations were found at each of the eight

surrounding points and interpolated linearly. The concentration of drops for each of the

591 drop sizes was obtained in this fashion, and their contribution to the overall rainfall

rate was estimated and summed to generate the final rain rate at the time step in

question. The rainfall rates at the beginning and end of each five minute interval were

then averaged to determine the total rainfall during that period.
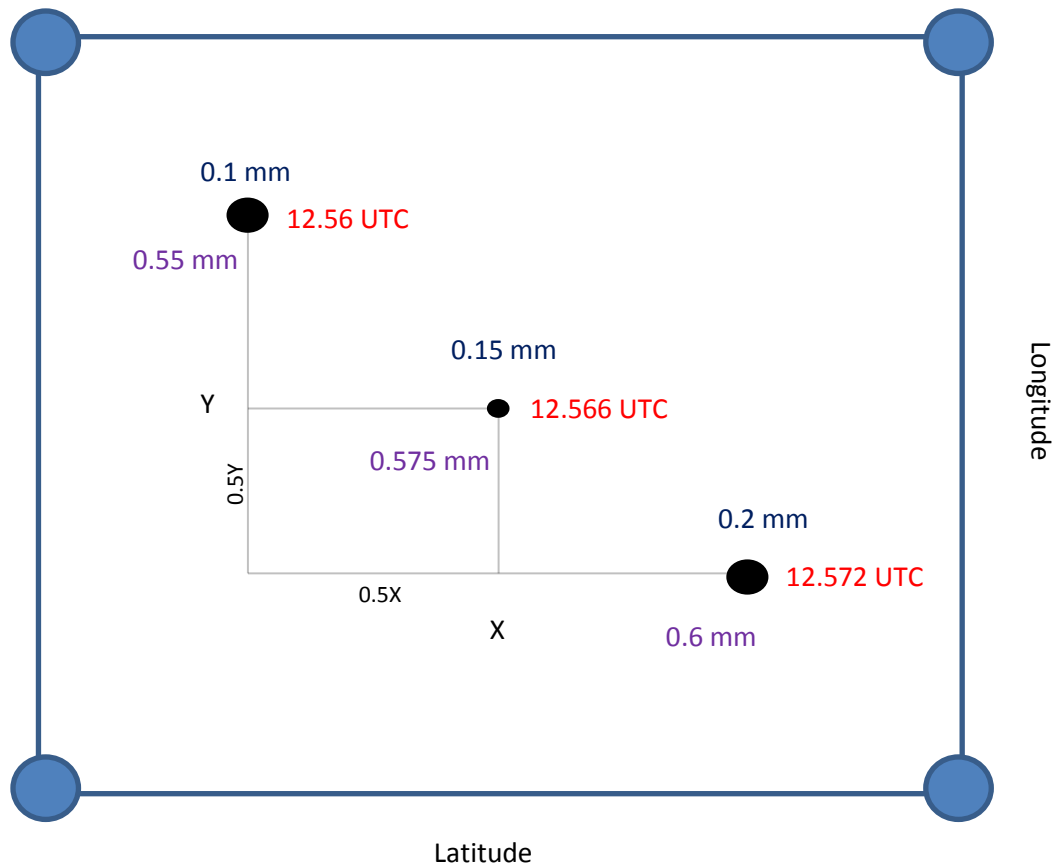
Figure 2.12. Illustration of the Drop Size Interpolation Process. The two larger black circles represent two hypothetical locations of origin for drops of 0.1 mm and 0.2 mm in diameter at the surface. Also shown for each drop is the time of origin in red and the drop size at point of origin in purple. X is the longitudinal distance between the larger black circles and Y is the latitudinal distance. The smaller black circle represents the interpolated location of origin for a drop of 0.15 mm in diameter at the surface; also present for the smaller black circle are the interpolated time and size information. The size interval for the 0.15 mm drop in this case would be 0.005 mm. This means that for calculation purposes, drops between 0.5725 mm and 0.5775 mm in diameter at the point of origin are considered to all be 0.15 mm in diameter when they reach the surface.

2.4 Evaluated Techniques and Implementation

2.4.1 Evaluated Techniques

Table 2.3 shows the conventional rainfall estimation techniques tested. Most of these

techniques were also evaluated in RGS05. In addition to these formulas, the "synthetic"

algorithm from RGS05 was also tested, albeit with slight alterations. The synthetic

algorithm calculates rainfall rates using different formulas for different rain intensities.

Equations 2.8-2.12 describe the synthetic algorithm.

$$R = \frac{\overline{R(Z)}}{f_1(\overline{Z_{dr}})} \ \ if \ \overline{R(Z)} < 6 \ mm \ hr^{-1} \tag{2.8}$$

$$R = \frac{\overline{R(K_{DP})}}{f_2(\overline{Z_{dr}})} \ \ if \ 6 < \overline{R(Z)} < 50 \ mm \ hr^{-1} \tag{2.9}$$

$$R = \overline{R(K_{DP})} \ \ if \ 6 < \overline{R(Z)} < 50 \ mm \ hr^{-1} \tag{2.10}$$

$$f_1(\langle Z_{dr} \rangle) = 0.4 + 5.0 \ |\langle Z_{dr} \rangle - 1|^{1.3} \tag{2.11}$$

$$f_2(\langle Z_{dr} \rangle) = 0.4 + 3.5 \ |\langle Z_{dr} \rangle - 1|^{1.7} \tag{2.12}$$

In this case, $\langle Z_{dr} \rangle$ is the differential reflectivity in linear units. $\overline{R(Z)}$ is (2) from Table 1

and $\overline{R(K_{DP})}$ is (9) from Table 2.3. The bar denotes mean values, using an averaging

scheme described in RGS05. For this study, the only manipulation of Z and Z$_{DR}$ was done

in the merging process mentioned earlier. K$_{DP}$ values were smoothed using a simple

filter that consisted of averaging the immediate surrounding cells with the cell in

question.

As mentioned in Chapter 1, hail causes many problems when it comes to rainfall

estimation using radar. A simple hail adjustment algorithm was implemented to reduce

the effects of hail on the results, similar to the one described in the WSR-88D paper

(Fulton et al. 1998). In this algorithm, reflectivity values were capped at 52 dBZ. A fuzzy

logic scheme was implemented for reflectivity values between 45 and 52 dBZ. The fuzzy

logic was designed to reduce reflectivity values for points where hail was more likely to

be present, which in this case corresponded to Z$_{DR}$ values below the threshold of 3 dB. A

detailed description of the fuzzy logic scheme is given in Appendix B.

Two other algorithms were used to improve the quality of the results. For the trace

techniques, the minimum value allowed for Z$_{DR}$ was 0.5 dB. This was implemented due

to the range of μ values (Equation 2.4) utilized within the program. μ was allowed to

vary between -5 and 16, resulting in a Z$_{DR}$ range of 9.33 to 0.47.

The last algorithm dealt with conventional formulas dependent on K$_{DP}$. This algorithm

assumed a rain rate of zero for any location where reflectivity was below 20 dBZ,

regardless of the K$_{DP}$ value. Implementation of this algorithm helped reduce noise within

the K_{DP}-reliant formulas; applying the 20 dBZ minimum provided assurance that the

radar was actually picking up a significant signal at that location.

Table 2.3 Conventional Rainfall Formulas (R in mm/hr)

$Z = aR^b$	a	b
1	200	1.6
2	300	1.4
3	250	1.2
4	303	1.44
5	527	1.41

$R(K_{DP}) = a\lvert K_{DP}\rvert^b sign(K_{DP})$	a	b
6	50.7	0.85
7	54.3	0.806
8	51.6	0.71
9	44.0	0.822
10	50.3	0.812
11	47.3	0.791

$R(Z, Z_{DR}) = aZ^b Z_{dr}{}^c$	a	b	c
12	$6.7 * 10^{-3}$	0.927	-3.43
13	$7.46 * 10^{-3}$	0.945	-4.76
14	$1.42 * 10^{-2}$	0.770	-1.67
15	$1.59 * 10^{-2}$	0.737	-1.03
16	$1.44 * 10^{-2}$	0.761	-1.51

$R(K_{DP}, Z_{DR}) = a\lvert K_{DP}\rvert^b Z_{dr}{}^c sign(K_{DP})$	a	b	c
17	90.8	0.93	-1.69
18	136	0.968	-2.86
19	52.9	0.852	-0.53
20	63.6	0.851	-0.72

2.4.2 Trace Method and Z_{DR} adjustments

The five trace techniques evaluated are shown in Table 2.4. Also shown is the

adjustments to Z_{DR} that were tested. The reason for these adjustments was possible bias

in Z_{DR} values noted by the NWS (Hoban et al. 2014).

Table 2.4 Trace Techniques

Description	Label	ZDR Adjustments
Drift, Evaporation	T1	+0, 0.2, 0.3, 0.4, 0.5, 0.6, 0.7, 0.8, 0.9, 1.0, 1.1, 1.5, 2.0, 2.6
No Drift, No Evaporation, Instant	T2	+0.4, 0.6, 0.8, 1.0, 1.2, 1.4, 1.6, 1.8, 2.0, 2.2, 2.4, 2.6
No Drift, Evaporation	T3	+0, 0.2, 0.3, 0.4, 0.5, 0.6, 0.7, 0.8, 0.9, 1.0, 1.1, 1.5, 2.0, 2.6
No Drift, No Evaporation	T4	+0.4, 0.6, 0.8, 1.0, 1.2, 1.4, 1.6, 1.8, 2.0, 2.2, 2.4, 2.6
Drift, No Evaporation	T5	+0.4, 0.6, 0.8, 1.0, 1.2, 1.4, 1.6, 1.8, 2.0, 2.2, 2.4, 2.6

2.4.2 Evaluation Methods

The initial phase of program development focused on implementing conventional

rainfall estimation techniques. These included simple Z-R relationships, and more

complicated techniques that used combinations of Z, Z_{DR}, and K_{DP}. The next step

involved implementing the calculation of parameters describing method effectiveness.

The parameters chosen are listed in Table 2.5.

**Table 2.5 Evaluation
Methods**

Evaluation Method	Formula	
Fractional Bias	$FB = \dfrac{\langle T_R - T_G \rangle}{\langle T_G \rangle}$	(2.13)
Fractional Absolute Difference	$FAD = \dfrac{\langle \lvert T_R - T_G \rvert \rangle}{\langle T_G \rangle}$	(2.14)
Fractional Root Mean Square Error	$FRMSE = \dfrac{\langle (T_R - T_G)^2 \rangle^{1/2}}{\langle T_G \rangle}$	(2.15)
Fractional Standard Deviation	$FSD = (FRMSE^2 - FB^2)^{1/2}$	(2.16)

In Table 2.5 T_R is the total radar estimated rainfall, T_G is the total gauge rainfall, and the

brackets indicate averaging over all values. The pairs of corresponding rain gauge and

radar estimated rainfall data had to fulfill two criteria before inclusion in the method

effectiveness calculations. Double zero values were disqualified, as well as pairs where

the rain gauge recorded zero accumulation and the radar estimated rainfall was at or

below half the minimum possible rain gauge accumulation. For these rain gauges the minimum possible accumulation was 0.01 inches, or 0.254 millimeters.

The simplest graphical depiction of method effectiveness was an XY scatterplot with radar estimated rainfall on the x-axis and gauge rainfall on the y-axis. Figure 2.13 shows an example of this type of graphic.

In order to fulfill the "Flexibility" criterion, it was necessary to develop a control program. This program would take inputs like which formulas to use (and which constants to use with those formulas) and generate understandable results. A more detailed description of how this program functions is found in Appendix B.

$$r = 0.0159 * Z^{0.737} * Zdr^{-1.03} \quad \text{60 Minute Interval}$$
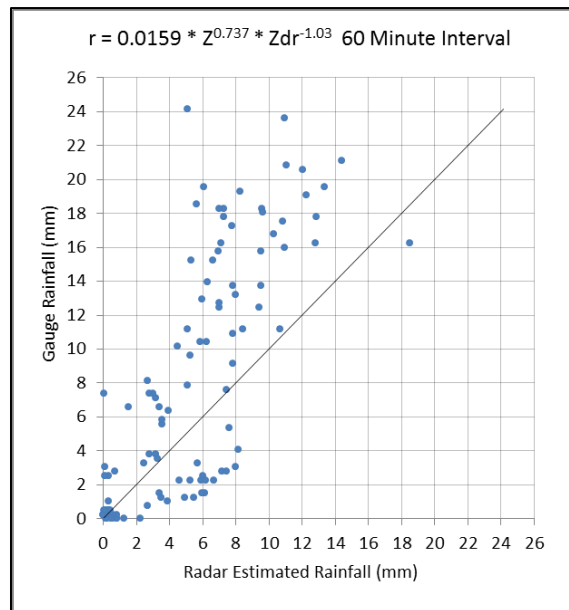
Figure 2.13. Sample X-Y Scatter plot of Radar Estimated Rainfall vs. Gauge Rainfall. The formula tested is shown in the top left corner.

Chapter 3. Results and Discussion

3.1 March 20, 2012

Several competing air masses and at least two low pressure centers set the stage for widespread precipitation over the central United States. Figure 3.1.1 is an HPC surface analysis for 03 UTC of March 21, 2012. The precipitation occurred in several waves, beginning the evening of March 20 and continuing through the early morning hours.

Figure 3.1.2 shows humidity versus height in percentile format for 20 UTC of March 20 through 22 UTC of March 21; the data used for this figure came from one of the high resolution models. The percentiles are references to the amount of time spent at a particular relative humidity level. If the 50th percentile showed relative humidity at 76%, that would mean half of the event duration was spent above 76% relative humidity and half below it. A clear dry layer between 500 and 1000 meters above sea level is readily visible from Figure 3.1.2. Figure 3.1.3 is a hodograph also based on high resolution model data; the U and V values in Figure 3.1.3 are based on averages throughout the time period. The point nearest to the origin shows the U and V wind values at the 1000 millibar level; each subsequent point represents the U and V wind values at a pressure level 25 millibars above. On March 20, a persistent southeasterly wind was present from 1000 to 700 millibars. The direction changed to a more southerly orientation higher up

in the atmosphere. The assumptions made in Figure 3.1.2 and Figure 3.1.3 were also made for the corresponding figures in other events.

3.1.1 Conventional Techniques

Table 3.1.1 shows the performance of the conventional techniques for this event. Of the conventional techniques, the most basic Z-R relationship, (1), proved to be the most effective. The parameters most used to describe method effectiveness were FAD and FRMSE. The lower these values were, the better the method performed. The formulas based on solely Z were roughly equal to those based on Z and Z_{DR} for these parameters. A general negative bias was present for these types of formulas.

The K_{DP} based formulas performed very poorly, as they did for most of the events. Some of this error is undoubtedly due to the general noisiness of K_{DP} data. The method used to calculate K_{DP} from ϕ_{DP} is another probable source of error. All the formulas using K_{DP} exhibited a positive bias, with the Synthetic formula being the most accurate for every parameter.

3.1.2 Tracing Techniques

Table 3.1.2 shows the performance of the various trace techniques and their permutations for this event. The general pattern for the tracing techniques was that an increase in Z_{DR} values resulted in reduced bias values. This makes sense due to the larger drops implied by larger Z_{DR} values. These larger drops produce higher reflectivity values for the same quantity of water in the atmosphere, and as a consequence reduce the total estimated rainfall.

47

Techniques T1 and T3 accounted for evaporation in their trace calculations. These techniques performed best in the +0.5 to +0.8 Z_{DR} range. The other techniques performed best in the +1.2 to +1.4 Z_{DR} range. It can be reasonably implied that for this date the evaporation that took place was roughly equivalent to a +0.6 to +0.7 increase in Z_{DR}.

If the events studied have a significant variation in the amount of evaporation occurring, the overall performance of the T2, T4, and T5 techniques at each individual category of Z_{DR} adjustment will be reduced.

Out of all the techniques evaluated, the effectiveness of the T3 +0.6 Z_{DR} was best for the FAD and FRMSE parameters.

3.1.3 Graphical Evaluation

Figure 3.1.4 is a histogram showing the FAD performance of each evaluated technique for this event. Figure 3.1.5 is the equivalent histogram showing FRMSE performance. For these and subsequent histograms, the techniques are grouped into six sections. The conventional formulas are the first group, and make up the 21 separate techniques on the left edge of each histogram. The number of the technique corresponds to the number given in Table 2.3. These conventional formulas are further sorted by color. The green bars represent the simple Z-R relations, the red bars are the K_{DP}-R relations, the dark blue bars are the Z,Z_{DR}-R relations, the purple bars are the K_{DP},Z_{DR}-R relations, and the brown bar is the synthetic formula. The five other sections of techniques are the

trace techniques, all light blue in color. Within each trace section are the varying ZDR

adjustments used for that particular technique from Table 2.4.

Figure 3.1.6 shows a combination of scatterplots of radar-derived rainfall versus rain

gauge rainfall for the conventional formulas. The techniques illustrated were the top

performers in each category. Figure 3.1.7 is identical to 3.1.6, except it depicts the best

performers of the trace techniques. These types of charts can be used to make a

qualitative assessment of method performance, rather than quantitative.
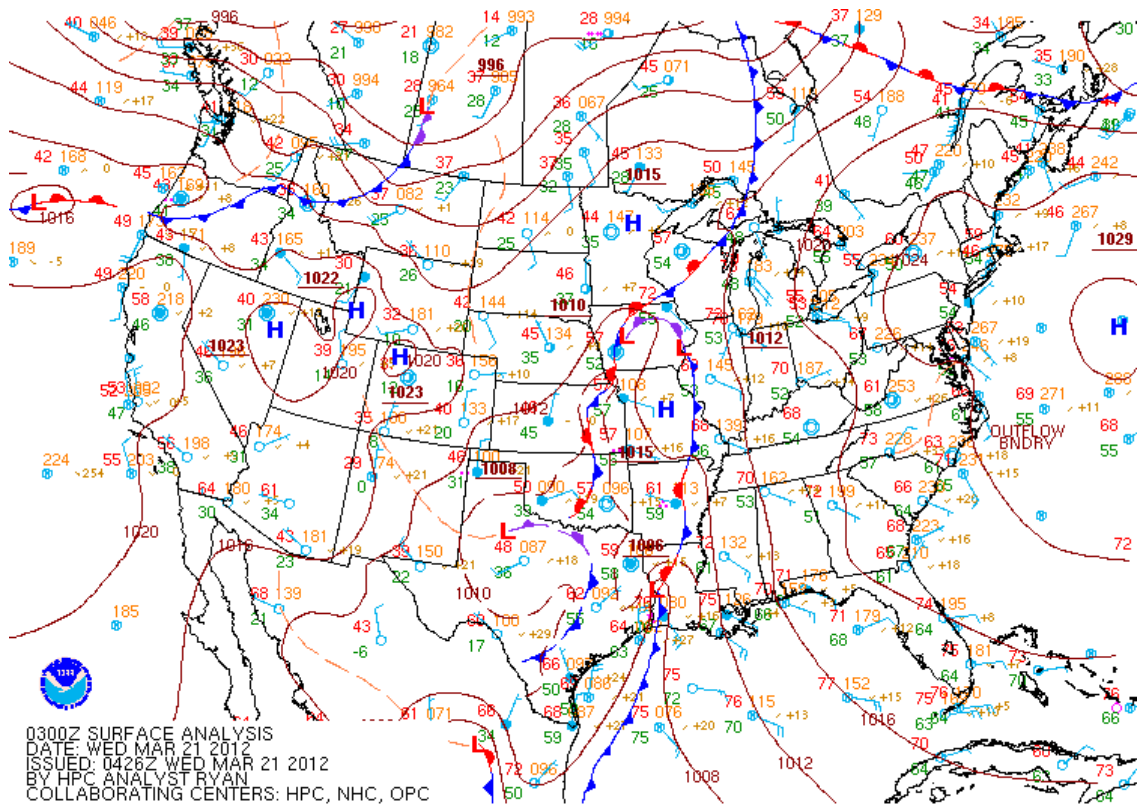
Figure 3.1.1. Surface Analysis 0300 UTC March 21, 2012.
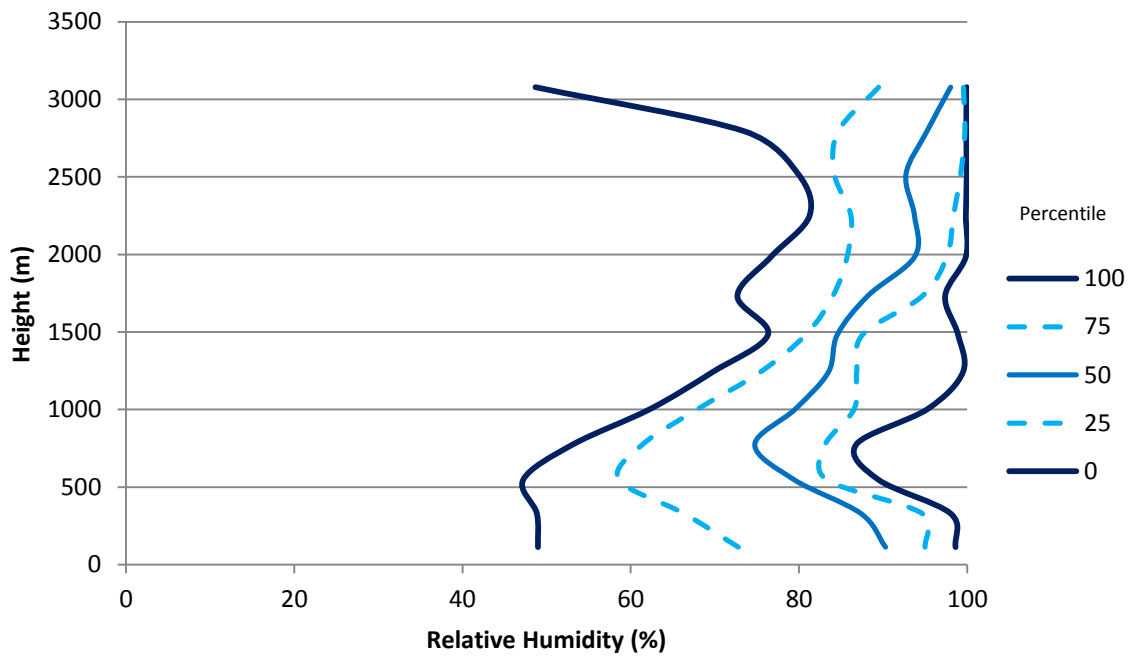
Figure 3.1.2. Relative Humidity Profile March 20, 2012.
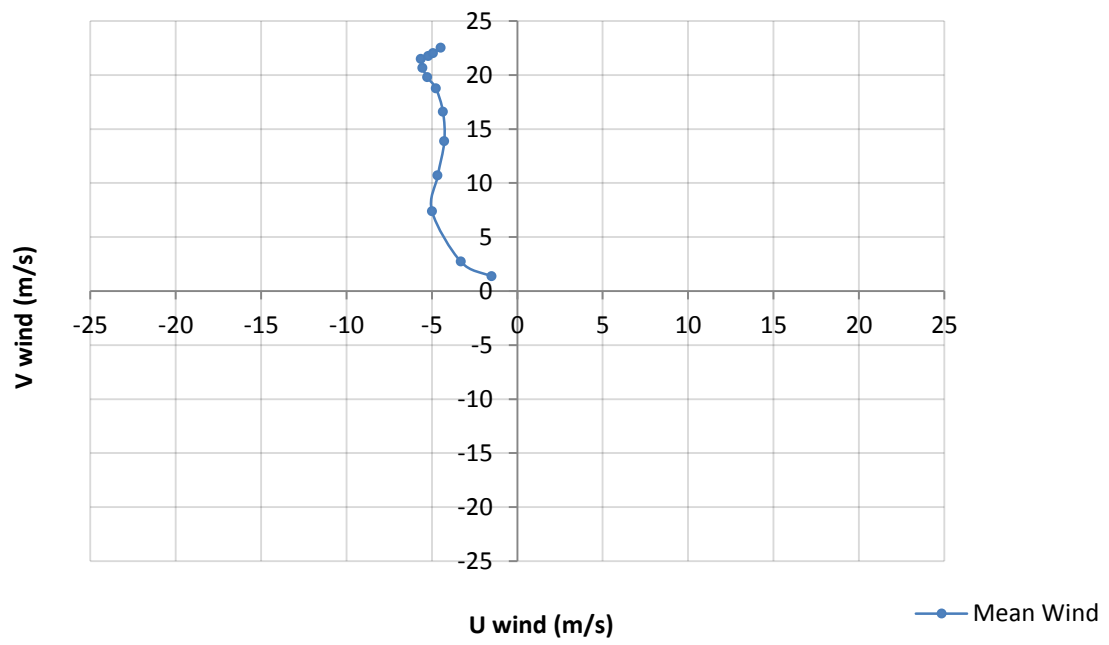
Figure 3.1.3. Hodograph March 20, 2012.

Table 3.1.1 Conventional Techniques, March 20, 2012

$Z = aR^b$	#	FB(%)	FAD(%)	FRMSE(%)	FSD(%)
1	168	-10.42	34.77	48.18	47.04
2	166	-19.69	35.65	50.89	46.93
3	165	15.90	39.30	56.43	54.14
4	166	-22.87	37.47	53.87	48.78
5	157	-46.88	51.83	75.06	58.62
$R(K_{DP}) = a|K_{DP}|^b sign(K_{DP})$					
6	175	63.67	148.58	203.00	192.75
7	175	80.92	167.02	227.79	212.93
8	175	84.56	172.29	232.90	217.01
9	175	44.91	130.70	176.78	170.98
10	175	66.86	152.08	207.31	196.23
11	175	59.32	144.76	196.46	187.29
$R(Z, Z_{DR}) = aZ^b Z_{dr}{}^c$					
12	160	-2.92	35.61	49.22	49.14
13	162	7.33	39.40	57.55	57.08
14	163	-20.91	35.57	50.99	46.51
15	164	-24.11	37.44	53.92	48.23
16	163	-23.32	36.79	52.85	47.42
$R(K_{DP}, Z_{DR}) = a|K_{DP}|^b Z_{dr}{}^c sign(K_{DP})$					
17	176	123.15	213.31	296.49	269.70
18	176	178.68	277.75	390.90	347.67
19	175	64.00	150.49	204.69	194.42
20	175	92.19	180.03	246.18	228.27
Synthetic					
21	174	19.94	51.71	89.29	87.04

Table 3.1.2 Trace Techniques, March 20, 2012

	Z_{DR} +	#	FB(%)	FAD(%)	FRMSE(%)	FSD(%)
T1	0	151	17.25	43.85	77.94	76.01
	0.2	152	8.51	39.63	67.03	66.49
	0.3	152	3.72	38.17	62.25	62.14
	0.4	152	-1.10	37.77	58.35	58.34
	0.5	151	-5.93	37.75	55.30	54.98
	0.6	151	-10.58	38.12	53.63	52.57
	0.7	150	-15.26	38.32	52.40	50.13
	0.8	150	-19.77	38.84	52.22	48.34
	0.9	149	-24.13	39.50	52.61	46.75
	1	149	-28.24	40.64	53.82	45.81
	1.1	149	-32.17	41.98	55.59	45.33
	1.5	149	-45.39	48.61	65.62	47.39
	2	149	-57.26	58.63	78.36	53.49
	2.6	149	-67.19	67.74	90.55	60.70
T2	0.4	160	75.64	85.83	146.09	124.99
	0.6	159	46.82	62.81	104.52	93.44
	0.8	156	23.22	48.25	74.43	70.72
	1	154	4.37	39.41	55.95	55.78
	1.2	154	-10.30	36.32	48.76	47.66
	1.4	151	-21.99	37.53	49.01	43.80
	1.6	149	-31.38	39.93	53.38	43.18
	1.8	149	-39.01	44.12	59.36	44.74
	2	149	-45.38	48.96	65.45	47.15
	2.2	149	-50.80	53.47	71.19	49.88
	2.4	149	-55.46	57.38	76.48	52.66
	2.6	149	-59.53	60.90	81.30	55.37
T3	0	150	10.88	41.28	63.57	62.63
	0.2	150	2.69	37.49	54.80	54.73
	0.3	150	-1.85	36.08	50.84	50.80
	0.4	150	-6.52	35.03	47.89	47.44
	0.5	150	-11.19	34.41	46.14	44.77
	0.6	150	-15.78	34.38	45.53	42.71
	0.7	150	-20.28	34.60	46.02	41.31
	0.8	149	-24.63	35.51	47.29	40.37
	0.9	149	-28.71	37.00	49.43	40.24
	1	149	-32.56	38.72	52.06	40.62
	1.1	149	-36.17	41.02	54.97	41.39
	1.5	149	-48.36	51.04	67.09	46.51
	2	149	-59.46	60.68	80.21	53.83
	2.6	149	-68.86	69.28	92.22	61.34

Table 3.1.2 Trace Techniques, March 20, 2012 (Continued)

	Z_{DR} +	#	FB(%)	FAD(%)	FRMSE(%)	FSD(%)
T4	0.4	163	75.79	83.90	146.58	125.47
	0.6	160	46.88	60.36	103.89	92.71
	0.8	156	23.23	45.77	72.77	68.96
	1	156	4.44	38.03	54.23	54.05
	1.2	155	-10.28	35.12	46.76	45.62
	1.4	151	-22.01	35.46	46.93	41.45
	1.6	149	-31.39	38.19	51.59	40.94
	1.8	149	-39.02	43.23	57.88	42.75
	2	149	-45.40	48.60	64.22	45.42
	2.2	149	-50.81	53.21	70.16	48.39
	2.4	149	-55.47	57.22	75.60	51.37
	2.6	149	-59.53	60.77	80.54	54.25
T5	0.4	158	86.88	94.92	170.38	146.57
	0.6	156	57.17	71.01	127.77	114.27
	0.8	156	32.26	53.83	94.91	89.26
	1	155	12.26	43.89	71.06	70.00
	1.2	152	-3.87	39.19	56.41	56.28
	1.4	152	-16.48	38.52	51.78	49.09
	1.6	151	-26.64	39.84	53.09	45.92
	1.8	151	-34.91	42.91	57.53	45.74
	2	151	-41.76	46.37	62.99	47.16
	2.2	151	-47.58	50.52	68.58	49.38
	2.4	149	-52.65	54.64	73.41	51.16
	2.6	149	-56.98	58.41	78.33	53.75
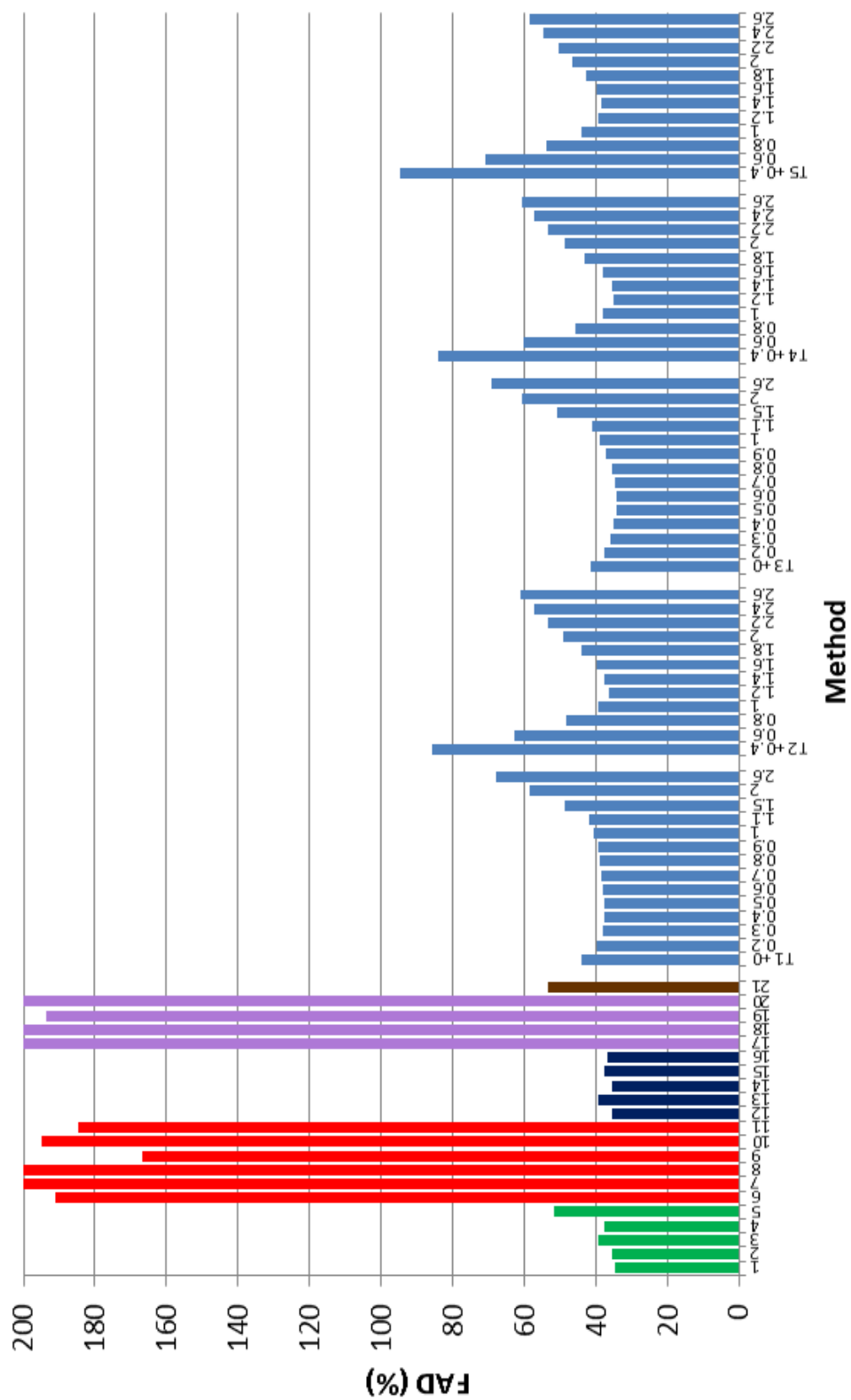
Figure 3.1.4. FAD Performance March 20, 2012.

Figure 3.1.5. FRMSE Performance March 20, 2012.
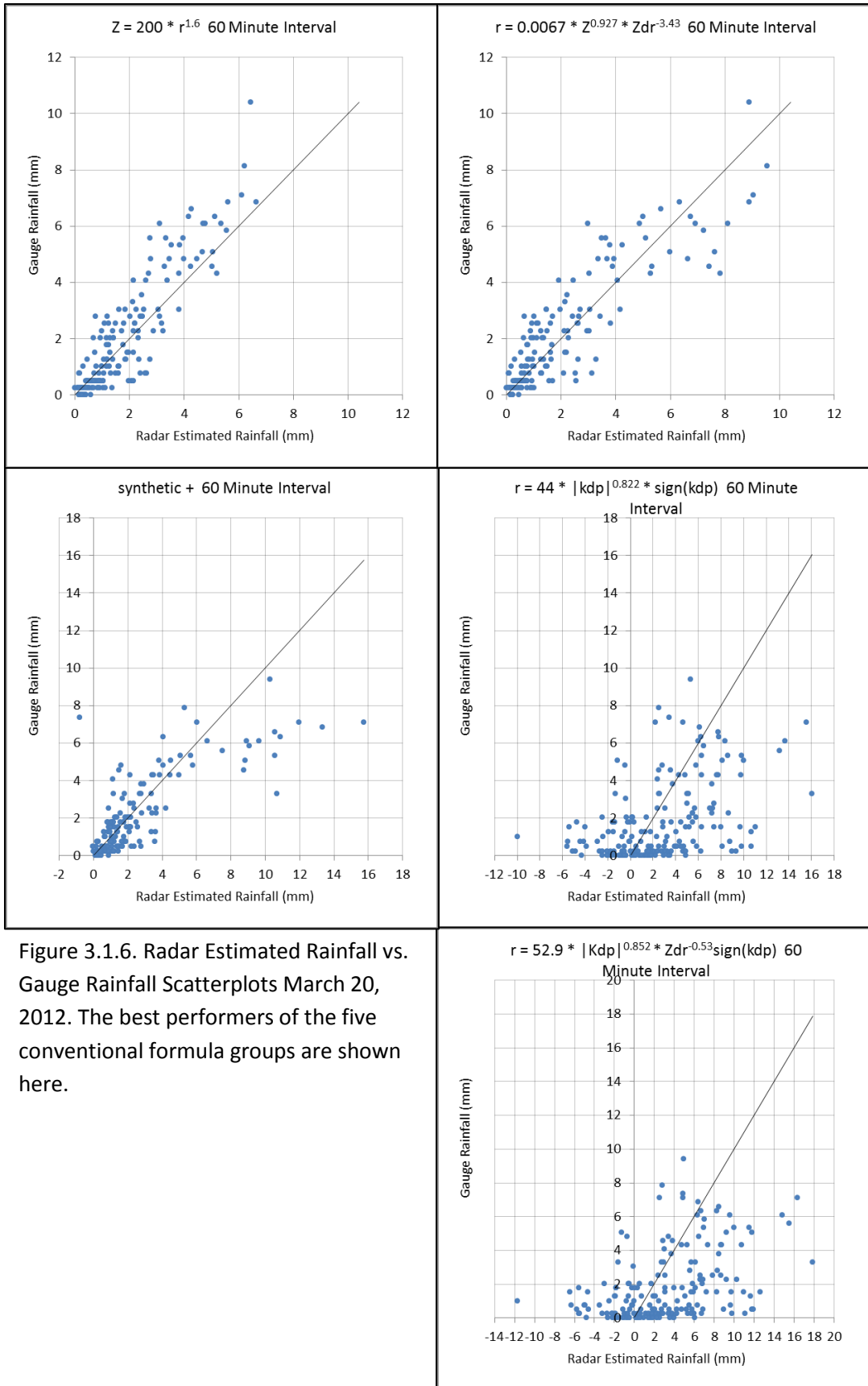
Figure 3.1.6. Radar Estimated Rainfall vs. Gauge Rainfall Scatterplots March 20, 2012. The best performers of the five conventional formula groups are shown here.

57
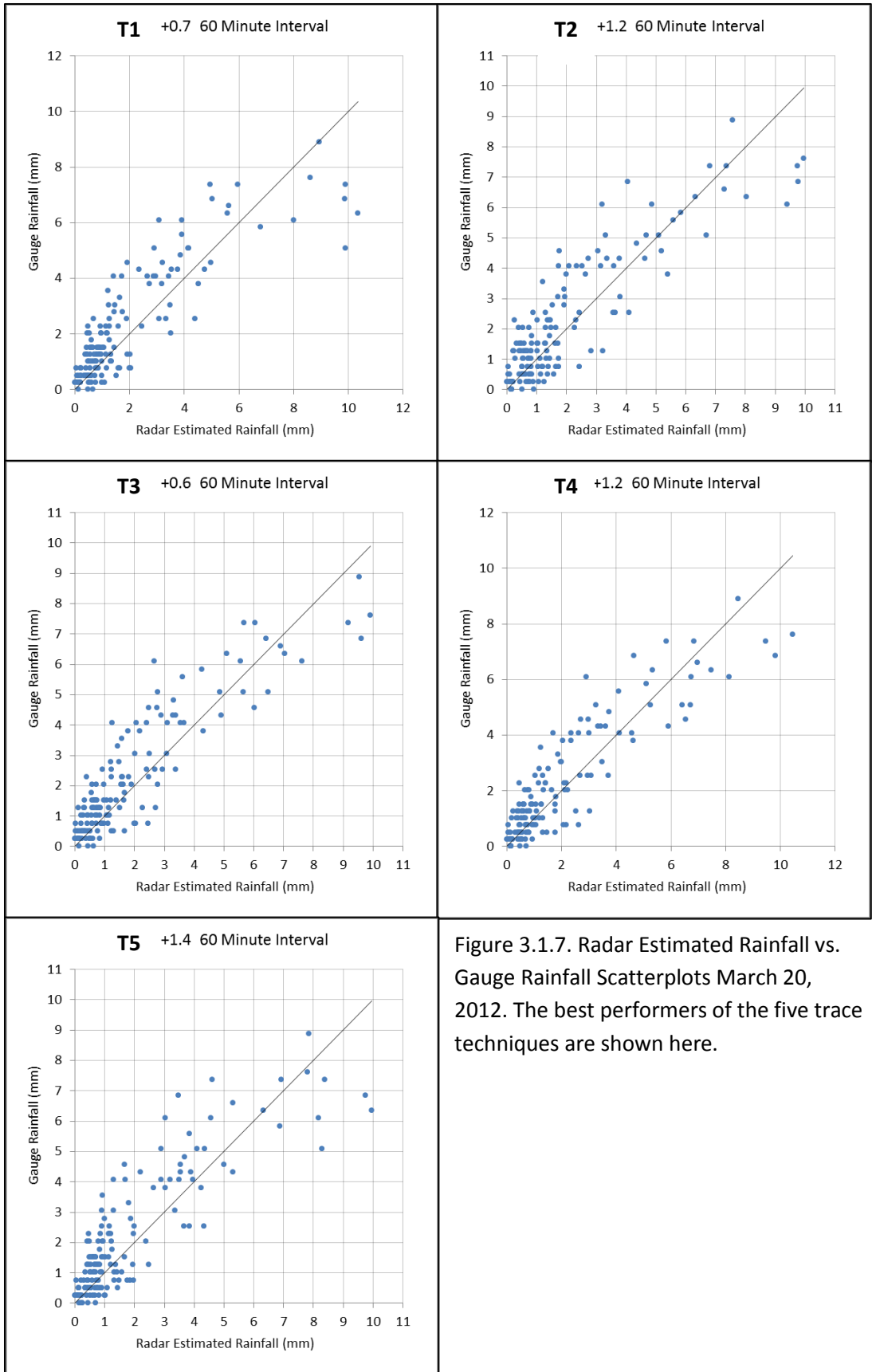
Figure 3.1.7. Radar Estimated Rainfall vs. Gauge Rainfall Scatterplots March 20, 2012. The best performers of the five trace techniques are shown here.

3.2 April 13, 2012

The morning hours of April 13, 2012, saw precipitation overrun a warm front in the central United States. Figure 3.2.1 is an HPC surface analysis for 12 UTC of April 13, 2012. Figure 3.2.2 shows humidity versus height in percentile format for 04 UTC through 13 UTC of April 13. An exceptionally dry layer was present at about 500 meters above sea level throughout the examined period. Figure 3.2.3 is a hodograph for April 13. In the hodograph, a southeasterly wind at the surface transitions to southerly at 900 millibars, and southwesterly above 900.

3.2.1 Conventional Formulas

Due to extreme noise in the K_{DP} data, formulas involving K_{DP} were not evaluated for the precipitation events of April 13, April 14, and April 15 of 2012.

Table 3.2.1 shows the performance of the conventional techniques for this event. Of the conventional formulas evaluated, (5), was most effective. Three outliers are present in formulas (3), (12), and (13). (3) is the formula associated with tropical rain, so it is not unexpected that it would perform poorly in a frontal situation like this. (12) and (13) maybe have been affected by the Z_{DR} bias mentioned in Chapter 2. A general positive bias was present for the conventional formulas tested in this event. Overall the conventional formulas performed worse on the FAD and FRMSE parameters when compared to March 20 of 2012.

3.2.2 Tracing Techniques

Table 3.2.2 shows the performance of the various trace techniques and their permutations for this event. Techniques T2, T4, and T5 were most effective at the highest range of + Z_{DR} values (2.6). Even then the associated values for FAD and FRMSE were higher for these than for techniques T1 and T3. The extremely dry layer at 500 meters is likely the cause of this. The techniques that take into account evaporation were much better suited to handle the precipitation reaching the ground.

The T4 technique performed the best out of the techniques that did not take into account evaporation. It is worth noting that the change from +2.4 Z_{DR} to +2.6 Z_{DR} resulted in improvements for the FAD and FRMSE values for the T2, T4, and T5 techniques. However, at this point the biases switched sign, so any significant further improvements from additional increases in Z_{DR} were unlikely. T1 values for FAD and FRMSE were smaller than those for T3 but not by a great margin.

A significant decrease in FAD and FRMSE occurred with T1 and T3 at their best ZDR adjustment compared to the conventional techniques for this event.

3.2.3 Graphical Evaluation

Figure 3.2.4 is a histogram showing the FAD performance of each evaluated technique for this event. Figure 3.2.5 is the equivalent histogram showing FRMSE performance.

Figure 3.2.6 shows a combination of scatterplots of radar-derived rainfall versus rain gauge rainfall for the conventional formulas. The techniques illustrated were the top performers in each category. Figure 3.2.7 is identical to 3.2.6, except it depicts the best performers of the trace techniques.
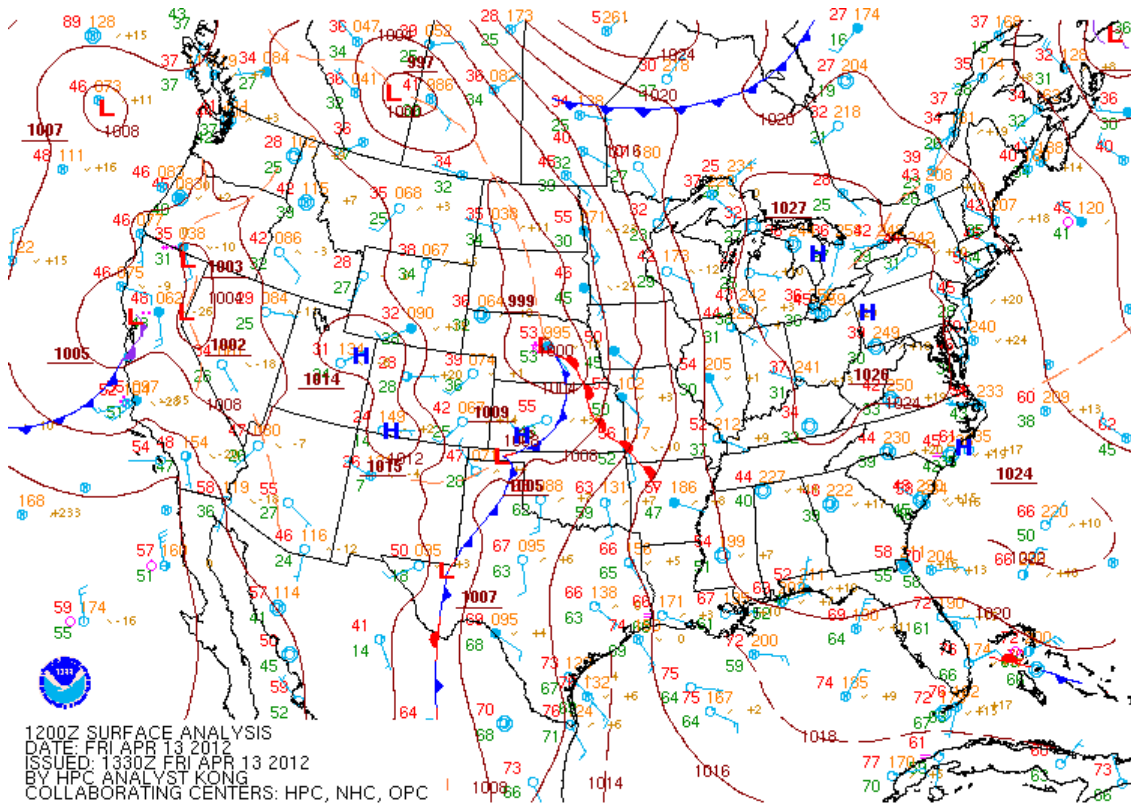
Figure 3.2.1. Surface Analysis 1200 UTC April 13, 2012.
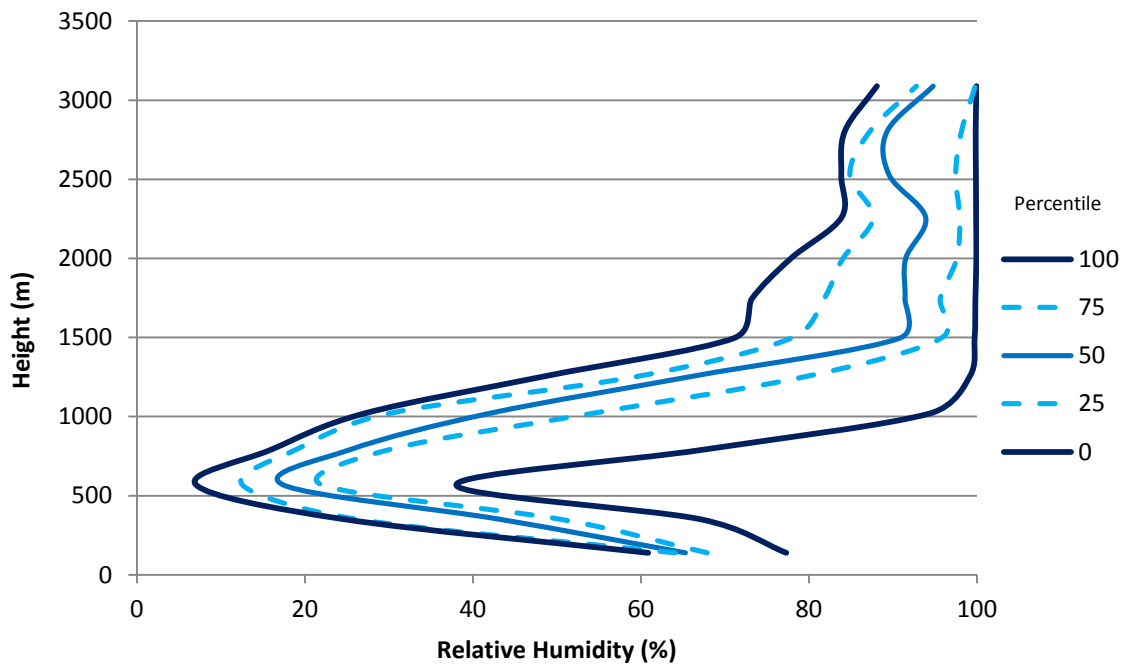
Figure 3.2.2. Relative Humidity Profile April 13, 2012.
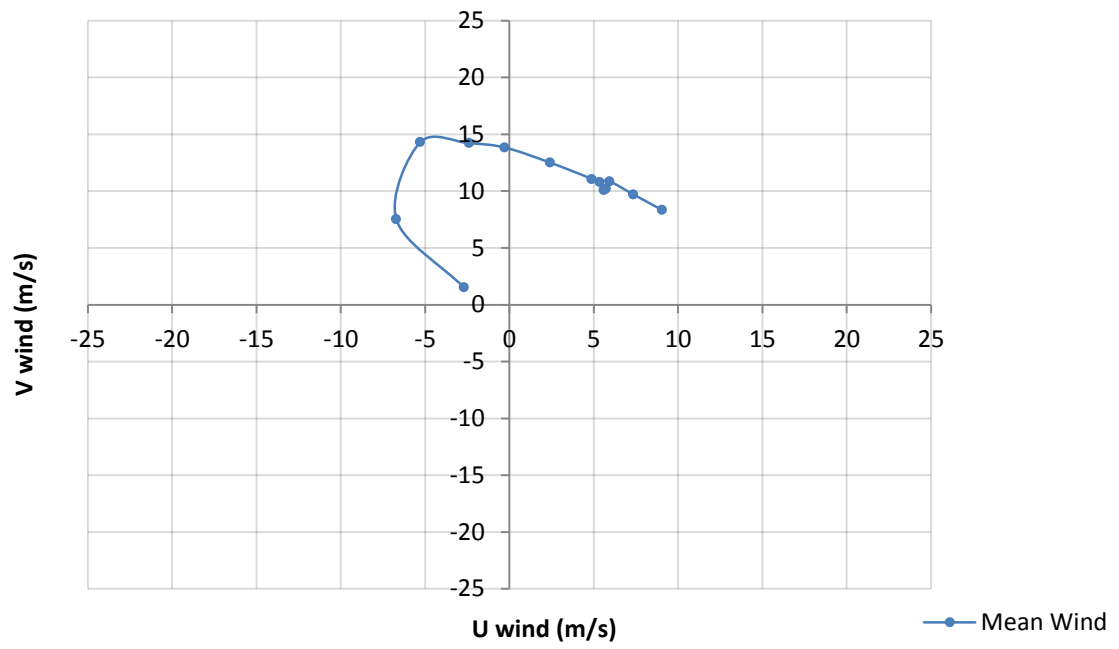
Figure 3.2.4. Hodograph April 13, 2012.

Table 3.2.1 Conventional Techniques, April 13, 2012

$Z = aR^b$	#	FB(%)	FAD(%)	FRMSE(%)	FSD(%)
1	24	45.79	63.72	84.15	70.60
2	22	50.36	63.52	81.19	63.68
3	22	164.17	164.17	217.20	142.21
4	22	39.83	58.05	73.85	62.18
5	20	-1.28	47.50	58.89	58.88
$R(Z, Z_{DR}) = aZ^b Z_{dr}{}^c$					
12	22	55.18	75.15	106.58	91.18
13	24	60.32	86.69	132.68	118.17
14	22	23.85	58.35	77.07	73.29
15	22	22.46	54.66	72.10	68.52
16	22	20.82	57.35	75.12	72.17

Table 3.2.2 Trace Techniques, April 13, 2012

	Z_{DR} +	#	FB(%)	FAD(%)	FRMSE(%)	FSD(%)
T1	0	19	-10.07	20.41	26.55	24.57
	0.2	19	-7.57	19.48	26.04	24.92
	0.3	19	-6.70	19.28	26.08	25.20
	0.4	19	-6.01	18.99	26.24	25.55
	0.5	19	-5.61	18.89	26.66	26.07
	0.6	19	-5.45	19.64	27.47	26.92
	0.7	19	-5.55	20.91	28.64	28.10
	0.8	20	-5.59	22.52	31.05	30.54
	0.9	20	-6.18	23.99	33.26	32.68
	1	20	-7.00	25.76	35.70	35.01
	1.1	20	-8.65	26.75	36.99	35.96
	1.5	19	-17.15	29.92	40.57	36.77
	2	19	-29.37	36.32	49.31	39.60
	2.6	19	-42.67	46.60	62.30	45.39
T2	0.4	27	183.59	183.59	243.33	159.70
	0.6	27	148.50	148.50	200.95	135.37
	0.8	26	120.03	120.03	165.76	114.31
	1	25	96.73	98.64	138.47	99.09
	1.2	25	77.98	82.13	120.32	91.63
	1.4	25	61.55	69.04	102.93	82.49
	1.6	25	46.95	58.15	88.13	74.59
	1.8	25	33.58	51.28	75.78	67.94
	2	23	21.52	46.14	64.53	60.84
	2.2	23	10.97	41.97	58.85	57.82
	2.4	23	1.64	39.71	56.11	56.08
	2.6	23	-7.08	39.36	55.49	55.03
T3	0	19	-5.64	21.69	28.56	28.00
	0.2	19	-5.37	22.15	29.87	29.38
	0.3	20	-5.26	22.44	31.34	30.90
	0.4	21	-5.56	23.09	33.18	32.71
	0.5	21	-6.35	24.08	34.41	33.82
	0.6	21	-7.39	25.07	35.78	35.01
	0.7	22	-8.35	26.25	38.12	37.19
	0.8	22	-9.80	26.94	39.43	38.19
	0.9	22	-11.45	27.53	40.76	39.12
	1	22	-13.10	28.58	42.23	40.15
	1.1	22	-14.77	29.73	43.78	41.21
	1.5	22	-21.50	34.25	50.66	45.87
	2	20	-32.46	39.42	57.16	47.05
	2.6	19	-44.93	49.09	66.86	49.51

Table 3.2.2 Trace Techniques, April 13, 2012 (Continued)

	Z_{DR} +	#	FB(%)	FAD(%)	FRMSE(%)	FSD(%)
T4	0.4	22	179.80	179.80	222.23	130.61
	0.6	22	145.17	145.17	183.62	112.44
	0.8	22	117.32	117.32	154.41	100.40
	1	22	94.54	98.09	131.62	91.57
	1.2	22	76.01	83.31	114.42	85.53
	1.4	22	59.78	70.27	98.04	77.71
	1.6	22	45.34	58.84	84.21	70.96
	1.8	22	32.11	51.47	72.71	65.23
	2	22	20.61	46.47	64.81	61.44
	2.2	22	10.14	41.97	59.28	58.40
	2.4	22	0.87	39.27	56.56	56.55
	2.6	22	-7.79	38.46	55.86	55.32
T5	0.4	25	188.04	188.04	231.25	134.61
	0.6	25	153.76	153.76	193.41	117.32
	0.8	24	126.82	126.82	162.63	101.81
	1	24	105.51	105.51	142.80	96.23
	1.2	23	85.62	85.76	120.03	84.11
	1.4	23	68.40	71.40	102.38	76.18
	1.6	23	52.70	60.04	85.83	67.75
	1.8	23	39.10	51.85	72.66	61.25
	2	23	26.57	44.85	61.45	55.41
	2.2	22	15.07	40.50	52.29	50.07
	2.4	22	5.06	37.00	48.20	47.93
	2.6	20	-4.35	35.20	45.27	45.06
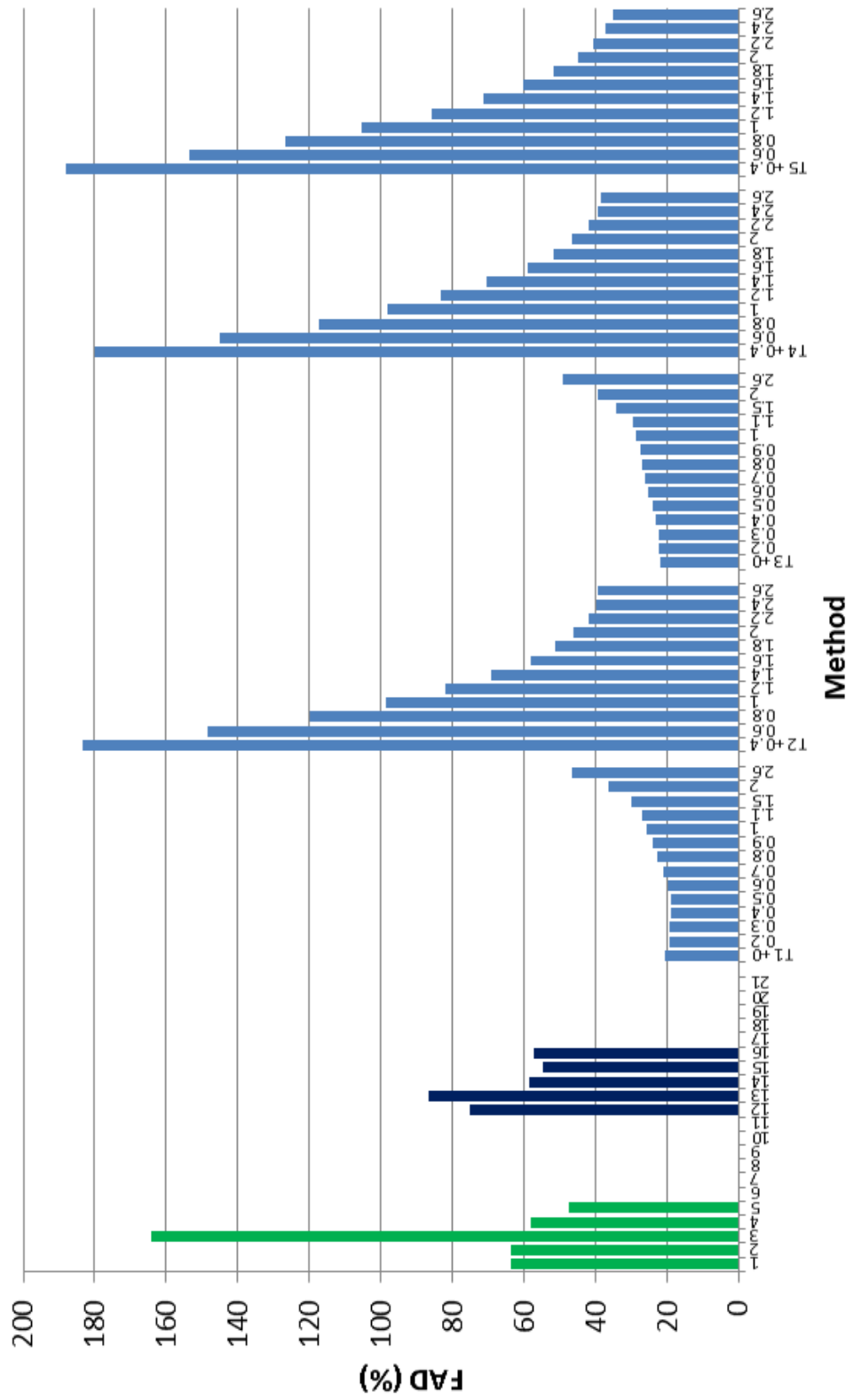
Figure 3.2.4. FAD Performance April 13, 2012.
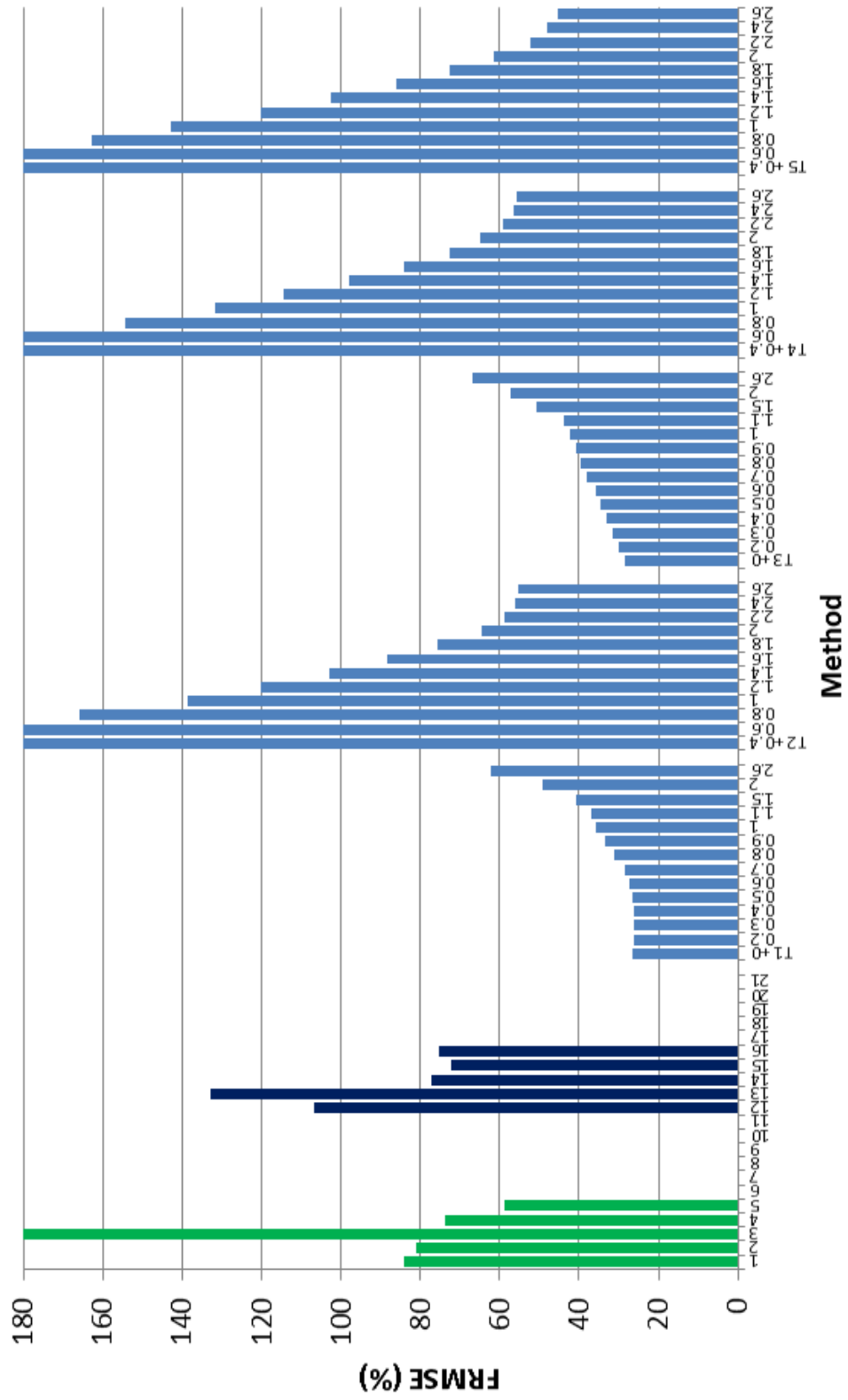
Figure 3.2.5. FRMSE Performance April 13, 2012.
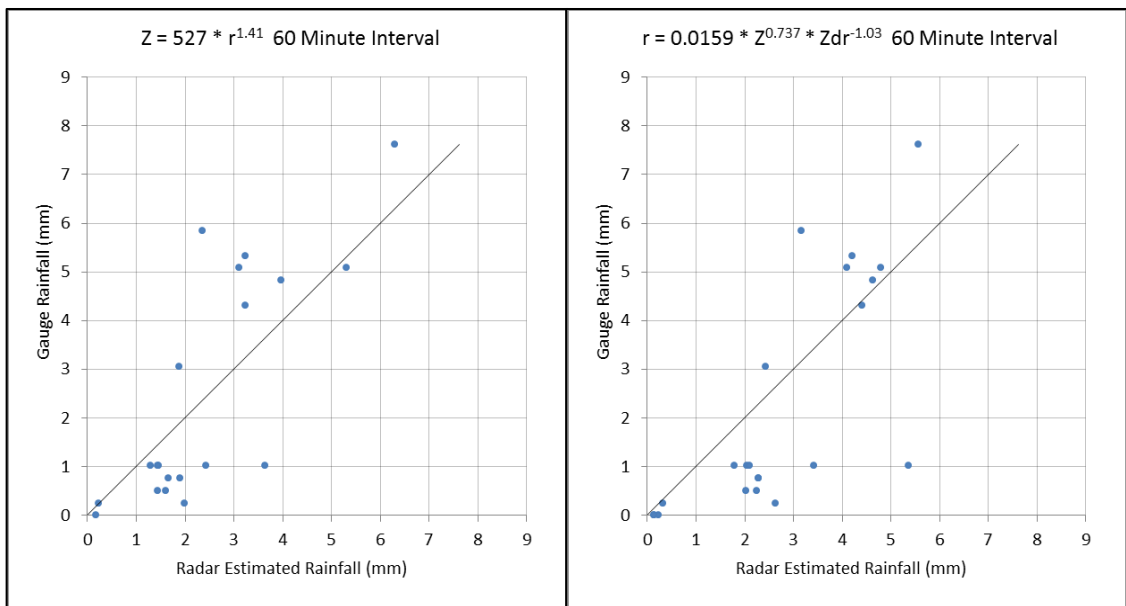
Figure 3.2.4. Radar Estimated Rainfall vs. Gauge Rainfall Scatterplots April 13, 2012. The best performers of the two evaluated conventional formula groups are shown here.
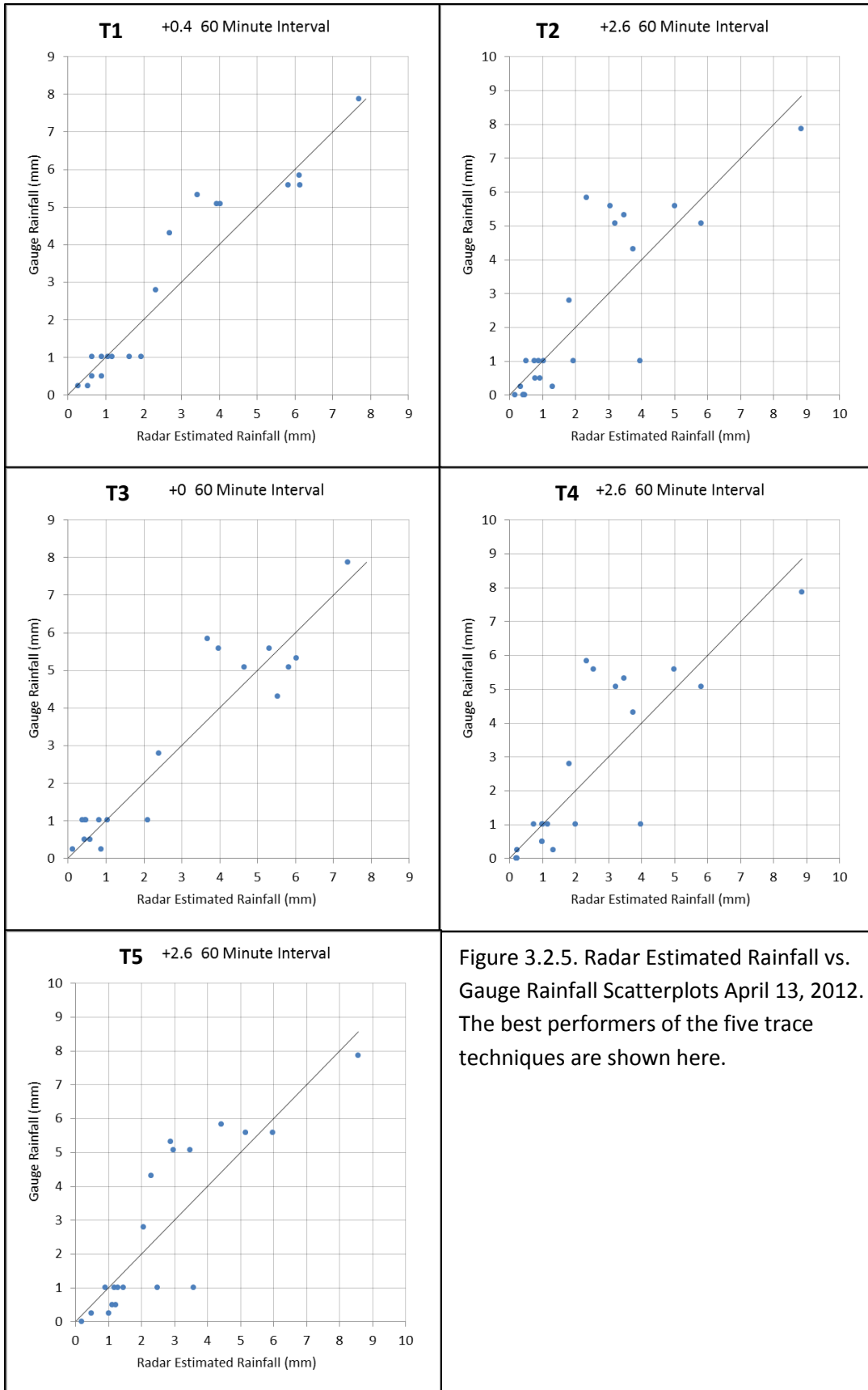
Figure 3.2.5. Radar Estimated Rainfall vs. Gauge Rainfall Scatterplots April 13, 2012. The best performers of the five trace techniques are shown here.

3.3 April 14, 2012

The same system that brought precipitation to central Missouri on April 13 continued to affect the area on the 14th. Figure 3.3.1 is an HPC surface analysis for 09 UTC of April 14, 2012. Figure 3.3.2 shows humidity versus height in percentile format for 01 UTC through 10 UTC of April 14. The dry layer at 500 meters was still present, but was much weaker in magnitude. Figure 3.3.3 is a hodograph for the 14th. The hodograph indicates the wind direction on the 14th became more westerly (or less easterly) at all levels shown. Figure 3.3.4 is a four panel radar image from KLSX for 0924 UTC of April 14.

3.3.1 Conventional Formulas

Due to extreme noise in the K_{DP} data, formulas involving K_{DP} were not evaluated for the precipitation events of April 13, April 14, and April 15 of 2012.

Table 3.3.1 shows the performance of the conventional techniques for this event. (2), the standard WSR-88D formula, was most effective of all the conventional formulas. Only one outlier, (3), was present, likely for the same reasons as it was an outlier on the 13th. There was a mix of positive and negative biases for the conventional formulas on this date.

3.3.2 Tracing Techniques

Table 3.3.2 shows the performance of the various trace techniques and their permutations for this event. Not many patterns were present for the tracing technique results on the 14th of April, 2012. The optimal ZDR adjustment varied considerably

across the tracing techniques. Several anomalously low FAD were present, suggesting outlying data points.

3.3.3 Graphical Evaluation

Figure 3.3.5 is a histogram showing the FAD performance of each evaluated technique for this event. Figure 3.3.6 is the equivalent histogram showing FRMSE performance.

Figure 3.3.7 shows a combination of scatterplots of radar-derived rainfall versus rain gauge rainfall for the conventional formulas. The techniques illustrated were the top performers in each category. Figure 3.3.8 is identical to 3.3.7, except it depicts the best performers of the trace techniques.
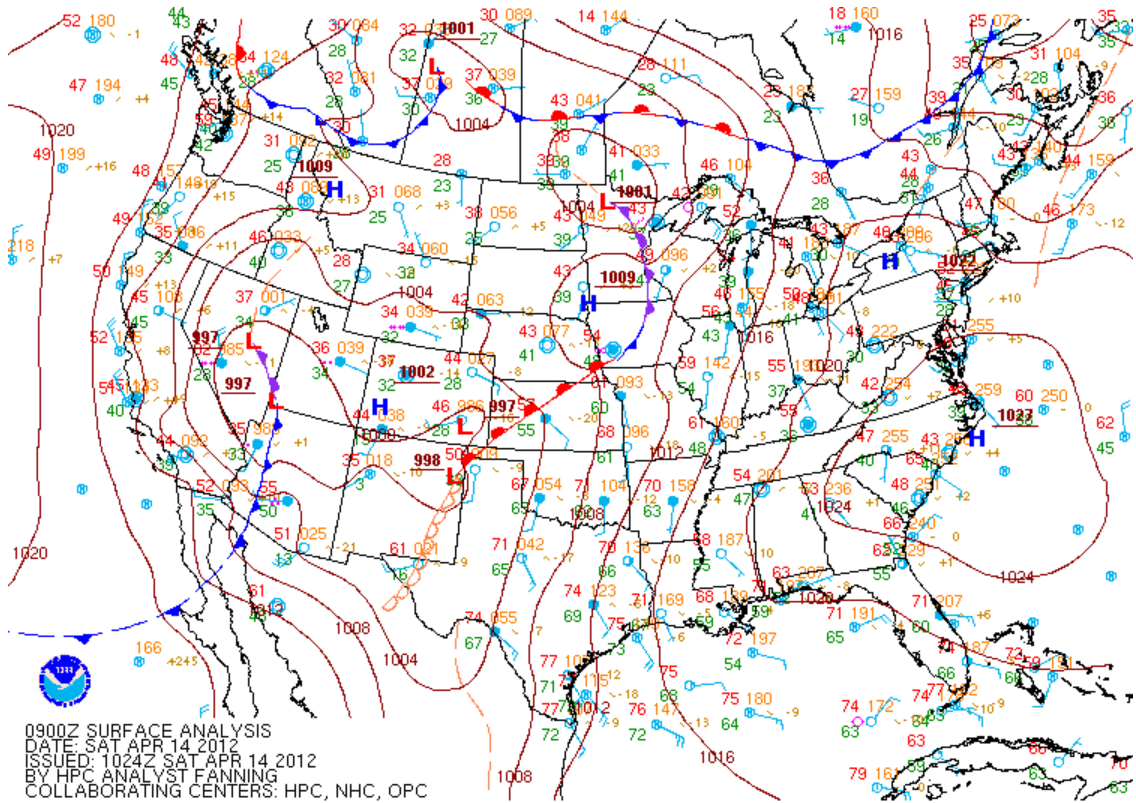
Figure 3.3.1. Surface Analysis 0900 UTC April 14, 2012.
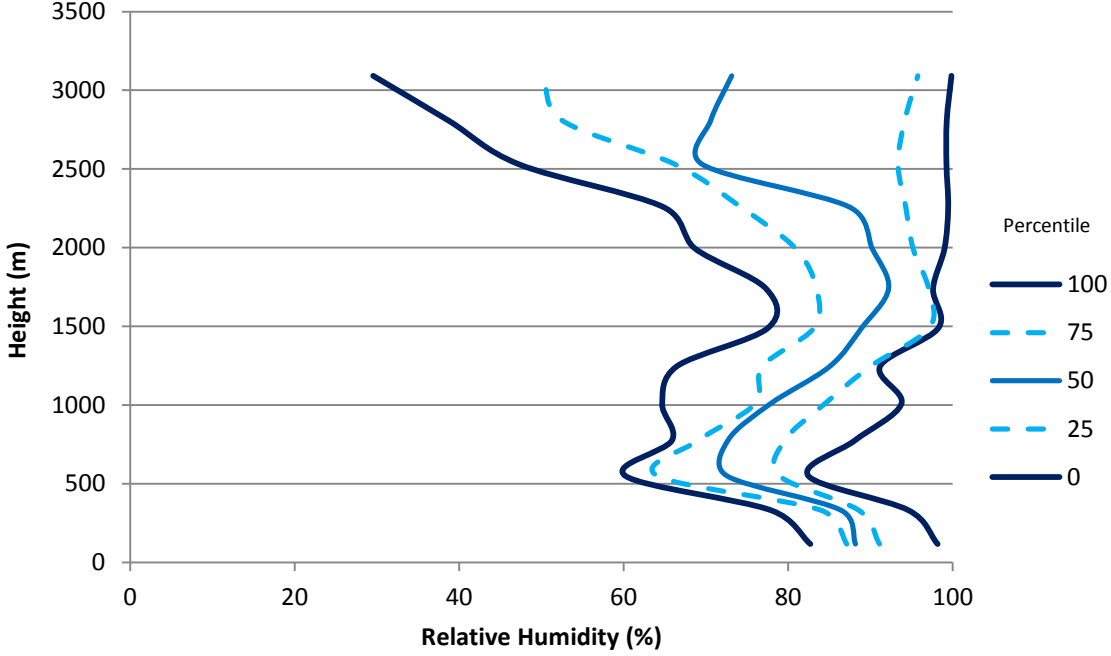
Figure 3.3.2. Relative Humidity Profile April 14, 2012.
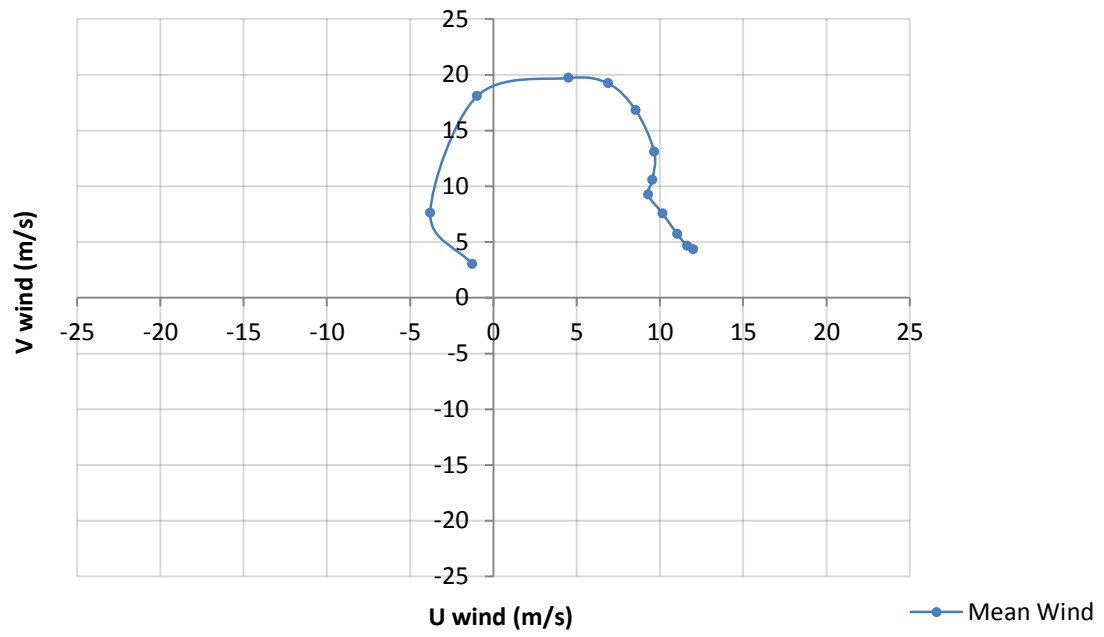
Figure 3.3.3. Hodograph April 14, 2012.
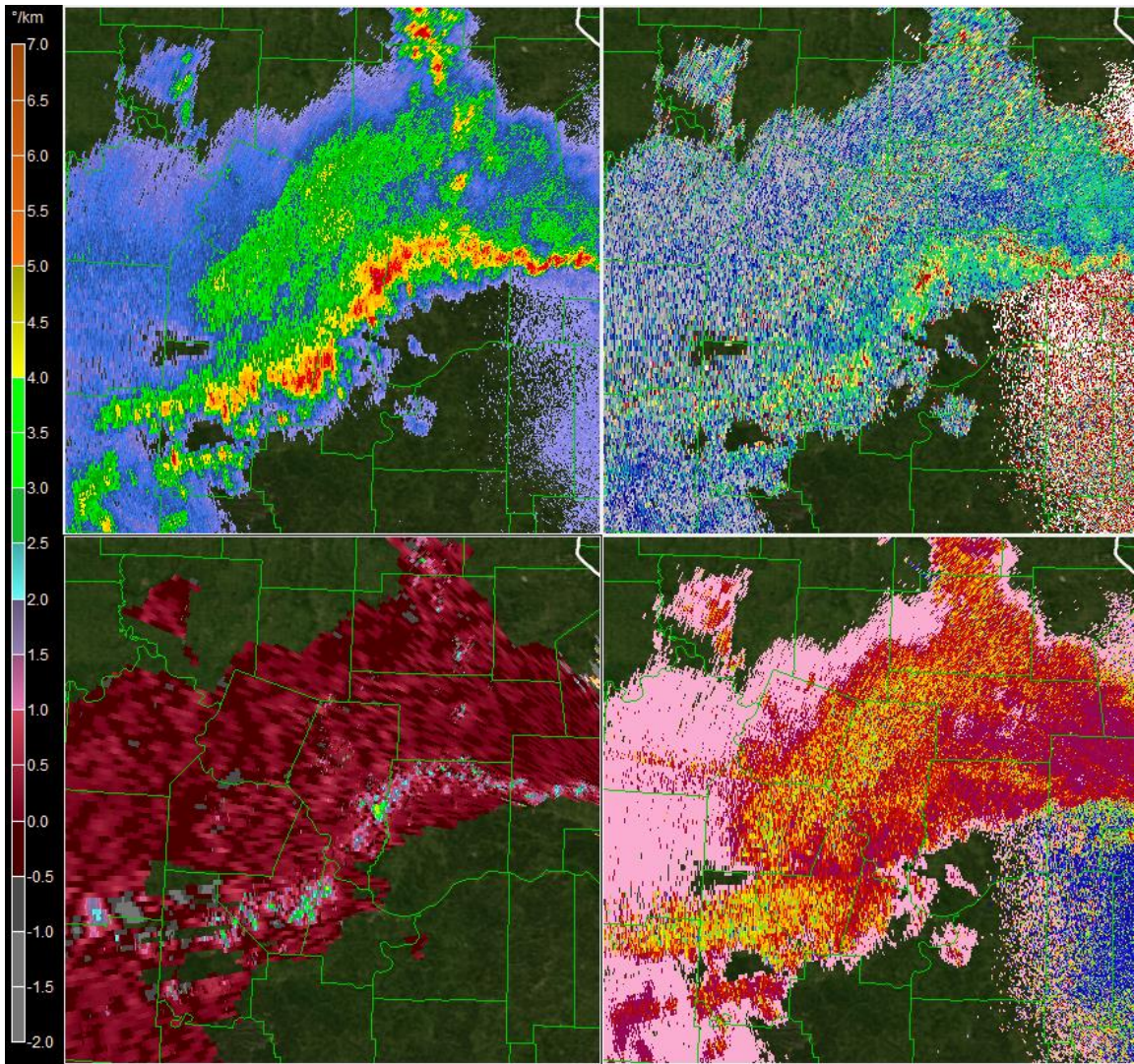
Figure 3.3.4. Four Panel Radar Image for 0924 UTC April 14, 2012. The top left is reflectivity (Z), top right is differential reflectivity (Z_{DR}), bottom left is specific phase differential (K_{DP}), and bottom right is correlation coefficient. The scale on the left corresponds to the bottom left image (K_{DP}). The elevation angle used here was 0.5^{o}.

Table 3.3.1 Conventional Techniques, April 14, 2012

$Z = aR^b$	#	FB(%)	FAD(%)	FRMSE(%)	FSD(%)
1	29	-10.95	41.62	68.85	67.97
2	28	-3.97	36.03	62.18	62.05
3	29	79.68	82.23	156.05	134.17
4	28	-11.58	39.31	66.10	65.08
5	24	-37.45	49.69	83.86	75.03
$R(Z, Z_{DR}) = aZ^b Z_{dr}{}^c$					
12	26	-3.77	33.85	66.38	66.27
13	26	-5.16	36.62	69.18	68.99
14	26	-25.02	46.29	76.40	72.19
15	28	-25.50	46.81	79.85	75.66
16	26	-26.87	47.22	78.14	73.37

Table 3.3.2 Trace Techniques, April 14, 2012

	Z_{DR} +	#	FB(%)	FAD(%)	FRMSE(%)	FSD(%)
T1	0	31	56.17	64.08	126.38	113.21
	0.2	28	48.06	56.55	108.84	97.65
	0.3	28	44.39	53.14	103.57	93.58
	0.4	28	40.89	50.12	99.08	90.25
	0.5	27	37.04	46.70	92.74	85.02
	0.6	25	33.06	43.06	85.03	78.34
	0.7	25	29.43	39.67	81.18	75.66
	0.8	25	25.74	36.41	77.93	73.55
	0.9	25	22.07	33.69	74.76	71.43
	1	25	18.51	31.43	72.14	69.73
	1.1	25	14.92	29.21	69.93	68.32
	1.5	25	0.65	30.57	65.81	65.81
	2	24	-15.99	35.51	67.17	65.24
	2.6	23	-34.30	45.74	79.10	71.27
T2	0.4	26	101.06	103.62	186.65	156.92
	0.6	25	77.65	80.97	145.45	122.99
	0.8	25	59.51	63.56	117.34	101.13
	1	25	43.42	48.05	94.19	83.58
	1.2	24	29.59	36.36	75.15	69.08
	1.4	24	18.26	31.27	63.73	61.06
	1.6	24	7.88	26.32	56.61	56.06
	1.8	23	-1.38	24.44	52.87	52.85
	2	23	-10.06	27.56	53.94	52.99
	2.2	23	-17.94	32.82	57.74	54.89
	2.4	23	-24.99	37.54	63.20	58.05
	2.6	23	-31.30	41.89	69.36	61.89
T3	0	23	12.25	28.02	67.28	66.16
	0.2	23	6.22	26.30	61.97	61.65
	0.3	23	2.96	25.88	59.76	59.69
	0.4	23	-0.22	26.38	58.07	58.07
	0.5	23	-3.25	27.30	56.93	56.84
	0.6	23	-6.10	28.08	56.29	55.96
	0.7	23	-8.87	28.76	56.16	55.46
	0.8	23	-11.51	29.73	56.52	55.33
	0.9	23	-14.68	31.55	57.50	55.59
	1	23	-17.64	33.25	58.86	56.15
	1.1	23	-20.47	34.89	60.52	56.95
	1.5	23	-30.62	40.96	68.97	61.81
	2	23	-42.47	49.49	82.23	70.41
	2.6	23	-54.46	58.62	97.98	81.45

Table 3.3.2 Trace Techniques, April 14, 2012 (Continued)

	Z_{DR} +	#	FB(%)	FAD(%)	FRMSE(%)	FSD(%)
T4	0.4	27	72.63	75.13	145.58	126.17
	0.6	26	53.29	56.54	112.71	99.32
	0.8	26	38.19	45.60	91.16	82.78
	1	26	24.44	36.27	74.28	70.14
	1.2	25	12.73	31.50	62.35	61.04
	1.4	25	3.19	28.45	57.44	57.35
	1.6	24	-5.79	26.15	55.28	54.98
	1.8	23	-13.75	28.95	56.23	54.52
	2	23	-21.24	34.01	60.74	56.91
	2.2	23	-28.04	38.64	66.52	60.32
	2.4	23	-34.14	43.07	72.76	64.25
	2.6	23	-39.62	47.21	79.03	68.38
T5	0.4	37	148.52	148.74	283.99	242.06
	0.6	34	121.55	121.83	228.09	193.01
	0.8	32	100.26	100.63	188.50	159.63
	1	29	82.33	82.92	154.28	130.47
	1.2	29	67.03	67.81	133.36	115.29
	1.4	29	53.44	57.19	116.11	103.08
	1.6	27	40.81	47.56	97.36	88.40
	1.8	26	29.41	38.96	83.74	78.41
	2	25	18.38	30.46	72.53	70.16
	2.2	24	7.70	26.85	64.89	64.43
	2.4	24	-1.74	29.11	62.79	62.77
	2.6	24	-10.18	32.18	63.96	63.14
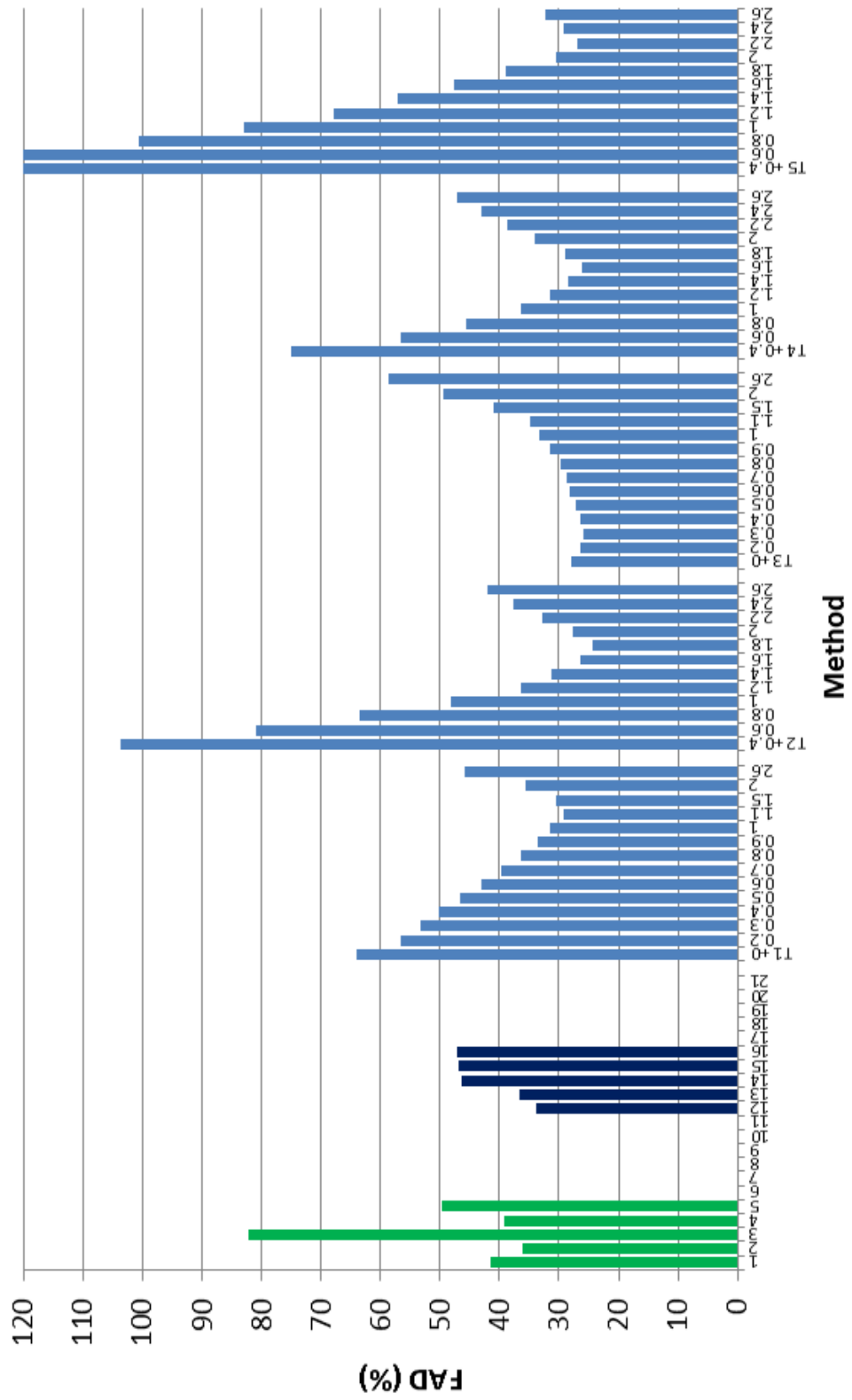
Figure 3.3.5. FAD Performance April 14, 2012.
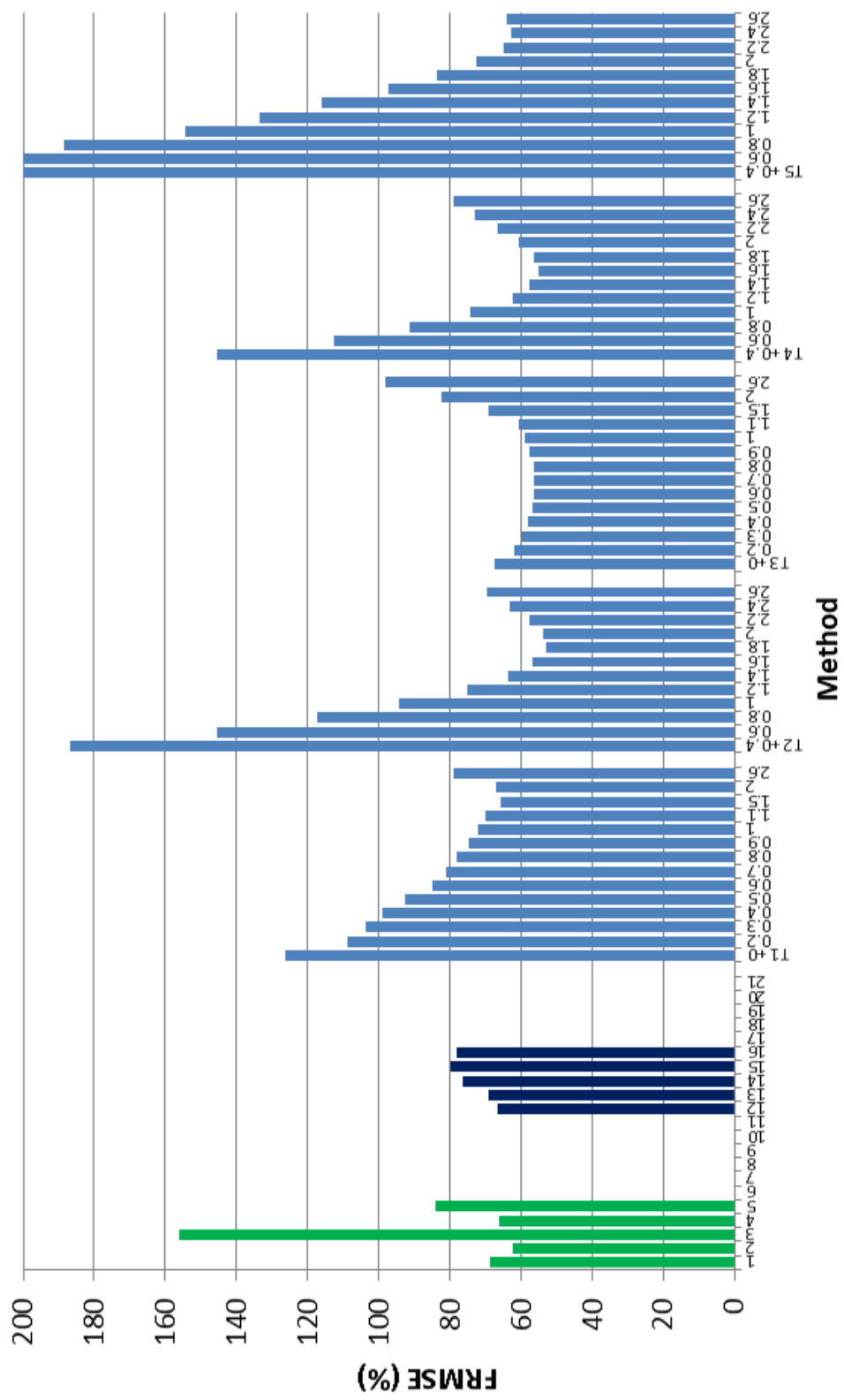
Figure 3.3.6. FRMSE Performance April 14, 2012.
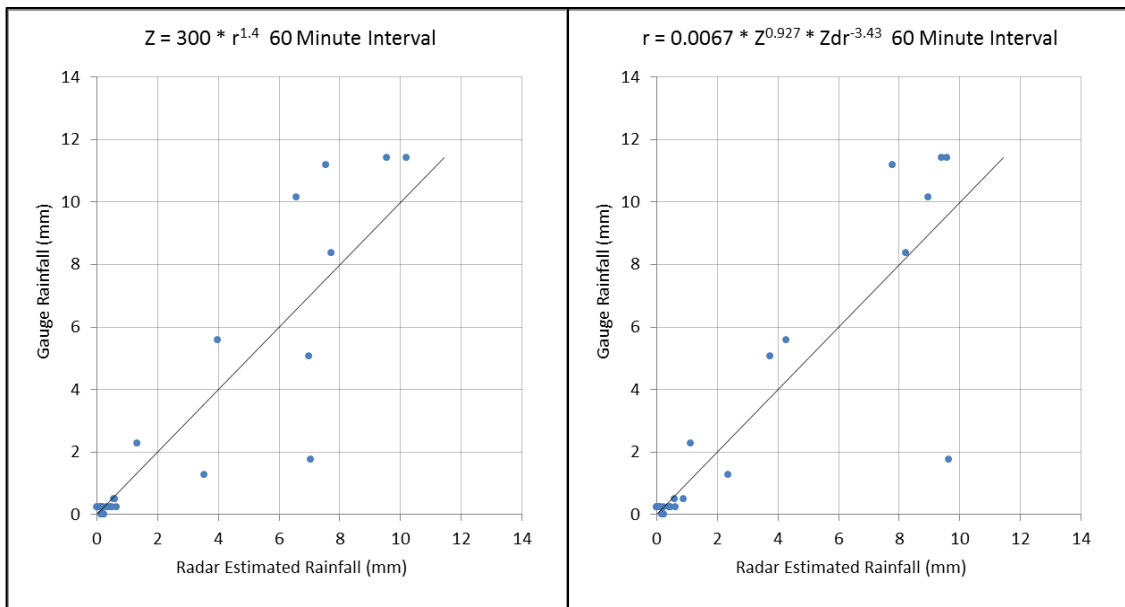
Figure 3.3.7. Radar Estimated Rainfall vs. Gauge Rainfall Scatterplots April 14, 2012.
The best performers of the five conventional formula groups are shown here.
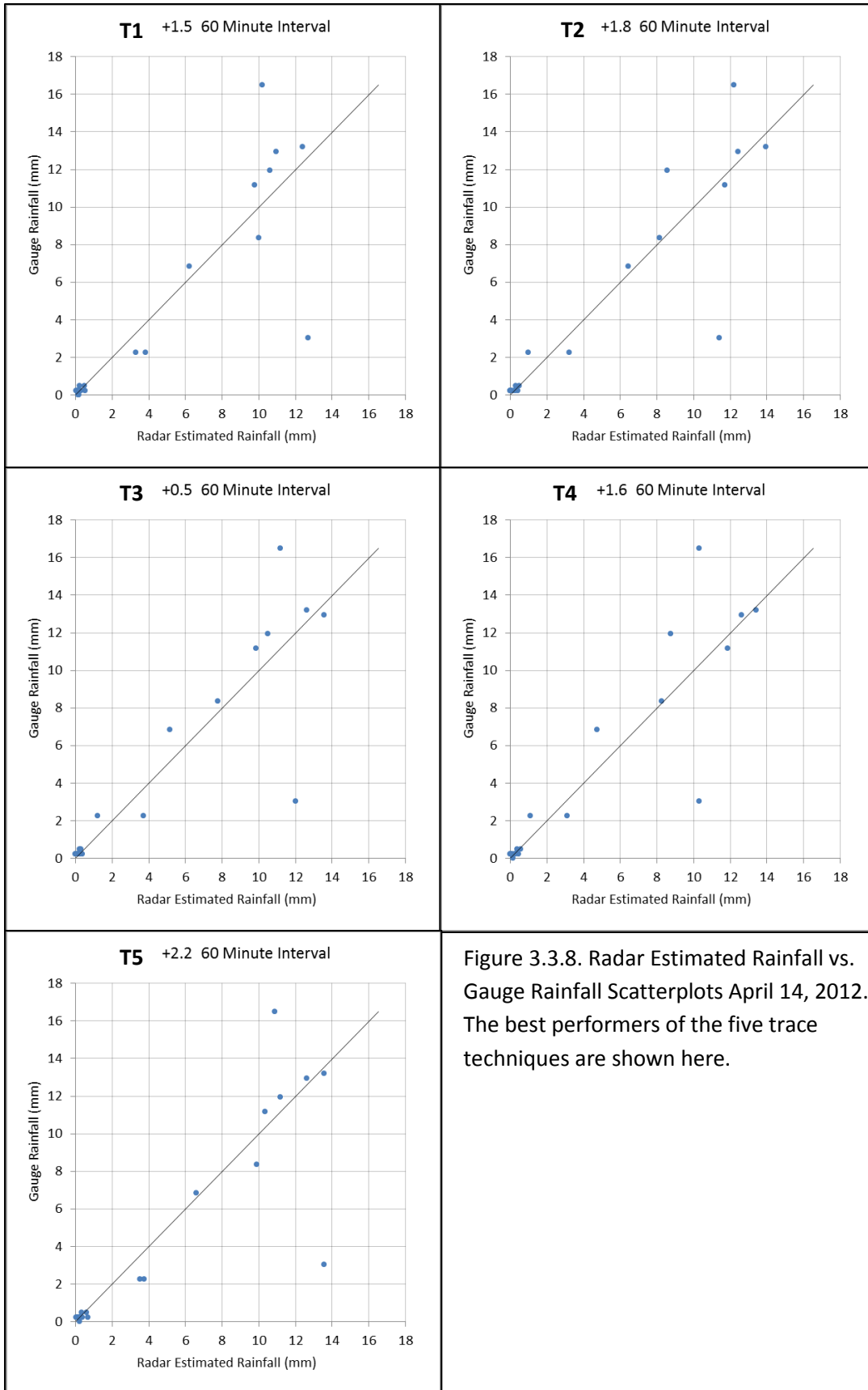
Figure 3.3.8. Radar Estimated Rainfall vs. Gauge Rainfall Scatterplots April 14, 2012. The best performers of the five trace techniques are shown here.

3.4 April 15, 2012

On the 15th of April, the system affecting the area finally began to move. Figure 3.4.1 is

an HPC surface analysis for 15 UTC of April 15, 2012. The precipitation on the 15th

occurred ahead of the cold front that would move through late in the evening of the

15th. Figure 3.4.2 shows humidity versus height in percentile format for 10 UTC through

20 UTC of April 15. The humidity profile was not drastically different from the 14th.

Figure 3.4.3 is a hodograph for the 15th of April. The hodograph shows that a very strong

southwesterly wind was present from 900 millibars and up.

3.4.1 Conventional Formulas

Due to extreme noise in the K_{DP} data, formulas involving K_{DP} were not evaluated for the

precipitation events of April 13, April 14, and April 15 of 2012.

Table 3.4.1 shows the performance of the conventional techniques for this event. (5)

was most effective of the formulas evaluated. Three outliers were present, the same

ones from April 13 (3, 12, and 13). Biases for the conventional techniques were mostly

positive for this date.

3.4.2 Tracing Techniques

Table 3.4.2 shows the performance of the various trace techniques and their

permutations for this event. Techniques T2, T4, and T5 were most effective at the $+Z_{DR}$

values of around 2, while T1 and T3 were most effective at $+Z_{DR}$ values near 1.

The overall effectiveness of the tracing techniques was similar to the conventional

formulas on the 15th.

3.4.3 Graphical Evaluation

Figure 3.4.4 is a histogram showing the FAD performance of each evaluated technique for this event. Figure 3.4.5 is the equivalent histogram showing FRMSE performance.

Figure 3.4.6 shows a combination of scatterplots of radar-derived rainfall versus rain gauge rainfall for the conventional formulas. The techniques illustrated were the top performers in each category. Figure 3.4.7 is identical to 3.4.6, except it depicts the best performers of the trace techniques.
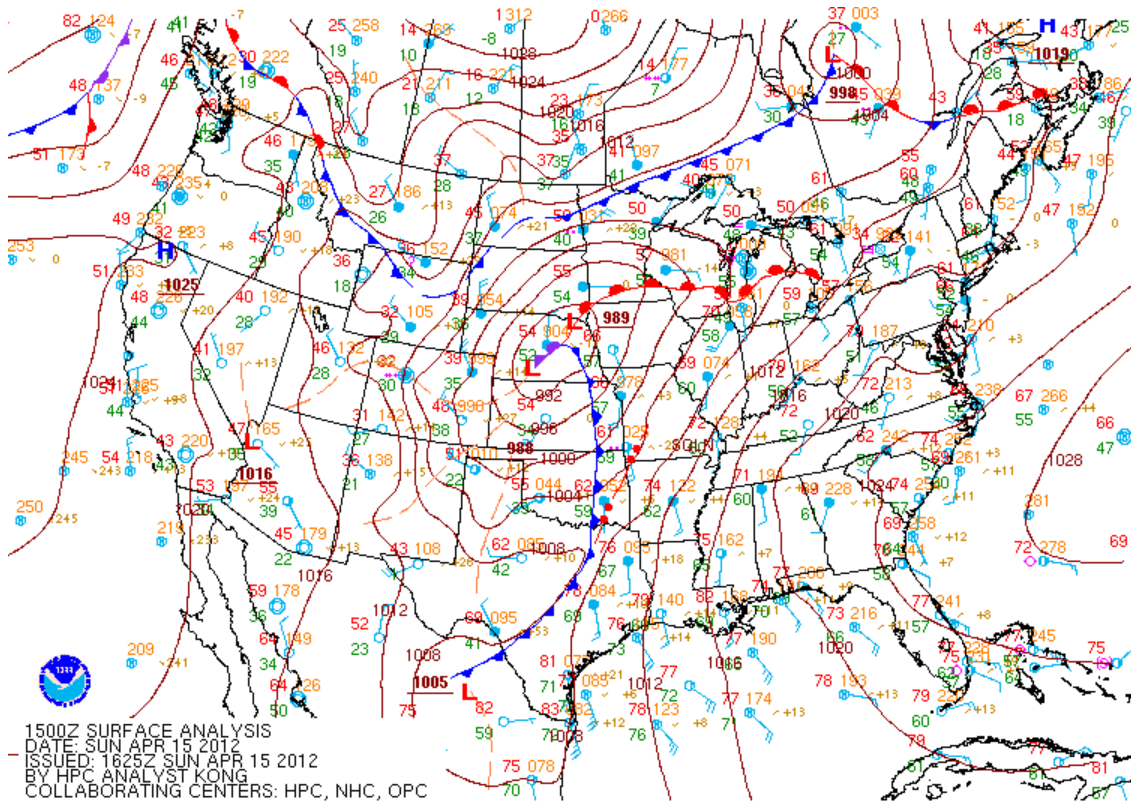
Figure 3.4.1. Surface Analysis 1500 UTC April 15, 2012.
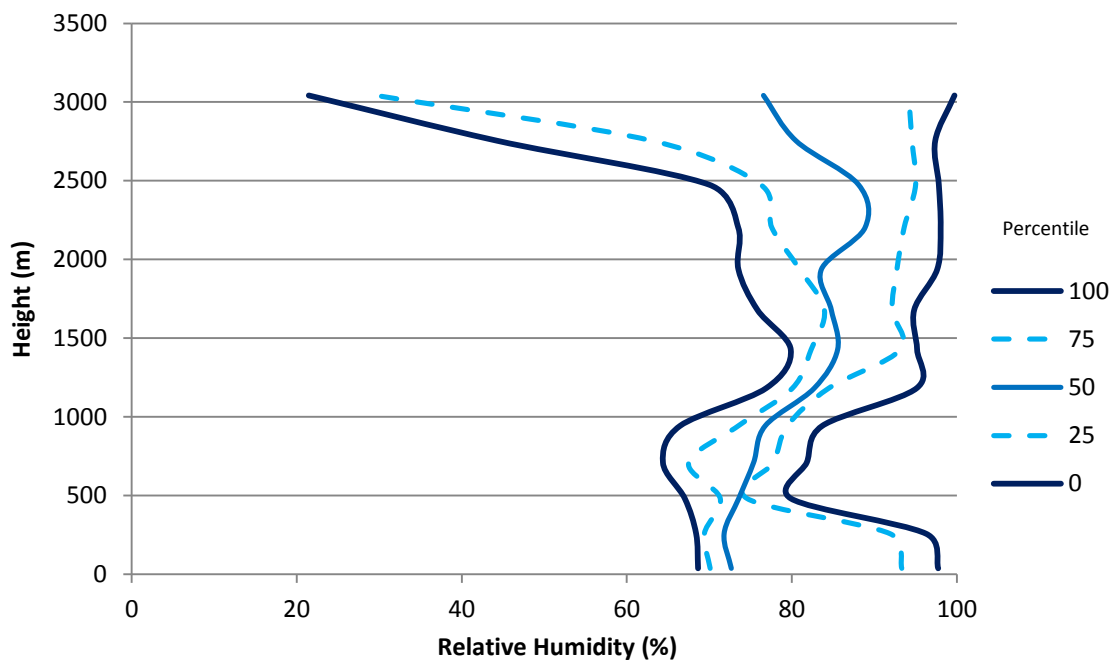
Figure 3.4.2. Relative Humidity Profile April 15, 2012.
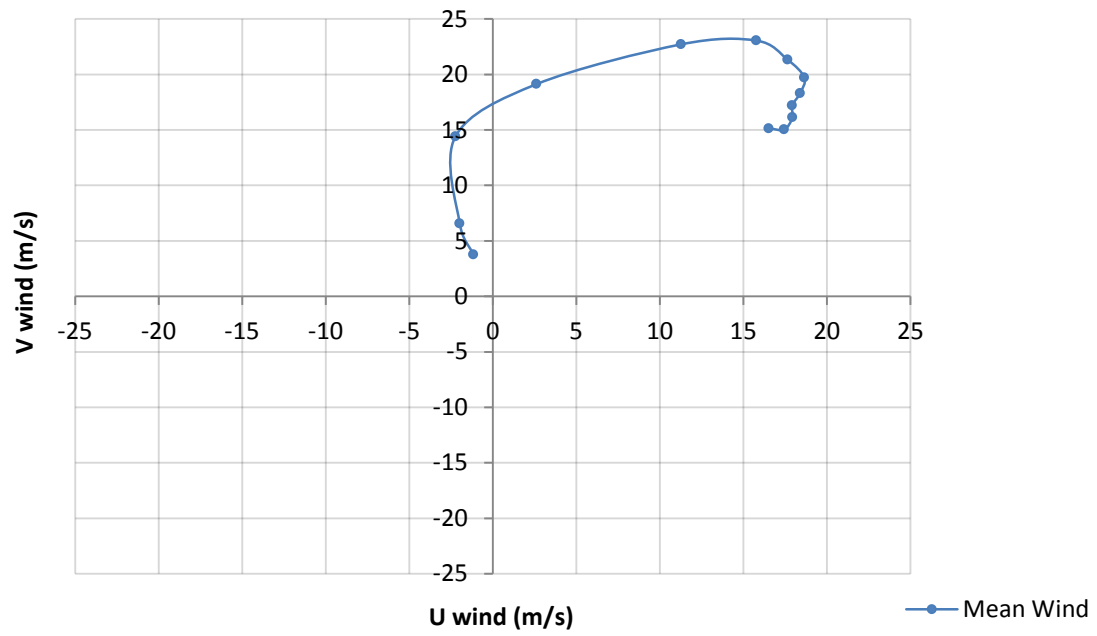
Figure 3.4.3. Hodograph April 15, 2012.

Table 3.4.1 Conventional Techniques, April 15, 2012

$Z = aR^b$	#	FB(%)	FAD(%)	FRMSE(%)	FSD(%)
1	27	27.31	40.66	50.70	42.72
2	25	23.05	37.82	46.98	40.94
3	25	96.74	105.06	132.01	89.83
4	25	16.12	31.96	40.91	37.60
5	24	-18.78	24.57	35.82	30.50
$R(Z, Z_{DR}) = aZ^b Z_{dr}{}^c$					
12	25	58.55	73.54	94.92	74.71
13	25	71.58	87.34	113.66	88.30
14	25	20.33	37.57	48.01	43.49
15	25	14.36	31.53	41.55	38.99
16	25	16.34	34.12	44.31	41.19

Table 3.4.2 Trace Techniques, April 15, 2012

	Z_{DR} +	#	FB(%)	FAD(%)	FRMSE(%)	FSD(%)
T1	0	24	41.06	52.72	68.34	54.63
	0.2	24	34.83	47.65	60.77	49.80
	0.3	24	31.10	44.50	56.65	47.35
	0.4	24	27.00	41.58	52.81	45.39
	0.5	24	22.69	38.73	49.31	43.78
	0.6	24	18.34	35.92	46.44	42.66
	0.7	24	13.77	33.54	44.26	42.07
	0.8	24	9.05	32.12	42.35	41.37
	0.9	24	4.45	31.46	41.03	40.79
	1	24	-0.03	31.16	40.45	40.45
	1.1	24	-4.26	31.57	40.76	40.54
	1.5	24	-19.74	34.07	45.61	41.11
	2	24	-35.79	39.06	55.97	43.03
	2.6	24	-49.99	49.99	69.75	48.63
T2	0.4	27	206.38	210.00	313.31	235.74
	0.6	26	158.24	162.52	240.54	181.16
	0.8	26	118.02	125.62	183.49	140.51
	1	24	85.05	95.47	133.13	102.42
	1.2	24	60.59	74.01	101.54	81.48
	1.4	24	41.42	57.49	78.12	66.23
	1.6	24	25.89	44.65	60.95	55.18
	1.8	24	12.71	34.54	48.80	47.11
	2	24	1.28	29.07	41.45	41.43
	2.2	24	-8.50	25.57	39.10	38.17
	2.4	24	-16.99	25.77	40.60	36.87
	2.6	24	-24.41	28.05	44.35	37.03
T3	0	24	58.34	71.54	90.62	69.34
	0.2	24	49.51	63.66	81.00	64.10
	0.3	24	44.75	59.30	75.76	61.13
	0.4	24	39.78	54.76	70.43	58.13
	0.5	24	34.60	50.04	65.12	55.17
	0.6	24	29.29	45.43	59.94	52.29
	0.7	24	23.96	41.23	55.11	49.63
	0.8	24	18.69	37.58	50.77	47.21
	0.9	24	13.50	34.68	47.12	45.14
	1	24	8.45	32.65	44.29	43.48
	1.1	24	3.58	30.77	42.37	42.22
	1.5	24	-13.44	27.58	42.92	40.77
	2	24	-30.35	35.36	53.12	43.60
	2.6	24	-45.69	47.25	67.04	49.05

Table 3.4.2 Trace Techniques, April 15, 2012 (Continued)

	Z_{DR} +	#	FB(%)	FAD(%)	FRMSE(%)	FSD(%)
T4	0.4	24	202.72	206.41	265.93	172.12
	0.6	24	155.47	161.45	207.18	136.93
	0.8	24	115.78	124.93	157.46	106.72
	1	24	83.82	95.44	118.39	83.62
	1.2	24	59.60	73.20	90.06	67.52
	1.4	24	40.61	55.82	69.53	56.44
	1.6	24	25.21	42.64	55.31	49.23
	1.8	24	12.14	34.58	46.29	44.67
	2	24	0.78	30.05	42.06	42.05
	2.2	24	-8.95	27.82	42.13	41.17
	2.4	24	-17.38	28.59	45.00	41.50
	2.6	24	-24.76	31.76	49.29	42.62
T5	0.4	26	180.34	183.01	232.50	146.75
	0.6	26	139.84	143.02	184.00	119.60
	0.8	26	103.41	107.37	142.10	97.46
	1	24	73.46	78.89	104.34	74.10
	1.2	24	50.51	58.38	80.66	62.89
	1.4	24	32.08	44.14	63.34	54.62
	1.6	24	16.53	34.48	49.34	46.49
	1.8	24	3.85	31.07	41.83	41.65
	2	24	-6.83	30.24	39.87	39.28
	2.2	24	-15.94	32.05	41.93	38.79
	2.4	24	-23.82	34.16	46.17	39.54
	2.6	24	-30.71	36.44	51.28	41.06
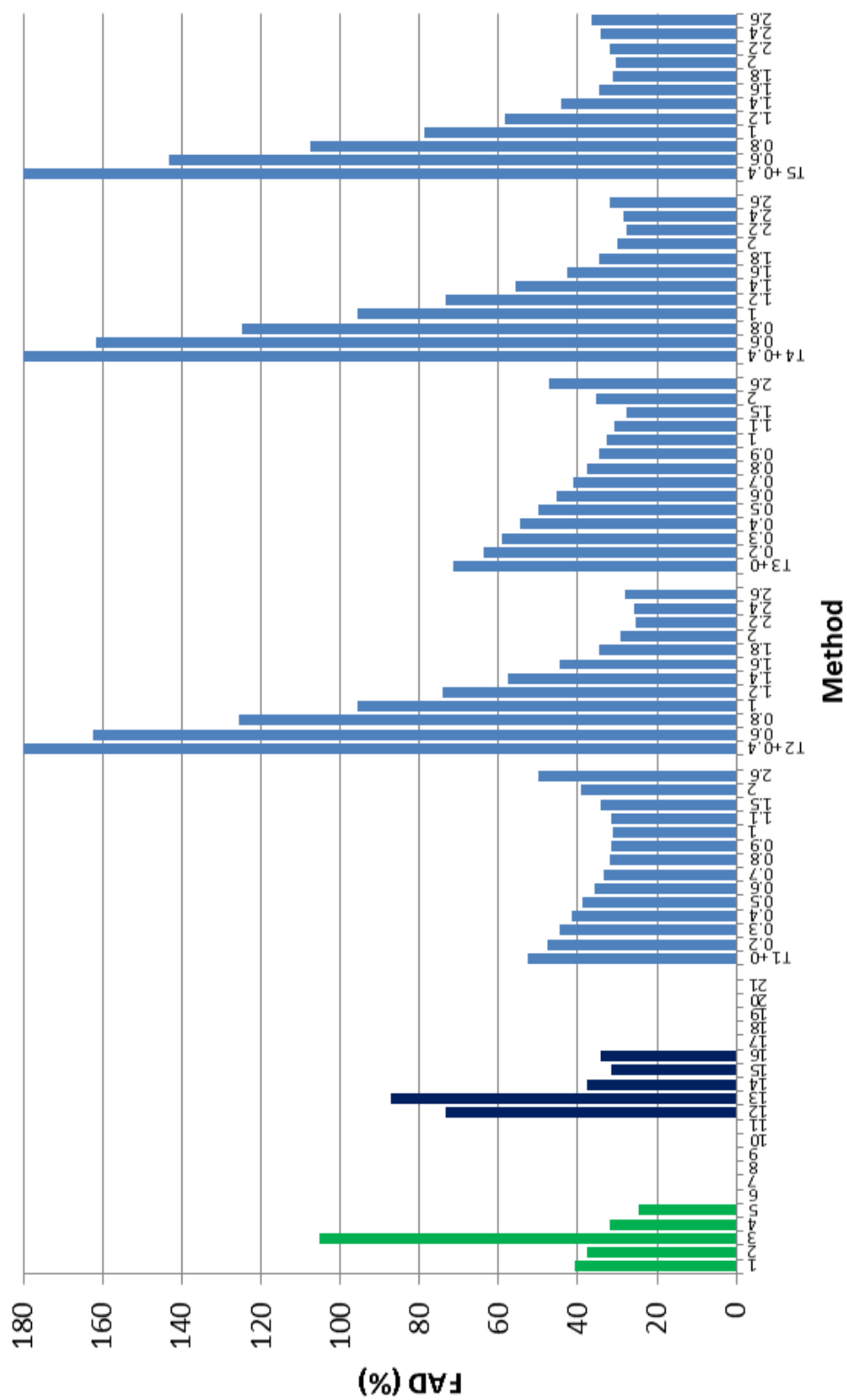
Figure 3.4.4. FAD Performance April 15, 2012.
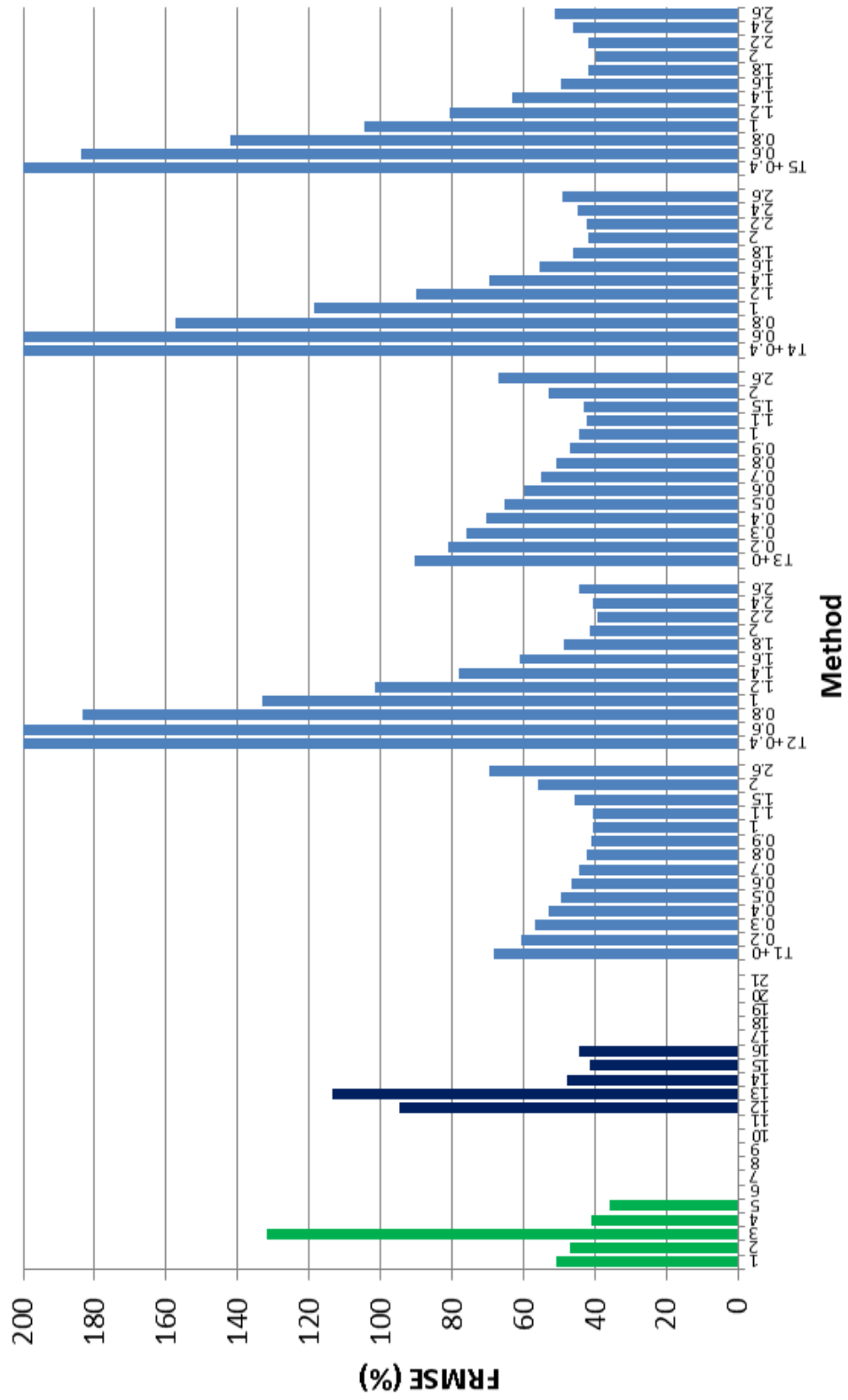
Figure 3.4.5. FRMSE Performance April 15, 2012.

Figure 3.4.6. Radar Estimated Rainfall vs. Gauge Rainfall Scatterplots April 15, 2012.
The best performers of the five conventional formula groups are shown here.
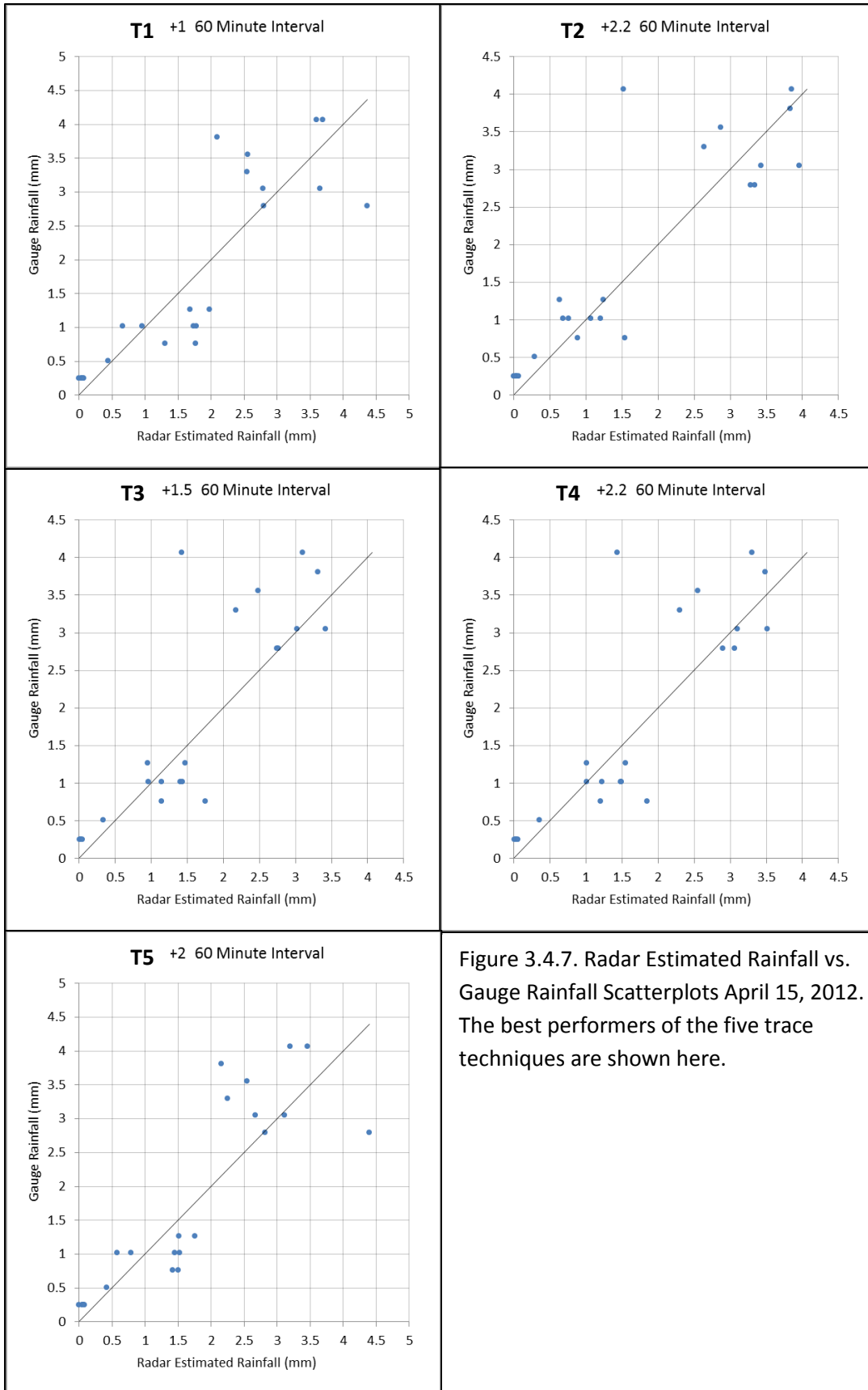
Figure 3.4.7. Radar Estimated Rainfall vs. Gauge Rainfall Scatterplots April 15, 2012. The best performers of the five trace techniques are shown here.

3.5 June 16, 2012

The event on the 16th of June occurred when a squall line passed through Central

Missouri ahead of a cold front. Figure 3.5.1 is an HPC surface analysis for 00 UTC of June

17, 2012. The precipitation on this day came from several strong thunderstorms moving

through the area. Figure 3.5.2 shows humidity versus height in percentile format for 18

UTC of June 16 through 03 UTC of June 17. The atmosphere was relatively dry for this

event, especially in the lower levels. Figure 3.5.3 is a hodograph for the 16th of June. The

hodograph shows a weak southwesterly wind at the surface turning more in a west

southwesterly direction higher up. Figure 3.5.4 is a four panel radar image from KLSX for

0021 UTC of June 17.

3.5.1 Conventional Formulas

Table 3.5.1 shows the performance of the conventional formulas for this event. (19) was

most effective of the conventional formulas evaluated. The simple Z-R formulas

performed relatively poorly. The K_{DP}-reliant formulas had their best showing in this

event, performing better than the Z-R formulas at several points. One outlier, (3), was

present. Biases for the conventional techniques were mostly positive for this date.

3.5.2 Tracing Techniques

Table 3.5.2 shows the performance of the various trace techniques and their

permutations for this event. The no-evaporation techniques were most effective at $+Z_{DR}$

values of around 2, while T1 and T3 were most effective at $+Z_{DR}$ values from 1 to 1.5.

The optimal T3 and T5 techniques performed better than any conventional formulas for this event. The other trace techniques performed similarly to the conventional formulas. The evaporation techniques exhibited negative biases at all Z_{DR} adjustments.

3.5.3 Graphical Evaluation

Figure 3.5.5 is a histogram showing the FAD performance of each evaluated technique for this event. Figure 3.5.6 is the equivalent histogram showing FRMSE performance.

Figure 3.5.7 shows a combination of scatterplots of radar-derived rainfall versus rain gauge rainfall for the conventional formulas. The techniques illustrated were the top performers in each category. Figure 3.5.8 is identical to 3.5.7, except it depicts the best performers of the trace techniques.
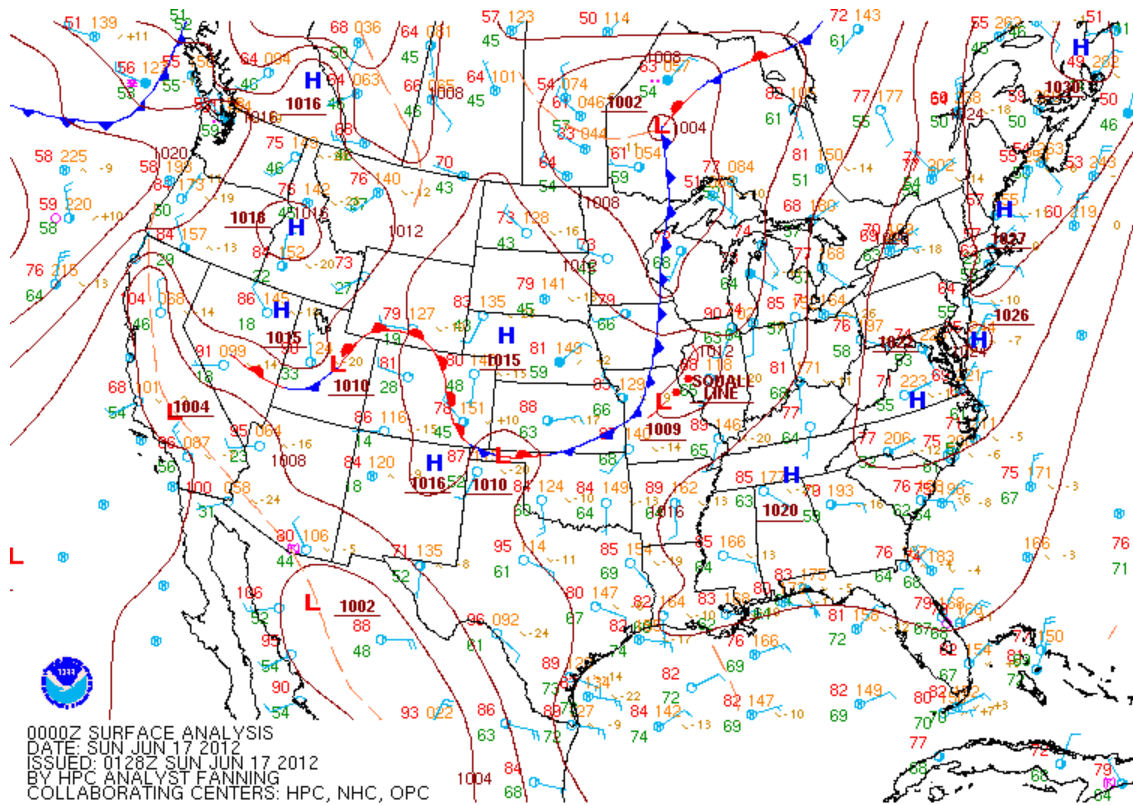
Figure 3.5.1. Surface Analysis 0000 UTC June 17, 2012.
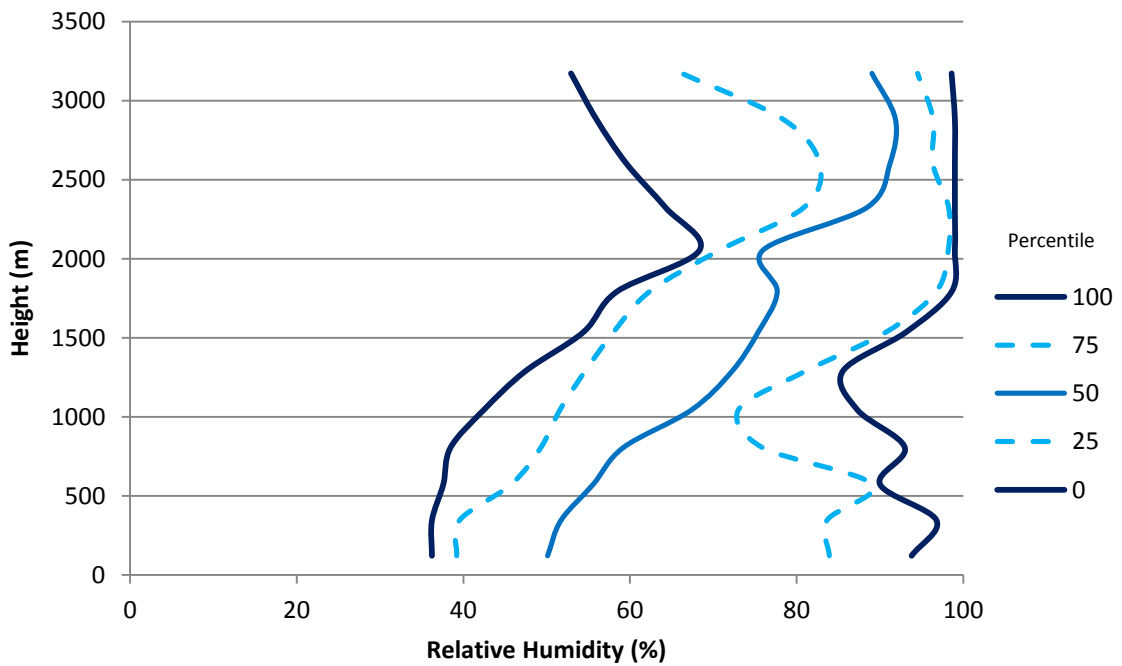
Figure 3.5.2. Relative Humidity Profile June 16, 2012.

Figure 3.5.3. Hodograph June 16, 2012.

Figure 3.5.4. Four Panel Radar Image for 0021 UTC June 17, 2012. The top left is reflectivity (Z), top right is differential reflectivity (Z_{DR}), bottom left is specific phase differential (K_{DP}), and bottom right is correlation coefficient. The scale on the left corresponds to the bottom left image (K_{DP}). The elevation angle used here was 0.5°.

Table 3.5.1 Conventional Techniques, June 16, 2012

$Z = aR^b$	#	FB(%)	FAD(%)	FRMSE(%)	FSD(%)
1	30	-0.94	49.59	72.92	72.92
2	30	15.59	41.62	69.31	67.53
3	30	139.15	139.81	219.40	169.63
4	30	4.65	45.62	69.84	69.69
5	30	-24.30	56.86	88.30	84.89
$R(K_{DP}) = a|K_{DP}|^b sign(K_{DP})$					
6	33	26.31	45.12	66.54	61.11
7	33	36.57	54.13	77.57	68.41
8	33	33.07	52.63	74.20	66.43
9	33	10.27	37.43	57.47	56.55
10	33	26.34	45.64	66.78	61.37
11	33	19.38	41.69	61.62	58.49
$R(Z, Z_{DR}) = aZ^b Z_{dr}{}^c$					
12	30	-39.27	65.55	109.07	101.75
13	30	-49.94	71.09	122.93	112.33
14	30	-39.79	67.28	109.83	102.37
15	30	-34.25	65.37	104.09	98.30
16	30	-39.84	67.41	109.90	102.42
$R(K_{DP}, Z_{DR}) = a|K_{DP}|^b Z_{dr}{}^c sign(K_{DP})$					
17	32	25.82	53.39	70.90	66.03
18	33	26.40	63.87	82.58	78.25
19	33	10.74	39.97	58.89	57.90
20	32	24.81	48.47	66.82	62.04
Synthetic					
21	32	24.00	38.73	62.58	57.80

Table 3.5.2 Trace Techniques, June 16, 2012

	Z_{DR} +	#	FB(%)	FAD(%)	FRMSE(%)	FSD(%)
T1	0	23	-22.76	35.60	57.84	53.17
	0.2	23	-23.92	35.93	58.20	53.05
	0.3	24	-24.32	36.14	59.59	54.41
	0.4	23	-24.79	36.16	58.44	52.92
	0.5	23	-25.06	36.18	58.43	52.78
	0.6	23	-25.20	36.09	58.27	52.54
	0.7	22	-25.26	35.82	56.66	50.72
	0.8	22	-25.07	35.60	56.13	50.22
	0.9	22	-24.71	35.27	55.40	49.59
	1	23	-24.25	34.80	55.69	50.13
	1.1	23	-24.14	34.25	54.85	49.25
	1.5	23	-25.29	33.04	53.78	47.47
	2	22	-35.63	41.23	66.01	55.57
	2.6	21	-48.50	52.07	82.53	66.78
T2	0.4	30	63.69	66.03	111.31	91.29
	0.6	29	59.37	62.09	104.29	85.75
	0.8	29	58.21	60.97	101.88	83.62
	1	29	55.39	58.29	95.03	77.22
	1.2	29	49.06	52.12	85.24	69.70
	1.4	29	41.83	45.02	75.94	63.38
	1.6	29	33.39	38.88	67.32	58.46
	1.8	29	23.39	35.44	59.31	54.50
	2	29	13.08	34.85	55.28	53.71
	2.2	29	3.61	36.68	55.90	55.78
	2.4	29	-4.89	39.29	59.77	59.57
	2.6	28	-12.63	42.65	64.38	63.13
T3	0	26	-10.76	34.53	52.66	51.55
	0.2	27	-10.43	34.94	53.21	52.18
	0.3	27	-10.17	34.76	52.45	51.45
	0.4	26	-9.80	34.30	50.49	49.52
	0.5	26	-9.14	33.69	49.27	48.41
	0.6	26	-8.25	32.86	47.84	47.12
	0.7	27	-7.08	31.85	47.03	46.50
	0.8	27	-5.81	30.49	45.04	44.67
	0.9	26	-5.01	29.14	42.39	42.09
	1	26	-4.94	28.29	40.97	40.67
	1.1	26	-5.78	28.38	40.77	40.36
	1.5	26	-11.68	30.98	45.41	43.89
	2	26	-24.62	39.02	61.47	56.32
	2.6	25	-39.60	50.47	81.24	70.93

Table 3.5.2 Trace Techniques, June 16, 2012 (Continued)

	Z_{DR} +	#	FB(%)	FAD(%)	FRMSE(%)	FSD(%)
T4	0.4	30	64.06	64.25	110.03	89.46
	0.6	30	59.87	60.67	105.56	86.94
	0.8	30	58.77	60.11	104.09	85.91
	1	29	55.92	57.69	95.98	78.00
	1.2	29	49.61	51.71	86.09	70.35
	1.4	28	42.32	44.69	75.21	62.18
	1.6	28	33.88	37.55	66.21	56.88
	1.8	28	23.87	33.17	57.30	52.09
	2	28	13.54	31.93	52.25	50.46
	2.2	28	4.05	34.04	52.12	51.96
	2.4	28	-4.47	35.95	55.62	55.44
	2.6	28	-12.17	39.56	61.25	60.03
T5	0.4	31	35.36	40.77	72.74	63.56
	0.6	30	28.63	36.71	64.54	57.84
	0.8	30	24.58	34.05	60.24	54.99
	1	29	22.52	32.22	56.58	51.90
	1.2	29	20.37	30.32	52.53	48.42
	1.4	28	17.70	28.10	47.38	43.95
	1.6	28	12.58	24.68	43.37	41.50
	1.8	28	4.65	22.05	41.61	41.34
	2	28	-4.07	26.39	44.45	44.26
	2.2	28	-12.15	31.00	50.95	49.48
	2.4	28	-19.38	35.12	58.80	55.52
	2.6	28	-25.89	39.36	66.94	61.73
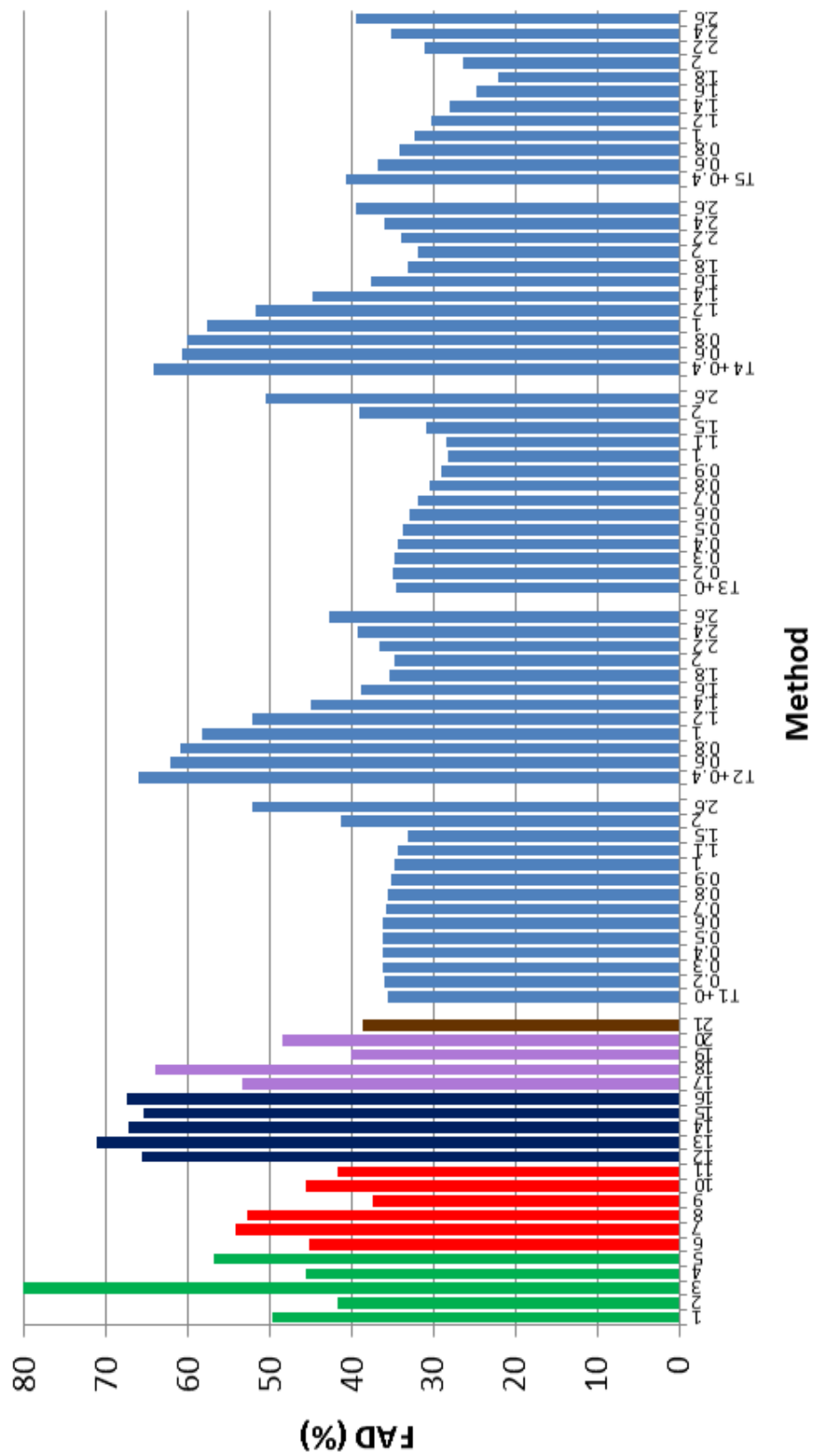
Figure 3.5.5. FAD Performance June 16, 2012.

Figure 3.5.6. FRMSE Performance June 16, 2012.

Z = 300 * r^{1.4} 60 Minute Interval

Gauge Rainfall (mm)

Radar Estimated Rainfall (mm)

r = 0.0159 * Z^{0.737} * Zdr^{-1.03} 60 Minute Interval

Gauge Rainfall (mm)

Radar Estimated Rainfall (mm)

synthetic + 60 Minute Interval

Gauge Rainfall (mm)

Radar Estimated Rainfall (mm)

r = 44 * |kdp|^{0.822} * sign(kdp) 60 Minute Interval

Gauge Rainfall (mm)

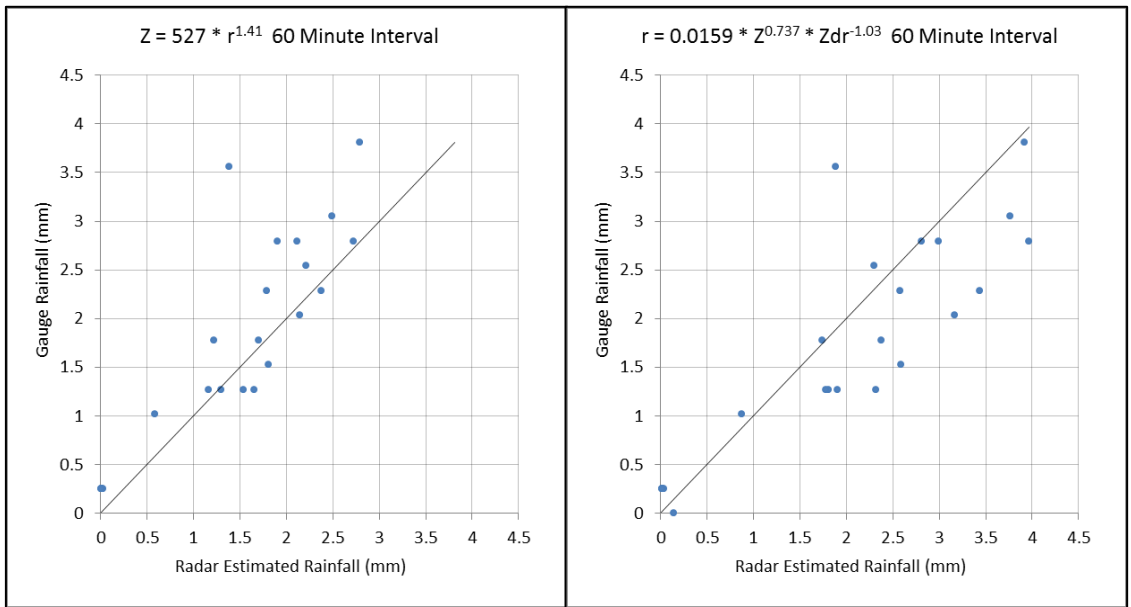Radar Estimated Rainfall (mm)

Figure 3.5.7. Radar Estimated Rainfall vs. Gauge Rainfall Scatterplots June 16, 2012. The best performers of the five conventional formula groups are shown here.

r = 63.6 * |Kdp|^{0.851} * Zdr^{-0.72}sign(kdp) 60 Minute Interval

Gauge Rainfall (mm)

Radar Estimated Rainfall (mm)

104

Figure 3.5.8. Radar Estimated Rainfall vs. Gauge Rainfall Scatterplots June 16, 2012. The best performers of the five trace techniques are shown here.

3.6 August 31, 2012

On the 31st of August the remnants of Hurricane Isaac passed through Central Missouri,

helping to ease the severe drought conditions affecting the region. Figure 3.6.1 is an

HPC surface analysis for 15 UTC of August 31, 2012. The precipitation on this day came

in the form of continuous, heavy rainfall. Figure 3.6.2 shows humidity versus height in

percentile format for 11 UTC through 22 UTC of August 31. Initially the atmosphere was

relatively dry, but quickly became fully saturated. Figure 3.6.3 is a hodograph for the 31st

of August. The hodograph shows an easterly wind at the surface turning more in a

southeasterly direction higher up. These wind directions are expected considering

Central Missouri's position on the northern side of the cyclone. Figure 3.6.4 is a four

panel radar image from KLSX for 1537 UTC of August 31.

3.6.1 Conventional Formulas

Table 3.6.1 shows the performance of the conventional formulas for this event. The

synthetic formula, (21), was the most effective of the conventional formulas evaluated.

The tropical Z-R relationship, (3), had its best showing, and the least negative bias out of

all the conventional formulas. The K_{DP}-reliant formulas performed slightly worse overall,

except for (21). Every conventional formula tested showed a significant negative bias for

this event.

3.6.2 Tracing Techniques

Table 3.6.2 shows the performance of the various trace techniques and their permutations for this event. All five tracing techniques were most effective at $+Z_{DR}$ values of around 0.8 on this date. This optimal $+Z_{DR}$ value was anomalously low for T2, T4, and T5.

The overall effectiveness of the optimal tracing techniques was superior to the conventional techniques for this event.

3.6.3 Graphical Evaluation

Figure 3.6.5 is a histogram showing the FAD performance of each evaluated technique for this event. Figure 3.6.6 is the equivalent histogram showing FRMSE performance.

Figure 3.6.7 shows a combination of scatterplots of radar-derived rainfall versus rain gauge rainfall for the conventional formulas. The techniques illustrated were the top performers in each category. Figure 3.6.8 is identical to 3.6.7, except it depicts the best performers of the trace techniques.
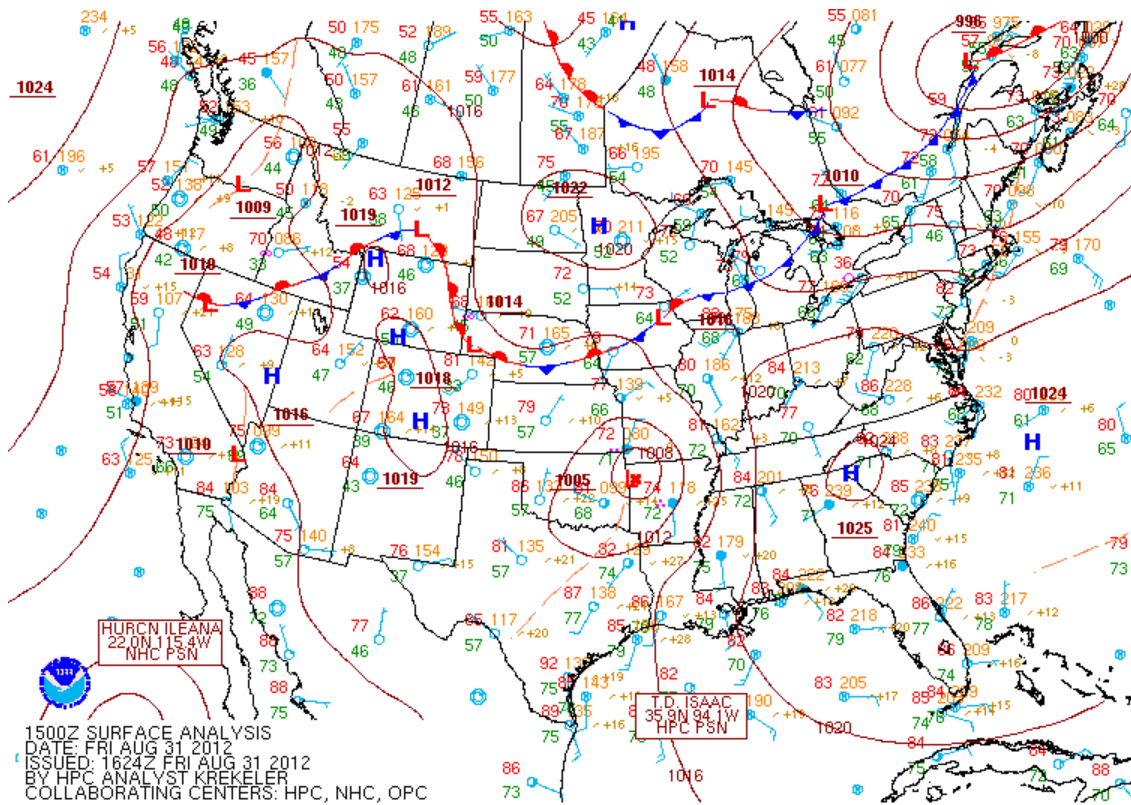
Figure 3.6.1. Surface Analysis 1500 UTC August 31, 2012.
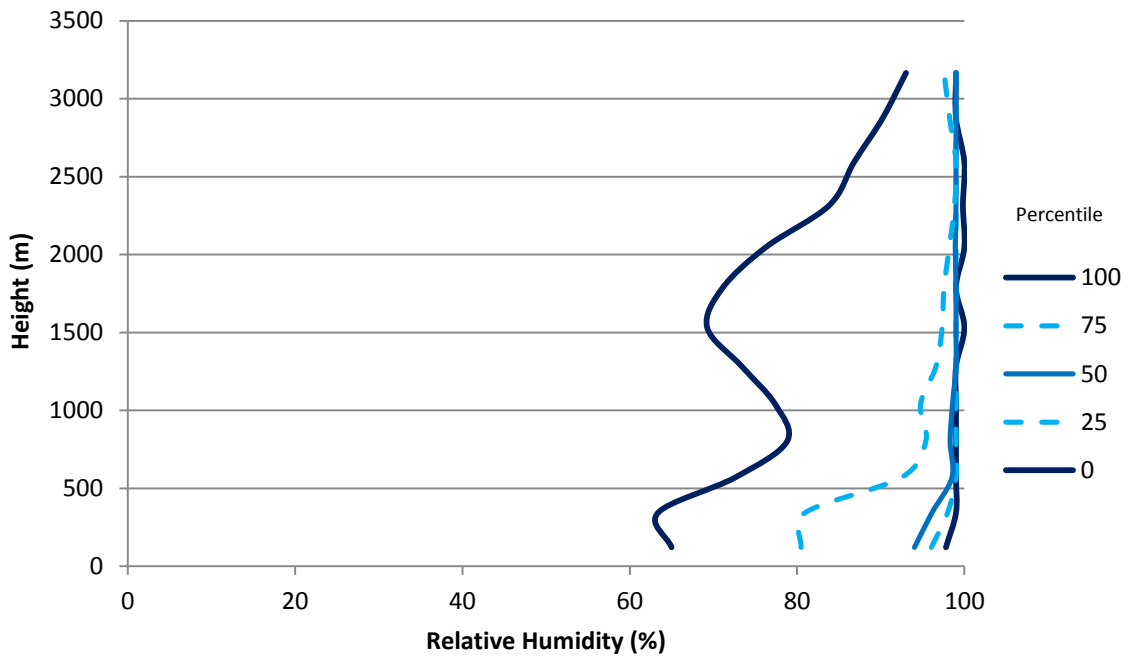
Figure 3.6.2. Relative Humidity Profile August 31, 2012.
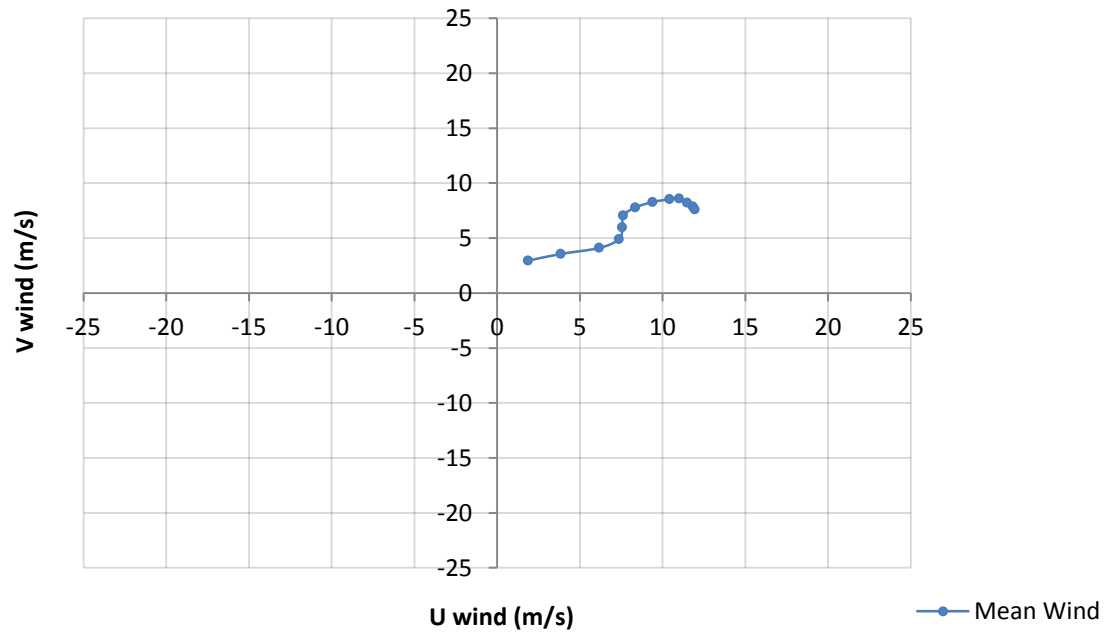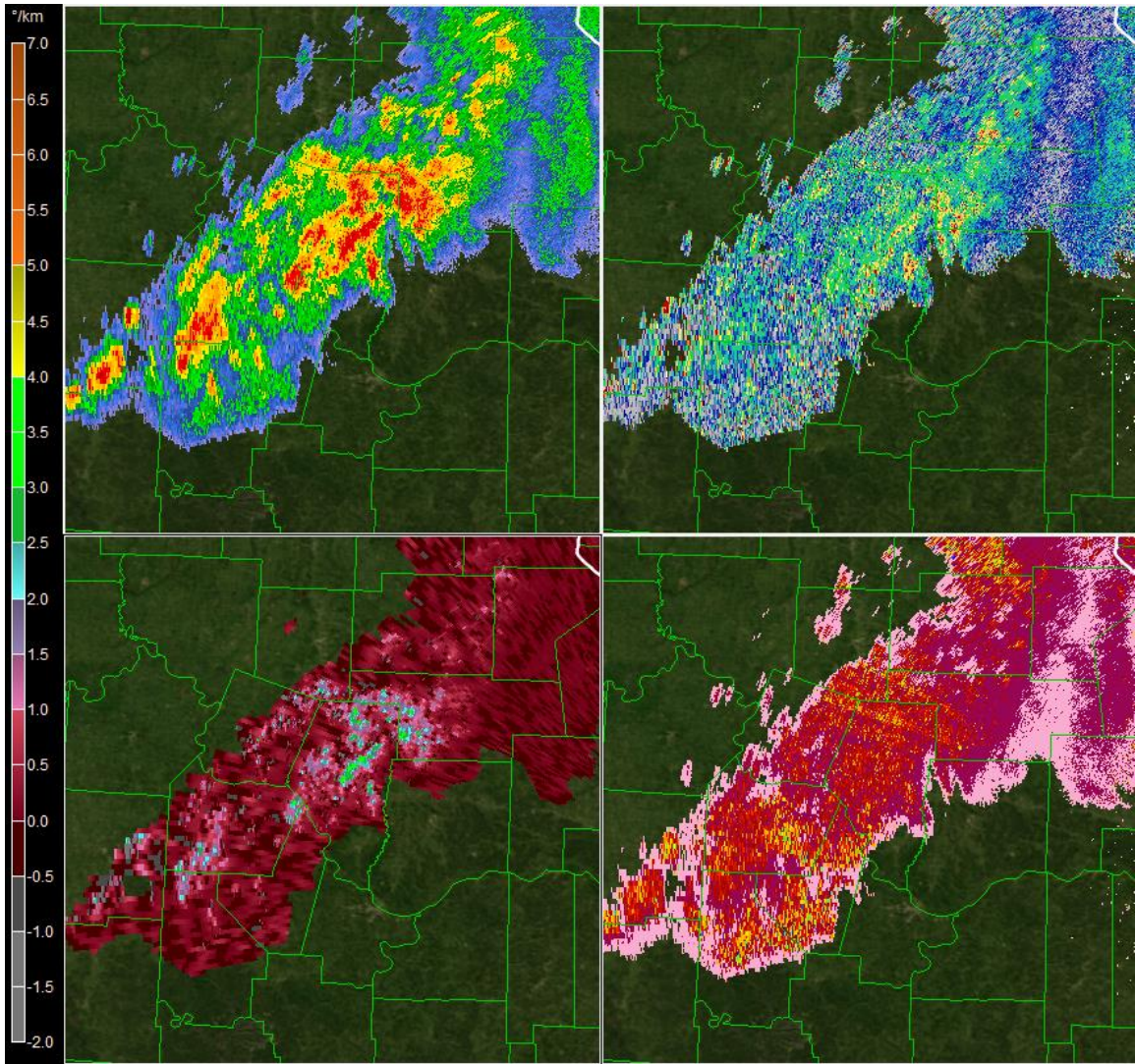
Figure 3.6.3. Hodograph August 31, 2012.

Figure 3.6.4. Four Panel Radar Image for 1537 UTC August 31, 2012. The top left is reflectivity (Z), top right is differential reflectivity (Z_{DR}), bottom left is specific phase differential (K_{DP}), and bottom right is correlation coefficient. The scale on the left corresponds to the top left image (Z). The elevation angle used here was 0.5°.

Table 3.6.1 Conventional Techniques, August 31, 2012

$Z = aR^b$	#	FB(%)	FAD(%)	FRMSE(%)	FSD(%)
1	74	-35.44	48.53	67.25	57.15
2	74	-40.04	50.08	69.41	56.70
3	74	-10.47	42.85	52.89	51.84
4	74	-42.82	51.63	72.03	57.92
5	74	-60.21	63.08	88.25	64.53
$R(K_{DP}) = a|K_{DP}|^b sign(K_{DP})$					
6	72	-46.45	64.12	82.94	68.71
7	72	-38.28	63.21	81.17	71.57
8	72	-31.01	63.87	80.37	74.14
9	72	-51.31	64.96	84.38	66.99
10	72	-43.40	63.48	81.82	69.36
11	72	-44.87	63.44	81.92	68.54
$R(Z, Z_{DR}) = aZ^b Z_{dr}{}^c$					
12	74	-25.40	38.94	52.75	46.23
13	74	-20.42	35.68	48.61	44.11
14	74	-39.96	48.82	67.44	54.33
15	74	-42.79	50.92	70.76	56.36
16	74	-41.87	50.06	69.35	55.28
$R(K_{DP}, Z_{DR}) = a|K_{DP}|^b Z_{dr}{}^c sign(K_{DP})$					
17	73	-32.97	72.71	90.24	84.00
18	73	-19.36	87.01	107.57	105.81
19	72	-47.31	65.87	84.72	70.28
20	73	-38.25	66.36	84.80	75.69
Synthetic					
21	73	-17.89	36.42	46.99	43.45

Table 3.6.2 Trace Techniques, August 31, 2012

	Z_{DR} +	#	FB(%)	FAD(%)	FRMSE(%)	FSD(%)
T1	0	73	88.35	105.03	146.74	117.16
	0.2	73	54.11	73.64	97.60	81.22
	0.3	73	39.63	61.74	79.13	68.49
	0.4	73	26.99	51.63	64.59	58.68
	0.5	73	16.06	44.74	53.93	51.48
	0.6	73	6.49	39.87	46.98	46.53
	0.7	73	-1.95	36.80	43.36	43.32
	0.8	73	-9.41	34.38	42.55	41.49
	0.9	73	-16.05	33.06	43.77	40.73
	1	73	-21.94	33.75	46.25	40.71
	1.1	73	-27.20	35.98	49.39	41.23
	1.5	73	-43.46	46.54	63.17	45.84
	2	73	-56.99	58.89	77.51	52.53
	2.6	73	-67.78	68.92	89.98	59.18
T2	0.4	73	33.33	53.68	67.04	58.17
	0.6	73	10.06	39.86	47.45	46.37
	0.8	73	-7.54	35.06	43.01	42.34
	1	73	-20.91	36.82	47.21	42.32
	1.2	73	-31.34	41.23	54.17	44.19
	1.4	73	-39.69	46.25	61.35	46.78
	1.6	73	-46.53	51.10	67.95	49.52
	1.8	73	-52.23	55.57	73.83	52.19
	2	73	-57.05	59.69	79.03	54.68
	2.2	73	-61.20	63.44	83.61	56.97
	2.4	73	-64.79	66.69	87.67	59.06
	2.6	73	-67.93	69.54	91.27	60.96
T3	0	73	83.15	94.69	129.61	99.42
	0.2	73	51.55	66.01	86.18	69.07
	0.3	73	37.33	53.55	68.25	57.13
	0.4	73	24.57	43.14	53.94	48.02
	0.5	73	13.39	35.09	43.86	41.76
	0.6	73	3.64	31.12	38.19	38.02
	0.7	73	-4.93	29.85	36.61	36.27
	0.8	73	-12.41	30.41	37.98	35.90
	0.9	73	-18.96	32.09	41.08	36.45
	1	73	-24.74	34.44	44.99	37.57
	1.1	73	-29.86	36.86	49.15	39.04
	1.5	73	-45.62	48.15	64.68	45.84
	2	73	-58.66	59.98	79.31	53.37
	2.6	73	-69.03	69.75	91.58	60.19

Table 3.6.2 Trace Techniques, August 31, 2012 (Continued)

|	Z_{DR} +	#	FB(%)	FAD(%)	FRMSE(%)	FSD(%)
T4	0.4	73	33.32	50.28	63.35	53.88
	0.6	73	10.06	34.49	42.86	41.66
	0.8	73	-7.54	31.83	38.63	37.89
	1	73	-20.91	34.48	43.81	38.50
	1.2	73	-31.34	38.89	51.61	41.01
	1.4	73	-39.69	44.05	59.37	44.15
	1.6	73	-46.53	49.33	66.37	47.33
	1.8	73	-52.23	54.29	72.54	50.34
	2	73	-57.06	58.64	77.94	53.10
	2.2	73	-61.20	62.50	82.69	55.60
	2.4	73	-64.79	65.85	86.87	57.87
	2.6	73	-67.94	68.80	90.58	59.91
T5	0.4	73	35.76	58.62	73.68	64.42
	0.6	73	12.97	44.03	51.97	50.32
	0.8	73	-4.44	37.04	44.07	43.84
	1	73	-18.02	34.44	45.73	42.03
	1.2	73	-28.72	38.05	51.51	42.75
	1.4	73	-37.34	42.92	58.27	44.74
	1.6	73	-44.41	47.93	64.82	47.22
	1.8	73	-50.33	52.97	70.81	49.81
	2	73	-55.34	57.57	76.17	52.33
	2.2	73	-59.65	61.53	80.94	54.71
	2.4	73	-63.38	64.97	85.18	56.91
	2.6	73	-66.66	68.00	88.97	58.93
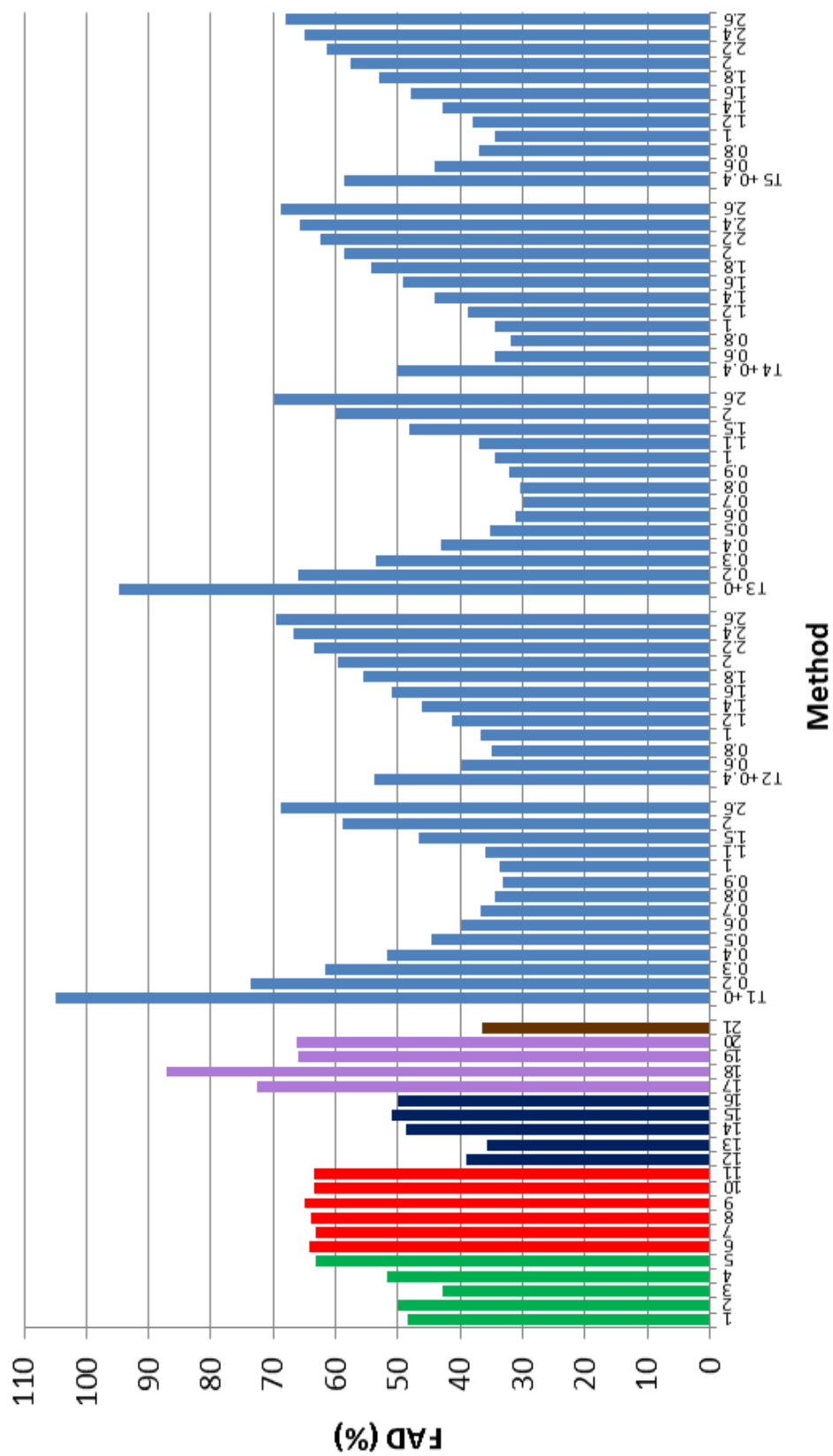
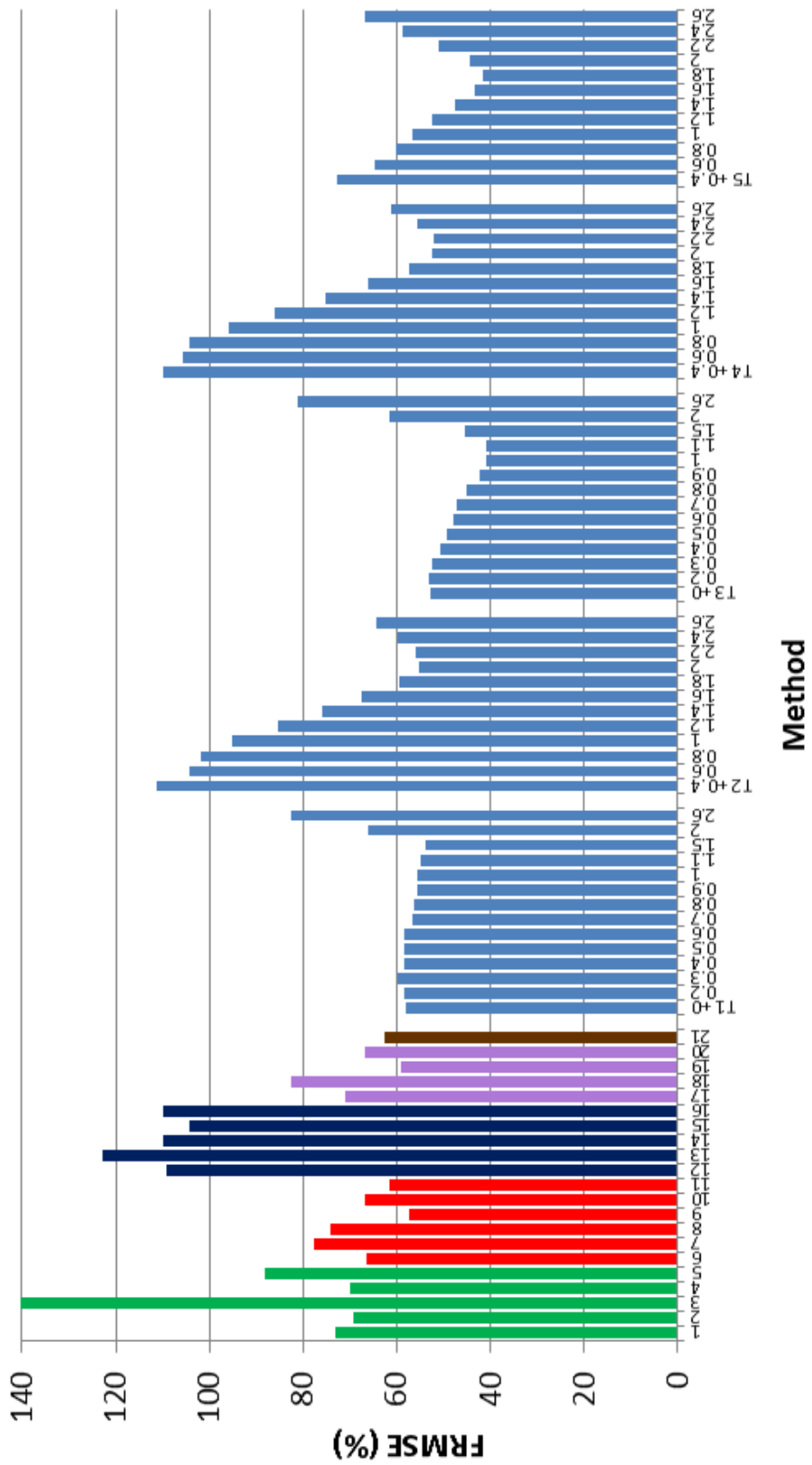Figure 3.6.5. FAD Performance August 31, 2012.
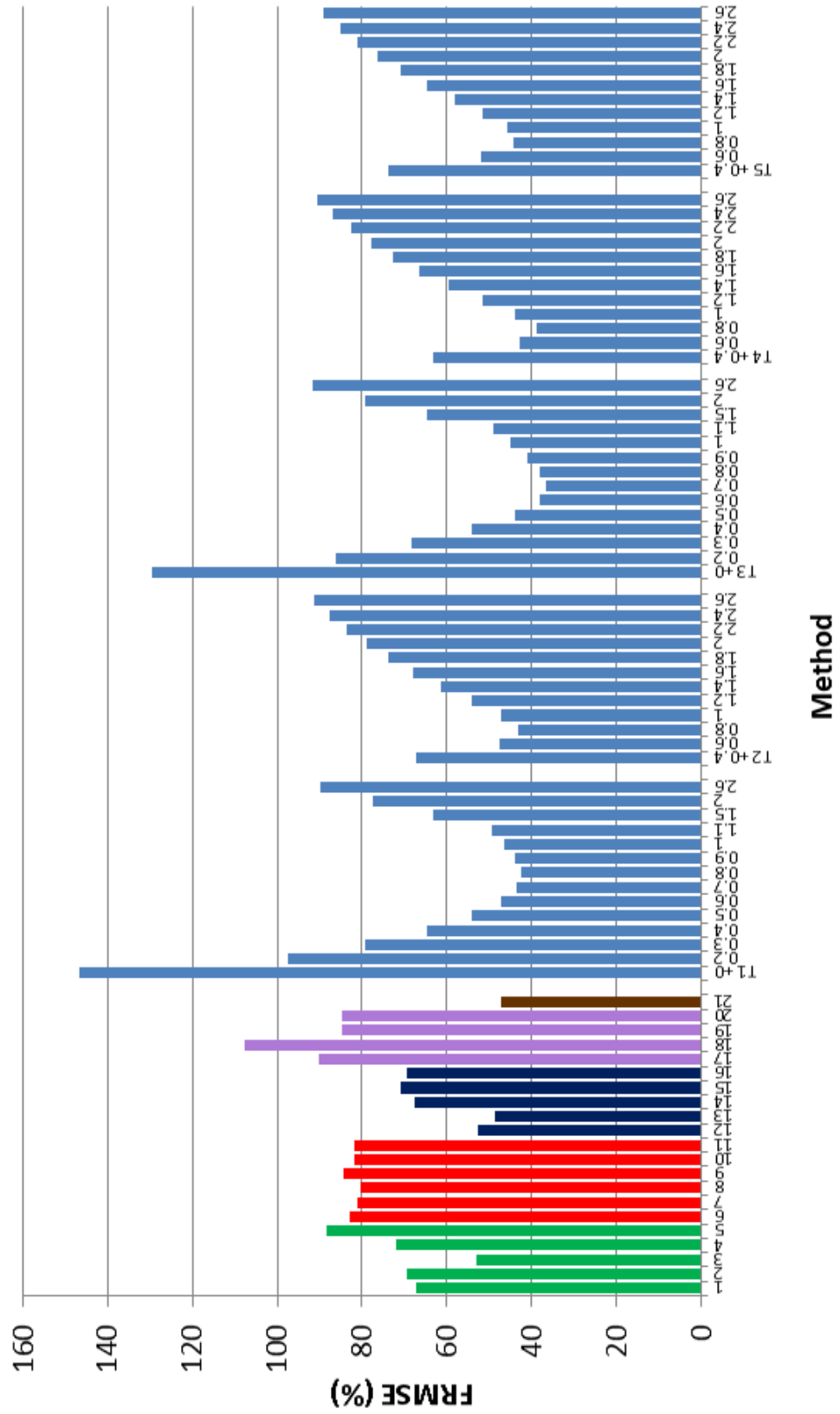
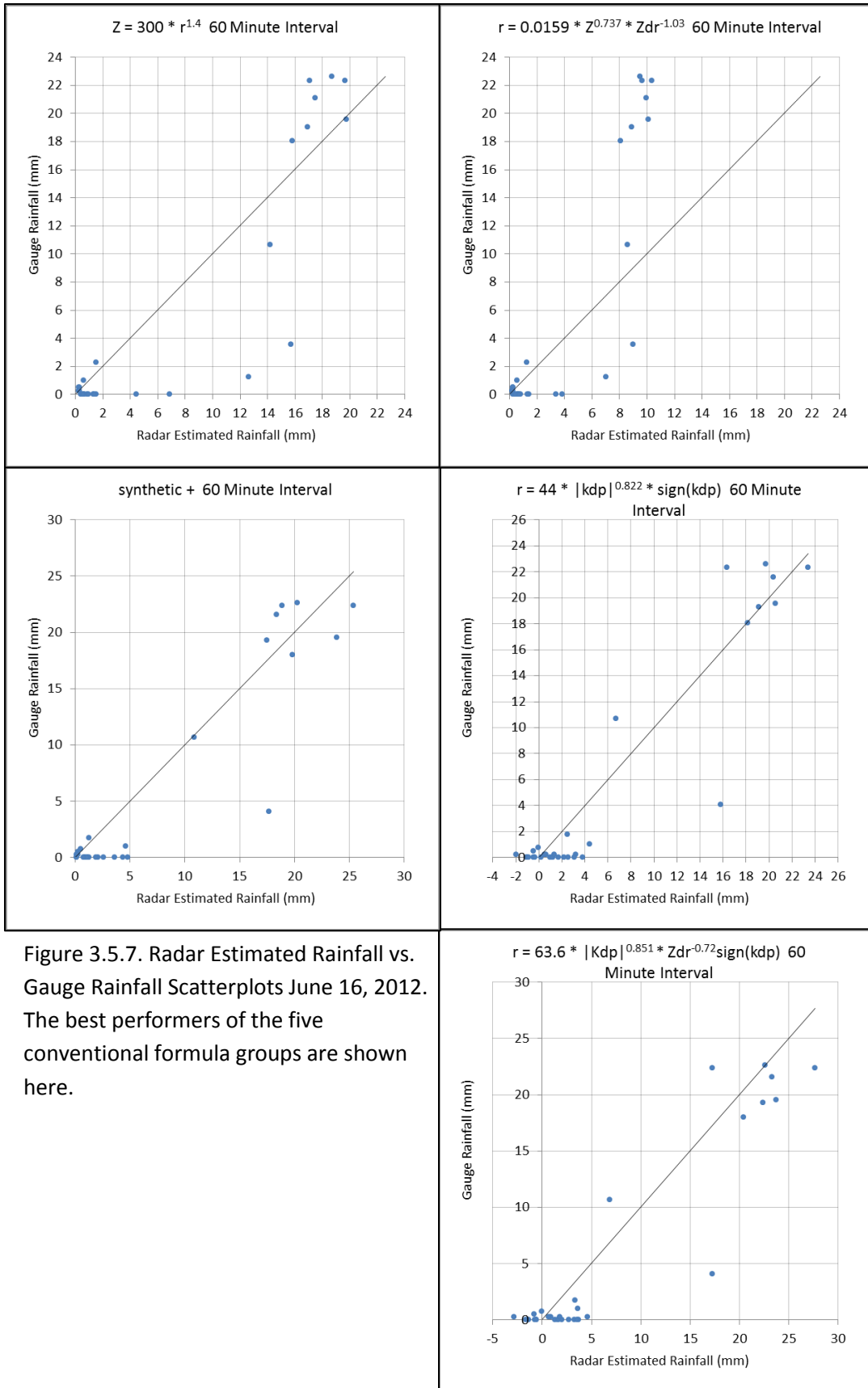Figure 3.6.6. FRMSE Performance August 31, 2012.

Figure 3.6.7. Radar Estimated Rainfall vs. Gauge Rainfall Scatterplots August 31, 2012. The best performers of the five conventional formula groups are shown here.
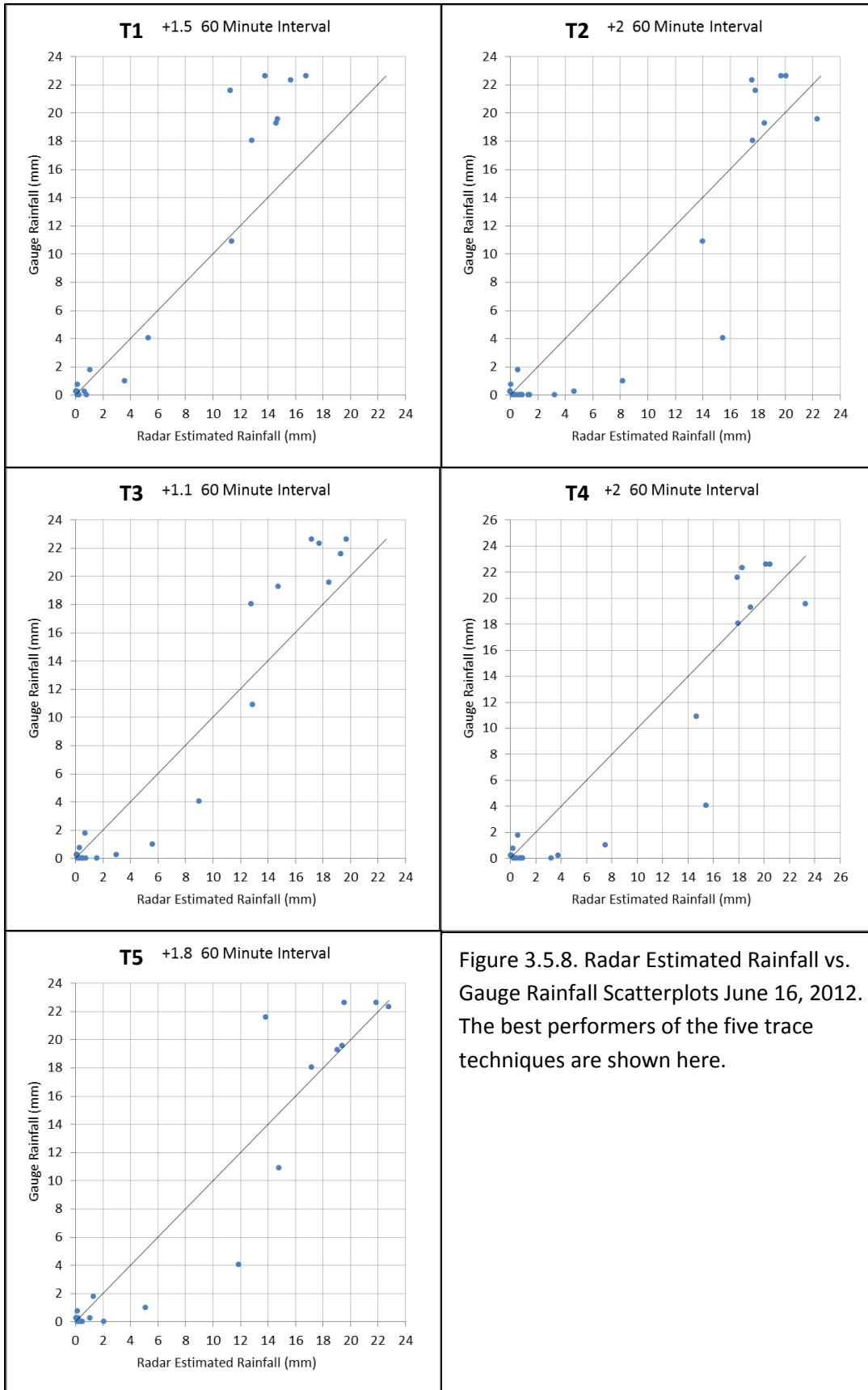
Figure 3.6.8. Radar Estimated Rainfall vs. Gauge Rainfall Scatterplots August 31, 2012. The best performers of the five trace techniques are shown here.

117

3.7 September 7, 2012

The afternoon of September 7 saw a severe hailstorm pass through Columbia, Missouri.

Figure 3.7.1 is an HPC surface analysis for 21 UTC of September 7, 2012. The storms

were associated with a cold front and low pressure center moving from the northwest

to southeast. Reflectivity values for the storm passing through Columbia reached

between 65 and 70 dBZ, a clear indication of hail. Figure 3.7.2 shows humidity versus

height in percentile format for 19 UTC of September 7 through 01 UTC of September 8.

On this afternoon, the atmosphere made a rapid transition from dry to moist. Figure

3.7.3 is a hodograph for the 31st of August. The hodograph shows a northwesterly wind

at the surface turning northerly at 925 millibars, and transitioning to westerly higher up.

Figure 3.7.4 is a four panel radar image from KLSX for 2107 UTC of September 7.

3.7.1 Conventional Formulas

Table 3.7.1 shows the performance of the conventional formulas for this event. The

presence of large hail contributed to extremely poor performance for all of the

conventional formulas. The best performer was the synthetic formula (21). Overall the

K_{DP}-reliant formulas outperformed the other formulas for this event. Three outliers were

present, (3, 12, and 13). Biases for the conventional techniques were all very positive for

this date.

3.7.2 Tracing Techniques

Table 3.7.2 shows the performance of the various trace techniques and their permutations for this event. The optimal T1 and T3 techniques performed significantly better than the other tracing techniques and all of the conventional formulas. The optimal Z_{DR} adjustment for all five tracing techniques was again roughly +0.8. The performance of the other tracing techniques was roughly on par with the conventional formulas. Every trace technique permutation tested exhibited a positive bias for this event.

3.5.3 Graphical Evaluation

Figure 3.7.5 is a histogram showing the FAD performance of each evaluated technique for this event. Figure 3.7.6 is the equivalent histogram showing FRMSE performance.

Figure 3.7.7 shows a combination of scatterplots of radar-derived rainfall versus rain gauge rainfall for the conventional formulas. The techniques illustrated were the top performers in each category. Figure 3.7.8 is identical to 3.7.7, except it depicts the best performers of the trace techniques.
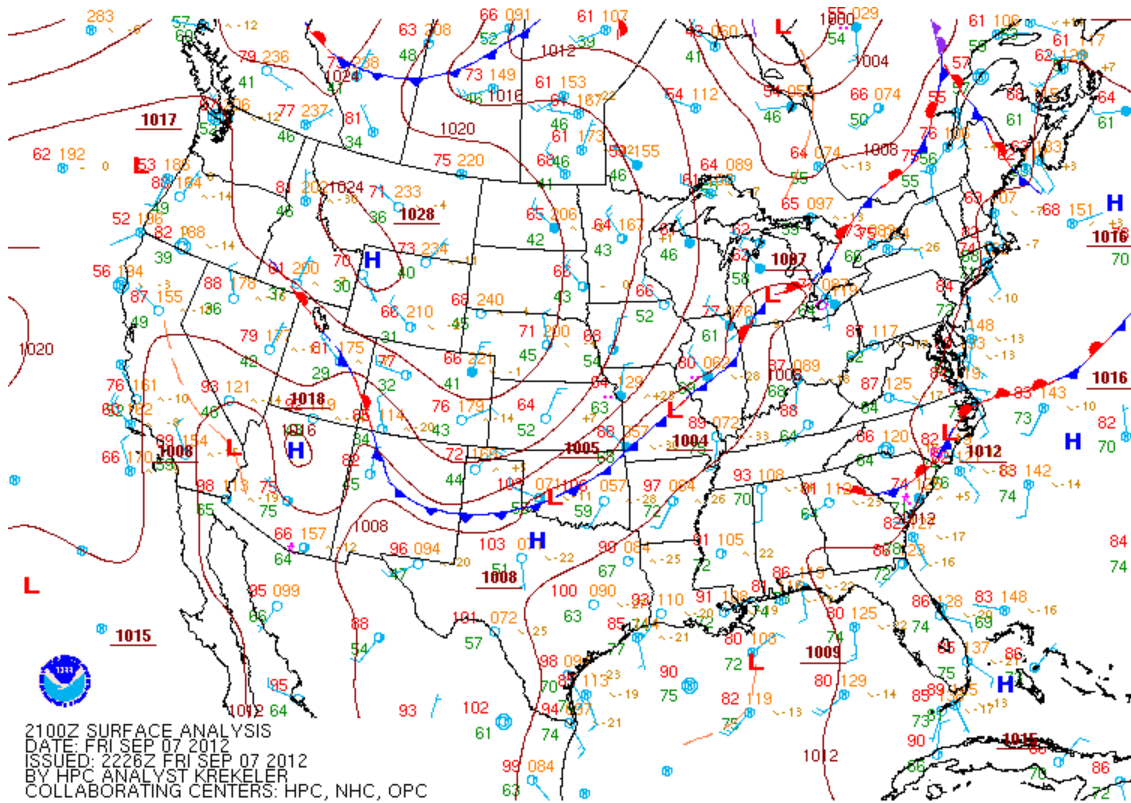
Figure 3.7.1. Surface Analysis 2100 UTC September 7, 2012.
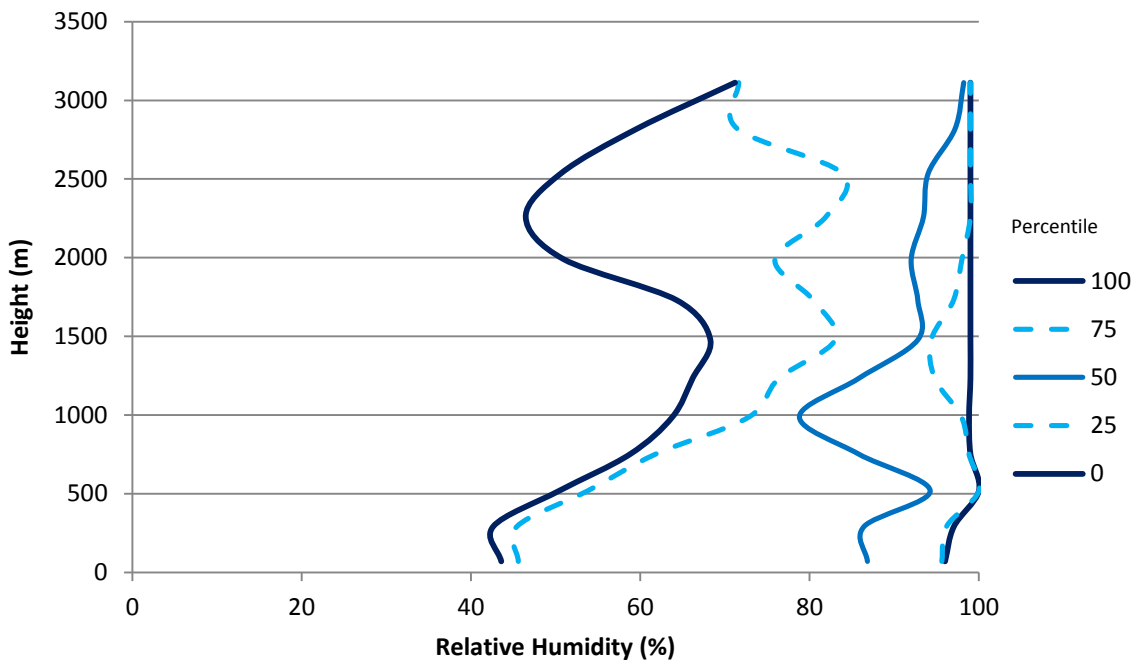
Figure 3.7.2. Relative Humidity Profile September 7, 2012.
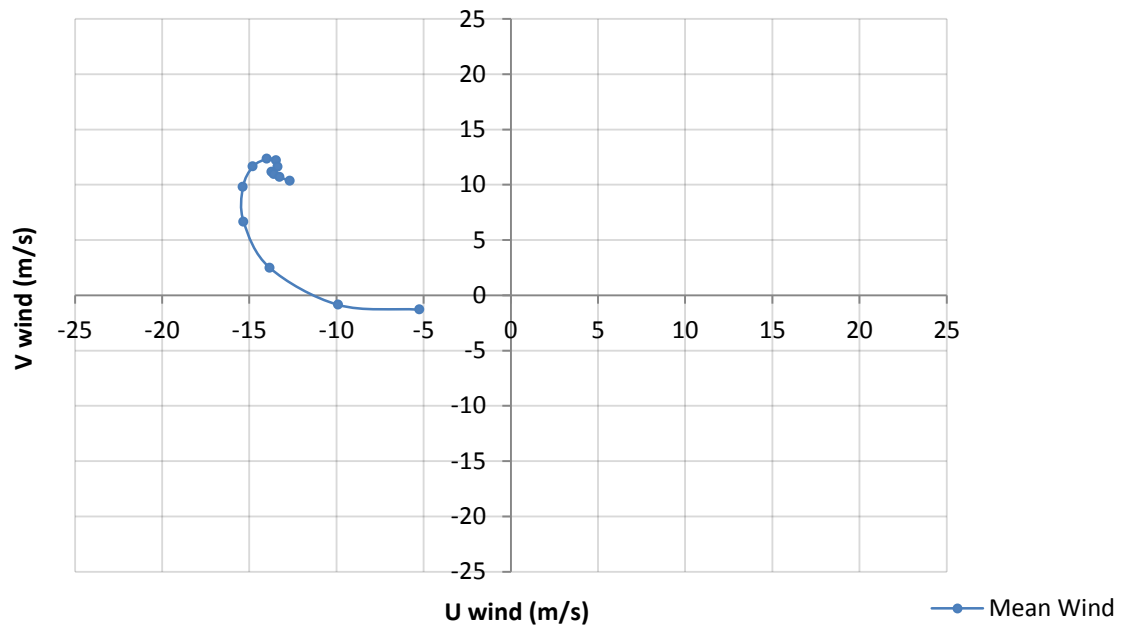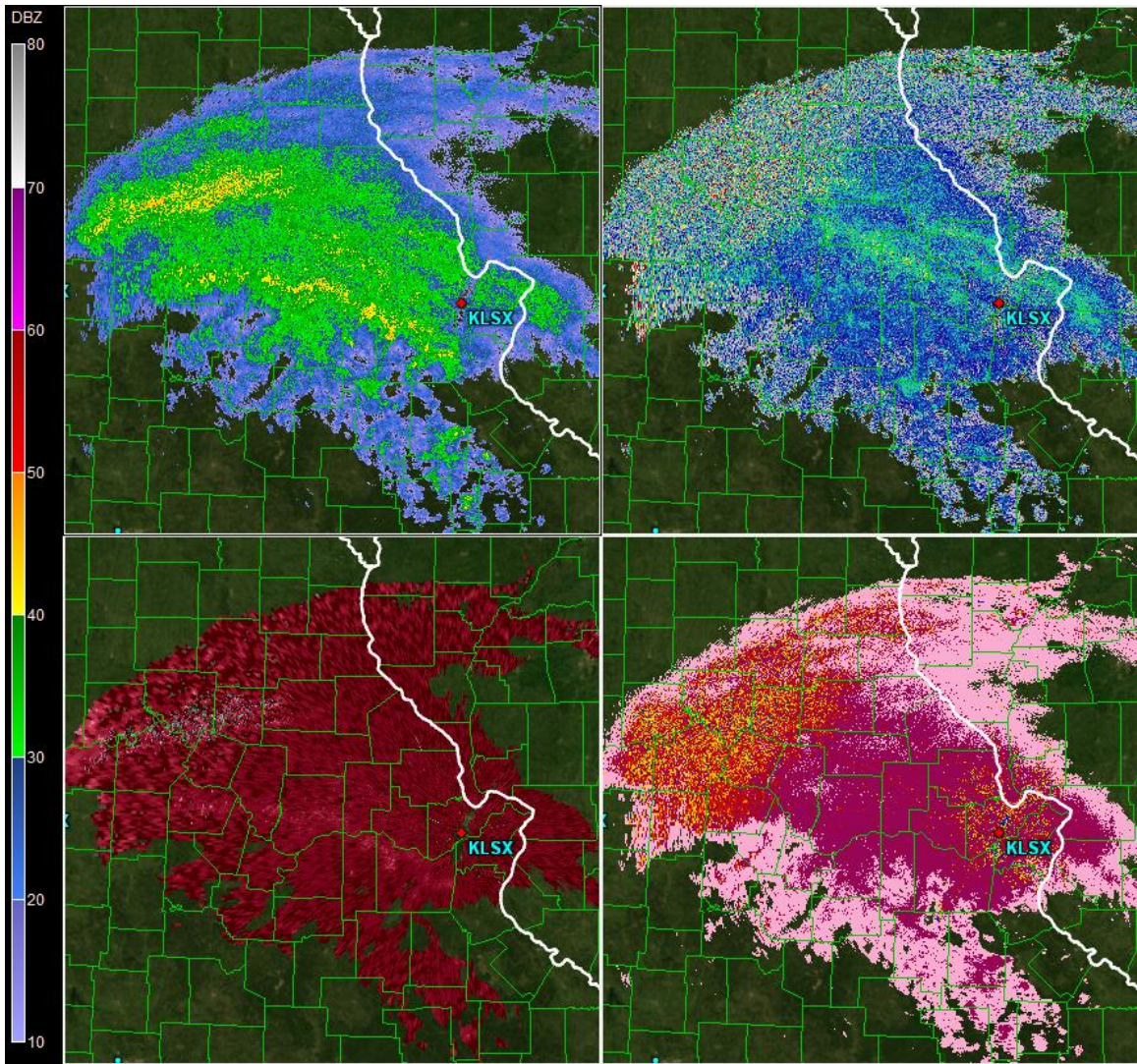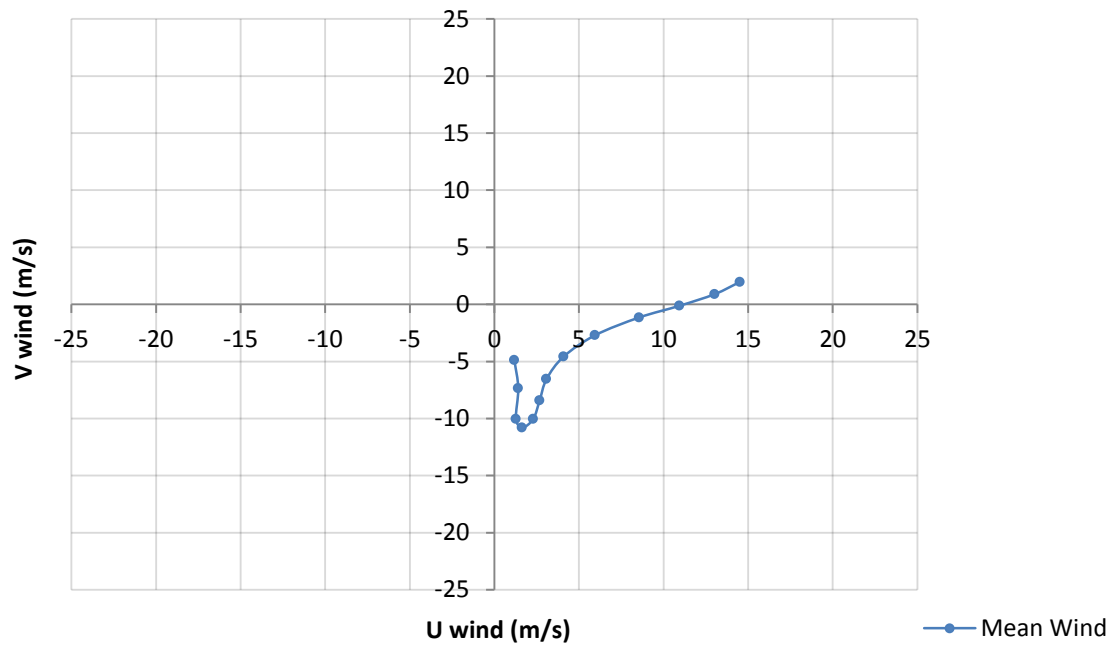
Figure 3.7.3. Hodograph September 7, 2012.
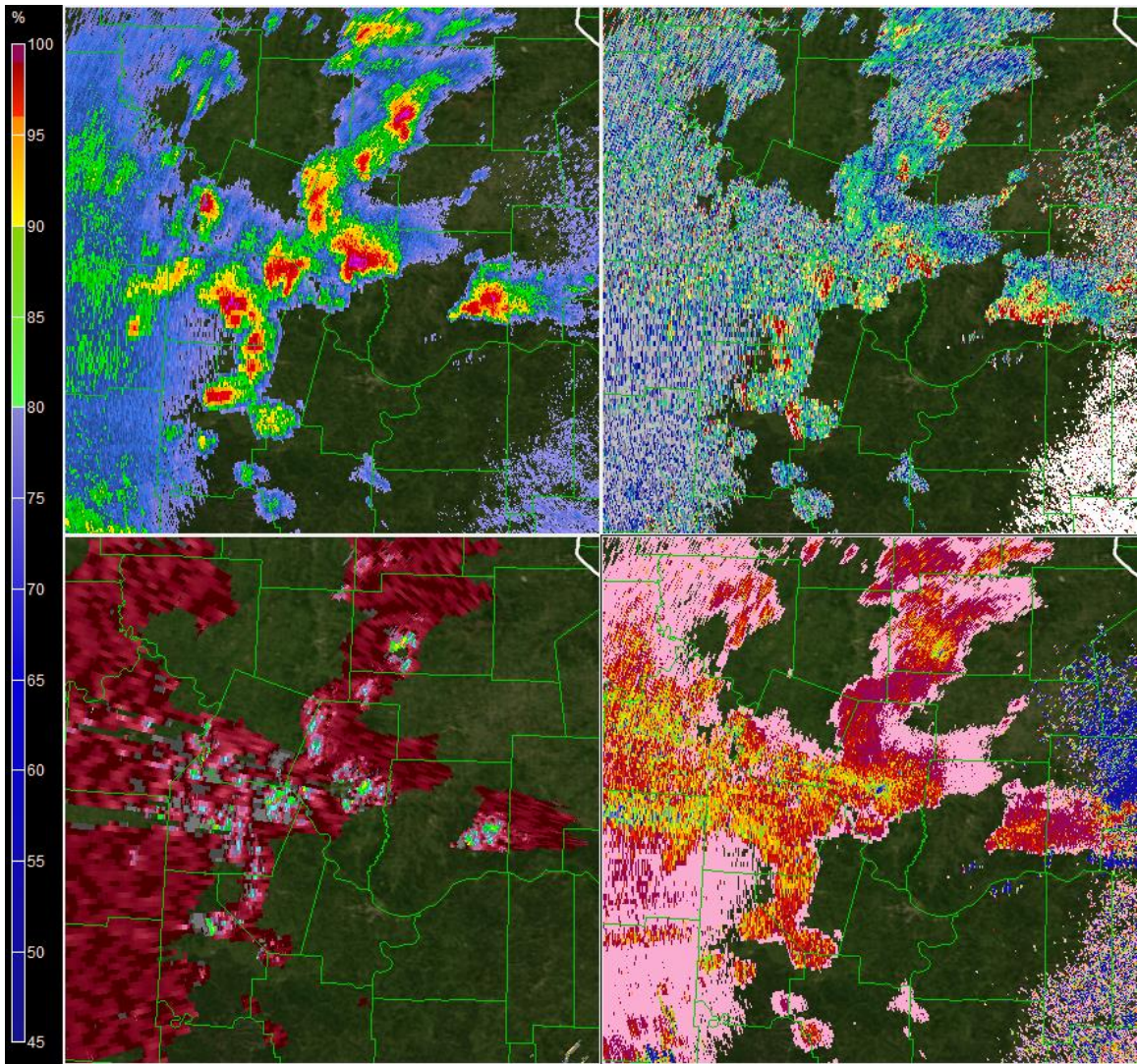
Figure 3.7.4. Four Panel Radar Image for 2107 UTC September 7, 2012. The top left is reflectivity (Z), top right is differential reflectivity (Z_{DR}), bottom left is specific phase differential (K_{DP}), and bottom right is correlation coefficient. The scale on the left corresponds to the bottom right image (correlation coefficient). The elevation angle used here was 0.5°.

Table 3.7.1 Conventional Techniques, September 7, 2012

$Z = aR^b$	#	FB(%)	FAD(%)	FRMSE(%)	FSD(%)
1	35	17.31	64.49	113.48	112.15
2	35	34.72	76.21	142.59	138.30
3	35	179.27	192.10	363.50	316.22
4	35	22.23	70.13	128.58	126.64
5	35	-11.73	68.78	113.94	113.33
$R(K_{DP}) = a|K_{DP}|^b sign(K_{DP})$					
6	35	83.47	120.77	164.77	142.06
7	36	100.26	136.54	186.94	157.78
8	36	99.35	135.72	184.83	155.85
9	35	61.07	99.72	137.83	123.56
10	35	84.92	122.12	165.67	142.25
11	35	75.51	113.29	154.13	134.37
$R(Z, Z_{DR}) = aZ^b Z_{dr}{}^c$					
12	35	-30.37	50.93	89.34	84.03
13	35	-36.61	55.61	95.83	88.56
14	35	-33.42	53.11	93.70	87.54
15	35	-29.70	54.13	92.90	88.03
16	35	-33.99	53.68	94.48	88.15
$R(K_{DP}, Z_{DR}) = a|K_{DP}|^b Z_{dr}{}^c sign(K_{DP})$					
17	35	142.70	184.44	253.66	209.71
18	36	199.21	244.75	348.22	285.61
19	35	79.31	119.80	162.59	141.93
20	35	108.78	148.61	200.21	168.08
Synthetic					
21	34	45.75	79.41	121.47	112.53

Table 3.7.2 Trace Techniques, September 7, 2012

	Z_{DR} +	#	FB(%)	FAD(%)	FRMSE(%)	FSD(%)
T1	0	36	43.35	62.76	92.82	82.08
	0.2	36	34.08	53.56	78.07	70.24
	0.3	36	30.03	49.73	72.60	66.11
	0.4	36	26.70	46.38	68.79	63.40
	0.5	36	23.99	44.13	66.16	61.66
	0.6	36	21.38	41.81	63.67	59.97
	0.7	33	19.03	39.55	59.77	56.66
	0.8	32	17.58	38.69	59.12	56.45
	0.9	32	16.80	38.67	60.62	58.25
	1	32	16.61	39.39	63.13	60.91
	1.1	32	16.82	41.60	66.77	64.62
	1.5	32	21.79	58.16	92.80	90.20
	2	31	25.69	73.91	121.15	118.40
	2.6	31	18.48	78.03	132.78	131.49
T2	0.4	36	67.86	80.61	125.68	105.79
	0.6	36	56.49	73.40	118.53	104.20
	0.8	35	47.82	70.27	113.62	103.07
	1	33	42.82	70.58	113.86	105.50
	1.2	32	40.46	72.87	121.12	114.17
	1.4	32	40.75	78.07	136.40	130.17
	1.6	32	42.95	84.76	157.11	151.12
	1.8	32	45.87	91.90	178.50	172.51
	2	32	45.67	97.38	188.82	183.21
	2.2	31	40.12	97.26	184.66	180.25
	2.4	31	34.61	97.87	183.84	180.56
	2.6	31	30.30	99.35	186.22	183.74
T3	0	36	36.72	64.66	95.61	88.28
	0.2	36	28.83	56.87	86.73	81.80
	0.3	36	25.53	53.69	83.86	79.88
	0.4	36	22.68	51.10	81.85	78.65
	0.5	36	19.93	49.21	80.12	77.60
	0.6	36	16.84	47.18	77.52	75.66
	0.7	36	14.18	46.05	75.59	74.24
	0.8	36	12.17	45.71	74.75	73.75
	0.9	36	10.78	45.63	74.94	74.16
	1	36	9.82	45.75	76.14	75.50
	1.1	34	8.85	46.17	76.01	75.49
	1.5	32	9.46	52.69	90.70	90.21
	2	32	12.30	67.23	117.52	116.87
	2.6	32	1.30	70.53	122.59	122.58

Table 3.7.2 Trace Techniques, September 7, 2012 (Continued)

	Z_{DR} +	#	FB(%)	FAD(%)	FRMSE(%)	FSD(%)
T4	0.4	36	67.77	84.08	125.92	106.13
	0.6	36	56.38	73.82	116.31	101.73
	0.8	36	47.79	67.65	110.31	99.42
	1	36	42.95	67.14	111.18	102.55
	1.2	36	40.60	69.08	118.07	110.87
	1.4	35	40.69	72.85	129.13	122.55
	1.6	33	42.59	78.43	143.07	136.59
	1.8	32	45.37	85.29	159.95	153.39
	2	32	45.16	90.26	169.13	162.98
	2.2	32	39.73	89.90	168.37	163.62
	2.4	32	34.23	88.93	168.13	164.61
	2.6	32	29.90	88.71	170.89	168.25
T5	0.4	36	70.80	76.88	117.43	93.69
	0.6	36	61.03	68.65	106.46	87.23
	0.8	36	54.90	65.00	103.57	87.82
	1	34	52.44	65.41	105.81	91.90
	1.2	32	52.93	69.87	114.07	101.05
	1.4	32	56.49	78.05	132.23	119.55
	1.6	32	59.95	85.39	151.63	139.27
	1.8	32	63.18	93.44	169.96	157.78
	2	31	63.97	98.83	179.51	167.72
	2.2	31	60.38	99.80	183.22	172.99
	2.4	31	57.60	100.78	188.80	179.80
	2.6	31	54.83	101.06	193.16	185.21
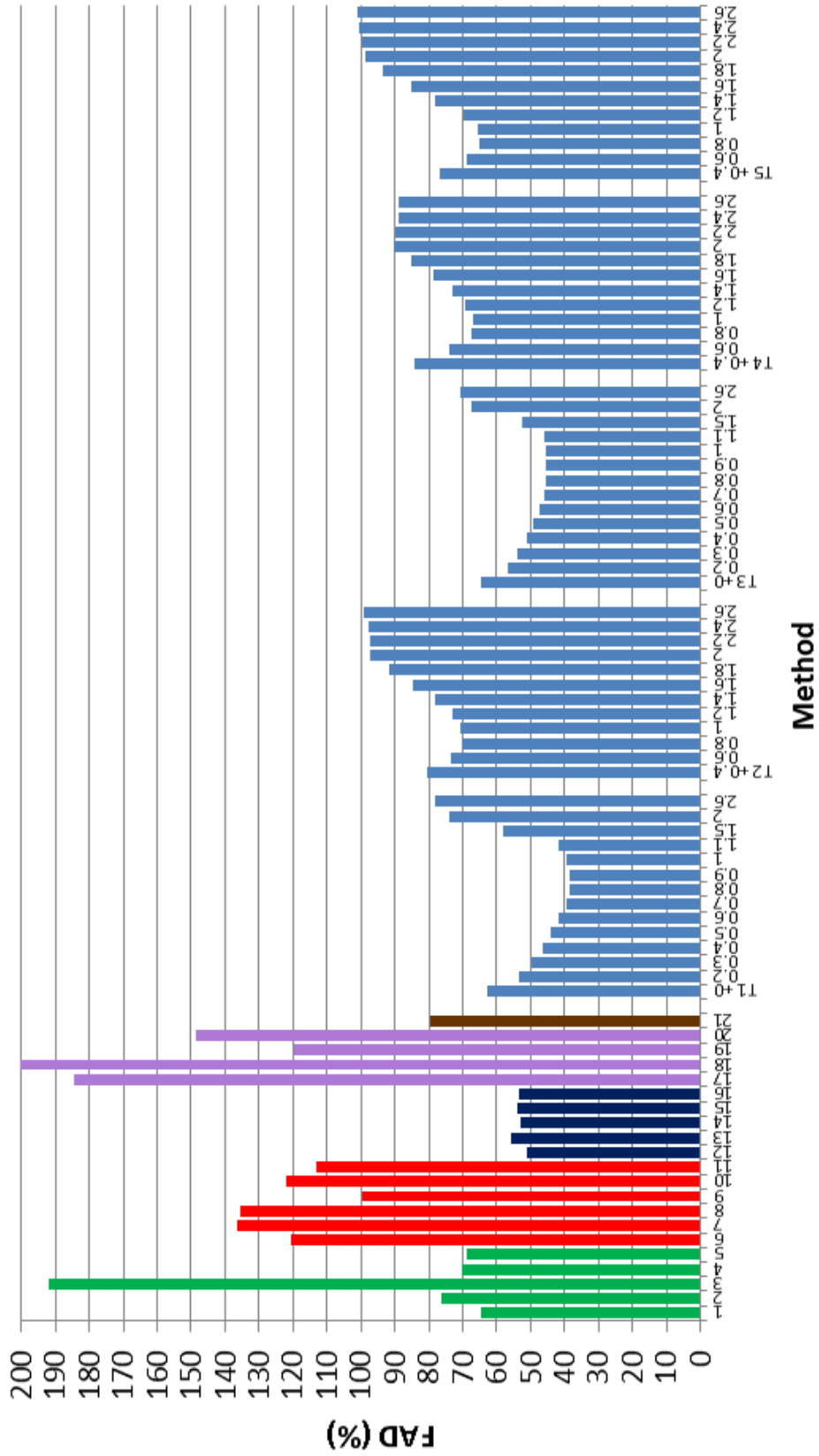
Figure 3.7.5. FAD Performance September 7, 2012.

126
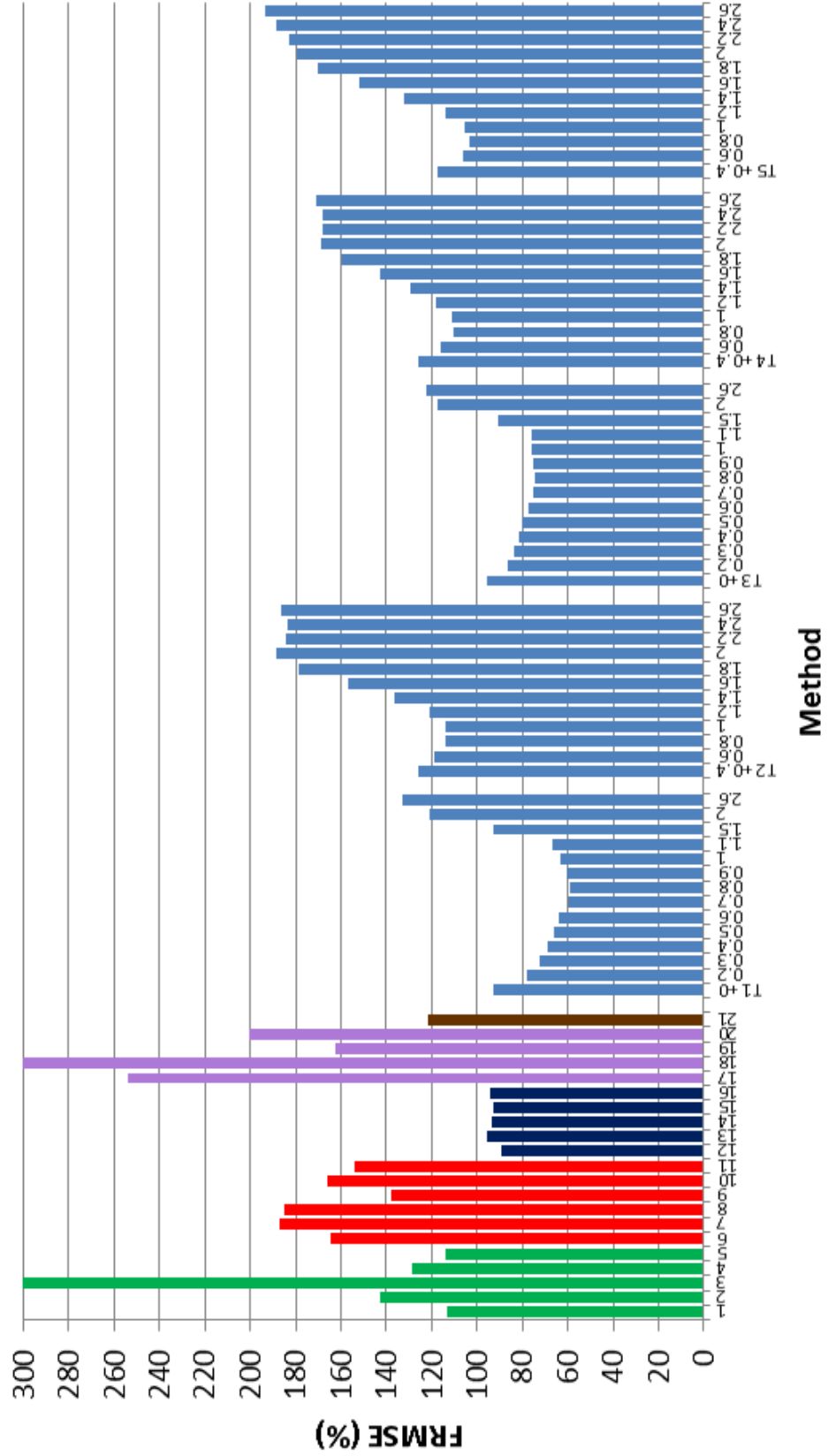
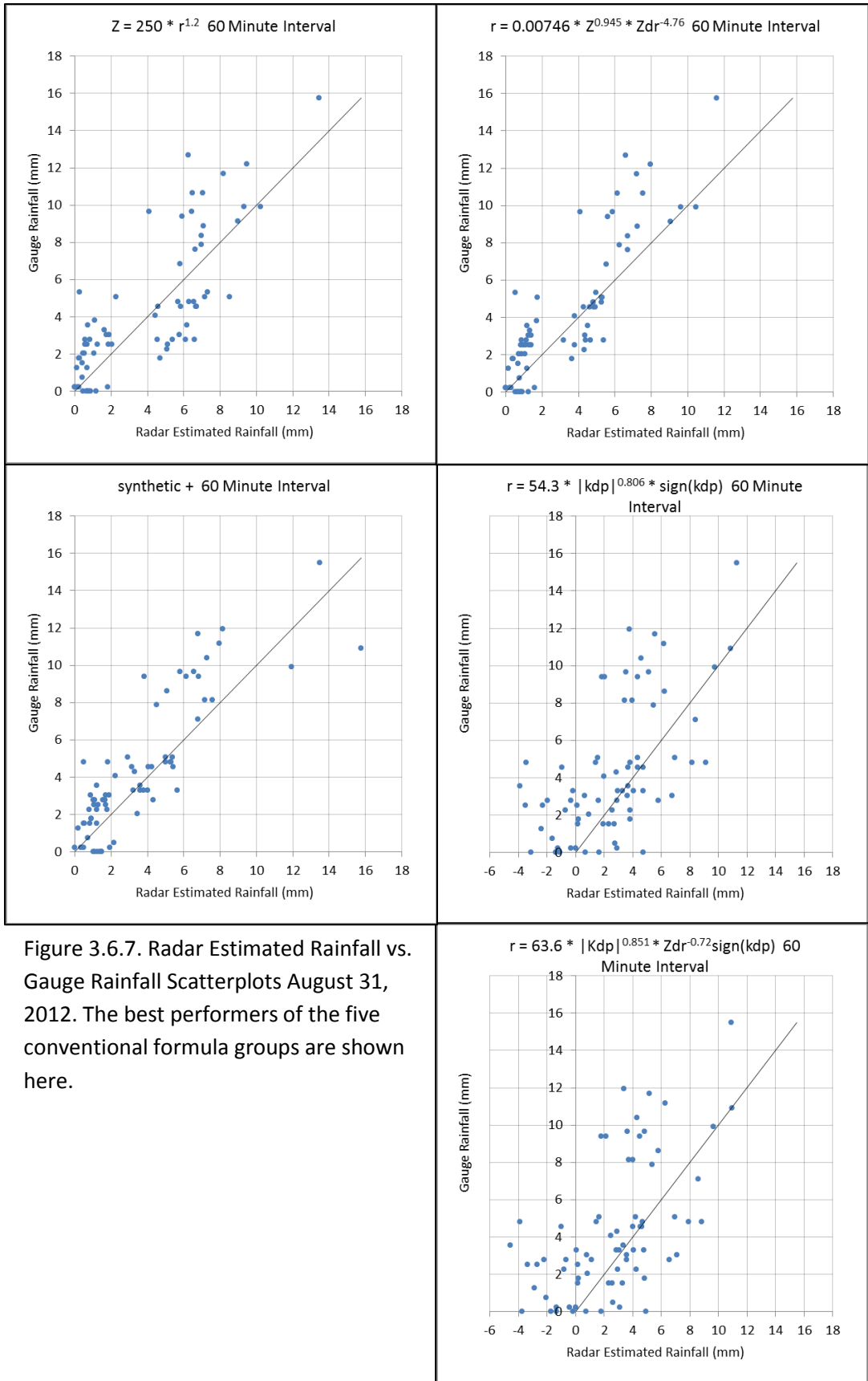Figure 3.7.6. FRMSE Performance September 7, 2012.

127

Figure 3.7.7. Radar Estimated Rainfall vs. Gauge Rainfall Scatterplots September 7, 2012. The best performers of the five conventional formula groups are shown here.
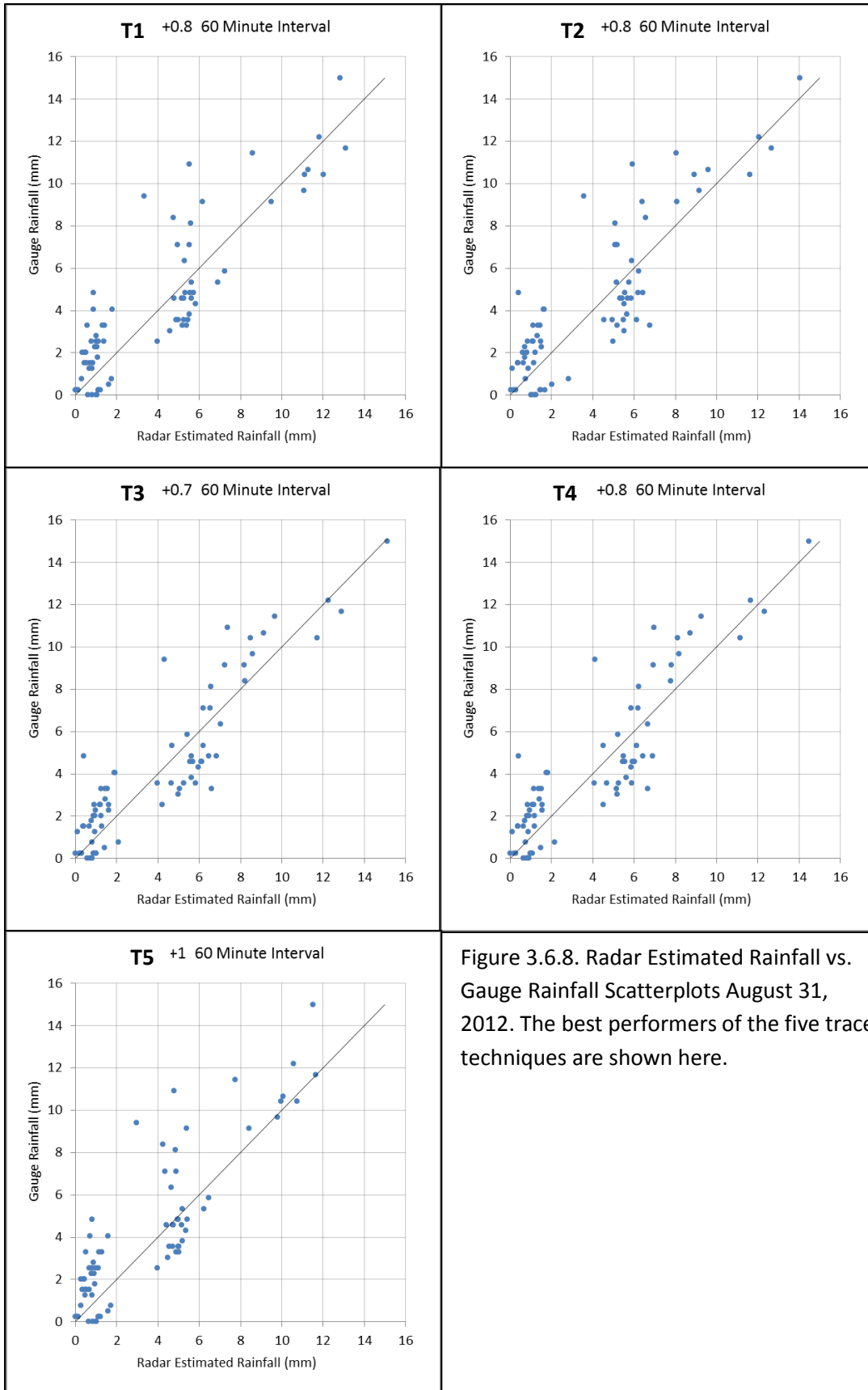
128

Figure 3.7.8. Radar Estimated Rainfall vs. Gauge Rainfall Scatterplots September 7, 2012. The best performers of the five trace techniques are shown here.

3.8 October 13, 2012

The rainfall event on October 13 was associated with two centers of low pressure to the northwest of the region. On the 13th of October several thunderstorm complexes moved through Central Missouri. Figure 3.8.1 is an HPC surface analysis for 03 UTC of October 14, 2012. Figure 3.8.2 shows humidity versus height in percentile format for 18 UTC of October 13 through 06 UTC of October 14. The atmosphere was very humid throughout this event. Figure 3.8.3 is a hodograph for the 13th of October. The hodograph shows a southerly wind at the surface turning southwesterly higher up.

3.8.1 Conventional Formulas

Table 3.8.1 shows the performance of the conventional formulas for this event. (1), (4), (14), (15), and (16) performed the best out of the conventional formulas. The tropical Z-R formula, (3), performed poorly again. All K_{DP}-reliant formulas also performed very poorly on this date. Biases for the conventional formulas were nearly all positive for this date.

3.8.2 Tracing Techniques

Table 3.8.2 shows the performance of the various trace techniques and their permutations for this event. The optimal tracing techniques as a whole performed slightly better than the (non-K_{DP} reliant) conventional formulas. The optimal Z_{DR} adjustment for all five tracing techniques was roughly +2, although this is less precise for T1 and T3 due to +1.8 and +2.2 Z_{DR} adjustments not being tested. This was an anomalously high optimal Z_{DR} adjustment for T1 and T3. This may have been caused by

inaccurate humidity data within the high resolution model. Figure 3.8.2 indicated a very saturated environment, which would reduce expected evaporation.

3.5.3 Graphical Evaluation

Figure 3.8.4 is a histogram showing the FAD performance of each evaluated technique for this event. Figure 3.8.5 is the equivalent histogram showing FRMSE performance.

Figure 3.8.6 shows a combination of scatterplots of radar-derived rainfall versus rain gauge rainfall for the conventional formulas. The techniques illustrated were the top performers in each category. Figure 3.8.7 is identical to 3.8.6, except it depicts the best performers of the trace techniques.
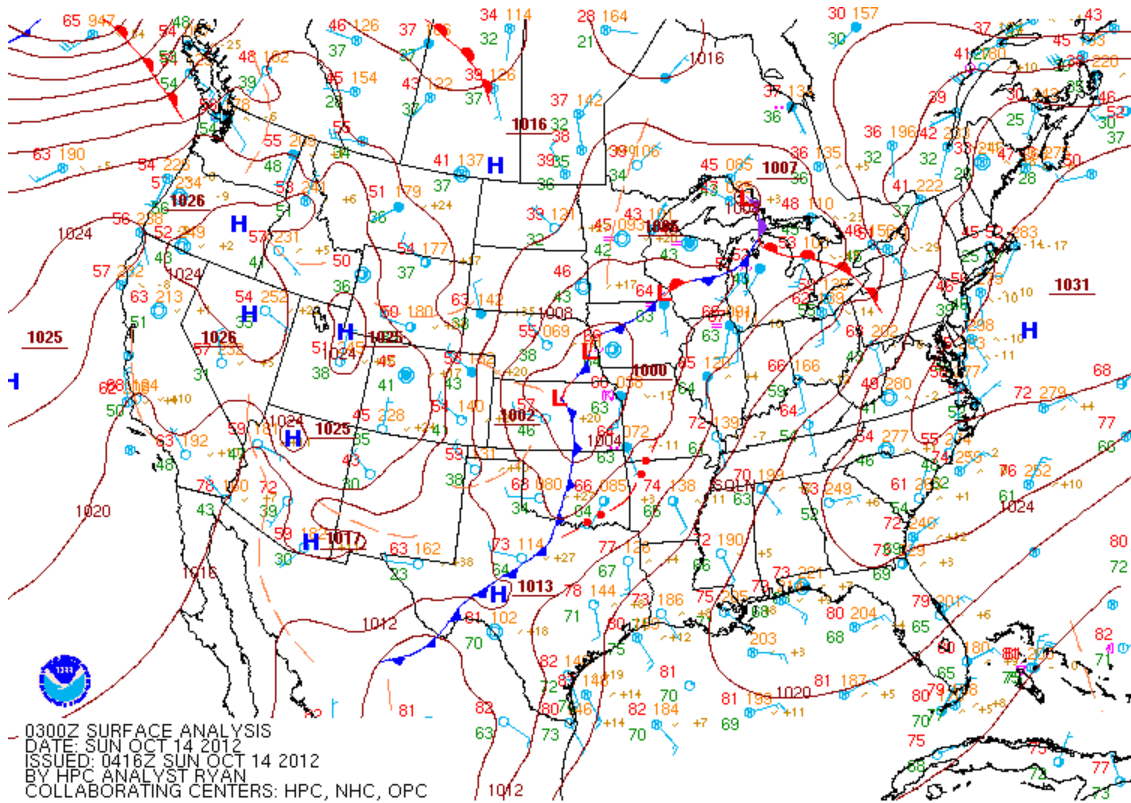
Figure 3.8.1. Surface Analysis 0300 UTC October 14, 2012.
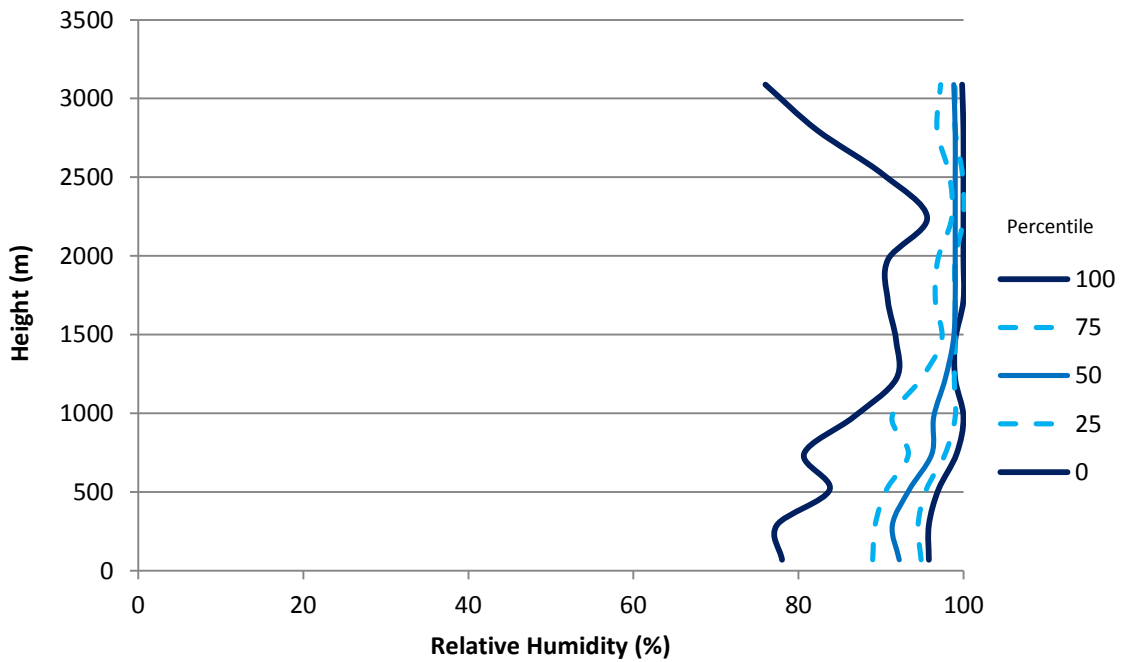
Figure 3.8.2. Relative Humidity Profile October 13, 2012.

132
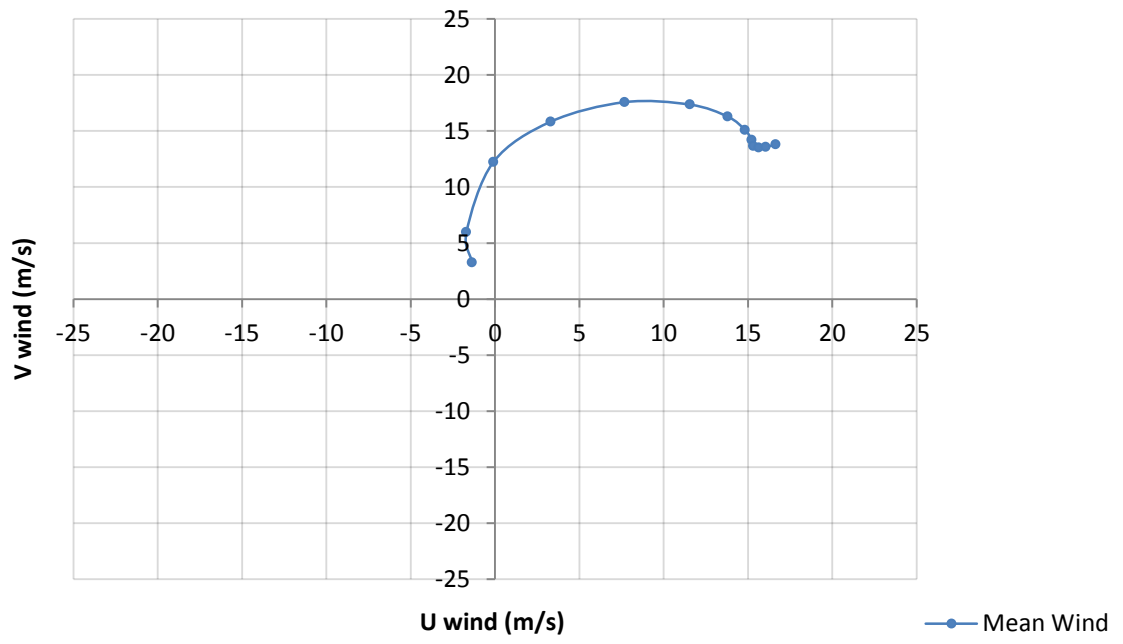
Figure 3.8.3. Hodograph October 13, 2012.

Table 3.8.1 Conventional Techniques, October 13, 2012

$Z = aR^b$	#	FB(%)	FAD(%)	FRMSE(%)	FSD(%)
1	72	14.67	42.26	60.87	59.08
2	72	14.86	44.48	63.63	61.87
3	72	91.72	93.74	141.29	107.47
4	72	7.66	42.33	60.89	60.41
5	72	-24.11	45.74	67.66	63.22
$R(K_{DP}) = a|K_{DP}|^b sign(K_{DP})$					
6	60	55.39	130.82	167.17	157.73
7	60	74.51	144.89	185.89	170.31
8	60	84.04	148.60	191.02	171.54
9	60	38.99	117.41	148.64	143.43
10	60	60.62	133.22	170.33	159.18
11	60	54.50	127.78	162.40	152.99
$R(Z, Z_{DR}) = aZ^b Z_{dr}{}^c$					
12	72	33.71	51.96	79.46	71.95
13	72	38.88	56.61	92.41	83.83
14	72	4.64	39.78	58.62	58.44
15	72	1.41	39.34	58.12	58.10
16	72	1.64	39.34	58.31	58.29
$R(K_{DP}, Z_{DR}) = a|K_{DP}|^b Z_{dr}{}^c sign(K_{DP})$					
17	60	90.31	183.23	238.72	220.98
18	62	121.69	238.29	319.96	295.92
19	60	52.60	132.66	168.86	160.46
20	60	77.35	155.93	200.16	184.61
Synthetic					
21	57	33.78	60.21	102.89	97.19

Table 3.8.2 Trace Techniques, October 13, 2012

	Z_{DR} +	#	FB(%)	FAD(%)	FRMSE(%)	FSD(%)
T1	0	72	187.44	187.46	247.60	161.79
	0.2	72	151.81	151.87	203.73	135.86
	0.3	72	134.66	134.75	182.82	123.65
	0.4	72	118.40	118.52	163.24	112.37
	0.5	72	103.44	103.57	145.70	102.61
	0.6	72	89.77	89.96	129.94	93.95
	0.7	72	77.37	77.81	116.16	86.64
	0.8	72	66.11	67.00	104.05	80.35
	0.9	72	55.78	58.14	93.29	74.78
	1	72	46.47	51.52	83.97	69.94
	1.1	72	37.90	46.74	75.60	65.42
	1.5	72	10.36	37.30	54.86	53.87
	2	72	-14.82	35.77	51.65	49.48
	2.6	72	-35.65	44.97	63.30	52.31
T2	0.4	72	153.35	154.20	225.54	165.37
	0.6	72	116.99	120.26	184.15	142.22
	0.8	72	87.27	95.41	150.71	122.88
	1	72	63.45	77.70	124.77	107.43
	1.2	72	44.62	65.81	106.54	96.75
	1.4	72	28.44	57.03	91.45	86.92
	1.6	72	15.10	53.14	81.48	80.07
	1.8	72	3.57	50.55	74.91	74.83
	2	72	-6.50	49.11	71.16	70.86
	2.2	72	-15.23	49.53	69.80	68.12
	2.4	72	-22.87	50.36	70.23	66.40
	2.6	72	-29.60	51.62	71.86	65.48
T3	0	72	184.40	184.40	246.65	163.80
	0.2	72	147.79	147.87	201.19	136.51
	0.3	72	130.46	130.63	179.96	123.96
	0.4	72	114.44	114.70	160.90	113.11
	0.5	72	99.91	100.49	144.19	103.96
	0.6	72	86.45	87.38	129.02	95.77
	0.7	72	74.24	76.10	115.65	88.68
	0.8	72	62.97	66.62	103.60	82.26
	0.9	72	52.78	59.18	93.06	76.64
	1	72	43.71	54.02	84.30	72.09
	1.1	72	35.56	49.85	77.14	68.45
	1.5	72	8.72	40.75	58.96	58.31
	2	72	-15.38	40.91	56.67	54.55
	2.6	72	-35.71	47.92	66.67	56.31

Table 3.8.2 Trace Techniques, October 13, 2012 (Continued)

	Z_{DR} +	#	FB(%)	FAD(%)	FRMSE(%)	FSD(%)
T4	0.4	72	151.80	151.85	207.52	141.49
	0.6	72	115.80	116.23	165.53	118.28
	0.8	72	86.33	87.59	132.09	99.97
	1	72	62.69	67.19	106.26	85.80
	1.2	72	43.97	55.10	87.87	76.08
	1.4	72	27.84	46.88	72.69	67.15
	1.6	72	14.55	42.84	63.45	61.76
	1.8	72	3.07	40.21	58.23	58.15
	2	72	-6.94	40.19	56.32	55.89
	2.2	72	-15.63	41.24	57.01	54.83
	2.4	72	-23.23	43.22	59.43	54.70
	2.6	72	-29.92	45.59	62.82	55.24
T5	0.4	72	157.73	157.81	212.56	142.49
	0.6	72	120.42	120.53	167.96	117.08
	0.8	72	90.42	90.87	133.53	98.26
	1	72	66.10	67.69	106.67	83.72
	1.2	72	46.33	52.87	85.54	71.90
	1.4	72	30.14	45.07	70.22	63.42
	1.6	72	16.20	40.22	59.36	57.11
	1.8	72	4.20	37.96	53.04	52.87
	2	72	-6.10	36.74	50.85	50.48
	2.2	72	-15.01	36.13	51.82	49.59
	2.4	72	-22.80	37.91	54.75	49.78
	2.6	72	-29.67	40.97	58.74	50.70
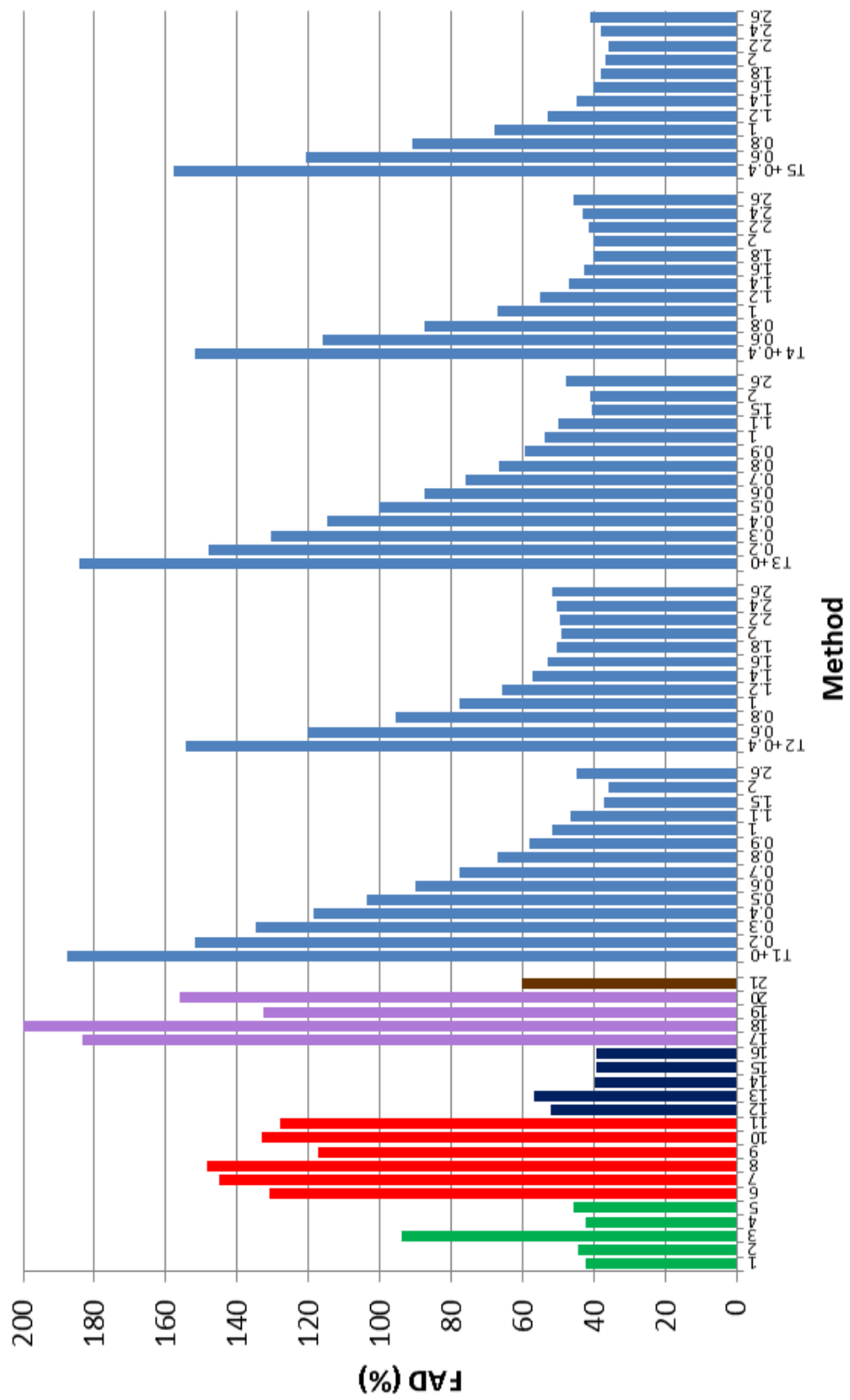
Figure 3.8.4. FAD Performance October 13, 2012.

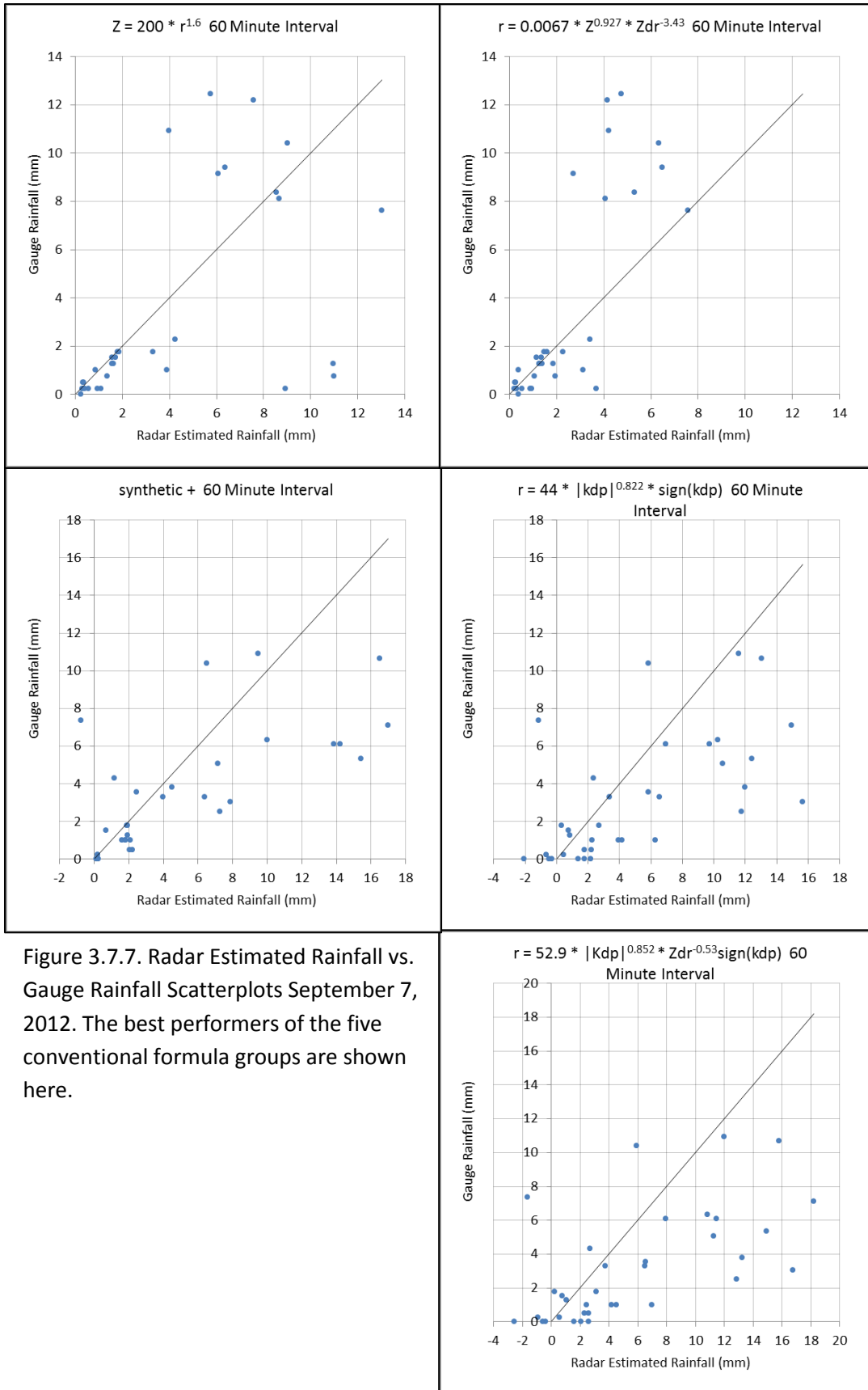137
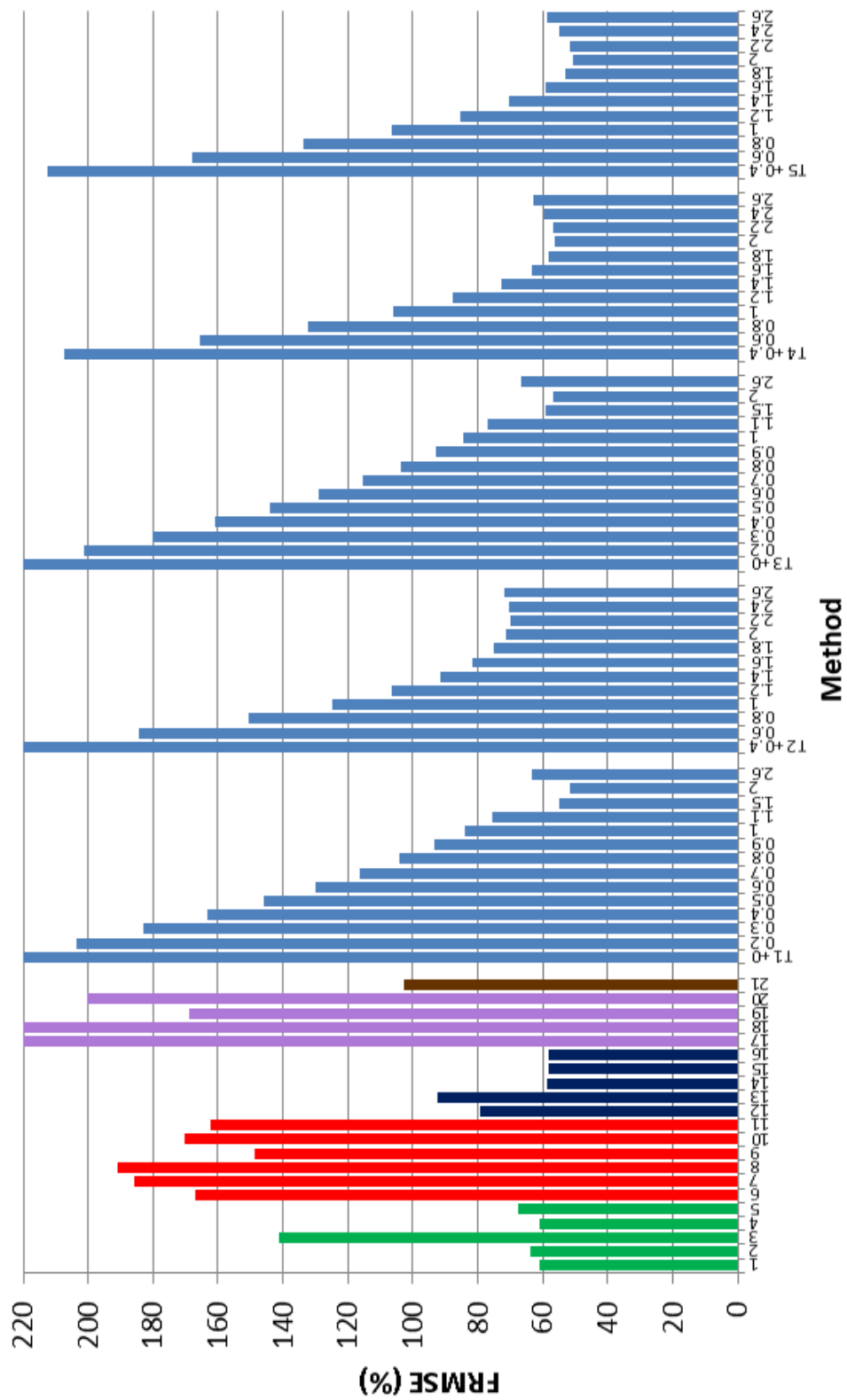
Figure 3.8.5. FRMSE Performance October 13, 2012.

138
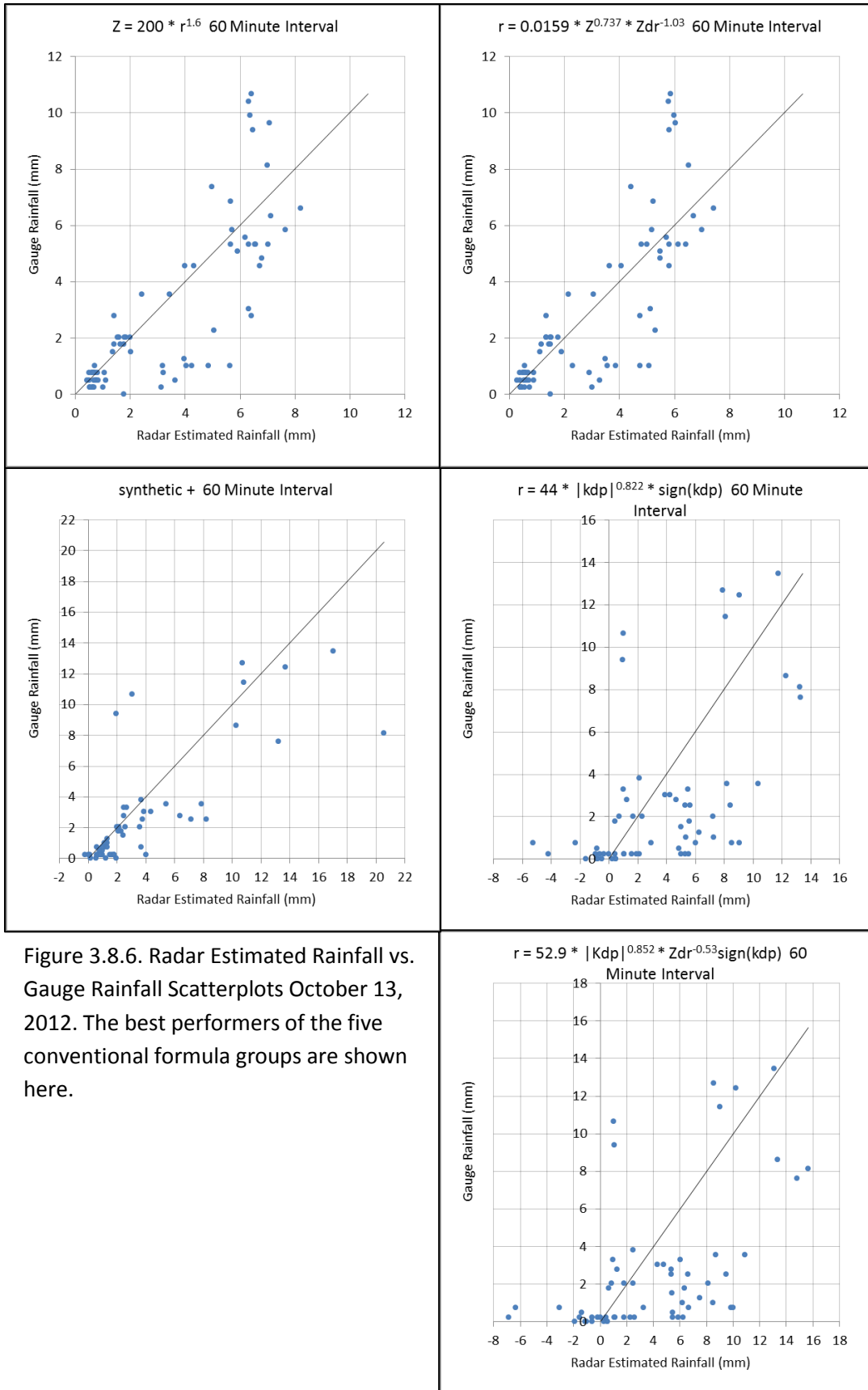
Figure 3.8.6. Radar Estimated Rainfall vs. Gauge Rainfall Scatterplots October 13, 2012. The best performers of the five conventional formula groups are shown here.
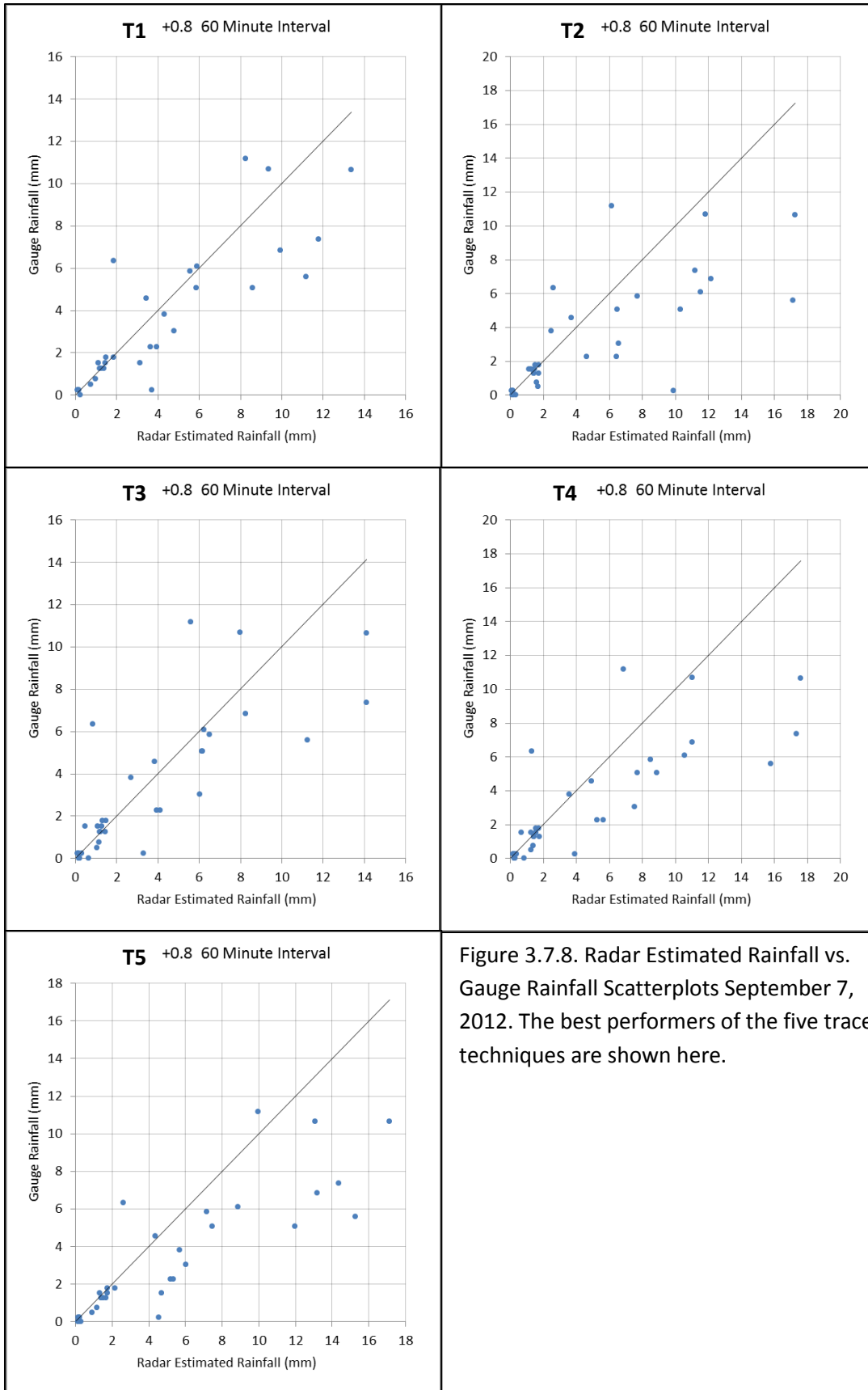
139
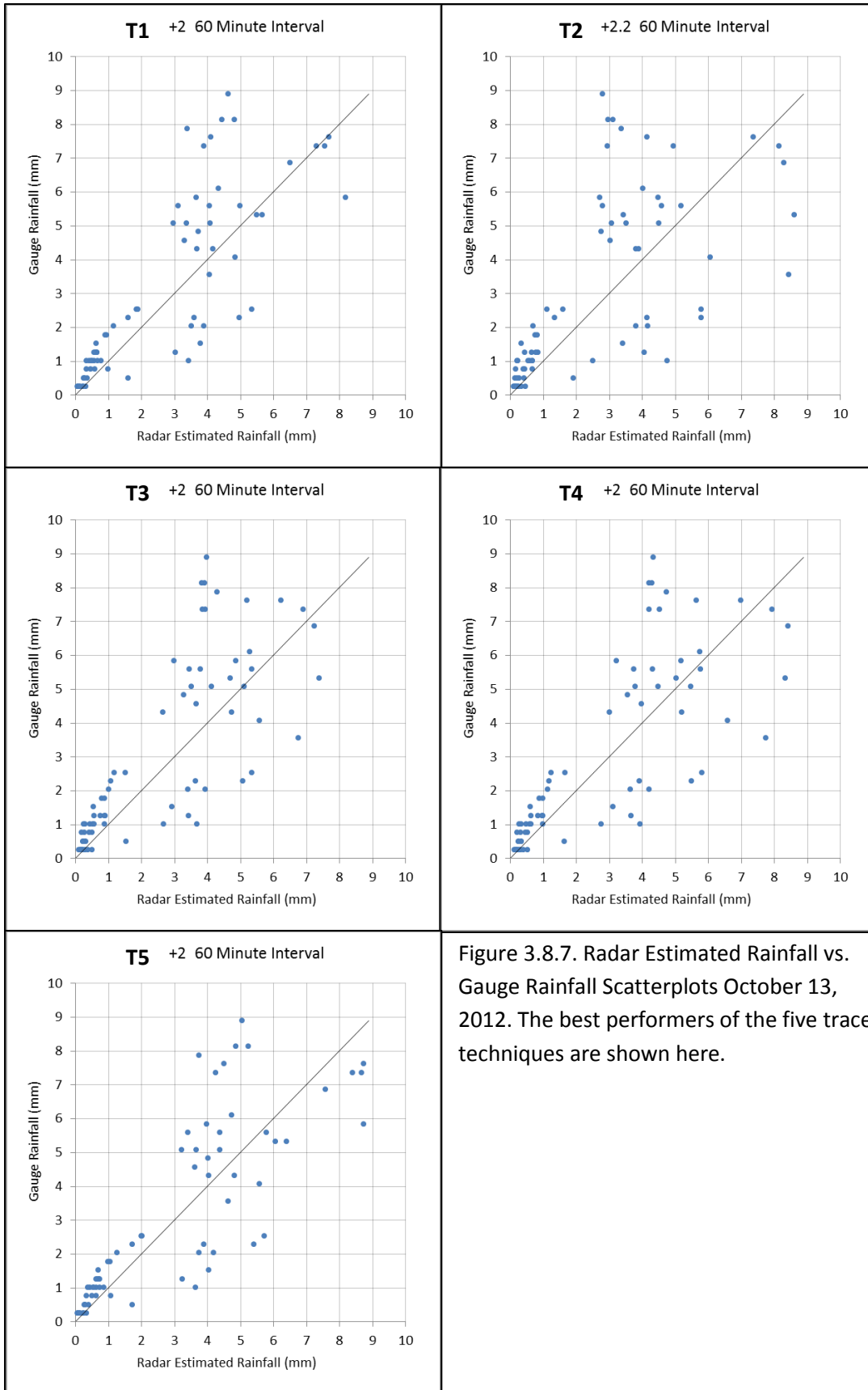
Figure 3.8.7. Radar Estimated Rainfall vs. Gauge Rainfall Scatterplots October 13, 2012. The best performers of the five trace techniques are shown here.

3.9 March 10, 2013

The rainfall event on March 10 took place to the east of an occluded low pressure center and several associated fronts. Figure 3.9.1 is an HPC surface analysis for 06 UTC of March, 2012. Figure 3.9.2 shows humidity versus height in percentile format for 01 UTC through 11 UTC of March 10. The atmosphere was very dry near the surface initially, but moistened as the event progressed. Figure 3.9.3 is a hodograph for the 13th of October. The hodograph shows a southerly wind at the surface turning southwesterly higher up. Figure 3.9.4 is a four panel radar image from KLSX for 0631 UTC of March 10.

3.9.1 Conventional Formulas

Table 3.9.1 shows the performance of the conventional formulas for this event. (1), (2), and (4) performed the best out of the conventional formulas, and as a whole the Z-R formulas performed better than the Z,Z_{DR}-R formulas. All of the K_{DP}-reliant formulas performed very poorly for this date. The K_{DP}-reliant formulas exhibited very positive biases, while the other conventional formulas tended to have negative biases.

3.9.2 Tracing Techniques

Table 3.9.2 shows the performance of the various trace techniques and their permutations for this event. Techniques T2, T4, and T5 were most effective at the $+Z_{DR}$ values of around 1.4, while T1 and T3 were most effective at $+Z_{DR}$ values near 1. The optimal tracing techniques performed similarly to the non-K_{DP} reliant conventional formulas for this event.

3.5.3 Graphical Evaluation

Figure 3.9.5 is a histogram showing the FAD performance of each evaluated technique

for this event. Figure 3.9.6 is the equivalent histogram showing FRMSE performance.

Figure 3.9.7 shows a combination of scatterplots of radar-derived rainfall versus rain

gauge rainfall for the conventional formulas. The techniques illustrated were the top

performers in each category. Figure 3.9.8 is identical to 3.9.7, except it depicts the best

performers of the trace techniques.
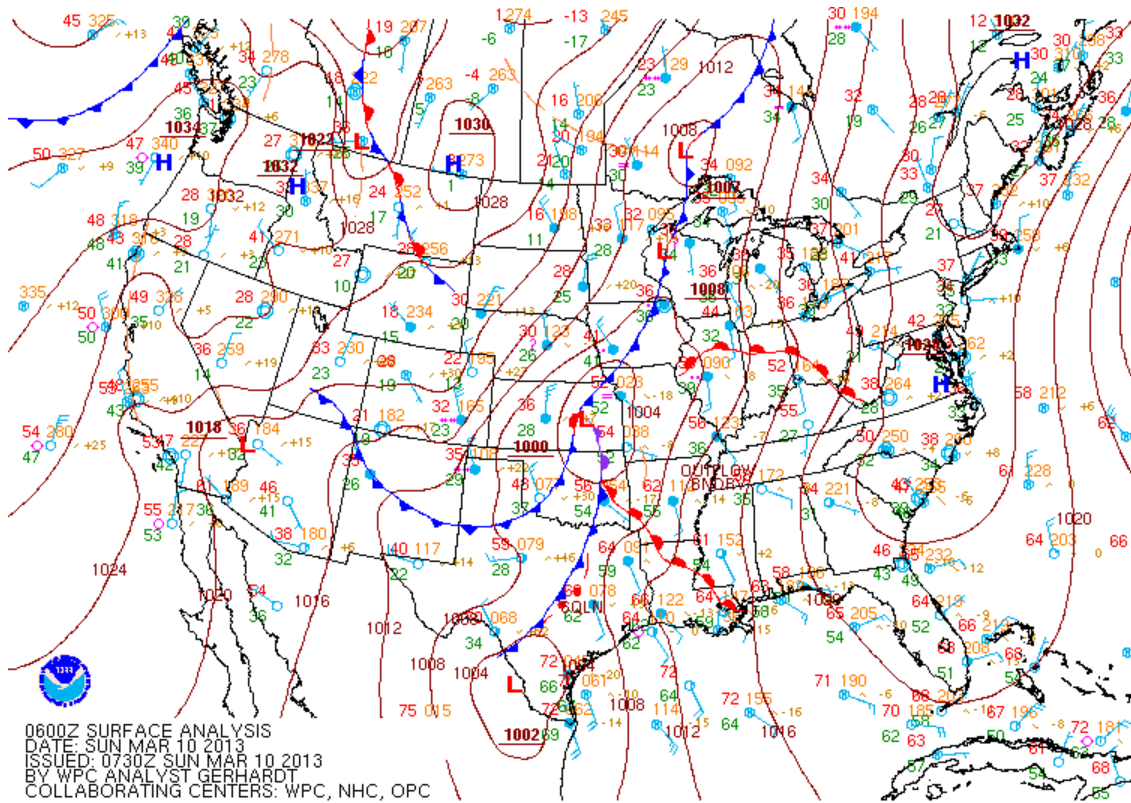
Figure 3.9.1. Surface Analysis 0600 UTC March 10, 2013.
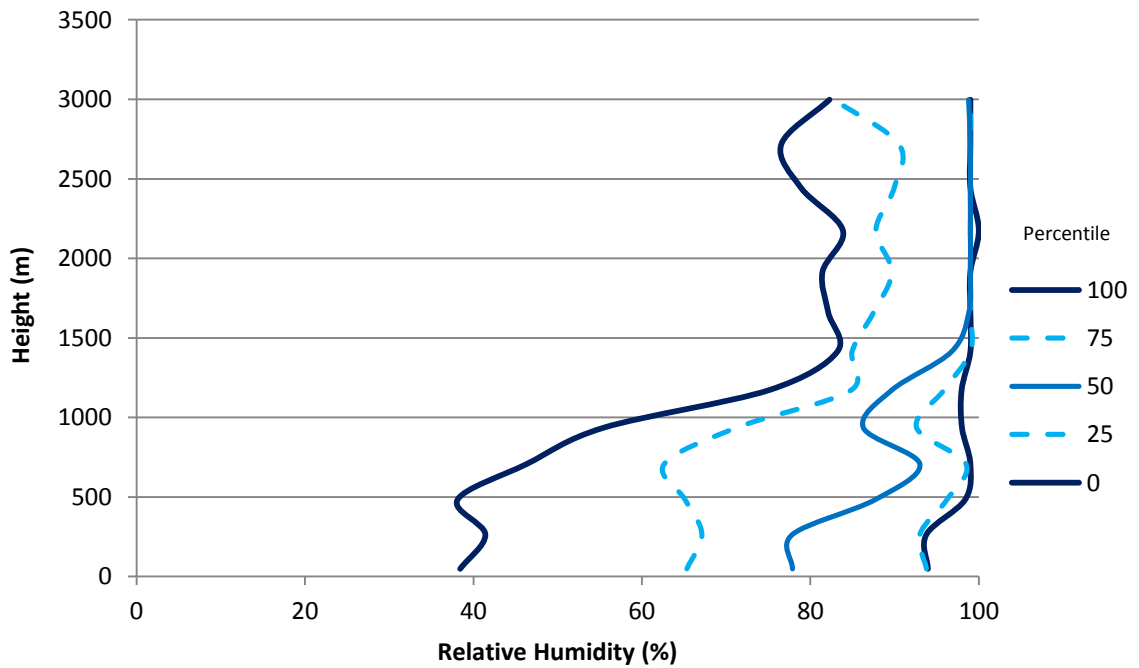
Figure 3.9.2. Relative Humidity Profile March 10, 2013.
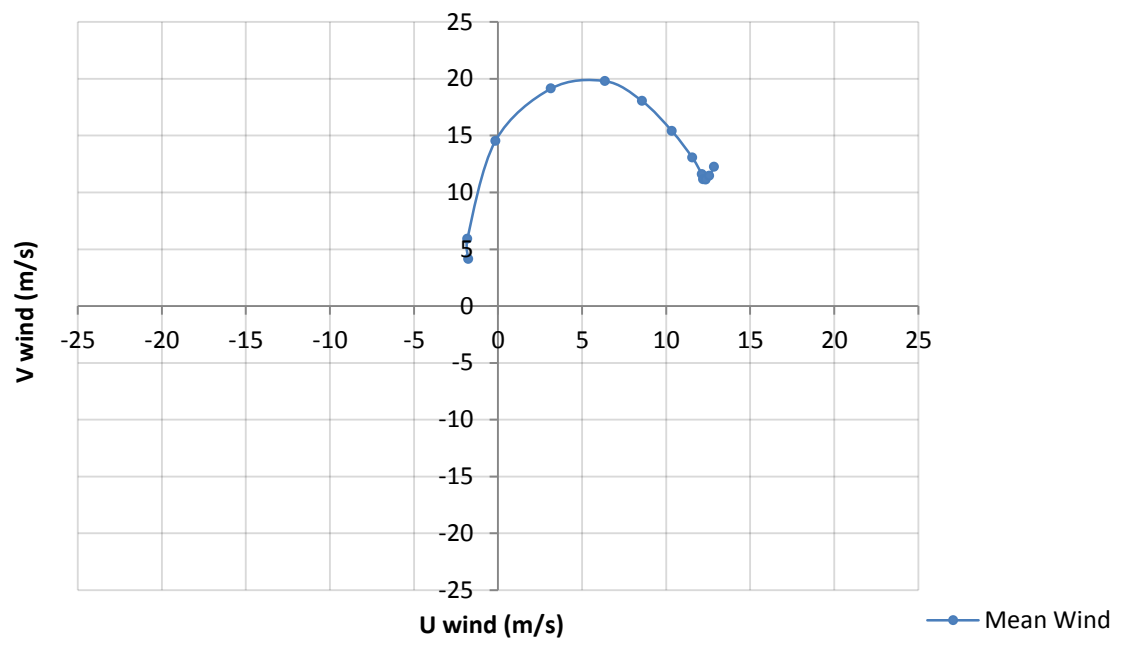
Figure 3.9.3. Hodograph March 10, 2013.
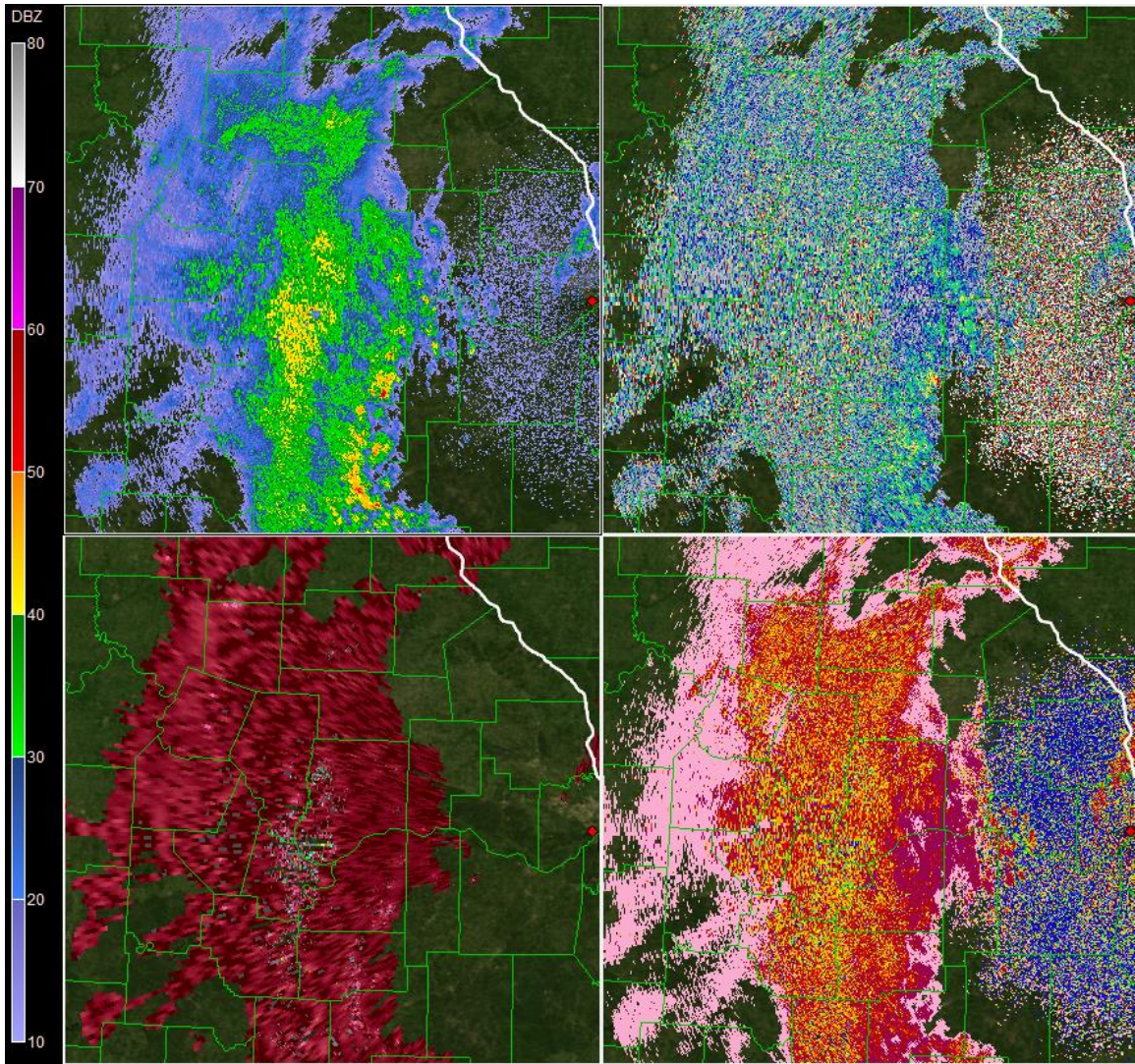
Figure 3.9.4. Four Panel Radar Image for 0631 UTC March 10, 2013. The top left is reflectivity (Z), top right is differential reflectivity (Z_{DR}), bottom left is specific phase differential (K_{DP}), and bottom right is correlation coefficient. The scale on the left corresponds to the top left image (Z). The elevation angle used here was 0.5°.

Table 3.9.1 Conventional Techniques, March 10, 2013

$Z = aR^b$	#	FB(%)	FAD(%)	FRMSE(%)	FSD(%)
1	45	-2.68	47.73	55.54	55.48
2	45	-13.28	47.45	57.40	55.84
3	45	22.93	57.41	69.13	65.21
4	45	-16.54	47.20	57.62	55.19
5	45	-42.32	51.10	68.21	53.49
$R(K_{DP}) = a|K_{DP}|^b sign(K_{DP})$					
6	52	63.19	212.88	278.71	271.45
7	52	78.86	235.74	308.69	298.44
8	52	78.98	240.24	311.52	301.35
9	51	43.59	188.04	241.39	237.43
10	52	65.16	216.95	283.07	275.47
11	52	57.05	206.75	268.57	262.45
$R(Z, Z_{DR}) = aZ^b Z_{dr}{}^c$					
12	45	6.41	59.47	70.50	70.20
13	45	24.86	69.76	86.29	82.63
14	45	-14.40	49.15	60.23	58.49
15	45	-18.04	48.18	59.49	56.69
16	45	-17.06	48.74	60.21	57.75
$R(K_{DP}, Z_{DR}) = a|K_{DP}|^b Z_{dr}{}^c sign(K_{DP})$					
17	53	142.18	326.26	424.72	400.22
18	53	224.51	452.05	579.75	534.51
19	53	65.77	217.09	284.59	276.88
20	53	95.78	258.59	340.27	326.51
Synthetic					
21	45	5.25	59.62	87.58	87.42

Table 3.9.2 Trace Techniques, March 10, 2013

	Z_{DR} +	#	FB(%)	FAD(%)	FRMSE(%)	FSD(%)
T1	0	45	53.66	71.04	87.90	69.62
	0.2	45	40.63	64.79	76.94	65.34
	0.3	45	33.73	61.60	71.72	63.30
	0.4	45	26.81	58.33	66.89	61.28
	0.5	45	19.90	55.36	62.90	59.67
	0.6	45	13.17	52.97	60.20	58.74
	0.7	45	6.65	50.61	58.26	57.88
	0.8	45	0.26	48.35	56.98	56.98
	0.9	45	-5.85	46.58	56.49	56.19
	1	45	-11.42	44.99	56.72	55.55
	1.1	45	-16.72	43.94	57.65	55.17
	1.5	45	-33.70	44.77	63.89	54.29
	2	45	-49.58	51.84	72.24	52.54
	2.6	45	-62.32	62.51	80.40	50.80
T2	0.4	46	82.40	100.27	137.62	110.22
	0.6	45	56.46	85.20	109.97	94.37
	0.8	45	32.20	71.36	88.90	82.87
	1	45	12.34	61.83	75.34	74.32
	1.2	45	-3.74	54.51	67.91	67.81
	1.4	45	-16.28	50.56	65.40	63.34
	1.6	45	-26.42	49.21	65.62	60.07
	1.8	45	-34.68	49.27	67.29	57.66
	2	45	-41.64	50.97	69.54	55.69
	2.2	45	-47.60	54.01	72.32	54.45
	2.4	45	-52.84	57.29	75.11	53.38
	2.6	45	-57.32	60.48	77.79	52.59
T3	0	45	54.23	67.86	93.93	76.70
	0.2	45	39.23	60.77	82.41	72.47
	0.3	45	32.00	58.43	77.52	70.60
	0.4	45	24.81	56.18	72.87	68.52
	0.5	45	17.68	54.10	68.68	66.37
	0.6	45	10.76	52.00	65.28	64.39
	0.7	45	3.74	49.55	62.35	62.24
	0.8	45	-2.93	47.65	60.31	60.24
	0.9	45	-9.15	46.16	59.25	58.54
	1	45	-14.87	45.41	59.05	57.15
	1.1	45	-20.19	45.23	59.47	55.94
	1.5	45	-37.15	48.19	64.54	52.78
	2	45	-51.71	54.90	72.46	50.75
	2.6	45	-63.78	64.89	80.79	49.58

Table 3.9.2 Trace Techniques, March 10, 2013 (Continued)

	Z_{DR} +	#	FB(%)	FAD(%)	FRMSE(%)	FSD(%)
T4	0.4	45	82.14	94.69	133.86	105.69
	0.6	45	56.34	80.70	107.58	91.64
	0.8	45	32.06	67.37	86.13	79.94
	1	45	12.21	58.27	72.62	71.58
	1.2	45	-3.87	51.47	65.44	65.33
	1.4	45	-16.40	46.84	63.34	61.18
	1.6	45	-26.53	46.13	64.02	58.27
	1.8	45	-34.78	47.60	66.06	56.16
	2	45	-41.73	50.43	68.60	54.45
	2.2	45	-47.67	53.61	71.57	53.38
	2.4	45	-52.91	56.55	74.49	52.43
	2.6	45	-57.39	59.83	77.27	51.74
T5	0.4	45	88.12	101.79	129.18	94.46
	0.6	45	62.53	86.22	105.64	85.15
	0.8	45	39.28	73.94	87.07	77.70
	1	45	18.86	63.06	73.26	70.79
	1.2	45	2.08	55.45	66.62	66.58
	1.4	45	-10.89	50.75	65.00	64.08
	1.6	45	-21.89	47.99	65.32	61.54
	1.8	45	-31.19	47.05	67.11	59.42
	2	45	-38.94	47.70	69.43	57.49
	2.2	45	-45.38	50.18	71.98	55.88
	2.4	45	-50.83	53.20	74.57	54.57
	2.6	45	-55.48	57.10	77.11	53.56
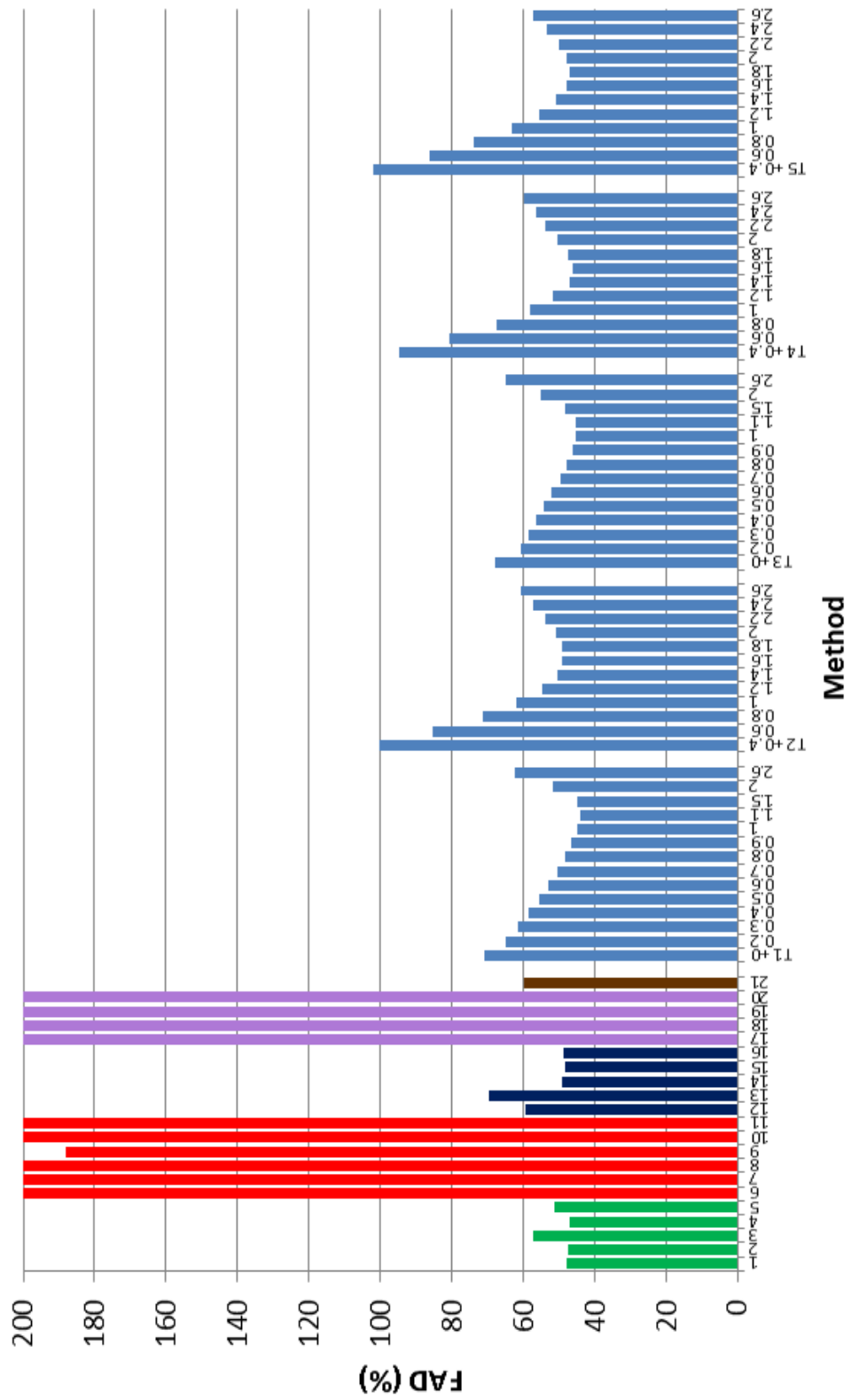
Figure 3.9.5. FAD Performance March 10, 2013.

149
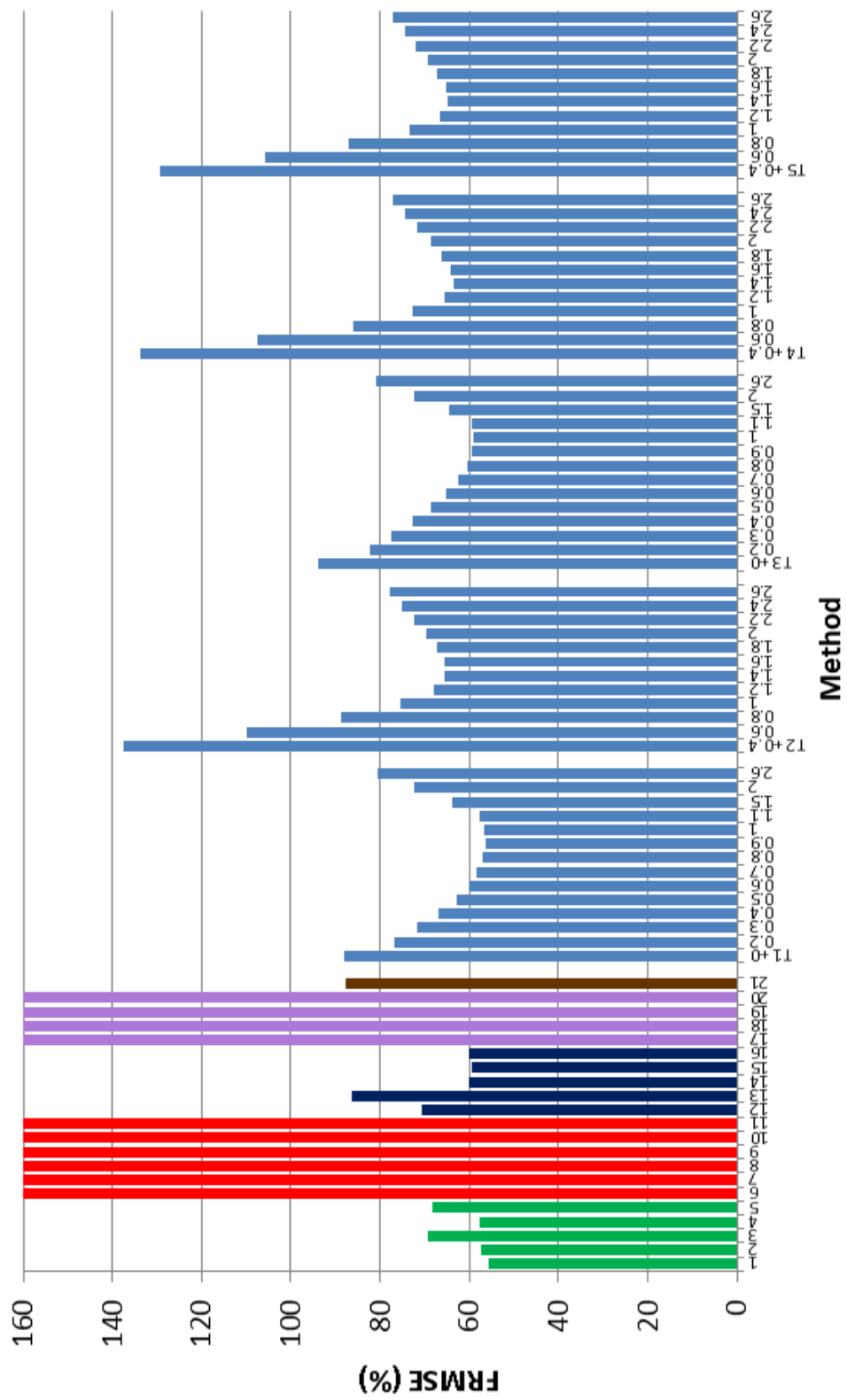
Figure 3.9.6. FRMSE Performance March 10, 2013.
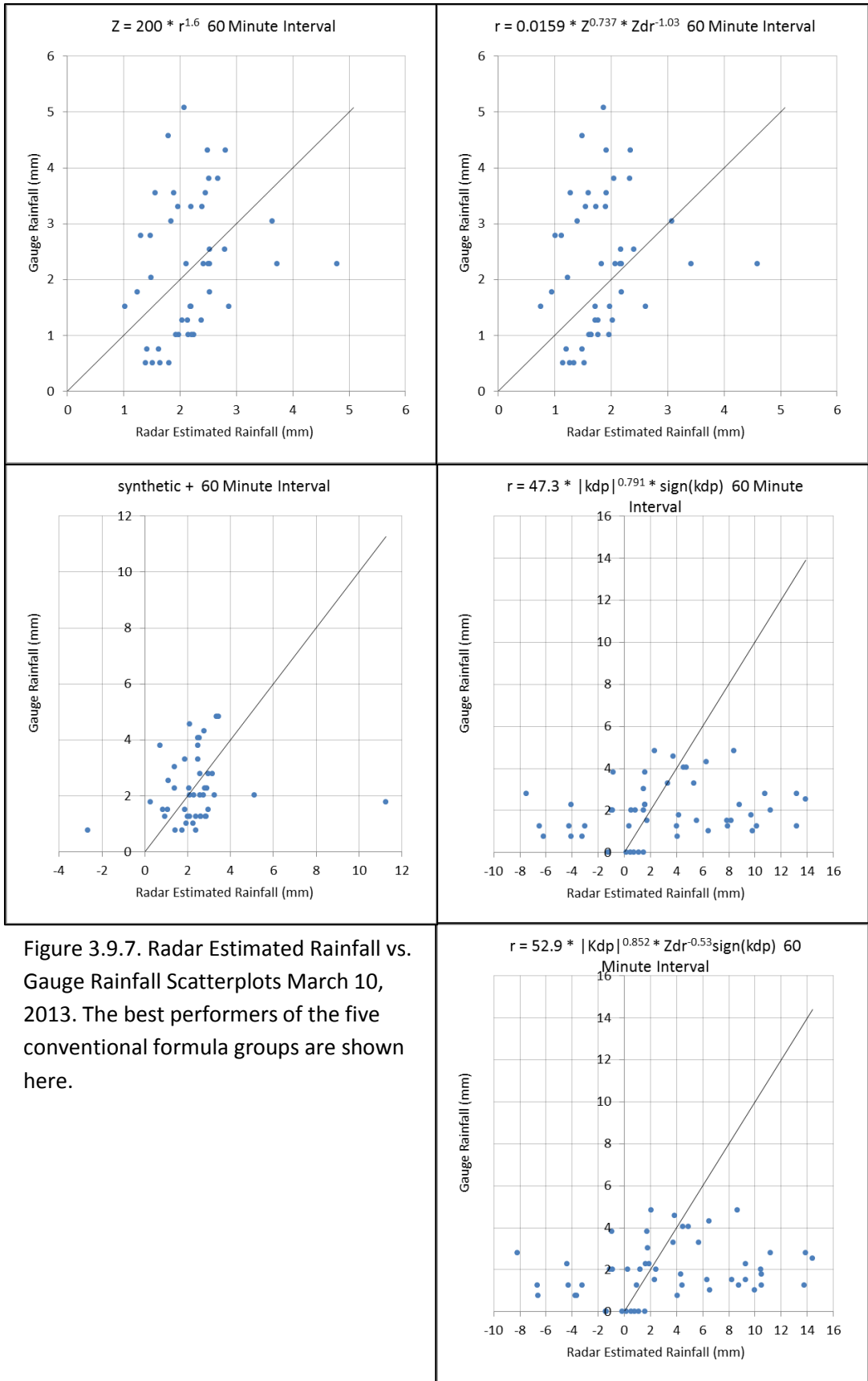
Figure 3.9.7. Radar Estimated Rainfall vs. Gauge Rainfall Scatterplots March 10, 2013. The best performers of the five conventional formula groups are shown here.

151
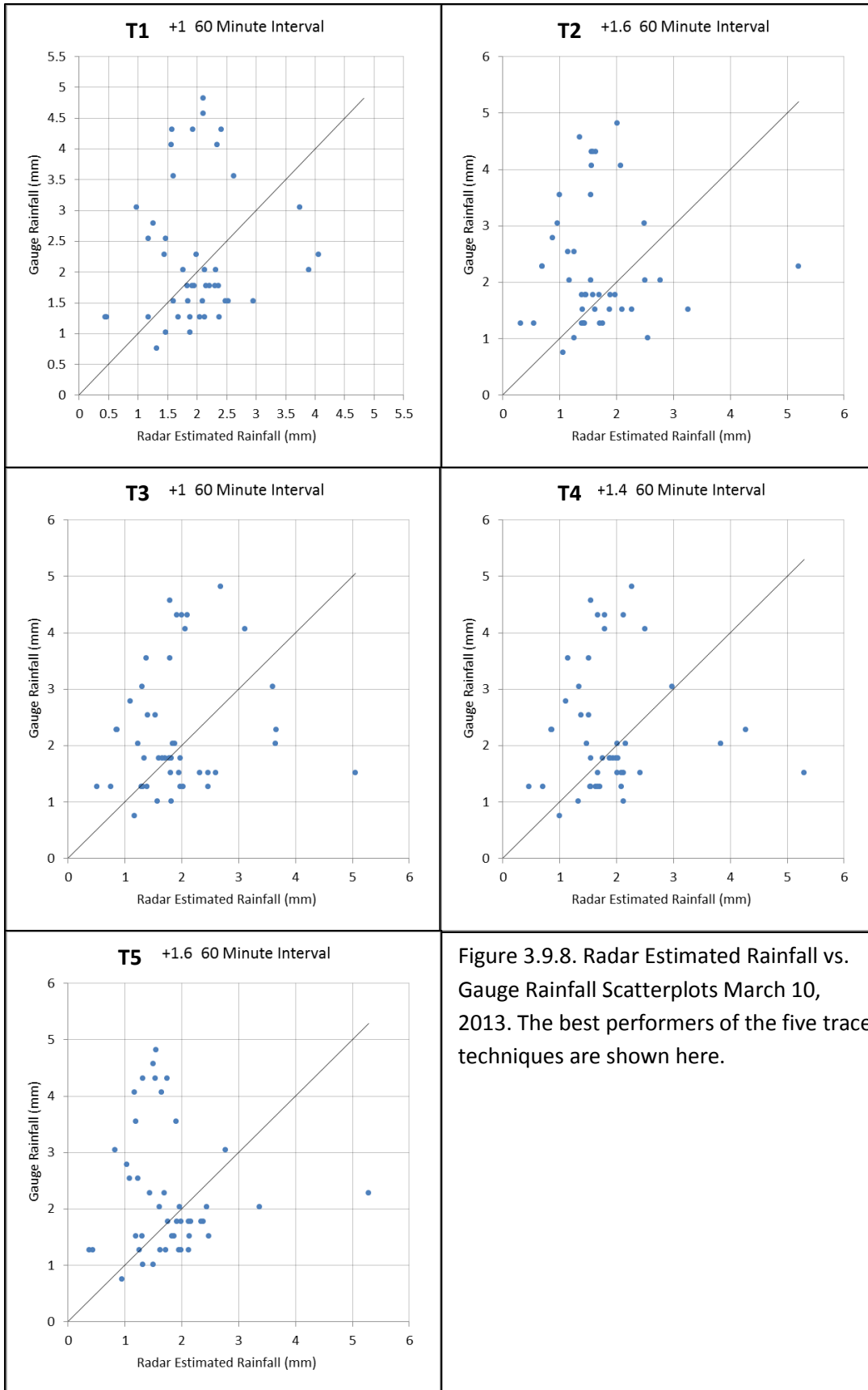
Figure 3.9.8. Radar Estimated Rainfall vs. Gauge Rainfall Scatterplots March 10, 2013. The best performers of the five trace techniques are shown here.

152

3.10 April 10, 2013

The event on April 10 was associated with two low pressure centers almost directly on top of Columbia. Figure 3.10.1 is an HPC surface analysis for 21 UTC of April 10. Figure 3.10.2 shows humidity versus height in percentile format for 19 UTC of April 10 through 05 UTC of April 11. The atmosphere was moist at the lowest layers throughout the event. Initially a dry layer was present above 750 meters, but it quickly reached saturation as the event progressed. Figure 3.10.3 is a hodograph for the 10th of April. The hodograph shows the wind direction turning clockwise with height, changing from northwesterly at the surface to southwesterly at 700 millibars. Figure 3.10.4 is a four panel radar image from KLSX for 2154 UTC of April 10.

3.10.1 Conventional Formulas

Table 3.10.1 shows the performance of the conventional formulas for this event. The most basic Z-R relationship, (1), was the top performer of the conventional formulas. Of the non-K_{DP} reliant formulas, three outliers were present, (3, 12, and 13 again). The K_{DP}-reliant formulas again performed poorly.

3.10.2 Tracing Techniques

Table 3.10.2 shows the performance of the various trace techniques and their permutations for this event. Techniques T1 and T5 were most effective at +Z_{DR} values of 2.6, while the other tracing techniques were most effective at +Z_{DR} values of 2. The first two in this case accounted for drift while the latter three did not. As a whole, the optimal tracing techniques performed slightly worse than the (non-K_{DP} reliant)

conventional formulas on this date. The April 10 event may have been another case where the modeled humidity was inaccurate (too high), due to the large optimal +Z_{DR} values for T1 and T3.

3.5.3 Graphical Evaluation

Figure 3.10.5 is a histogram showing the FAD performance of each evaluated technique for this event. Figure 3.10.6 is the equivalent histogram showing FRMSE performance.

Figure 3.10.7 shows a combination of scatterplots of radar-derived rainfall versus rain gauge rainfall for the conventional formulas. The techniques illustrated were the top performers in each category. Figure 3.10.8 is identical to 3.10.7, except it depicts the best performers of the trace techniques.
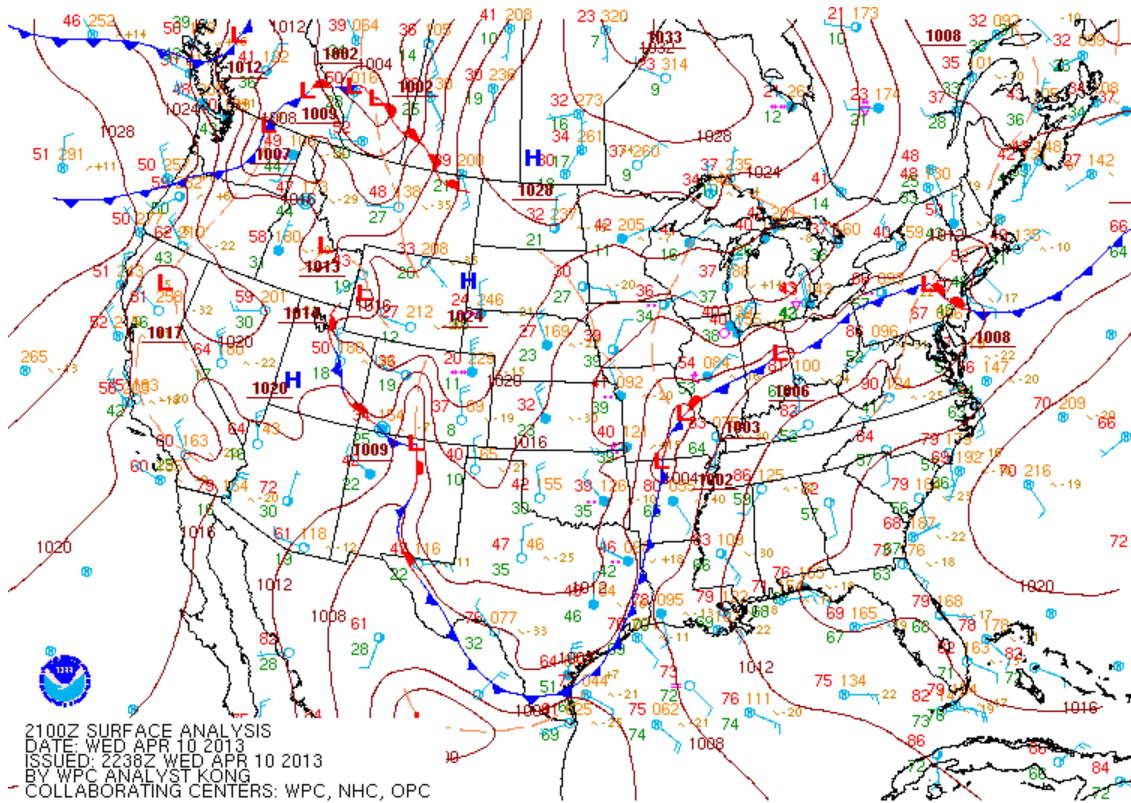
Figure 3.10.1. Surface Analysis 2100 UTC April 10, 2013.
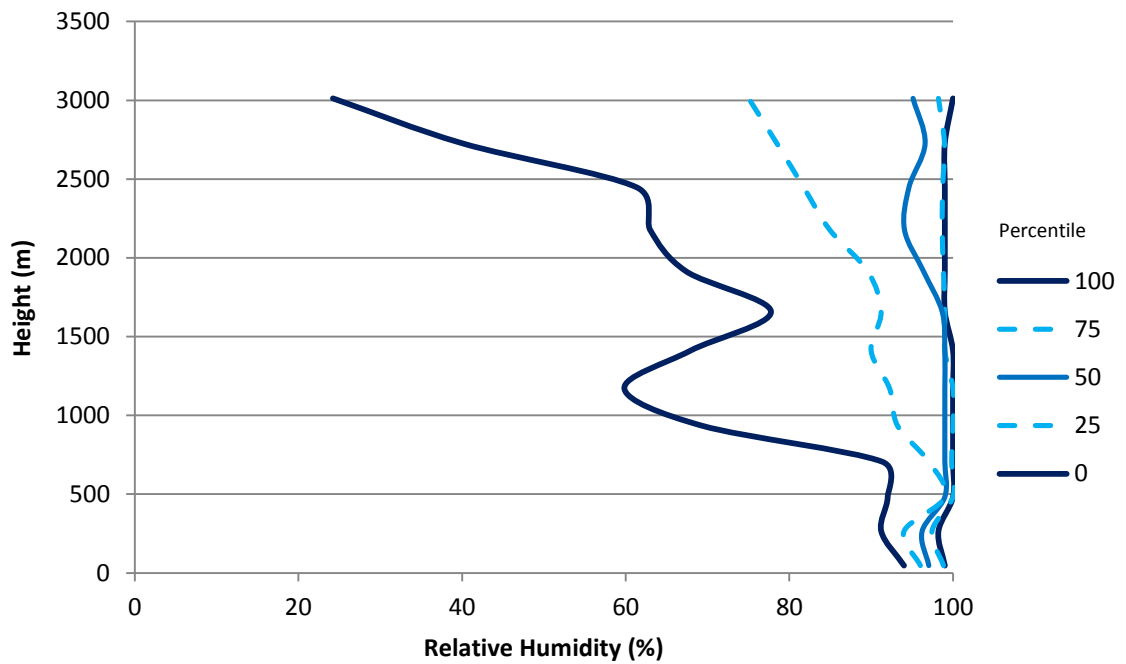
Figure 3.10.2. Relative Humidity Profile April 10, 2013.
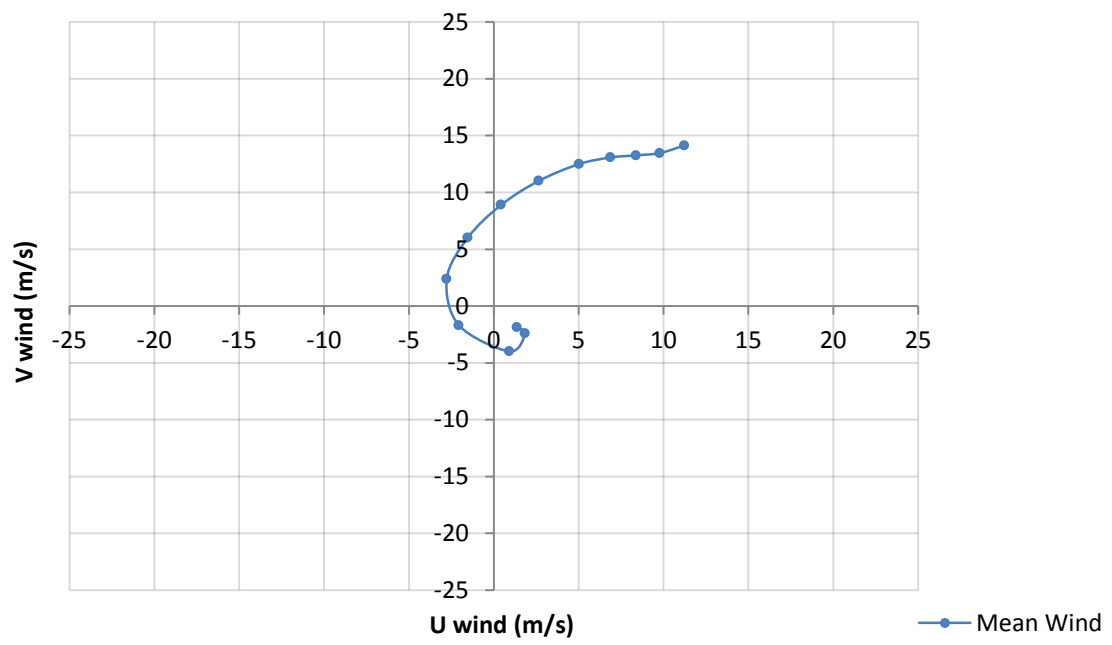
Figure 3.10.3. Hodograph April 10, 2013.
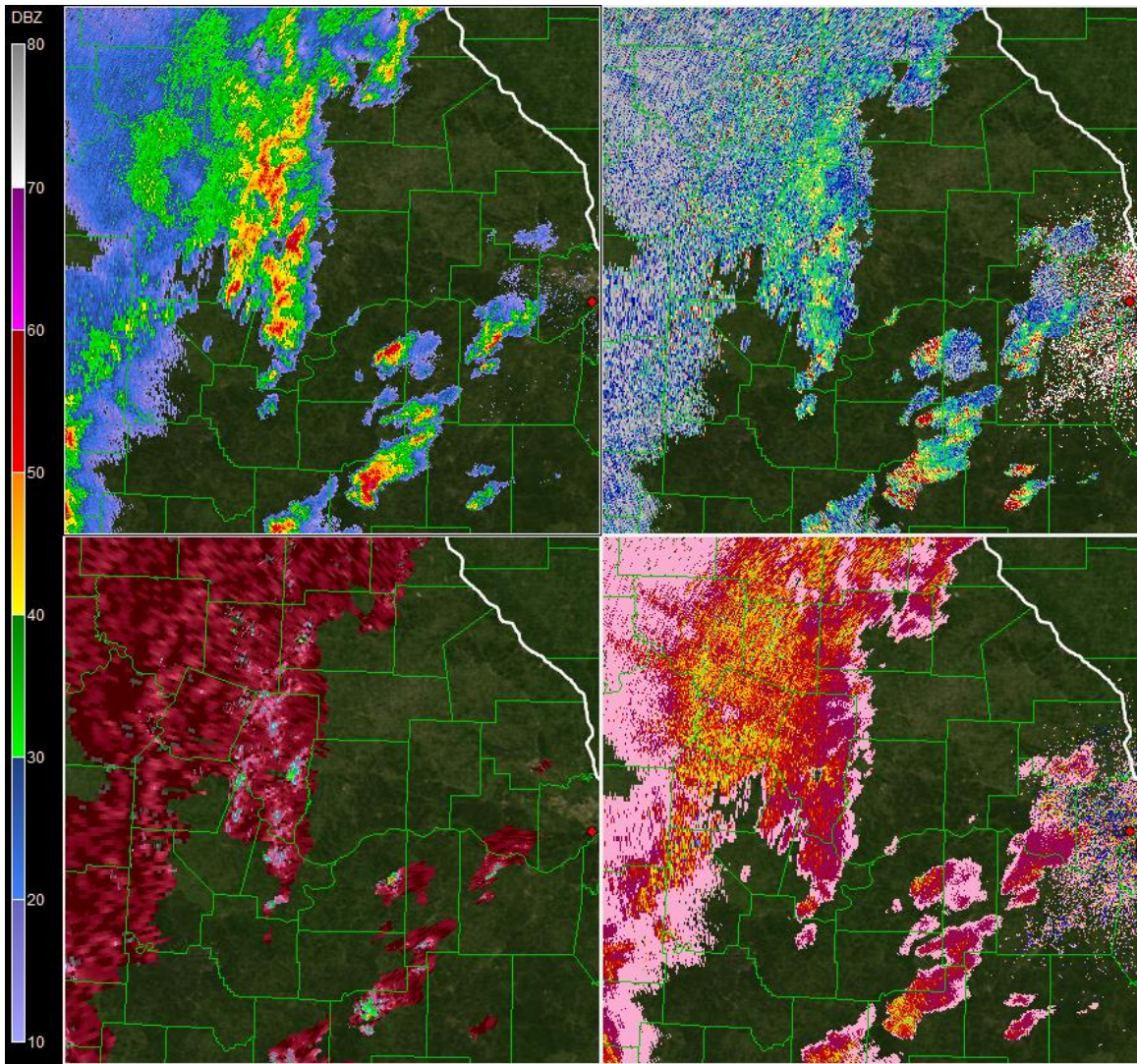
Figure 3.10.4. Four Panel Radar Image for 2154 UTC April 10, 2013. The top left is reflectivity (Z), top right is differential reflectivity (Z_{DR}), bottom left is specific phase differential (K_{DP}), and bottom right is correlation coefficient. The scale on the left corresponds to the top left image (Z). The elevation angle used here was 0.5^{o}.

Table 3.10.1 Conventional Techniques, April 10, 2013

$Z = aR^b$	#	FB(%)	FAD(%)	FRMSE(%)	FSD(%)
1	59	-6.02	31.72	47.56	47.18
2	59	3.07	36.04	59.11	59.03
3	59	96.13	114.49	205.86	182.04
4	59	-5.38	32.95	52.21	51.93
5	59	-32.26	39.10	57.52	47.62
$R(K_{DP}) = a|K_{DP}|^b sign(K_{DP})$					
6	61	32.54	82.19	129.99	125.85
7	61	45.20	91.17	143.65	136.36
8	61	45.52	90.53	138.30	130.59
9	61	16.68	70.97	109.81	108.54
10	61	34.08	82.98	129.64	125.07
11	61	27.50	78.19	120.42	117.24
$R(Z, Z_{DR}) = a Z^b Z_{dr}{}^c$					
12	59	-1.79	35.75	51.62	51.59
13	59	0.13	40.82	60.81	60.81
14	59	-23.02	33.98	49.56	43.89
15	59	-23.25	34.11	49.27	43.44
16	59	-24.80	34.73	50.65	44.17
$R(K_{DP}, Z_{DR}) = a|K_{DP}|^b Z_{dr}{}^c sign(K_{DP})$					
17	61	64.71	110.08	173.00	160.44
18	61	97.44	143.48	232.19	210.76
19	61	27.00	78.02	119.19	116.09
20	61	46.96	93.17	143.95	136.08
Synthetic					
21	61	12.86	60.77	99.45	98.61

Table 3.10.2 Trace Techniques, April 10, 2013

	Z_{DR} +	#	FB(%)	FAD(%)	FRMSE(%)	FSD(%)
T1	0	56	149.48	164.86	280.14	236.93
	0.2	56	124.93	141.86	246.03	211.95
	0.3	56	113.94	131.53	230.79	200.71
	0.4	56	103.49	121.69	216.01	189.61
	0.5	56	93.67	112.42	202.74	179.81
	0.6	55	84.47	103.98	189.31	169.42
	0.7	55	75.29	95.62	176.80	159.97
	0.8	54	66.54	88.22	163.24	149.07
	0.9	54	58.46	81.97	152.39	140.73
	1	54	50.65	75.86	141.86	132.51
	1.1	54	43.81	70.58	133.26	125.85
	1.5	54	21.05	55.28	106.70	104.60
	2	54	-1.53	44.50	82.90	82.89
	2.6	53	-23.14	42.76	72.42	68.63
T2	0.4	55	114.52	126.55	196.95	160.23
	0.6	55	89.70	103.80	163.20	136.34
	0.8	55	68.80	85.26	136.15	117.48
	1	55	51.77	70.90	115.92	103.72
	1.2	55	37.04	59.93	98.76	91.55
	1.4	55	25.06	52.55	87.13	83.45
	1.6	55	14.37	46.75	77.41	76.07
	1.8	55	4.91	43.87	72.00	71.84
	2	55	-3.22	41.74	70.48	70.41
	2.2	55	-10.14	43.38	72.22	71.50
	2.4	55	-15.97	46.60	76.54	74.85
	2.6	55	-21.47	50.56	80.72	77.81
T3	0	58	139.73	150.00	247.34	204.08
	0.2	58	115.61	127.76	213.18	179.11
	0.3	58	104.29	117.30	197.15	167.31
	0.4	58	94.01	108.46	182.85	156.83
	0.5	58	83.43	99.44	167.65	145.42
	0.6	58	73.10	90.62	153.18	134.62
	0.7	57	63.71	82.59	139.18	123.75
	0.8	56	55.05	75.41	126.51	113.90
	0.9	55	47.27	69.09	115.77	105.68
	1	55	40.20	63.54	107.13	99.30
	1.1	55	33.43	58.33	98.64	92.80
	1.5	55	11.66	42.95	75.43	74.52
	2	54	-9.03	35.97	64.40	63.76
	2.6	54	-25.77	45.00	75.01	70.44

Table 3.10.2 Trace Techniques, April 10, 2013 (Continued)

	Z_{DR} +	#	FB(%)	FAD(%)	FRMSE(%)	FSD(%)
T4	0.4	58	114.23	126.30	204.82	170.01
	0.6	58	89.45	103.77	170.60	145.28
	0.8	57	68.52	85.29	141.35	123.63
	1	55	51.43	70.60	117.84	106.02
	1.2	55	36.77	58.41	99.49	92.45
	1.4	55	24.85	49.65	86.63	82.99
	1.6	55	14.18	42.30	75.67	74.33
	1.8	54	4.71	36.46	68.45	68.29
	2	54	-3.40	35.60	66.05	65.96
	2.2	54	-10.30	36.59	67.19	66.40
	2.4	54	-16.12	38.87	71.26	69.42
	2.6	54	-21.61	42.86	75.46	72.29
T5	0.4	56	123.93	138.30	239.19	204.59
	0.6	56	101.40	116.72	210.30	184.24
	0.8	55	80.62	97.66	180.28	161.25
	1	54	62.44	81.84	154.17	140.96
	1.2	54	47.71	70.02	135.90	127.25
	1.4	54	34.98	60.28	120.44	115.25
	1.6	54	23.62	52.65	106.31	103.65
	1.8	54	13.45	46.77	94.27	93.31
	2	54	4.61	43.97	85.86	85.74
	2.2	54	-3.64	42.16	79.89	79.81
	2.4	53	-11.41	40.72	74.90	74.02
	2.6	53	-18.75	41.19	72.09	69.61
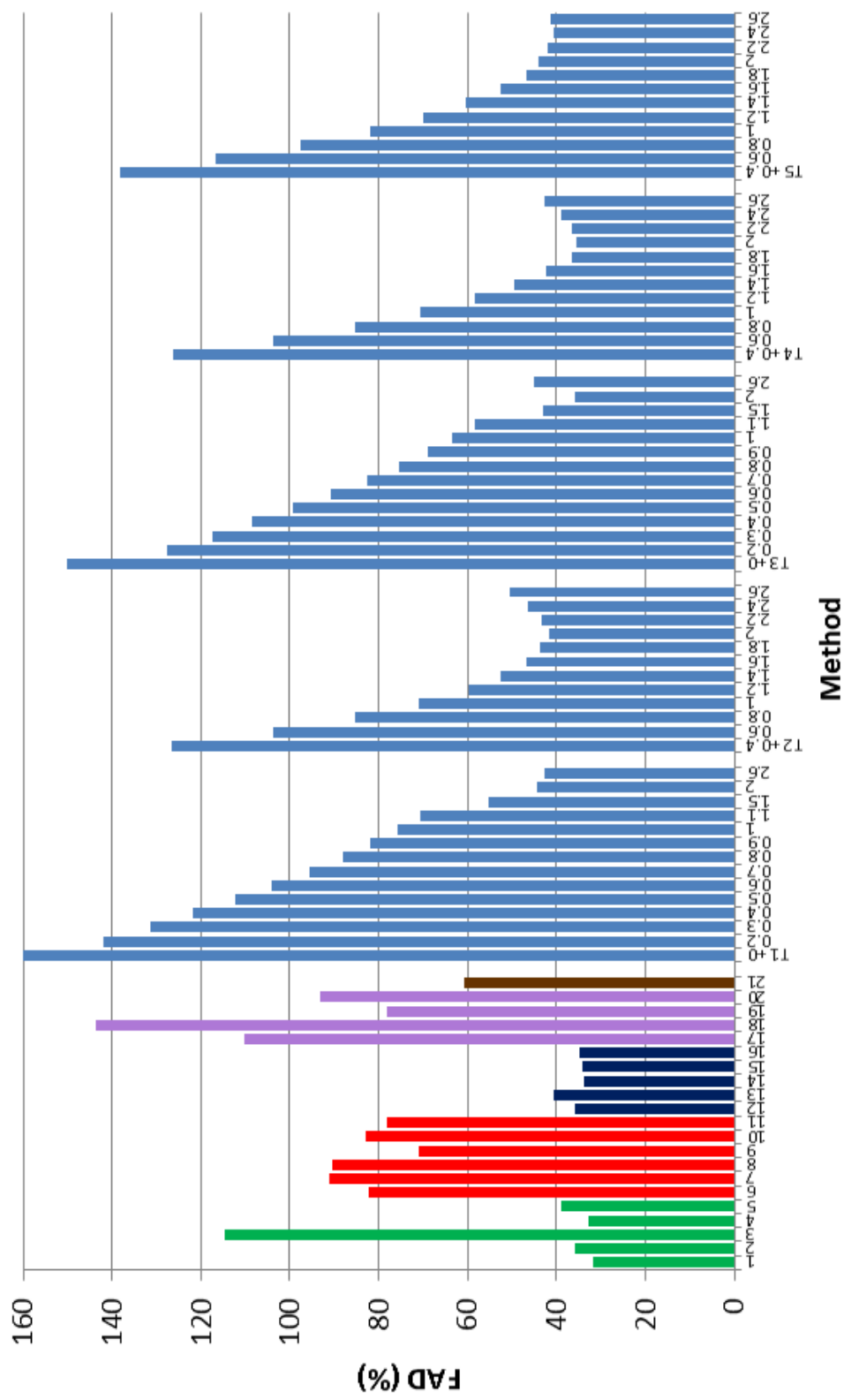
Figure 3.10.5. FAD Performance April 10, 2013.

161
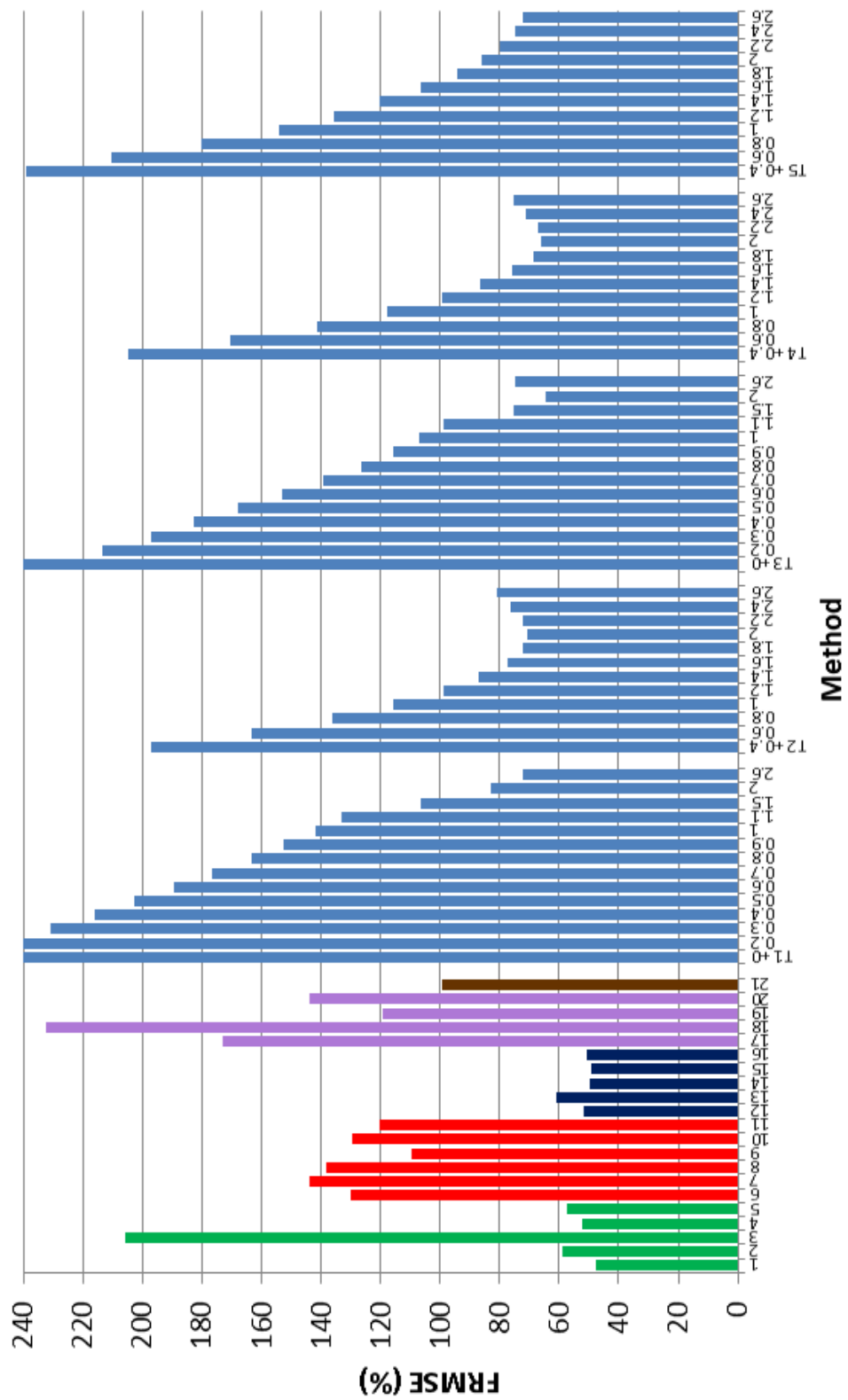
Figure 3.10.6. FRMSE Performance April 10, 2013.
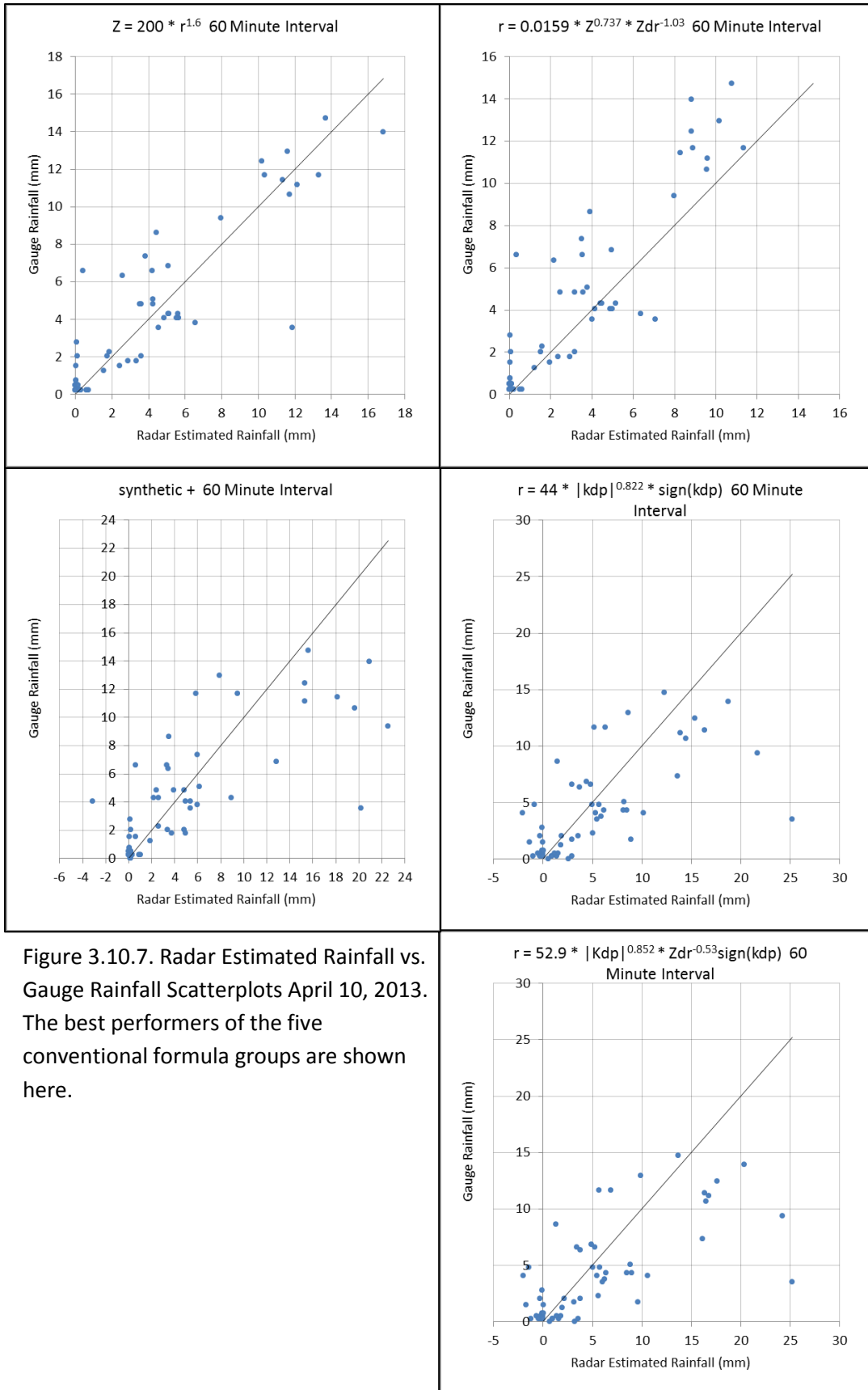
Figure 3.10.7. Radar Estimated Rainfall vs. Gauge Rainfall Scatterplots April 10, 2013. The best performers of the five conventional formula groups are shown here.
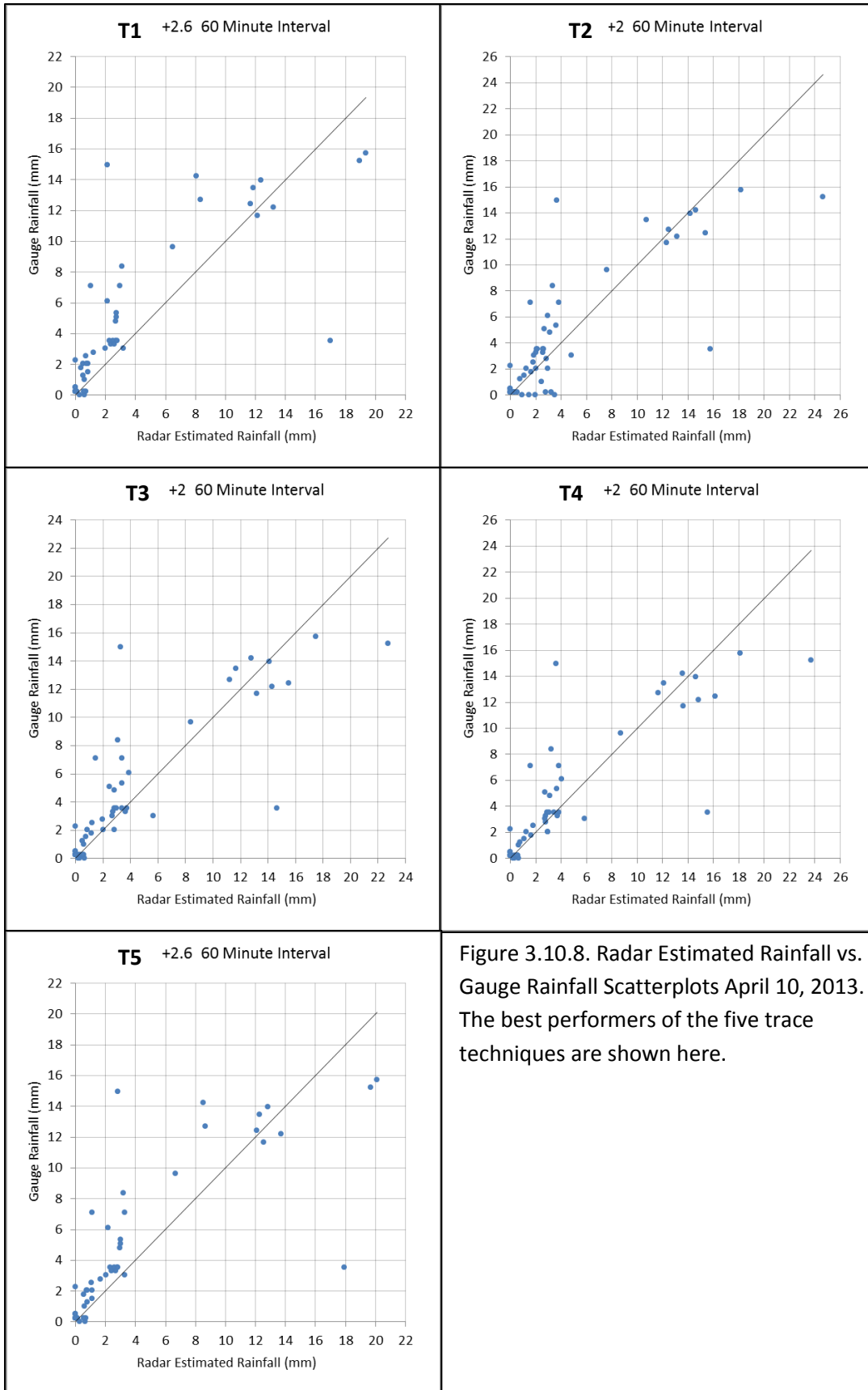
Figure 3.10.8. Radar Estimated Rainfall vs. Gauge Rainfall Scatterplots April 10, 2013. The best performers of the five trace techniques are shown here.

3.11 April 17, 2013

A second hail event occurred on the 17th of April. Up to baseball size hail was reported at locations around Central Missouri. This rainfall event took place along the stationary front located to the east of a low pressure center. Figure 3.11.1 is an HPC surface analysis for 00 UTC of April 18. Figure 3.11.2 shows humidity versus height in percentile format for 19 UTC of April 17 through 11 UTC of April 18. The same pattern seen earlier of a moistening atmosphere was present for this event. Figure 3.11.3 is a hodograph for the 10th of April. The hodograph shows the wind direction transitioning from southeasterly at the surface to southwesterly aloft. Figure 3.11.4 is a four panel radar image from KLSX for 0743 UTC of April 18.

3.11.1 Conventional Formulas

Formulas involving K_{DP} were not evaluated for the April 17 event due to lack of data.

Table 3.11.1 shows the performance of the conventional techniques for this event. The presence of large hail again caused poor performance for all conventional formulas. Mostly positive biases were present, and (3) was again an outlier.

3.11.2 Tracing Techniques

Table 3.11.2 shows the performance of the various trace techniques and their permutations for this event. Many of the same patterns from the hail event on September 7, 2012, were also present on this date. The optimal Z_{DR} adjustment for each of the five tracing techniques lay in the 1- 1.5 range, and the optimal T1 technique again performed the best. The optimal T1 and T3 techniques significantly outperformed all

other methods on this date. Biases for the tracing techniques were mostly positive for this event.

3.5.3 Graphical Evaluation

Figure 3.11.5 is a histogram showing the FAD performance of each evaluated technique for this event. Figure 3.11.6 is the equivalent histogram showing FRMSE performance.

Figure 3.11.7 shows a combination of scatterplots of radar-derived rainfall versus rain gauge rainfall for the conventional formulas. The techniques illustrated were the top performers in each category. Figure 3.11.8 is identical to 3.11.7, except it depicts the best performers of the trace techniques.
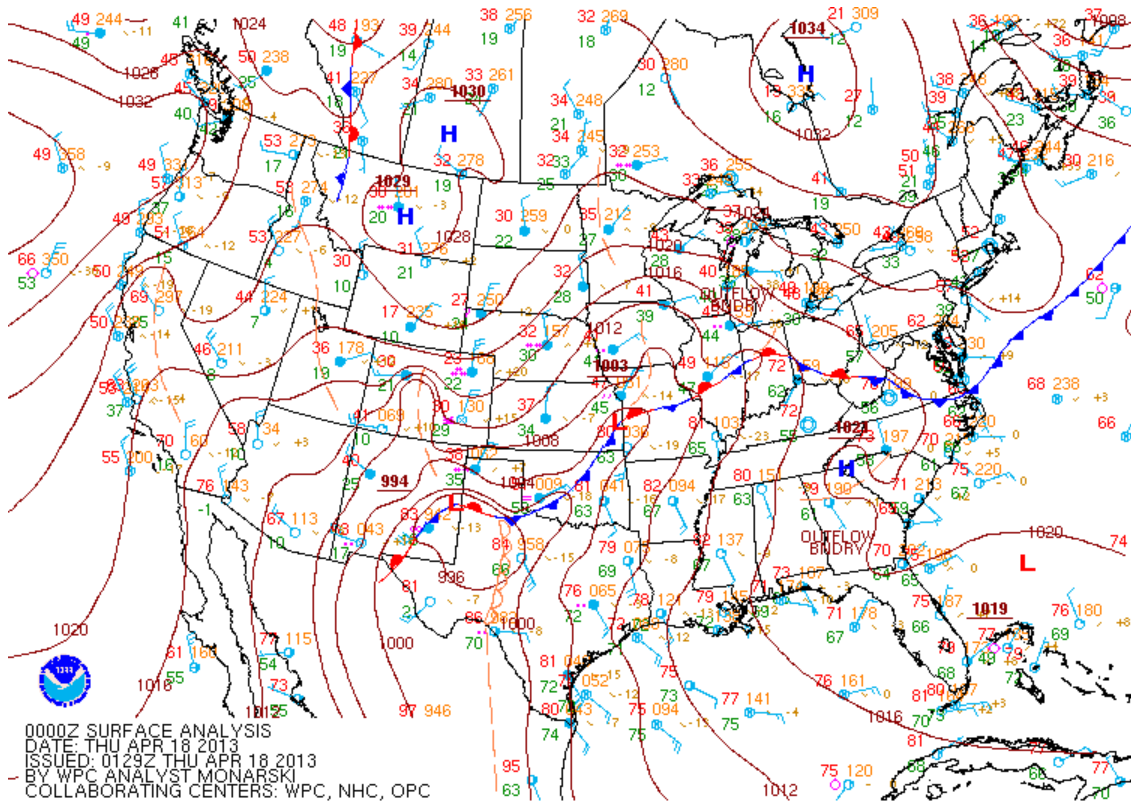
Figure 3.11.1. Surface Analysis 0000 UTC April 18, 2013.
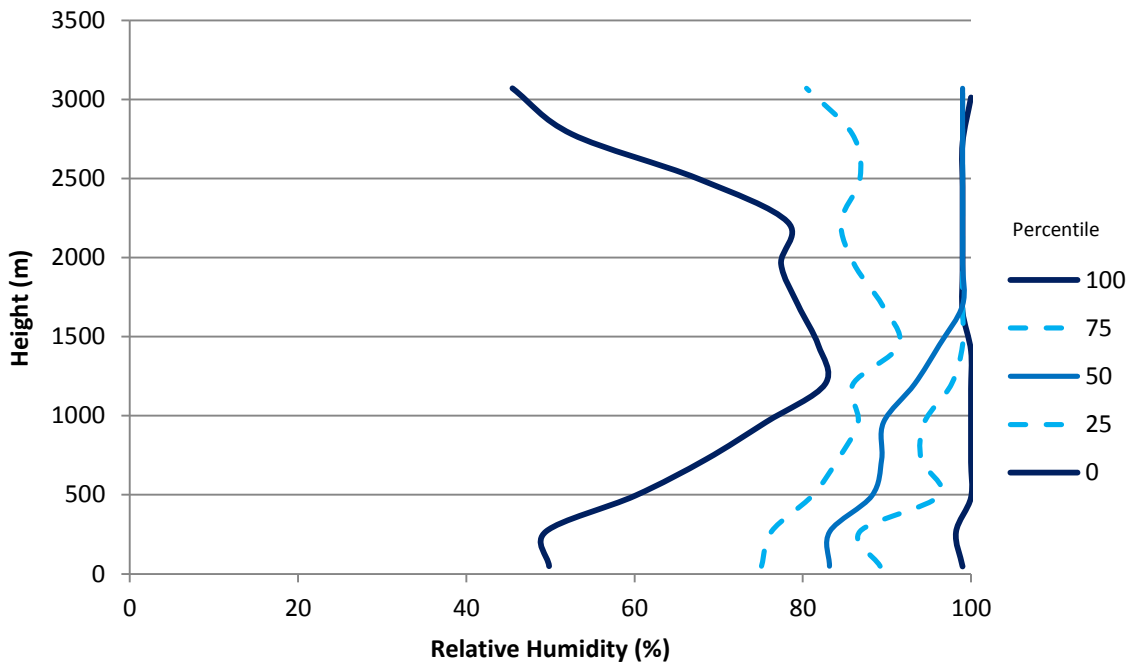
Figure 3.11.2. Relative Humidity Profile April 17, 2013.

167
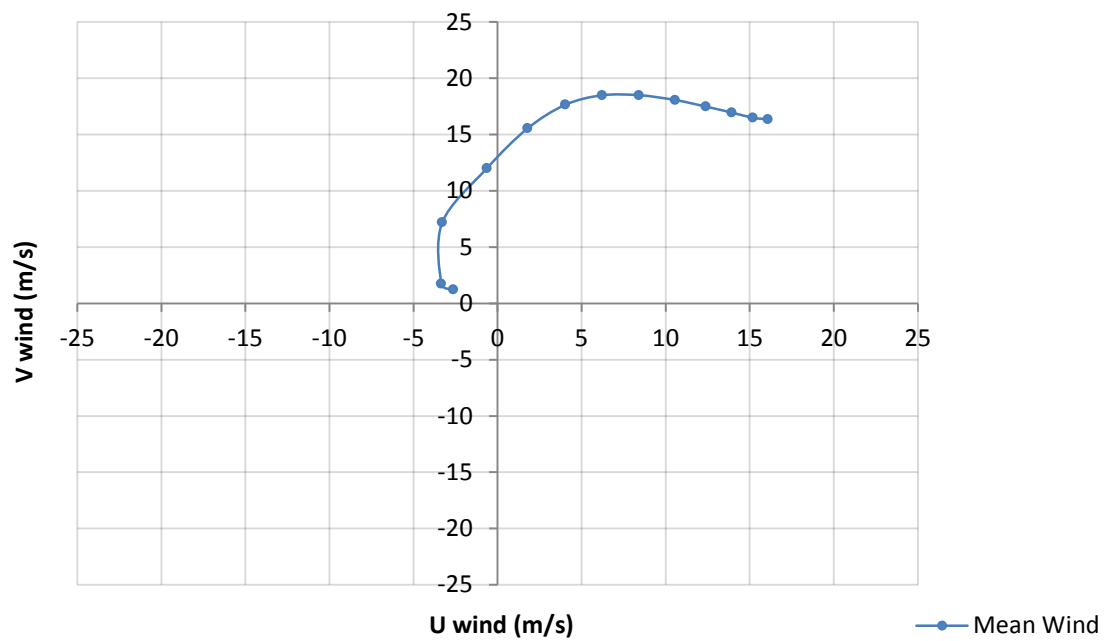
Figure 3.11.3. Hodograph April 17, 2013.
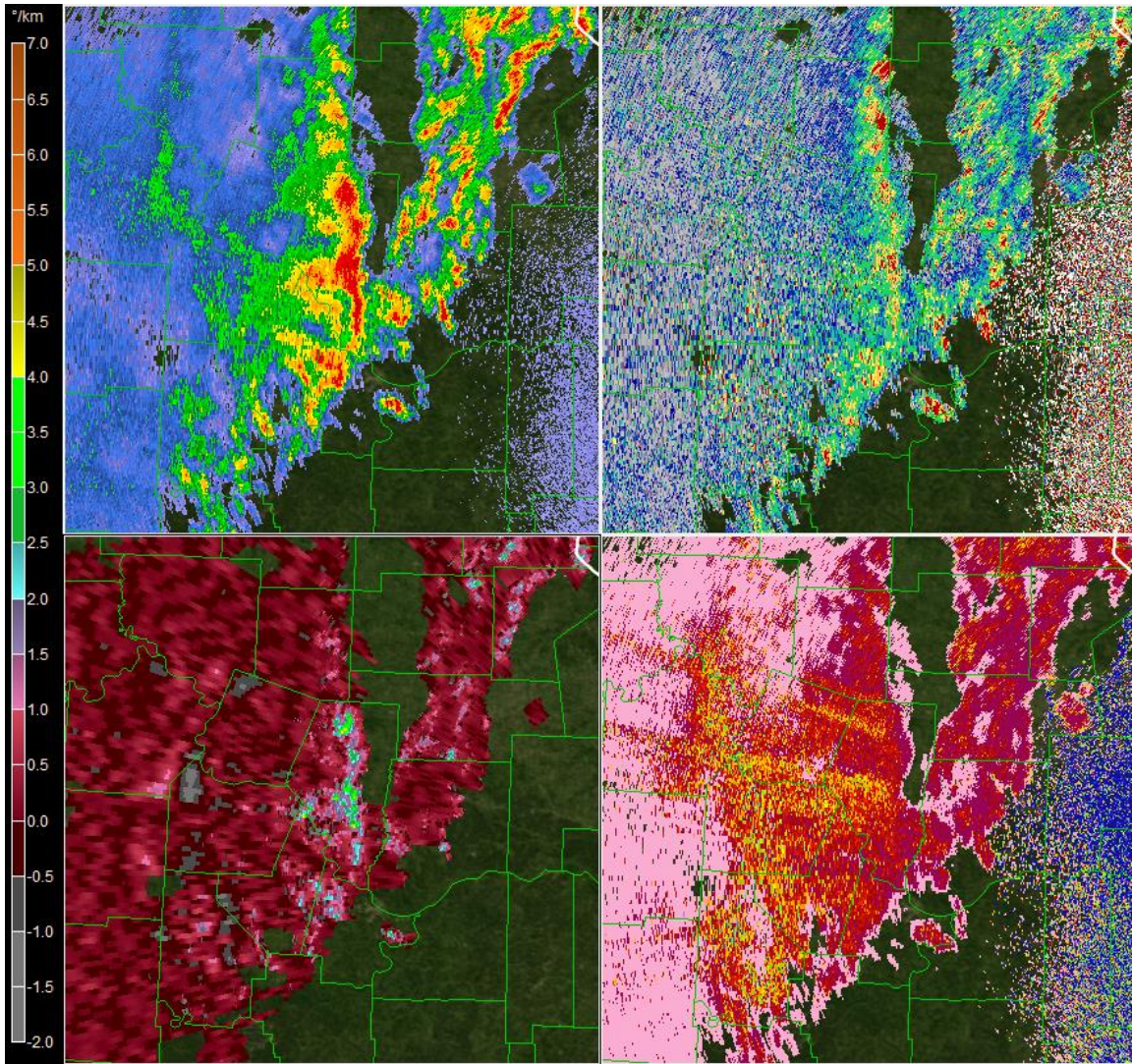
Figure 3.11.4. Four Panel Radar Image for 0743 UTC April 18, 2013. The top left is reflectivity (Z), top right is differential reflectivity (Z_{DR}), bottom left is specific phase differential (K_{DP}), and bottom right is correlation coefficient. The scale on the left corresponds to the bottom left image (K_{DP}). The elevation angle used here was 0.5°.

Table 3.11.1 Conventional Techniques, April 17, 2013

$Z = aR^b$	#	FB(%)	FAD(%)	FRMSE(%)	FSD(%)
1	83	13.61	48.69	79.70	78.53
2	79	30.64	61.91	104.96	100.38
3	79	169.17	181.25	336.78	291.21
4	79	18.52	54.96	90.14	88.22
5	75	-14.57	50.37	73.72	72.27
$R(Z, Z_{DR}) = aZ^b Z_{dr}{}^c$					
12	73	-29.48	54.70	82.33	76.87
13	71	-37.19	61.82	93.78	86.09
14	76	-33.15	52.32	80.61	73.47
15	77	-29.05	50.20	76.19	70.44
16	76	-33.66	52.57	80.48	73.10

Table 3.11.2 Trace Techniques, April 17, 2013

	Z_{DR} +	#	FB(%)	FAD(%)	FRMSE(%)	FSD(%)
T1	0	71	54.10	71.83	107.80	93.24
	0.2	71	43.13	61.46	89.07	77.94
	0.3	70	38.40	57.04	81.07	71.40
	0.4	70	34.50	53.21	75.48	67.13
	0.5	69	31.27	49.94	71.02	63.76
	0.6	69	28.56	47.00	68.16	61.89
	0.7	69	25.68	43.97	64.93	59.63
	0.8	69	22.72	41.48	61.44	57.09
	0.9	69	20.04	39.20	58.48	54.94
	1	69	17.63	37.07	56.32	53.49
	1.1	70	15.68	36.61	55.75	53.50
	1.5	70	9.72	40.15	60.25	59.46
	2	69	0.71	44.78	67.77	67.77
	2.6	69	-9.97	51.31	77.35	76.71
T2	0.4	78	74.70	82.45	129.43	105.70
	0.6	78	62.06	72.20	114.09	95.74
	0.8	77	52.26	64.68	102.70	88.41
	1	75	45.04	59.02	94.93	83.57
	1.2	74	39.37	55.20	91.00	82.04
	1.4	72	34.05	52.64	87.67	80.79
	1.6	71	29.88	52.98	88.77	83.60
	1.8	70	27.32	55.71	94.63	90.60
	2	70	26.04	60.40	105.15	101.88
	2.2	70	24.86	64.73	115.83	113.13
	2.4	70	22.50	67.92	123.09	121.01
	2.6	70	19.82	71.74	128.55	127.02
T3	0	75	66.02	85.86	129.85	111.82
	0.2	75	53.18	75.45	113.18	99.91
	0.3	75	47.40	70.67	105.93	94.73
	0.4	75	42.24	66.46	99.68	90.29
	0.5	73	37.49	62.69	93.28	85.42
	0.6	73	33.20	59.08	88.73	82.28
	0.7	73	29.30	55.92	84.59	79.36
	0.8	72	25.98	53.12	80.95	76.67
	0.9	72	23.09	50.47	78.11	74.62
	1	72	20.53	48.33	75.93	73.11
	1.1	72	18.23	46.48	74.14	71.86
	1.5	71	9.24	42.37	66.76	66.12
	2	70	3.07	47.59	73.14	73.08
	2.6	69	-3.34	56.94	88.37	88.31

Table 3.11.2 Trace Techniques, April 17, 2013 (Continued)

	Z_{DR} +	#	FB(%)	FAD(%)	FRMSE(%)	FSD(%)
T4	0.4	75	66.51	74.78	116.02	95.06
	0.6	75	55.21	66.16	104.43	88.65
	0.8	74	46.49	59.92	95.80	83.76
	1	72	40.13	55.33	89.93	80.49
	1.2	72	35.17	52.88	87.94	80.60
	1.4	71	30.40	51.87	86.10	80.55
	1.6	71	26.67	53.69	88.33	84.20
	1.8	71	24.47	57.23	95.04	91.84
	2	71	23.45	61.79	105.58	102.95
	2.2	70	22.45	65.91	115.44	113.23
	2.4	70	20.31	69.06	122.75	121.06
	2.6	69	17.79	72.96	127.33	126.09
T5	0.4	71	58.07	66.86	94.53	74.59
	0.6	71	50.37	60.99	88.33	72.55
	0.8	70	43.48	56.25	83.16	70.89
	1	70	37.92	53.01	82.05	72.76
	1.2	70	34.39	52.81	86.73	79.62
	1.4	70	31.69	54.92	93.88	88.37
	1.6	70	29.13	58.24	102.16	97.92
	1.8	70	25.69	60.56	107.79	104.69
	2	70	21.42	62.07	110.83	108.74
	2.2	70	17.38	63.25	114.03	112.70
	2.4	69	13.17	64.27	115.59	114.83
	2.6	69	9.37	66.26	118.15	117.78
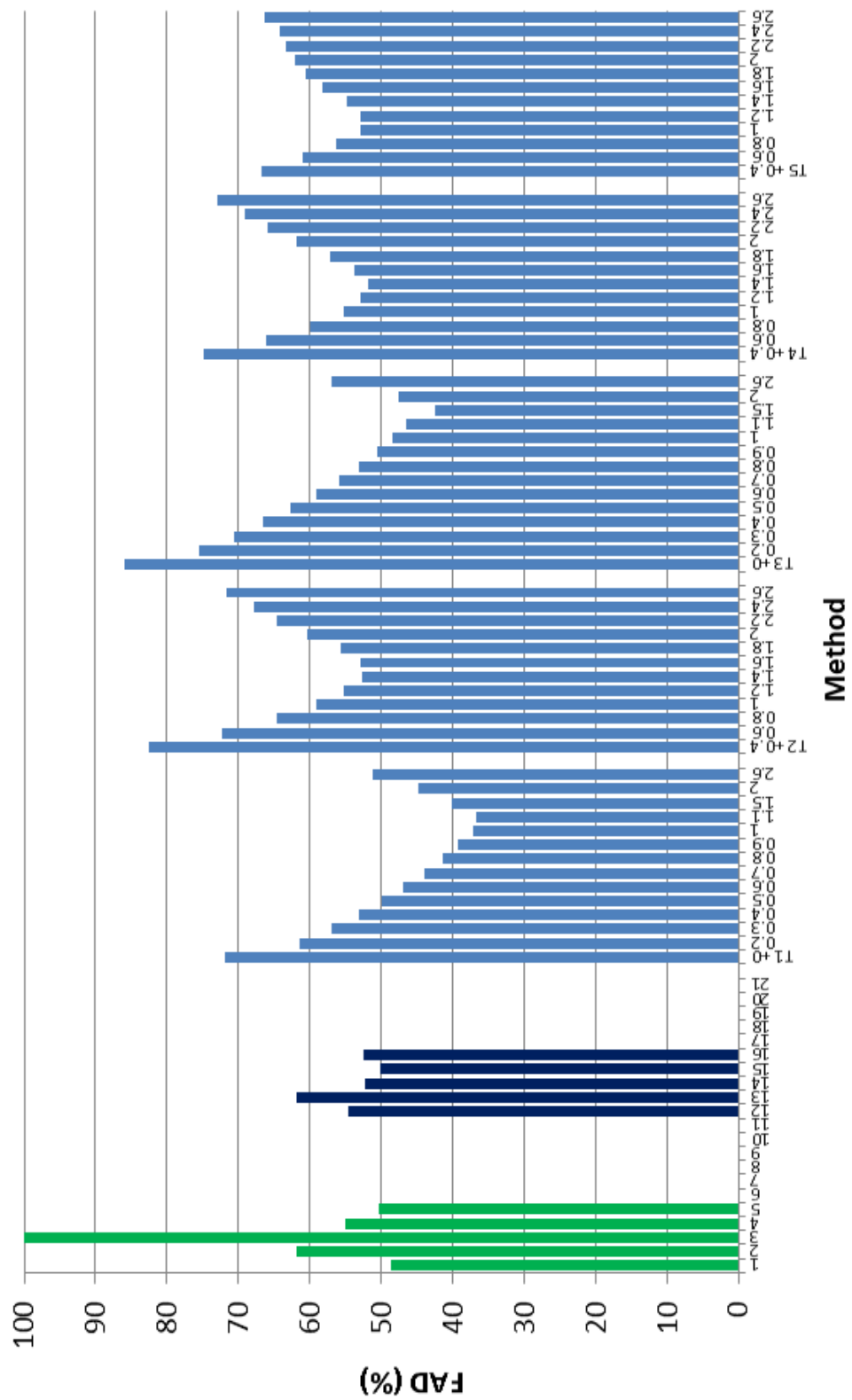
Figure 3.11.5. FAD Performance April 17, 2013.

173
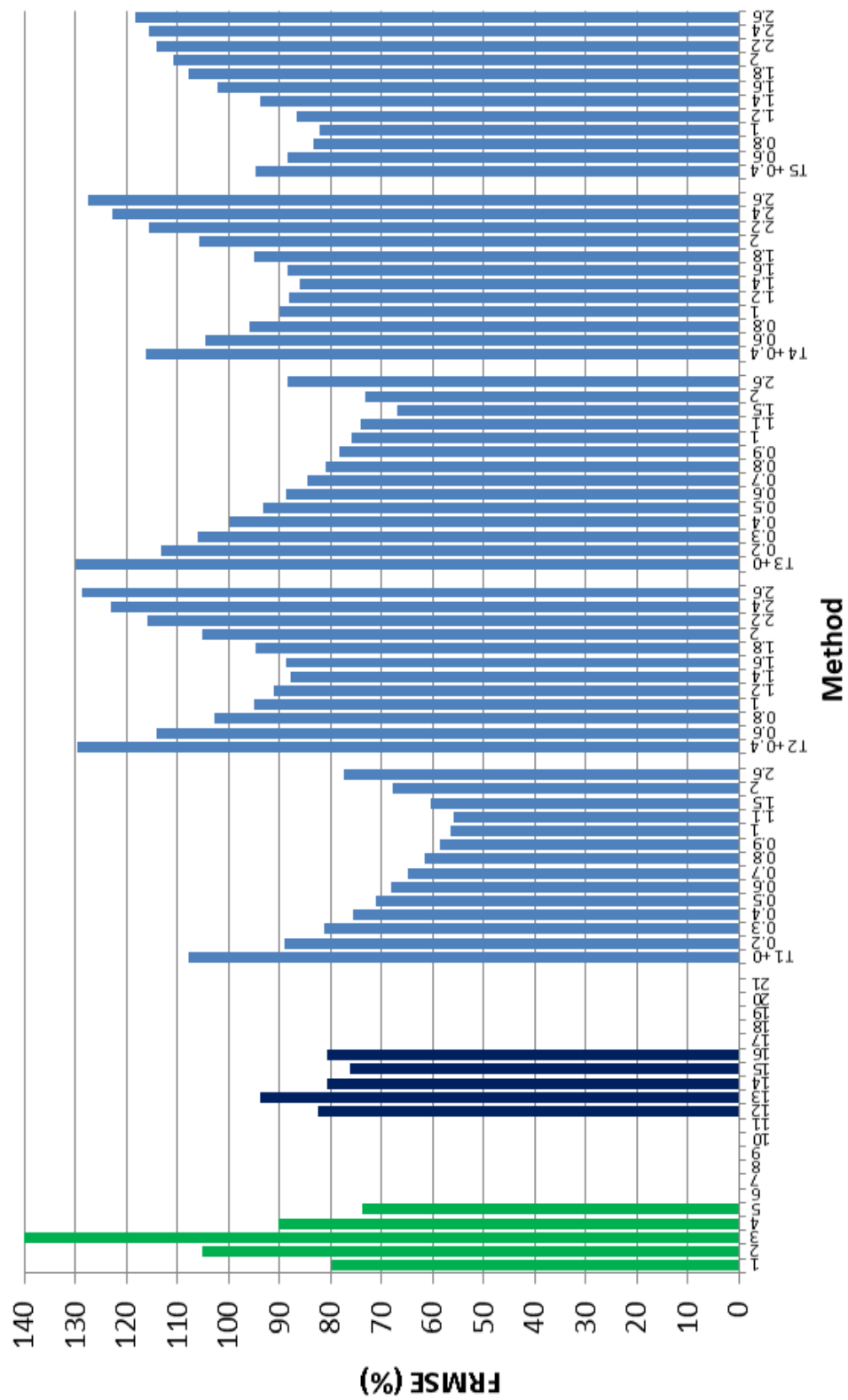
Figure 3.11.6. FRMSE Performance April 17, 2013.
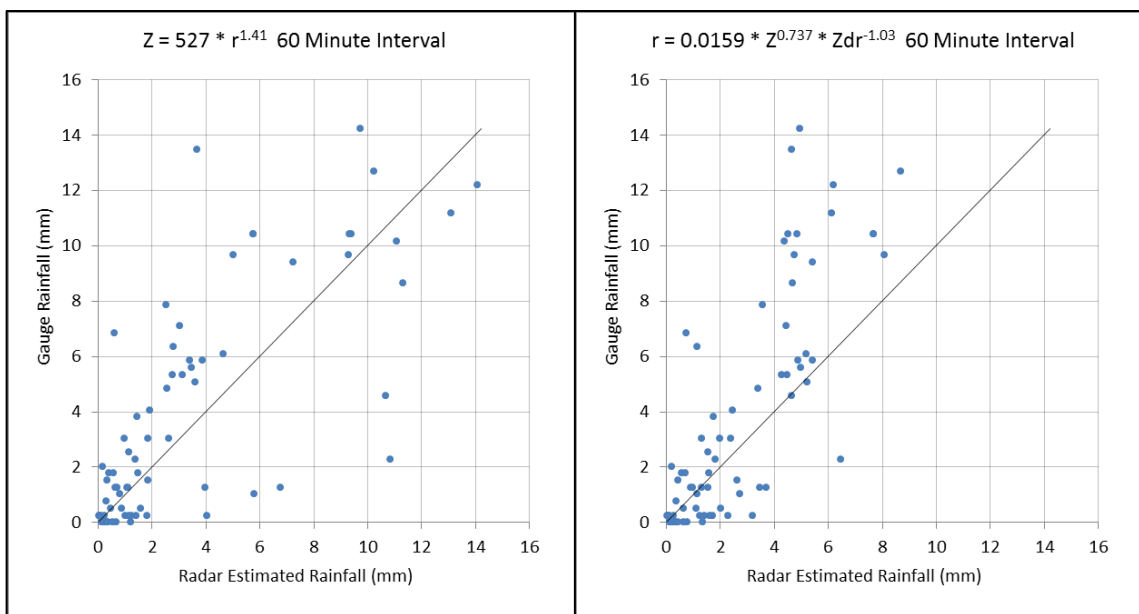
Figure 3.11.7. Radar Estimated Rainfall vs. Gauge Rainfall Scatterplots April 17, 2013.
The best performers of the five conventional formula groups are shown here.
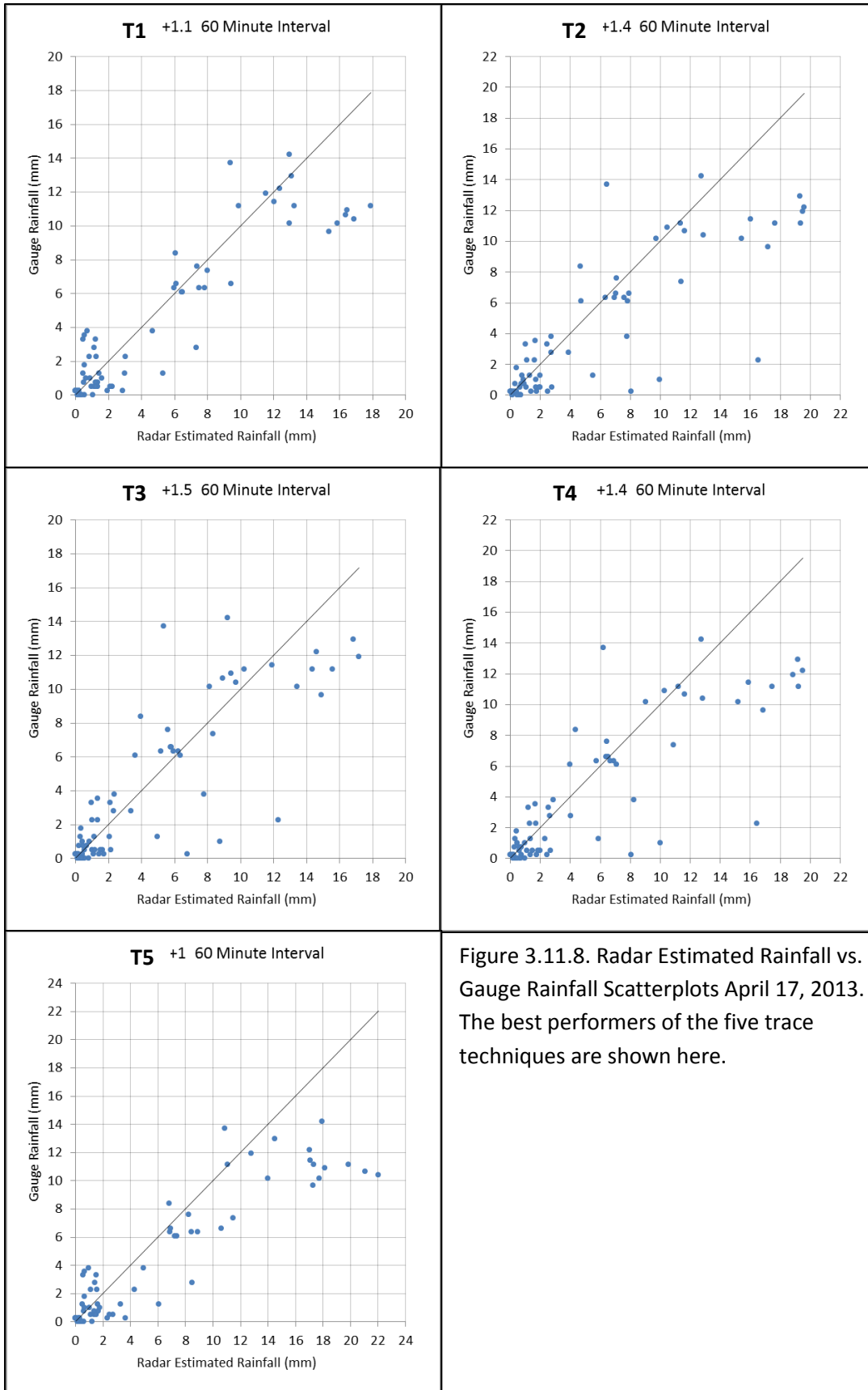
Figure 3.11.8. Radar Estimated Rainfall vs. Gauge Rainfall Scatterplots April 17, 2013. The best performers of the five trace techniques are shown here.

176

3.12 May 30, 2013

The May 30 rainfall event was both the longest and heaviest of the studied events.

More than 100 millimeters of rain fell over a two day period in several locations around

Central Missouri. The rain with this event was associated with two slow moving centers

of low pressure far to the west and northwest. Figure 3.12.1 is an HPC surface analysis

for 21 UTC of May 30. Figure 3.12.2 shows humidity versus height in percentile format

for 08 UTC of May 30 through 18 UTC of May 31. Due to the extended nature of the

event multiple drying and moistening periods were present, resulting in a very wide

range of relative humidity values (especially at higher levels). Figure 3.12.3 is a

hodograph for the 30th of May. The hodograph shows the wind direction transitioning

from southerly at the surface to southwesterly aloft. Figure 3.12.4 is a four panel radar

image from KLSX for 2044 UTC of May 30. Several waves of storms passed through

Central Missouri over the period of this event.

3.12.1 Conventional Formulas

Table 3.12.1 shows the performance of the conventional formulas for this event. The

most basic Z-R relationship, (1), was again the top performer of the conventional

formulas. Of the non-K_{DP} reliant formulas, one outlier was present, (3). The K_{DP}-reliant

formulas again performed poorly, though not as poorly as they did on other events. A

mix of positive and negative biases was present for the conventional formulas for this

event.

3.12.2 Tracing Techniques

Table 3.12.2 shows the performance of the various trace techniques and their permutations for this event. Techniques T2, T4, and T5 were most effective at the $+Z_{DR}$ values of around 2.6, T1 was most effective at $+Z_{DR}$ values near 0.2, and T3 was most effective at a $+Z_{DR}$ value of 2 (by FAD and FRMSE, FB was much worse at Z_{DR} +2). However, variation in the FAD and FRMSE evaluation parameters at all Z_{DR} adjustments for the T1 and T3 techniques was minimal. The tracing techniques as a whole performed slightly worse than the non-K_{DP} reliant conventional formulas for this event.

3.5.3 Graphical Evaluation

Figure 3.12.5 is a histogram showing the FAD performance of each evaluated technique for this event. Figure 3.12.6 is the equivalent histogram showing FRMSE performance.

Figure 3.12.7 shows a combination of scatterplots of radar-derived rainfall versus rain gauge rainfall for the conventional formulas. The techniques illustrated were the top performers in each category. Figure 3.12.8 is identical to 3.12.7, except it depicts the best performers of the trace techniques.
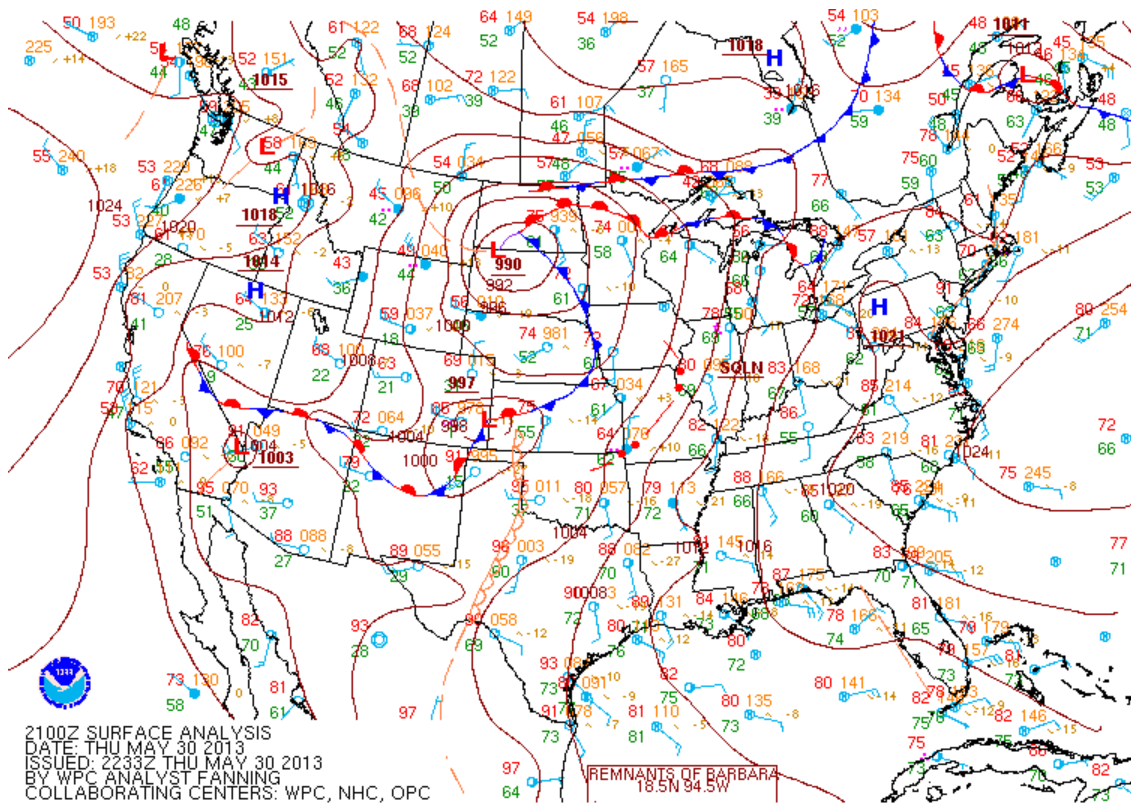
Figure 3.12.1. Surface Analysis 2100 UTC May 30, 2013.
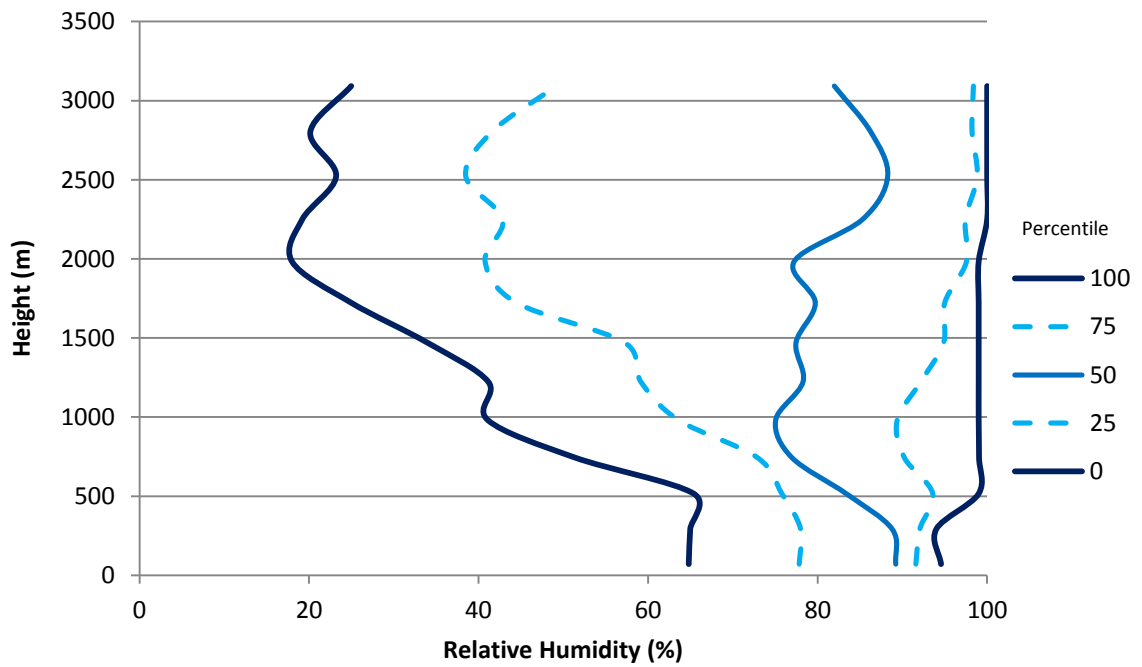
Figure 3.12.2. Relative Humidity Profile May 30, 2013.
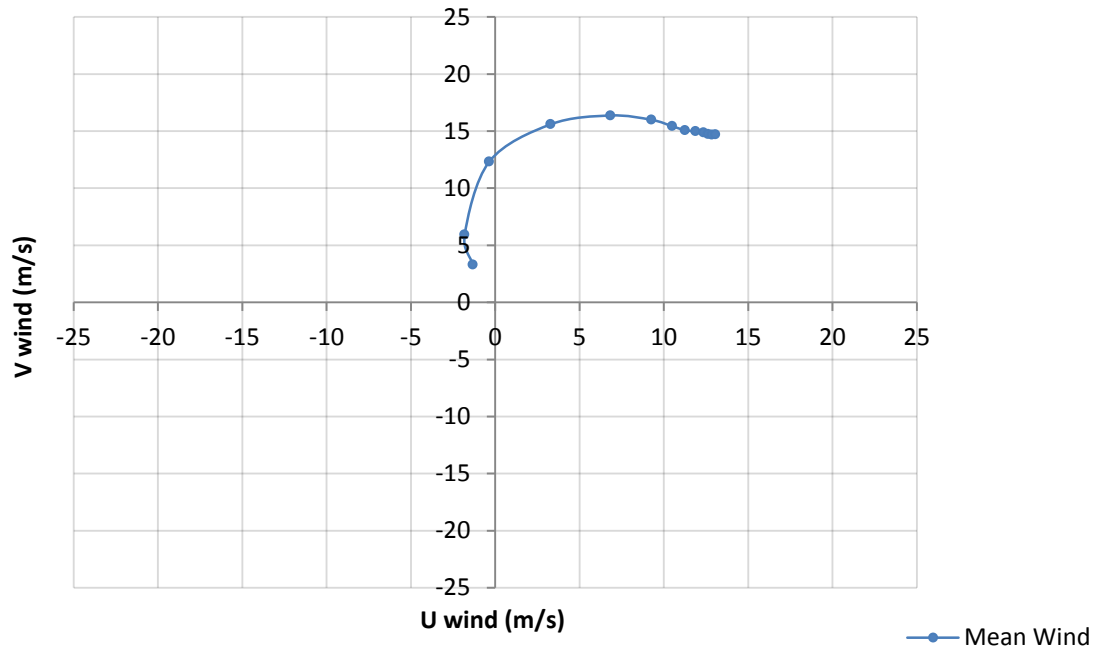
Figure 3.12.3. Hodograph May 30, 2013.
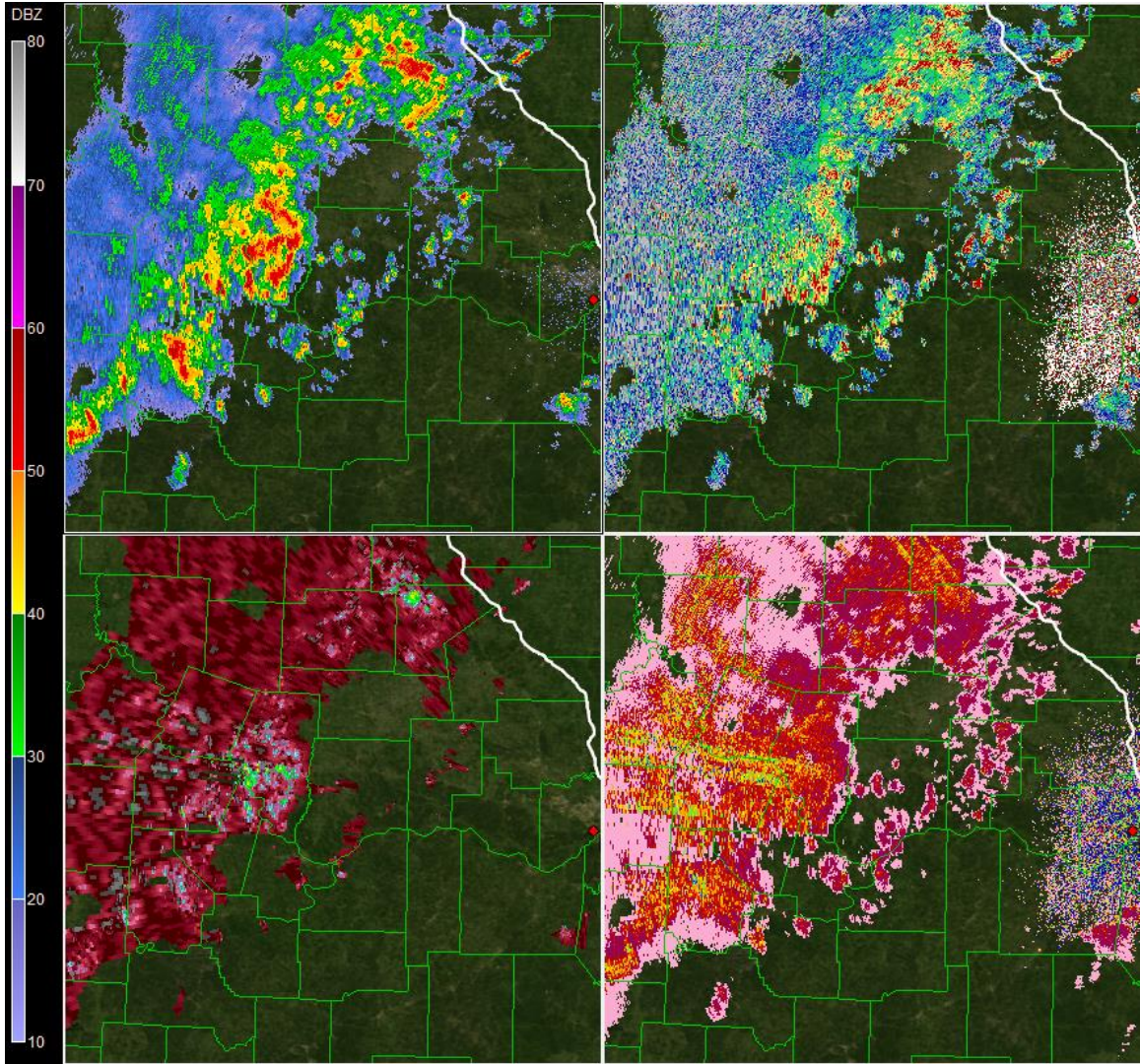
Figure 3.12.4. Four Panel Radar Image for 2044 UTC May 30, 2013. The top left is reflectivity (Z), top right is differential reflectivity (Z_{DR}), bottom left is specific phase differential (K_{DP}), and bottom right is correlation coefficient. The scale on the left corresponds to the top left image (Z). The elevation angle used here was 0.5°.

Table 3.12.1 Conventional Techniques, May 30, 2013

$Z = aR^b$	#	FB(%)	FAD(%)	FRMSE(%)	FSD(%)
1	114	-9.85	43.19	58.95	58.12
2	113	4.87	48.25	65.42	65.24
3	113	114.87	128.27	200.87	164.78
4	113	-4.96	45.24	61.36	61.15
5	112	-31.32	47.92	67.61	59.92
$R(K_{DP}) = a\lvert K_{DP}\rvert^b sign(K_{DP})$					
6	120	16.75	76.09	117.29	116.09
7	121	26.09	81.72	126.63	123.91
8	121	22.54	77.60	117.65	115.47
9	120	1.86	66.84	100.72	100.71
10	121	16.66	75.34	115.79	114.59
11	121	10.18	71.02	107.82	107.34
$R(Z, Z_{DR}) = a Z^b Z_{dr}{}^c$					
12	113	-30.23	60.87	81.79	76.00
13	113	-38.64	70.26	94.84	86.61
14	113	-37.66	56.93	76.76	66.89
15	113	-34.20	52.92	71.59	62.90
16	113	-38.24	56.62	76.51	66.26
$R(K_{DP}, Z_{DR}) = a\lvert K_{DP}\rvert^b Z_{dr}{}^c sign(K_{DP})$					
17	121	30.51	90.93	141.31	137.98
18	121	42.18	105.79	169.22	163.88
19	119	8.80	70.08	105.52	105.15
20	120	24.00	80.68	122.98	120.61
Synthetic					
21	111	-5.98	59.59	84.68	84.47

Table 3.12.2 Trace Techniques, May 30, 2013

	Z_{DR} +	#	FB(%)	FAD(%)	FRMSE(%)	FSD(%)
T1	0	107	-7.49	50.44	75.22	74.85
	0.2	107	-7.36	49.29	75.05	74.69
	0.3	107	-7.29	48.99	75.36	75.01
	0.4	106	-7.14	48.98	75.81	75.48
	0.5	106	-7.05	49.13	76.83	76.51
	0.6	106	-7.06	49.30	77.97	77.65
	0.7	106	-7.25	49.43	79.14	78.80
	0.8	106	-7.55	49.52	80.37	80.01
	0.9	106	-8.01	49.69	81.78	81.39
	1	106	-8.63	49.88	83.40	82.96
	1.1	106	-9.64	49.93	84.55	84.00
	1.5	105	-16.91	48.28	82.94	81.20
	2	103	-29.71	47.86	76.22	70.19
	2.6	102	-43.41	52.80	76.72	63.25
T2	0.4	108	77.04	88.17	133.62	109.18
	0.6	106	66.41	81.10	123.11	103.66
	0.8	106	57.18	75.81	116.22	101.18
	1	105	49.18	71.84	110.40	98.84
	1.2	104	41.08	67.84	103.55	95.05
	1.4	104	32.30	63.77	96.76	91.21
	1.6	104	23.10	59.91	89.22	86.18
	1.8	104	13.32	56.10	81.02	79.92
	2	103	3.91	52.89	73.84	73.74
	2.2	103	-4.74	50.04	69.09	68.93
	2.4	103	-12.62	47.92	66.40	65.19
	2.6	103	-19.73	46.93	65.55	62.51
T3	0	110	-8.52	49.44	75.25	74.76
	0.2	109	-8.73	47.54	73.17	72.64
	0.3	109	-8.65	47.25	73.35	72.84
	0.4	107	-8.56	47.34	73.46	72.96
	0.5	107	-8.49	47.63	74.57	74.09
	0.6	106	-8.37	48.26	75.87	75.41
	0.7	105	-8.39	48.87	77.21	76.75
	0.8	105	-8.87	49.12	77.96	77.46
	0.9	105	-9.44	49.30	78.65	78.08
	1	105	-10.30	49.19	78.64	77.96
	1.1	105	-11.42	48.87	78.11	77.27
	1.5	104	-18.63	47.50	75.03	72.69
	2	103	-31.17	47.60	71.57	64.43
	2.6	103	-44.78	51.66	74.78	59.89

Table 3.12.2 Trace Techniques, May 30, 2013 (Continued)

	Z_{DR} +	#	FB(%)	FAD(%)	FRMSE(%)	FSD(%)
T4	0.4	111	76.94	85.98	128.37	102.75
	0.6	109	66.33	78.88	117.31	96.76
	0.8	108	57.09	73.46	108.96	92.81
	1	107	49.10	68.74	102.29	89.73
	1.2	105	41.01	63.97	94.69	85.35
	1.4	105	32.24	59.08	87.84	81.71
	1.6	104	23.04	54.56	80.10	76.71
	1.8	104	13.27	50.40	72.66	71.44
	2	103	3.86	47.04	66.47	66.36
	2.2	103	-4.78	44.43	62.72	62.53
	2.4	103	-12.65	43.26	61.06	59.73
	2.6	103	-19.76	43.06	61.19	57.91
T5	0.4	107	74.01	81.96	117.09	90.73
	0.6	107	64.91	76.02	109.54	88.24
	0.8	106	57.30	72.15	104.54	87.44
	1	106	50.54	68.64	102.29	88.94
	1.2	106	43.04	64.18	98.99	89.15
	1.4	106	34.37	58.62	93.35	86.79
	1.6	105	24.92	52.15	85.40	81.68
	1.8	105	15.23	47.19	77.48	75.97
	2	105	5.87	43.99	71.27	71.03
	2.2	103	-2.85	42.66	66.31	66.25
	2.4	102	-10.73	42.23	63.77	62.86
	2.6	102	-17.87	43.01	63.28	60.70
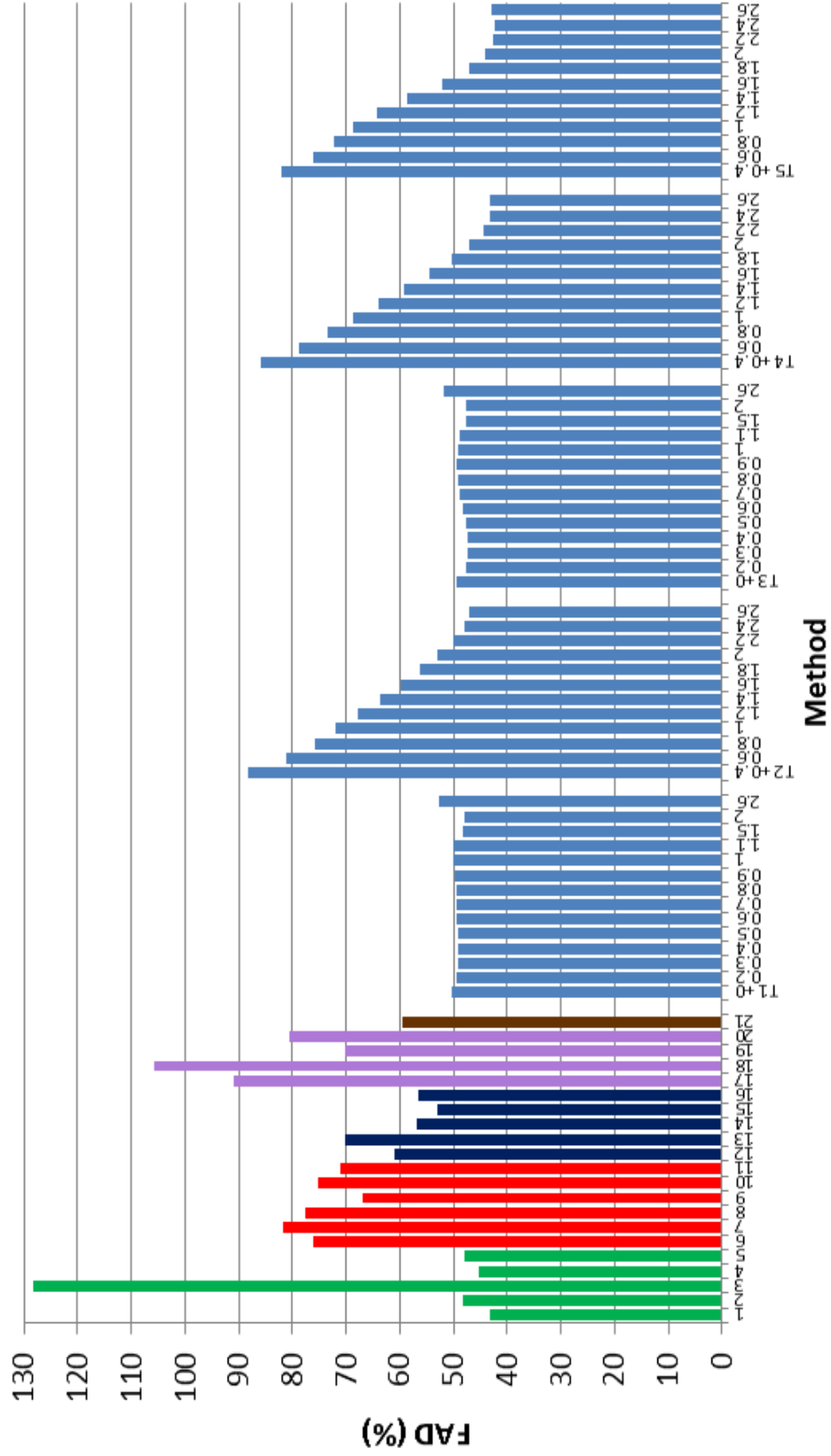
Figure 3.12.5. FAD Performance May 30, 2013.

185
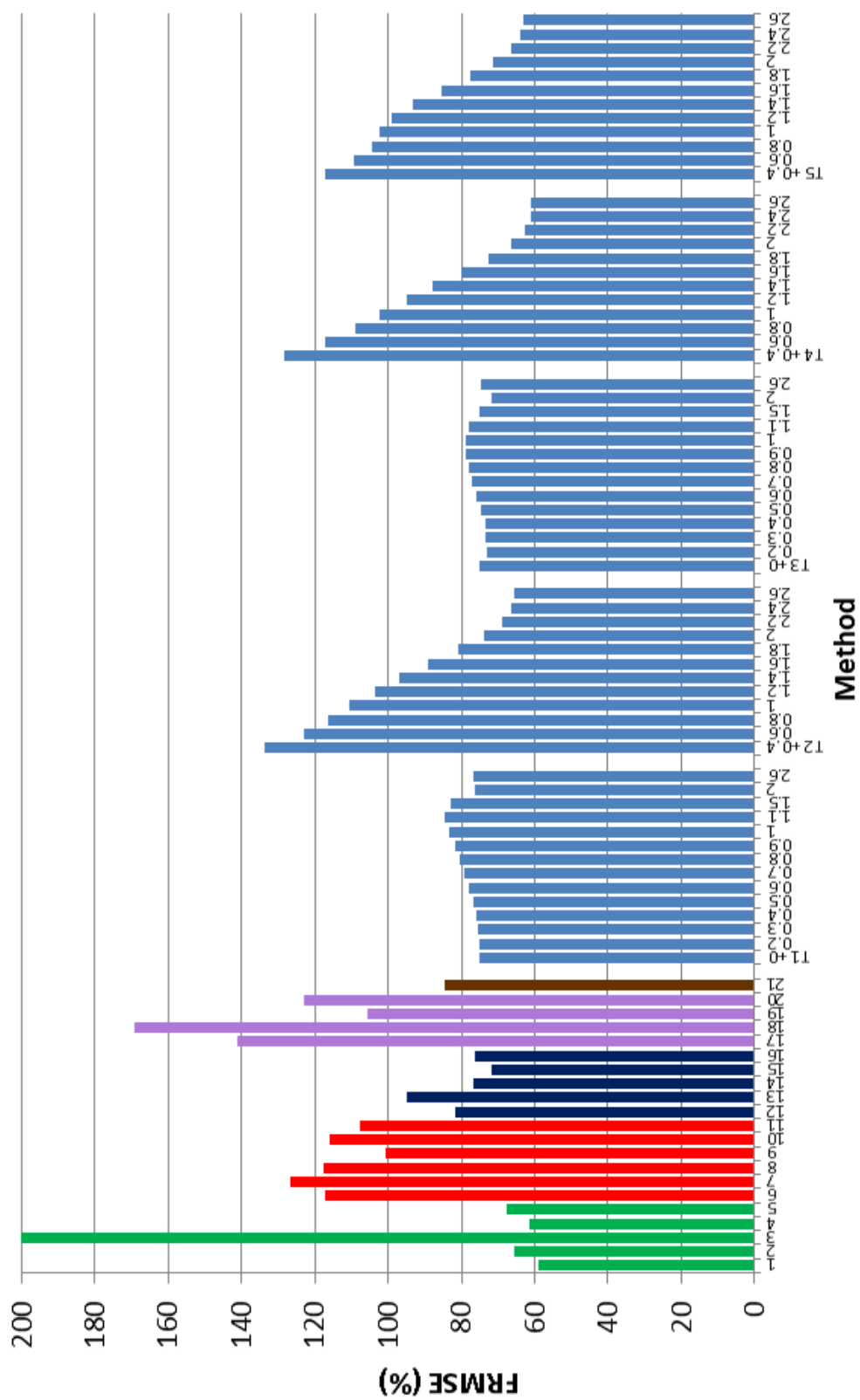
Figure 3.12.6. FRMSE Performance May 30, 2013.
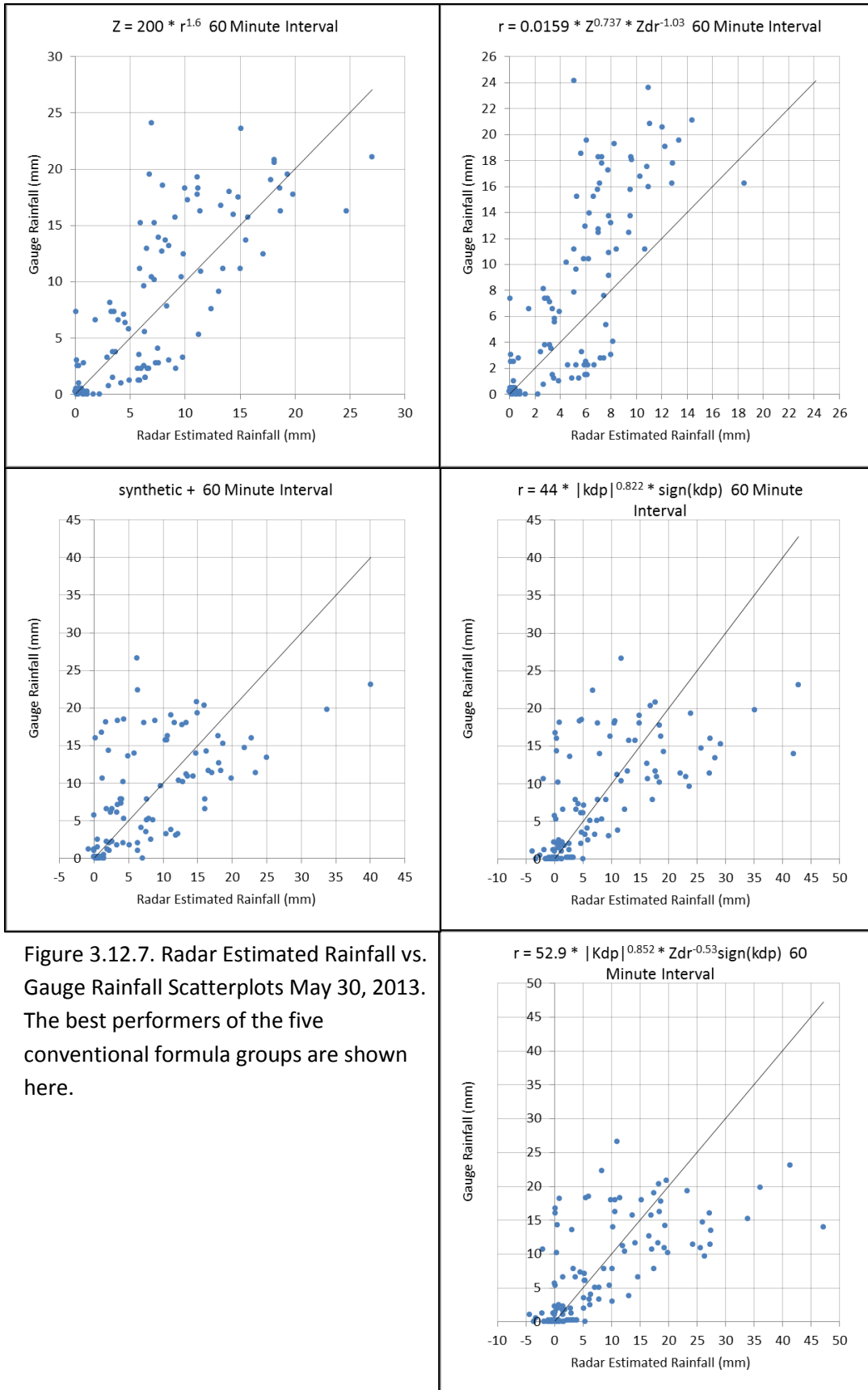
Figure 3.12.7. Radar Estimated Rainfall vs. Gauge Rainfall Scatterplots May 30, 2013. The best performers of the five conventional formula groups are shown here.
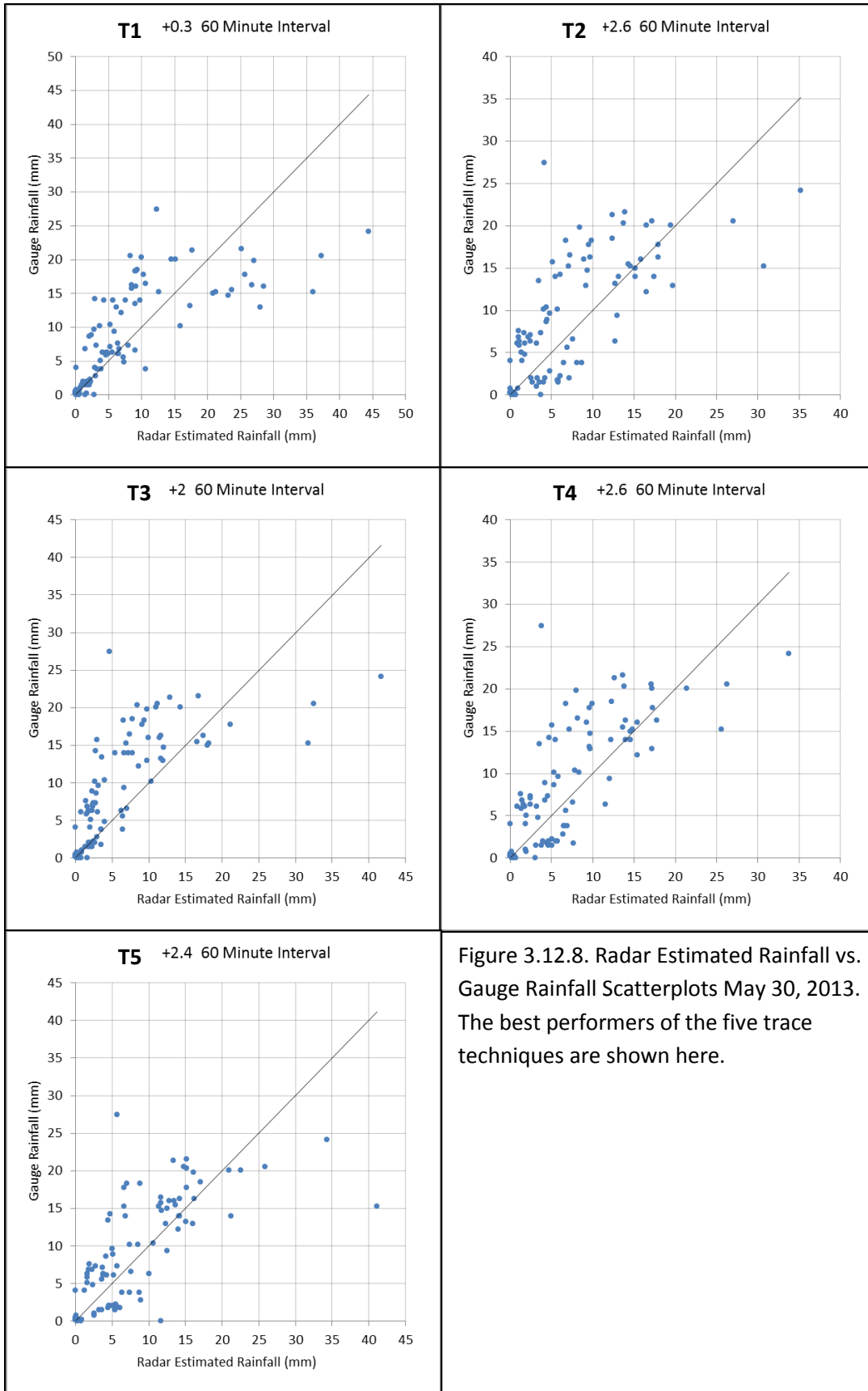
Figure 3.12.8. Radar Estimated Rainfall vs. Gauge Rainfall Scatterplots May 30, 2013. The best performers of the five trace techniques are shown here.

3.13 Statistical Analysis and Discussion

To determine the overall performance of each individual method for rainfall estimation, a statistical analysis was done. Each of the rainfall events was given equal weight for this analysis. The parameters chosen for analysis were bias, FAD, and FRMSE. Along with the mean values, five percentiles were calculated: 0th, 25th, 50th, 75th, and 100th. The 0th percentile for a method was equivalent to the minimum value of the parameter in question over all events examined. The 50th percentile was the median value and the 100th percentile was the maximum. For example, if method "A" showed a FAD of 30% for a first event, 40% for a second event, and 50% for a third event and there were three total events, the 0th percentile for the FAD parameter would be 30%, the 50th percentile would be 40%, and the 100th percentile would be 50%.

The choice to weight each event equally was made for several reasons. Successful rainfall estimation under different environmental conditions was the primary reason for weighting each event equally. This approach rewards a method for performing well in two shorter rainfall events, rather than one prolonged event. The other issues at play were time and technical constraints. Each of the April, 2012, events had an environmental factor that set the events apart from one another. The atmosphere on April 13, 2012, had a very dry layer, while the two subsequent days did not. On April 15, 2012, the precipitation occurred ahead of a cold front moving through the area, while the precipitation for the other two days was not associated with this front. The other candidate for "splitting" was the May 30-31, 2013, event. The wide range of relative humidity values was indicative of a very dynamic atmosphere. The storms during this

event, however, were not separated by significant time periods, as they were for the April, 2012, events.

Table 3.13.1 shows the mean and percentile performance analysis for the conventional formulas with respect to the FAD parameter. By median values, (1), (2), and (4) performed nearly identically. Mean values were only slightly different. Table 3.14.1 shows the mean and percentile performance analysis for the conventional formulas with respect to the FRMSE parameter. These values were generally higher, due to the outlier penalty introduced by the squaring. The same general patterns found in Table 3.13.1 were also present in Table 3.14.1.

Table 3.13.2 shows the mean and percentile performance analysis for the trace techniques with respect to the FAD parameter, while Table 3.14.2 shows the same analysis using the FRMSE parameter. Figure 3.13.1 shows the mean FAD performance of each of the five trace techniques as a function of Z_{DR} adjustment. Figure 3.13.2 is identical to Figure 3.13.1 except it shows the median FAD performance. Figure 3.13.3 and Figure 3.13.4 are the FRMSE equivalents to Figure 3.13.1 and 3.13.2. Figure 3.13.5 and Figure 3.13.6 are the Bias equivalents. For the FRMSE and FAD charts, the dotted line represents the best performing conventional formula. The optimal T1 and T3 techniques show some improvement over the best performing conventional formulas on the FRMSE and FAD charts.

At first glance all three pairs of graphs show a clear divide between the two techniques that account for evaporation and the other trace techniques. As a whole, T1 and T3

performed best at roughly the +1 Z_{DR} adjustment, while the other techniques performed

best near the +2 Z_{DR} adjustment. The optimal evaporation techniques significantly

outperformed the optimal no-evaporation techniques, and even the conventional

formulas. The difference in performance with respect to the mean FAD and FRMSE was

much greater than the difference with respect to the median FAD and FRMSE; this was

likely due to the hail events significantly skewing the means for the conventional

formulas.

The +2 Z_{DR} adjustment required for optimal performance for the no-evaporation

techniques was not very realistic. It essentially was a form of evaporation adjustment in

itself, in a one size fits all format. Adjusting the Z_{DR} as a means to account for

evaporation also reduced the effectiveness of the hail adjustment function.

The conclusion can be drawn from these results that accounting for evaporation is

necessary to accurately estimate rainfall amounts with radar. Significant improvements

to overall FAD and FRMSE were made when evaporation was taken into account. High

resolution model data describing atmospheric humidity can serve as a useful tool for

radar-derived rainfall estimation.

Overall any improvement due to accounting for drift was insignificant. However,

accounting for drift did result in noticeable performance improvement on September 7,

2012 and April 17, 2013. A very specific set of environmental conditions is necessary for

drift to have significant theoretical effect. If the storm is moving in the same direction as

the wind and stays at constant strength, the drift calculations only alter the time at

which the drops reach the ground. As discussed in Chapter 1, significant directional shear would be necessary to alter the paths of the drops away from the path of the storm. The degree to which the storms are scattered in nature also has theoretical implications on precipitation drift; if the precipitation covers a very broad area, it is unlikely that precipitation will drift to locations that are not similarly covered in precipitation.

Another factor for examination is time lag of precipitation. All of the conventional formulas and the T2 trace technique assumed precipitation instantly reaches the ground. Theoretically, the time it takes for the precipitation to reach the ground may alter which time slot the precipitation is recorded in, and thus affect the results. On an hourly scale, there are likely minimal amounts of this kind of clipping, but finer time scales may be more affected. The T2 and T4 techniques both did not take into account evaporation or precipitation drift, but the precipitation in the T4 technique did take time to reach the ground. The T4 technique did perform slightly better, but the difference was not significant.

Table 3.13.1 Conventional Formulas, FAD (%) by Percentile

Z $= aR^b$	Mean	0th	25th	50th	75th	100th
1	46.41	31.72	40.90	45.46	49.37	64.49
2	48.25	35.65	36.48	45.97	58.95	76.21
3	111.72	39.30	63.61	109.78	158.08	192.10
4	46.41	31.96	37.93	45.43	54.13	70.13
5	49.71	24.57	46.18	50.03	55.60	68.78
$R(K_{DP}) = a|K_{DP}|^b sign(K_{DP})$						
6	115.39	45.12	67.11	101.48	176.02	212.88
7	127.62	54.13	67.84	113.86	196.39	235.74
8	128.39	52.63	67.30	113.13	200.57	240.24
9	101.50	37.43	65.43	85.34	154.33	188.04
10	116.84	45.64	66.45	102.55	179.52	216.95
11	110.87	41.69	65.33	95.74	170.57	206.75
$R(Z,Z_{DR}) = aZ^b Z_{dr}{}^c$						
12	53.03	33.85	36.55	53.33	64.38	75.15
13	59.31	35.68	39.75	59.21	70.89	87.34
14	48.26	33.98	38.12	48.98	55.97	67.28
15	47.13	31.53	37.92	49.19	53.83	65.37
16	48.22	34.12	37.43	49.40	55.88	67.41
$R(K_{DP},Z_{DR}) = a|K_{DP}|^b Z_{dr}{}^c sign(K_{DP})$						
17	161.97	53.39	77.26	146.66	252.16	326.26
18	211.48	63.87	91.70	190.88	328.64	452.05
19	114.66	39.97	66.92	98.91	178.52	217.09
20	135.38	48.47	69.94	120.89	212.39	258.59
Synthetic						
21	56.04	36.42	42.44	59.61	60.63	79.41

Table 3.13.2 Trace Techniques, FAD (%) by Percentile

	Z_{DR} +	Mean	0th	25th	50th	75th	100th
T1	0	77.51	20.41	45.50	63.42	96.73	187.46
	0.2	66.31	19.48	41.63	55.06	71.42	151.87
	0.3	61.38	19.28	39.75	51.43	61.71	134.75
	0.4	56.95	18.99	38.73	49.55	57.05	121.69
	0.5	53.13	18.89	37.99	45.72	54.00	112.42
	0.6	49.81	19.64	36.60	42.43	52.05	103.98
	0.7	46.84	20.91	36.06	39.61	50.32	95.62
	0.8	44.43	22.52	34.68	38.76	49.22	88.22
	0.9	42.60	23.99	33.22	38.94	48.91	81.97
	1	41.35	25.76	32.01	38.23	48.66	75.86
	1.1	40.76	26.75	32.24	39.10	46.04	70.58
	1.5	42.22	29.92	33.30	42.46	48.53	58.16
	2	47.36	35.51	37.00	44.64	56.93	73.91
	2.6	55.29	42.76	45.96	51.69	66.43	78.03
T2	0.4	111.25	53.68	81.07	94.22	147.29	210.00
	0.6	91.06	39.86	65.16	81.04	116.14	162.52
	0.8	76.36	35.06	61.62	70.81	92.87	125.62
	1	65.71	36.82	50.61	66.21	76.23	98.64
	1.2	58.20	36.32	43.95	57.56	71.61	82.13
	1.4	53.43	31.27	45.33	52.60	62.20	78.07
	1.6	50.48	26.32	41.11	50.15	56.90	84.76
	1.8	49.40	24.44	37.55	49.91	55.67	91.90
	2	49.90	27.56	36.57	49.03	57.99	97.38
	2.2	51.07	25.57	38.00	49.79	61.08	97.26
	2.4	52.86	25.77	39.39	49.14	64.36	97.87
	2.6	55.26	28.05	42.08	51.09	67.38	99.35
T3	0	74.50	21.69	36.22	66.26	92.48	184.40
	0.2	63.90	22.15	35.57	58.82	73.09	147.87
	0.3	59.17	22.44	35.09	53.62	67.83	130.63
	0.4	55.08	23.09	34.48	49.22	63.89	114.70
	0.5	51.51	24.08	33.87	48.42	60.54	100.49
	0.6	48.46	25.07	31.55	46.31	57.31	90.62
	0.7	45.97	26.25	30.35	43.64	54.32	82.59
	0.8	44.02	26.94	30.43	41.65	52.12	75.41
	0.9	42.65	27.53	31.69	41.32	50.18	69.09
	1	41.85	28.29	32.80	42.07	48.97	63.54
	1.1	41.38	28.38	31.80	43.12	48.27	58.33
	1.5	42.28	27.58	35.87	42.66	48.18	52.69
	2	48.18	35.36	39.12	47.60	58.71	67.23
	2.6	56.78	45.00	48.21	54.30	68.18	70.53

Table 3.13.2 Trace Techniques, FAD (%) by Percentile (Continued)

	Z_{DR} +	Mean	0th	25th	50th	75th	100th
T4	0.4	106.45	50.28	74.87	85.03	145.46	206.41
	0.6	86.52	34.49	60.44	76.35	113.11	161.45
	0.8	72.24	31.83	49.30	67.51	87.02	124.93
	1	62.27	34.48	42.36	62.71	70.14	98.09
	1.2	55.39	31.50	42.04	53.99	67.80	83.31
	1.4	50.49	28.45	44.21	48.27	58.26	72.85
	1.6	47.55	26.15	39.22	44.49	54.34	78.43
	1.8	46.91	28.95	35.05	45.42	53.58	85.29
	2	47.92	30.05	34.40	46.75	56.59	90.26
	2.2	49.16	27.82	37.11	43.20	60.28	89.90
	2.4	50.82	28.59	38.97	43.24	63.69	88.93
	2.6	53.30	31.76	40.38	46.40	66.79	88.71
T5	0.4	111.48	40.77	69.37	98.35	155.54	188.04
	0.6	91.62	36.71	62.91	81.12	121.51	153.76
	0.8	76.30	34.05	54.43	73.05	99.89	126.82
	1	64.79	32.22	46.17	66.55	81.10	105.51
	1.2	57.06	30.32	42.59	56.91	69.36	85.76
	1.4	52.50	28.10	43.22	52.84	59.86	78.05
	1.6	49.26	24.68	39.94	47.96	56.84	85.39
	1.8	47.73	22.05	38.21	46.91	52.69	93.44
	2	47.43	26.39	32.03	44.42	55.10	98.83
	2.2	48.05	26.85	33.07	42.41	58.78	99.80
	2.4	49.51	29.11	35.59	41.47	61.86	100.78
	2.6	51.60	32.18	37.17	42.10	64.30	101.06

Table 3.14.1 Conventional Formulas, FRMSE (%) by Percentile

$Z = aR^b$	Mean	0th	25th	50th	75th	100th
1	67.35	47.56	51.91	64.06	78.01	113.48
2	72.76	46.98	57.82	64.53	78.24	142.59
3	179.28	52.89	84.85	178.46	218.85	363.50
4	68.95	40.91	54.81	63.73	73.39	128.58
5	73.24	35.82	61.07	70.97	87.15	113.94
$R(K_{DP}) = a\|K_{DP}\|^b sign(K_{DP})$						
6	157.08	66.54	91.53	147.38	228.74	278.71
7	173.60	77.57	92.53	164.77	255.41	308.69
8	172.61	74.20	89.69	161.56	259.98	311.52
9	137.18	57.47	88.47	123.82	200.02	241.39
10	158.37	66.78	90.31	147.65	232.98	283.07
11	149.68	61.62	88.40	137.28	221.01	268.57
$R(Z, Z_{DR}) = aZ^b Z_{dr}{}^c$						
12	77.83	49.22	56.16	80.62	93.53	109.07
13	89.05	48.61	62.90	93.09	109.21	132.68
14	70.77	48.01	52.90	71.92	79.72	109.83
15	69.15	41.55	54.97	71.18	78.93	104.09
16	70.86	44.31	54.21	72.23	79.90	109.90
$R(K_{DP}, Z_{DR}) = a\|K_{DP}\|^b Z_{dr}{}^c sign(K_{DP})$						
17	218.90	70.90	103.01	205.86	332.39	424.72
18	288.30	82.58	122.98	276.08	437.23	579.75
19	154.48	58.89	89.92	140.89	230.82	284.59
20	182.50	66.82	94.35	172.06	275.67	340.27
Synthetic						
21	87.23	46.99	68.11	89.89	102.03	121.47

Table 3.14.2 Trace Techniques, FRMSE (%) by Percentile

	Z_{DR} +	Mean	0th	25th	50th	75th	100th
T1	0	116.27	26.55	70.06	90.36	141.65	280.14
	0.2	98.95	26.04	62.34	77.51	106.03	246.03
	0.3	91.80	26.08	60.26	73.98	97.95	230.79
	0.4	85.48	26.24	58.37	67.84	93.27	216.01
	0.5	80.14	26.66	54.27	64.53	88.76	202.74
	0.6	75.59	27.47	48.64	61.93	83.27	189.31
	0.7	71.80	28.64	46.30	59.01	80.67	176.80
	0.8	68.95	31.05	44.97	58.05	79.76	163.24
	0.9	66.99	33.26	45.98	57.49	80.03	152.39
	1	65.79	35.70	48.14	56.52	80.59	141.86
	1.1	65.09	36.99	50.76	56.70	74.18	133.26
	1.5	66.33	40.57	54.05	63.53	78.66	106.70
	2	72.19	49.31	58.48	70.00	78.15	121.15
	2.6	81.43	62.30	70.42	78.23	88.12	132.78
T2	0.4	168.05	67.04	126.62	141.85	218.39	313.31
	0.6	138.02	47.45	105.88	120.82	178.91	240.54
	0.8	116.18	43.01	92.15	114.92	147.07	183.49
	1	99.93	47.21	80.05	102.71	122.56	138.47
	1.2	89.51	48.76	69.72	94.88	105.79	121.12
	1.4	82.99	49.01	64.15	82.62	95.44	136.40
	1.6	79.50	53.38	62.12	72.68	88.61	157.11
	1.8	78.19	48.80	59.32	72.92	79.71	178.50
	2	78.22	41.45	57.59	70.01	77.73	188.82
	2.2	79.19	39.10	58.02	70.50	80.79	184.66
	2.4	81.59	40.60	60.63	72.67	84.88	183.84
	2.6	84.74	44.35	64.67	74.83	88.78	186.22
T3	0	110.08	28.56	64.50	92.27	129.79	247.34
	0.2	94.74	29.87	56.59	81.70	106.57	213.18
	0.3	88.01	31.34	54.28	74.56	100.41	197.15
	0.4	82.13	33.18	51.35	71.65	95.22	182.85
	0.5	77.02	34.41	46.92	66.90	89.99	167.65
	0.6	72.76	35.78	46.10	62.61	85.93	153.18
	0.7	69.47	36.61	46.27	59.26	82.75	139.18
	0.8	66.76	37.98	45.60	58.42	80.20	126.51
	0.9	64.84	40.76	43.57	58.37	78.52	115.77
	1	63.72	40.97	44.46	58.95	78.01	107.13
	1.1	62.92	40.77	45.12	60.00	76.85	98.64
	1.5	64.26	42.92	52.74	65.72	73.52	90.70
	2	72.44	53.12	58.23	72.01	79.99	117.52
	2.6	83.76	66.67	68.97	81.02	92.06	122.59

Table 3.14.2 Trace Techniques, FRMSE (%) by Percentile (Continued)

|	Z_{DR} +	Mean	0th	25th	50th	75th	100th
T4	0.4	155.85	63.35	118.49	139.72	206.84	265.93
	0.6	128.13	42.86	104.71	114.51	169.34	207.18
	0.8	107.76	38.63	87.39	106.53	139.03	157.46
	1	93.20	43.81	73.03	99.13	116.17	131.62
	1.2	83.73	46.76	63.12	87.91	98.29	118.07
	1.4	77.69	46.93	60.36	73.95	87.54	129.13
	1.6	74.47	51.59	57.34	66.29	83.18	143.07
	1.8	73.61	46.29	57.44	67.26	72.70	159.95
	2	74.51	42.06	57.42	65.43	75.61	169.13
	2.2	76.27	42.13	57.58	66.85	79.91	168.37
	2.4	79.13	45.00	57.28	72.01	84.05	168.13
	2.6	82.63	49.29	61.20	76.36	88.07	170.89
T5	0.4	164.54	72.74	100.17	149.78	232.19	283.99
	0.6	136.50	51.97	92.66	118.66	191.06	228.09
	0.8	115.38	44.07	84.14	104.06	157.50	188.50
	1	99.92	45.73	71.61	103.32	133.77	154.28
	1.2	90.20	51.51	58.96	86.13	118.54	135.90
	1.4	84.53	47.38	59.54	81.78	112.68	132.23
	1.6	80.33	43.37	54.65	75.36	100.96	151.63
	1.8	78.15	41.61	54.16	71.73	91.64	169.96
	2	77.10	39.87	53.50	70.35	83.44	179.51
	2.2	77.24	41.93	51.93	67.44	80.67	183.22
	2.4	78.91	46.17	55.77	68.59	82.61	188.80
	2.6	81.44	45.27	59.88	69.51	86.31	193.16
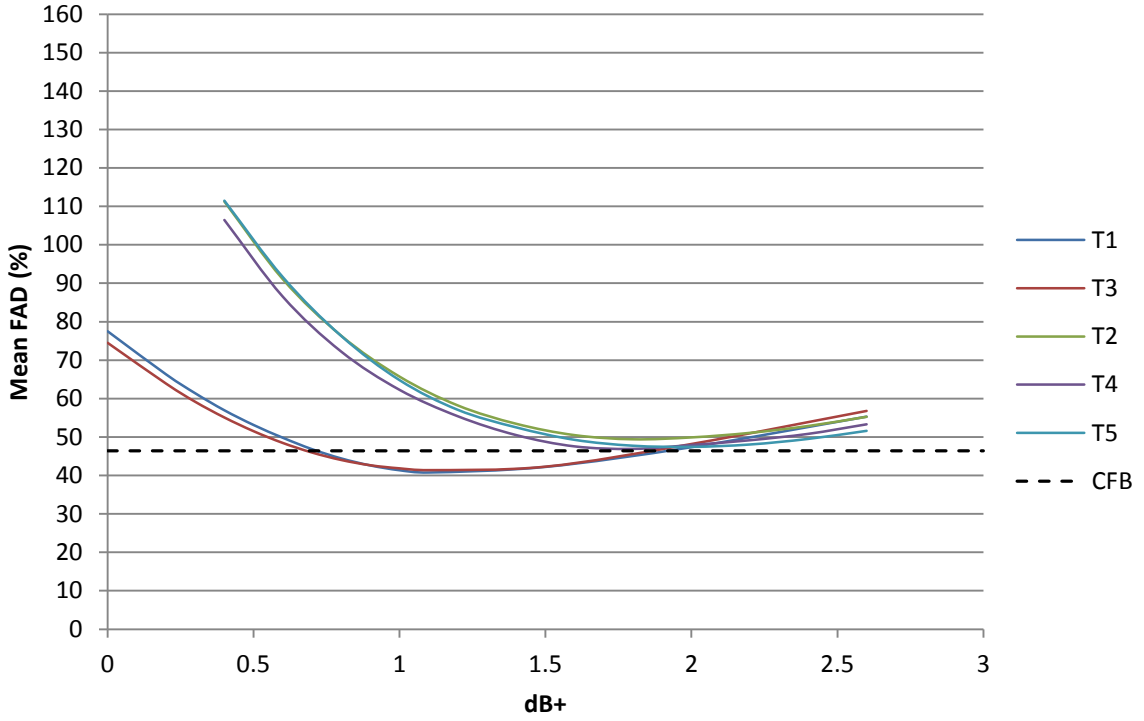
Figure 3.13.1. Mean FAD for the five trace techniques as a function of Z_{DR} adjustment.
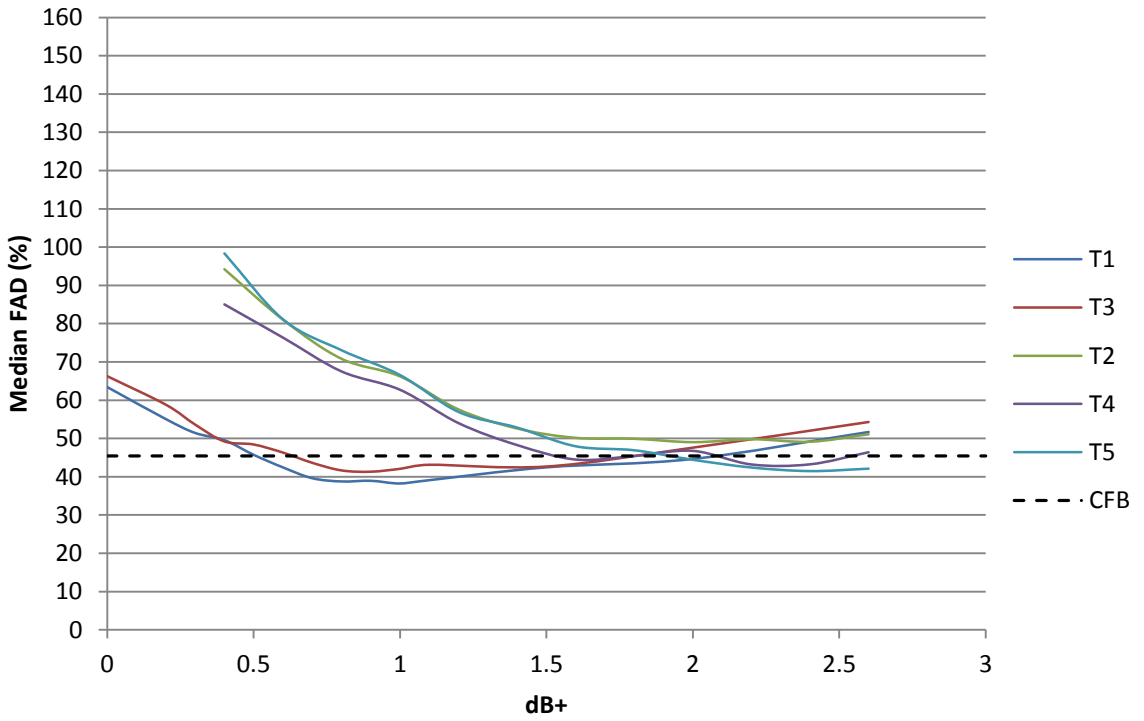

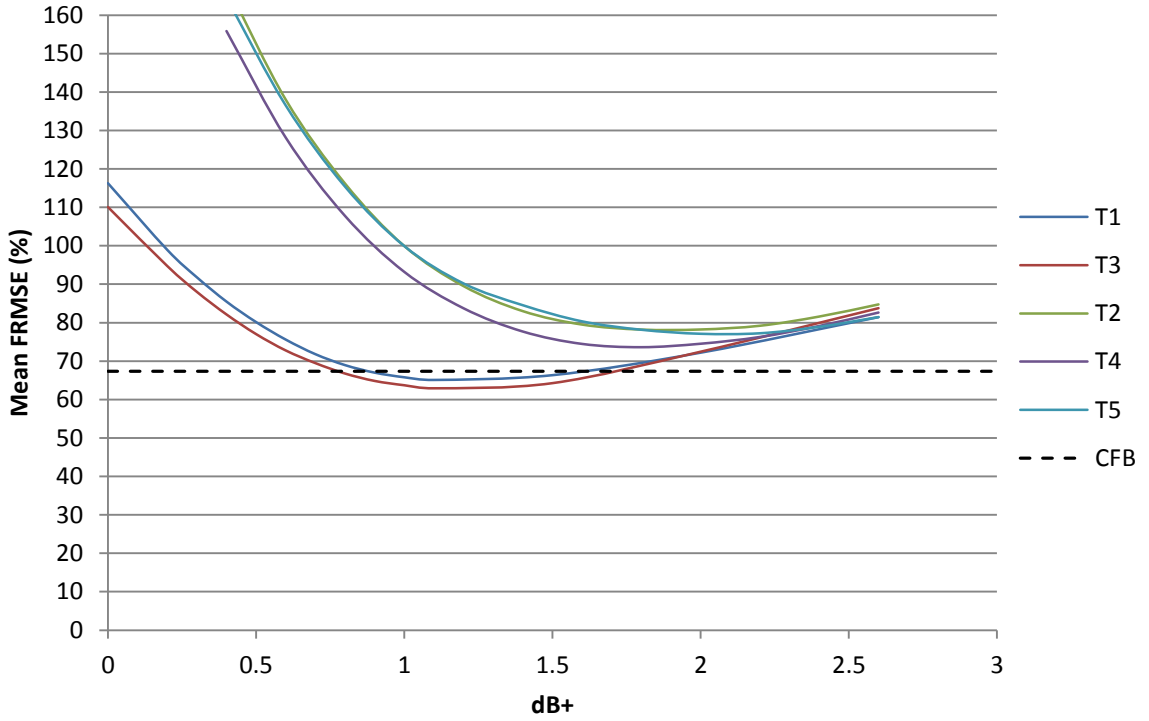Figure 3.13.2. Median FAD for the five trace techniques as a function of Z_{DR} adjustment.

Figure 3.13.3. Mean FRMSE for the five trace techniques as a function of Z_{DR} adjustment.
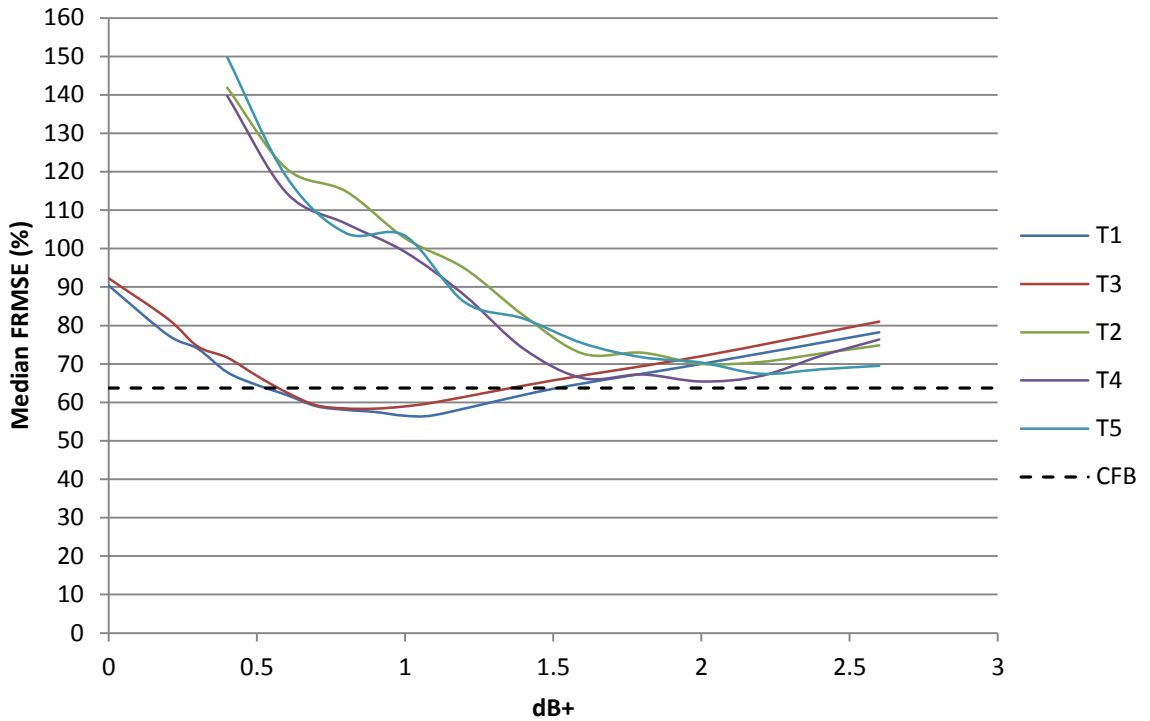

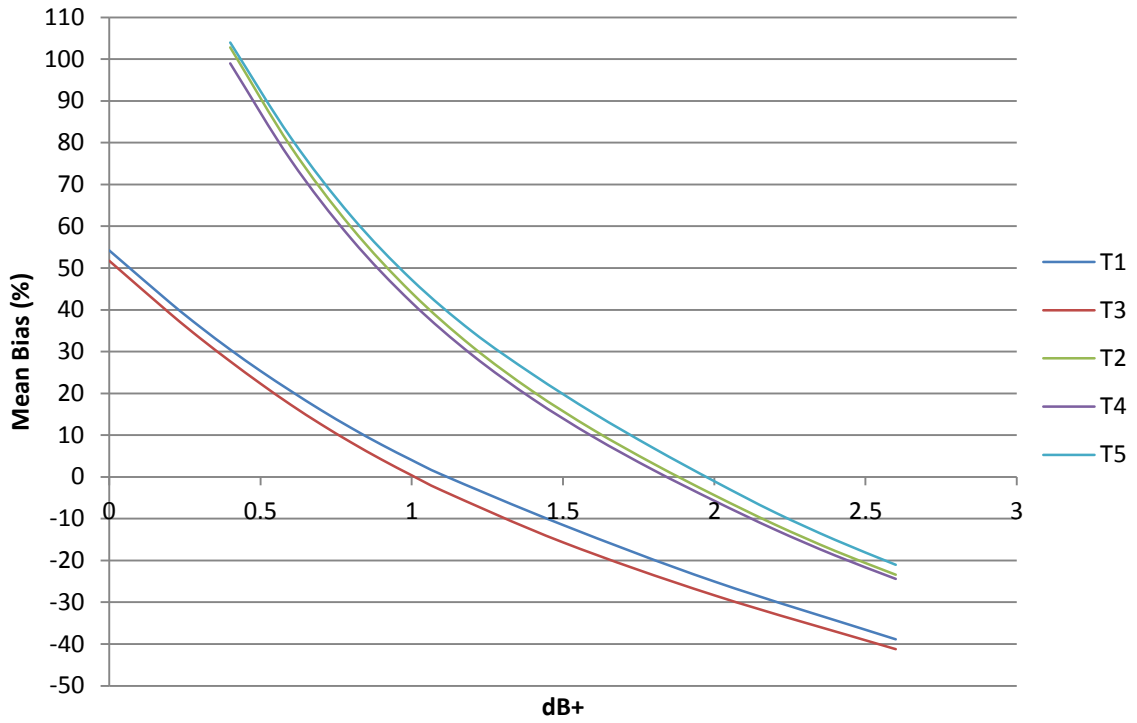Figure 3.13.4. Median FRMSE for the five trace techniques as a function of Z_{DR} adjustment.

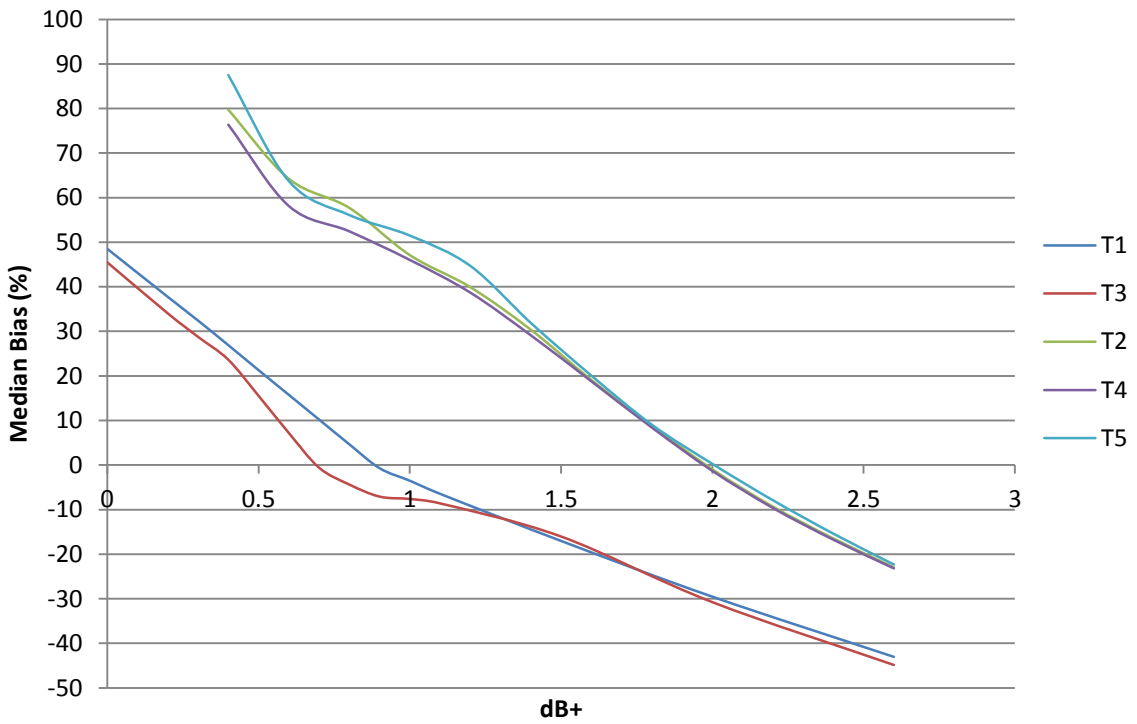Figure 3.13.5. Mean bias for the five trace techniques as a function of Z_{DR} adjustment.

Figure 3.13.6. Median bias for the five trace techniques as a function of Z_{DR} adjustment.

Chapter 4. Conclusions

Two primary objectives were discussed in the introduction and methodology. The first objective was to determine the most effective radar rainfall estimation technique for locations in Central Missouri. The second objective was to assess whether the introduction of high resolution model data could be used to improve radar rainfall estimation.

The optimal T1 and T3 trace techniques performed best overall given the assumptions in the study. T1 accounted for evaporation and precipitation drift, while T3 only accounted for evaporation. The mean overall FAD for the +1.1 Z_{DR} T1 technique was 40.76%, while the mean overall FAD for the +1.1 Z_{DR} T3 technique was 41.38%. The best mean overall FAD performance for the conventional formulas was a tie between (1) and (4) at 46.41%. This comes with the caveat that the K_{DP} data was extremely noisy, which likely degraded the performance of the formulas that rely on it significantly.

Median FAD values were similar to mean FAD values. The best performer with respect to median FAD was the +1.0 Z_{DR} T1 technique at 38.23%. The optimal T3 technique (+0.9 Z_{DR}) performed slightly worse at 41.32%. The best conventional technique was (4) at 45.43%.

With respect to FRMSE, the mean overall FRMSE for the +1.1 Z_{DR} T1 technique was

65.09%, while the mean overall FRMSE for the +1.1 Z_{DR} T3 technique was 62.92%. The

best mean overall FRMSE performance for the conventional formulas was (1) at 67.35%.

Median FRMSE values were moderately lower than mean FRMSE values, likely due to

the outlier penalty association with the FRMSE evaluation parameter. The top

performer with respect to median FRMSE was the +1.0 Z_{DR} T1 technique at 56.52%. The

optimal T3 technique (+0.9 Z_{DR}) was again slightly worse at 58.37%. The best of the

conventional formulas with respect to median FRMSE was (4) at 63.73%.

The FRMSE results obtained in this study did not differ significantly from those found in

RGS05 (optimal FRMSE in the ~50% range). The comparison is not exact for a variety of

reasons. The gauge locations for this study were much further from the radar than in

RGS05. The rainfall events were different, and the process in which the data from

differing events was combined was different. One point of interest is the relative

performance of the formulas dependent on just Z and those dependent on

combinations of Z, Z_{DR}, and K_{DP}. In RGS05 the formulas using the polarimetric

parameters performed slightly better than those just using Z, while the opposite was the

case for this study. One possible cause may be range from the radar affecting the quality

of the Z_{DR} data. The reason may also involve the problems with the K_{DP} data described in

Chapter 2.

Qualitative analysis of Figures 3.13.1-3.13.6 reveals a considerable difference between

the T1 and T3 trace techniques and the T2, T4, and T5 techniques. The minimum values

for FAD and FRMSE are reached at a difference of roughly 1 dB in Z_{DR} adjustment between the two sets. This is convincing evidence that evaporation plays a significant role in radar rainfall estimation and cannot be ignored (at least for locations far from the radar). This also makes the case for inclusion of high resolution model data into radar rainfall estimation, as calculating evaporation would be impossible without the model data.

Much less clear is the effect of precipitation drift on radar rainfall estimation. For some events it provided performance improvement, but for others it detracted from performance. This may be related to the beam broadening source of uncertainty discussed in the introduction. Studies from Chapter 1 indicated that the effects of precipitation drift would be most noticeable in high resolution situations. At the distance Columbia is from the radar, the resolution was probably a significant factor.

As noted in Section 3.13, a minor improvement in performance was seen when the time it took for precipitation to reach the ground was accounted for. This is an area where further investigation is warranted, particularly for finer timescales.

Chapter 5. Recommendations

5.1 Z_{DR} Adjustment

Several areas for further research with regard to the conventional formulas are

noteworthy. The formulas reliant on differential reflectivity may see some improvement

from Z_{DR} adjustment. Limited experimentation was done using various Z_{DR} alterations,

but the results proved inconclusive. Furthermore, the formulas reliant on Z_{DR} generally

exhibited negative biases, meaning a reduction in Z_{DR} would be necessary. This is the

opposite direction from which the trace techniques saw improvement, and would not

be physically expected, considering the already large number of negative Z_{DR} values.

5.2 Filtering

K_{DP} is an area for further investigation. Some of the extreme noise seen in the K_{DP} data

may have been the result of problems within the merging process described in Chapter

2. Further investigation into a proper filter is warranted.

Z_{DR} is another area where noise in the data can cause issues. For this project it remained

unfiltered due to several concerns. One concern was that filtering the Z_{DR} would cause

problems with the hail adjustment algorithm, negatively effecting results. Another issue

was that a simple filtering scheme could not be utilized due to Z_{DR} being ratio; an

adjustment would have to be made for reflectivity. Time constraints limited the amount

of complexity for certain parts of the project, and this is definitely an area that could be further investigated.

5.3 Resolution

Range degradation was a major issue affecting all techniques tested. Finding out how higher resolution radar data affects the performance of the trace techniques could prove insightful.

Another area where high vertical resolution could prove useful is tracking raindrops as they pass through different scanned elevation angles. Changes in DSD and reflectivity could provide information on what processes are occurring within the storm.

5.4 Drop Collisions

The tracing algorithm did not account for raindrop collisions. This is another area for improvement in the tracing scheme.

5.5 Evaporation Energy and Feedback into High Resolutions Models

Calculating the total amount of evaporation occurring within an atmospheric layer could prove useful in ways other than rainfall calculations. Total evaporative cooling within a storm could be estimated, and as a consequence the probably of a downburst occurring could also be calculated. This information could be fed back into the high resolution model, further improving the model forecast, as well as future rainfall estimation.

5.6 Operational Tracing

Several hurdles exist with respect to implementing an operational "trace technique" rainfall estimation program. The tracing technique developed in this project calculated drop paths at only nine distinct locations. Any operational program would require much greater spatial coverage. The computational power necessary would be immense. The infrastructure required to import model data in real time would have to be built as well.

Chapter 6. References

Andsager, K., K. V. Beard, and N. F. Laird, 1999: Laboratory Measurements of Axis Ratios for Large Raindrops. *Journal of the Atmospheric Sciences*, **56,** 2673-2683.

Auer, A. H., 1994: Hail recognition through the combined use of radar reflectivity and cloud-top temperatures. *Monthly Weather Review*, **122,** 2218-2221.

Beard, K. V., and C. Chuang, 1987: A New Model for the Equilibrium Shape of Raindrops. *Journal of the Atmospheric Sciences*, **44,** 1509-1524.

Best, A. C., 1950: Empirical formulae for the terminal velocity of water drops falling through the atmosphere. *Quarterly Journal of the Royal Meteorological Society*, **76,** 302-311.

Boxel, J. H. v., 1997: Numerical model for the fall speed of raindrops in a rainfall simulator. *International Workshop on Wind and Water Erosion*, Ghen, Belgium, 77-85.

Brandes, E. A., G. Zhang, and J. Vivekanandan, 2002: Experiments in Rainfall Estimation with a Polarimetric Radar in a Subtropical Environment. *Journal of Applied Meteorology*, **41,** 674-685.

——, 2004: Comparison of Polarimetric Radar Drop Size Distribution Retrieval Algorithms. *Journal of Atmospheric and Oceanic Technology*, **21,** 584-598.

Bringi, V. N., and V. Chandrasekar, 2001: *Polarimetric Doppler Weather Radar: Principles and Applications.* Cambridge University Press.

Dalezios, N. R., and N. Kouwen, 1990: Radar signal interpretation in warm season rainstorms. *Nordic hydrology*, **21,** 47-64.

Foote, G. B., and P. S. Du Toit, 1969: Terminal Velocity of Raindrops Aloft. *Journal of Applied Meteorology*, **8,** 249-253.

Fulton, R. A., J. P. Breidenbach, D. J. Seo, D. A. Miller, and T. O'Bannon, 1998: The WSR-88D rainfall algorithm. *Weather and Forecasting*, **13,** 377-395.

Goddard, J. W. F., K. L. Morgan, A. J. Illingworth, and H. Sauvageot, 1995: Dual-wavelength polarisation measurements in precipitation using the CAMRa and Rabelais radars. 196-198.

Gorgucci, E., V. Chandrasekar, V. N. Bringi, and G. Scarchilli, 2002: Estimation of Raindrop Size Distribution Parameters from Polarimetric Radar Measurements. *Journal of the Atmospheric Sciences*, **59,** 2373-2384.

Gossard, E. E., R. O. Strauch, and R. R. Rogers, 1990: Evolution of Dropsize Distributions in Liquid Precipitation Observed by Ground-Based Doppler Radar. *Journal of Atmospheric and Oceanic Technology*, **7,** 815-828.

Gossard, E. E., R. G. Strauch, D. C. Welsh, and S. Y. Matrosov, 1992: Cloud Layers, Particle Identification, and Rain-Rate Profiles from ZRVf Measurements by Clear-Air Doppler Radars. *Journal of Atmospheric and Oceanic Technology*, **9,** 108-119.

Gunn, R., and G. D. Kinzer, 1949: THE TERMINAL VELOCITY OF FALL FOR WATER DROPLETS IN STAGNANT AIR. *Journal of Meteorology*, **6,** 243-248.

Hoban, N. P., J. G. Cunningham, and D. Zittel, 2014: Using Bragg Scatter to Estimate Systematic Differential Reflectivity Biases on Operational WSR-88Ds. *30th Conference on Environmental Information Processing Technologies*.

Illingworth, A. J., and T. M. Blackman, 2002: The Need to Represent Raindrop Size Spectra as Normalized Gamma Distributions for the Interpretation of Polarization Radar Observations. *Journal of Applied Meteorology*, **41,** 286-297.

Keenan, T., and Coauthors, 2003: The Sydney 2000 World Weather Research Programme Forecast Demonstration Project: Overview and Current Status. *Bulletin of the American Meteorological Society*, **84,** 1041-1054.

Kinzer, G. D., and R. Gunn, 1951: The evaporation, temperature and thermal relaxation-time of freely falling waterdrops. *Journal of Atmospheric Sciences*, **8,** 71-83.

Kumjian, M. R., and A. V. Ryzhkov, 2010: The Impact of Evaporation on Polarimetric Characteristics of Rain: Theoretical Model and Practical Implications. *Journal of Applied Meteorology and Climatology*, **49,** 1247-1267.

Lack, S. A., 2004: Quantifying the Effect of Wind-drift on Radar-derived Surface Rainfall Estimations, University of Missouri.

Lakshmanan, V., T. Smith, G. Stumpf, and K. Hondl, 2007: The warning decision support system-integrated information. *Weather and Forecasting*, **22,** 596-612.

Lakshmanan, V., T. Smith, K. Hondl, G. J. Stumpf, and A. Witt, 2006: A real-time, three-dimensional, rapidly updating, heterogeneous radar merger technique for reflectivity, velocity, and derived products. *Weather and Forecasting*, **21,** 802-823.

Lauri, T., J. Koistinen, and D. Moisseev, 2011: Advection-Based Adjustment of Radar Measurements. *Monthly Weather Review*, **140,** 1014-1022.

Li, X., and R. C. Srivastava, 2001: An Analytical Solution for Raindrop Evaporation and Its Application to Radar Rainfall Measurements. *Journal of Applied Meteorology*, **40,** 1607-1616.

Marshall, J. S., and W. M. K. Palmer, 1948: THE DISTRIBUTION OF RAINDROPS WITH SIZE. *Journal of Meteorology*, **5,** 165-166.

Mittermaier, M. P., R. J. Hogan, and A. J. Illingworth, 2004: Using mesoscale model winds for correcting wind-drift errors in radar estimates of surface rainfall. *Quarterly Journal of the Royal Meteorological Society*, **130,** 2105-2123.

Parish, O. O., and T. W. Putnam, 1977: Equations for the Determination of Humidity from Dewpont and Psychometric Data. NASA, Ed.

Rosenfeld, D., D. B. Wolff, and D. Atlas, 1993: General Probability-matched Relations between Radar Reflectivity and Rain Rate. *Journal of Applied Meteorology*, **32,** 50-72.

Ryzhkov, A., and D. Zrnić, 1996: Assessment of Rainfall Measurement That Uses Specific Differential Phase. *Journal of Applied Meteorology*, **35,** 2080-2090.

Ryzhkov, A. V., S. E. Giangrande, and T. J. Schuur, 2005: Rainfall Estimation with a Polarimetric Prototype of WSR-88D. *Journal of Applied Meteorology*, **44,** 502-515.

Sánchez-Diezma, R., I. Zawadzki, and D. Sempere-Torres, 2000: Identification of the bright band through the analysis of volumetric radar data. *Journal of geophysical research*, **105,** 2225-2236.

Tokay, A., A. Kruger, and W. F. Krajewski, 2001: Comparison of Drop Size Distribution Measurements by Impact and Optical Disdrometers. *Journal of Applied Meteorology*, **40,** 2083-2097.

Tracy, C. R., W. r. Welch, and W. P. Porter, 1980: Properties of Air: A Manual for Use in Biophysical Ecology. Third ed.

Ulbrich, C. W., 1983: Natural Variations in the Analytical Form of the Raindrop Size Distribution. *Journal of Climate and Applied Meteorology*, **22,** 1764-1775.

Uplinger, W. G., 1981: NEW FORMULA FOR RAINDROP TERMINAL VELOCITY. 389-391.

Villarini, G., and W. Krajewski, 2010: Review of the Different Sources of Uncertainty in Single Polarization Radar-Based Estimates of Rainfall. *Surv Geophys*, **31,** 107-129.

Willis, P. T., and P. Tattelman, 1989: Drop-Size Distributions Associated with Intense Rainfall. *Journal of Applied Meteorology*, **28,** 3-15.

Appendix A. Data Processing

A.1 Radar Data

To convert the radar data into text format the ncks tool from the NCO toolbox was utilized, along with the AutoHotkey program. The AutoHotkey program allows the user to deliver input to the computer via code. The following passage contains a sample autohotkey code using the ncks tool as well as comments (in green) describing the functionality.

```
sendMode Input signals to the program that input is to be delivered.

sendMode Input


IfWinExist checks to see whether the appropriate window is open, and
activates this window if it is found.

IfWinExist NCO.lnk
(
    WinActivate
)

The following six variables are declared and assigned values
simultaneously. These variables define the number of radar images
associated with the event (given by the first number in the variable
name) and the type of data (denoted by the second number in the
variable name.

a0_1=274
a0_2=276
a0_3=276
a1_1=87
a1_2=87
a1_3=87

var=0

Loop 2
(

        var3=1
        Loop 3
        (
```

```
            var4 as defined here is the number of radar images to be
            processed for the particular date/type of data.

            var4=% a%var%_%var3%

            var5=1



            Each time the following code is executed one text file is
            written. The 9,44,80, and 123 describe the constraints
            for latitude and longitude, while the file paths specify
            the name of the text file to be created as well as the
            netcdf file used for the creation of the text file.

            Loop, %var4%
            (
                  var2=
                  (
                  ncks -d Lon,9,44 -d Lat,80,123 -F
                  E:/data/combined/v2/%var%_%var3%_%var5%.netcdf >
                  E:/data/combined/v2/%var%_%var3%_%var5%.txt
                  )
                  clipboard=%var2%

                  SendInput (Raw)%clipboard%
                  clipboard=""

                  Send, (Enter)
                  Sleep, 100
                  var5+=1
            )
            var3+=1

      )

      var+=1

)

Esc::ExitApp
```

A.2 Model Data

The wgrib2 tool requires two files to work, the control file and the index file. The following code describes how these files are created with an autohotkey script using the g2ctl.pl and gribmap tools.

```
sendMode Input

IfWinExist cmd.exe
(
    WinActivate
)

The following two variables contain the number of csv files to be
created for the event in question, which is specified by the number
within the variable.

a0=27
a1=11

var=0

Loop 2
(

        var4=% a%var%

        var5=1
        Loop, %var4%
        (
                The g2ctl tool is a perl script that creates the control
                file from the grb2 file.

                var2=
                (
                perl g2ctl.pl
                E:/data/grbdownload/march/namechange/%var%_%var5%.grb2 >
                E:/data/grbdownload/march/namechange/%var%_%var5%.ctl
                )
                clipboard=%var2%

                SendInput (Raw)%clipboard%
                clipboard=""

                Send, (Enter)
                Sleep, 200
```

```
            The gribmap tool creates the index file from the control
            file.

            var6=gribmap -0 -i
            E:/data/grbdownload/march/namechange/%var%_%var5%.ctl
            clipboard=%var6%

            SendInput (Raw)%clipboard%
            clipboard=""

            Send, (Enter)
            Sleep, 100

            The wgrib2 tool creates a comma separated variable file
            containing the information from the grb2 file.

            var7=
            (
            wgrib2
            E:/data/grbdownload/march/namechange/%var%_%var5%.grb2 -
            csv E:/data/grbdownload/march/namechange/%var%_%var5%.csv
            )
            clipboard=%var7%

            SendInput (Raw)%clipboard%
            clipboard=""

            Send, (Enter)
            Sleep, 200
            var5+=1
       )

       var+=1

)

Esc::ExitApp
```

Appendix B. Program Information

B.1 Program Description

The VBA program created for this project contains more than 3000 lines of code. Figure

B.1 is a simplified flowchart describing how the program functions.

B.2 Hail Adjustment

A simple algorithm was created for this project to adjust for hail. The hail adjustment

algorithm takes reflectivity and differential reflectivity as input, and alters them as

described by the following lines of VBA code.

```vba
Function hailadj(ByRef z As Double, ByRef zdr As Double)
Dim extra As Double
Dim var1 As Double

A reflectivity cap of 52 dBZ is established.

If z > 52 Then
z = 52
End If

Adjustments to Z based on differential reflectivity are made if the
following criteria are met.

If z > 45 And zdr < 3 Then

If zdr < 1 Then
zdr = 1
End If
var1 = (3 - zdr) / 2

extra = z - 45

z = 45 + extra * (1 - var1)

For reflectivity values exceeding 45, a minimum differential
reflectivity of 3 dB is set.

zdr = 3
```
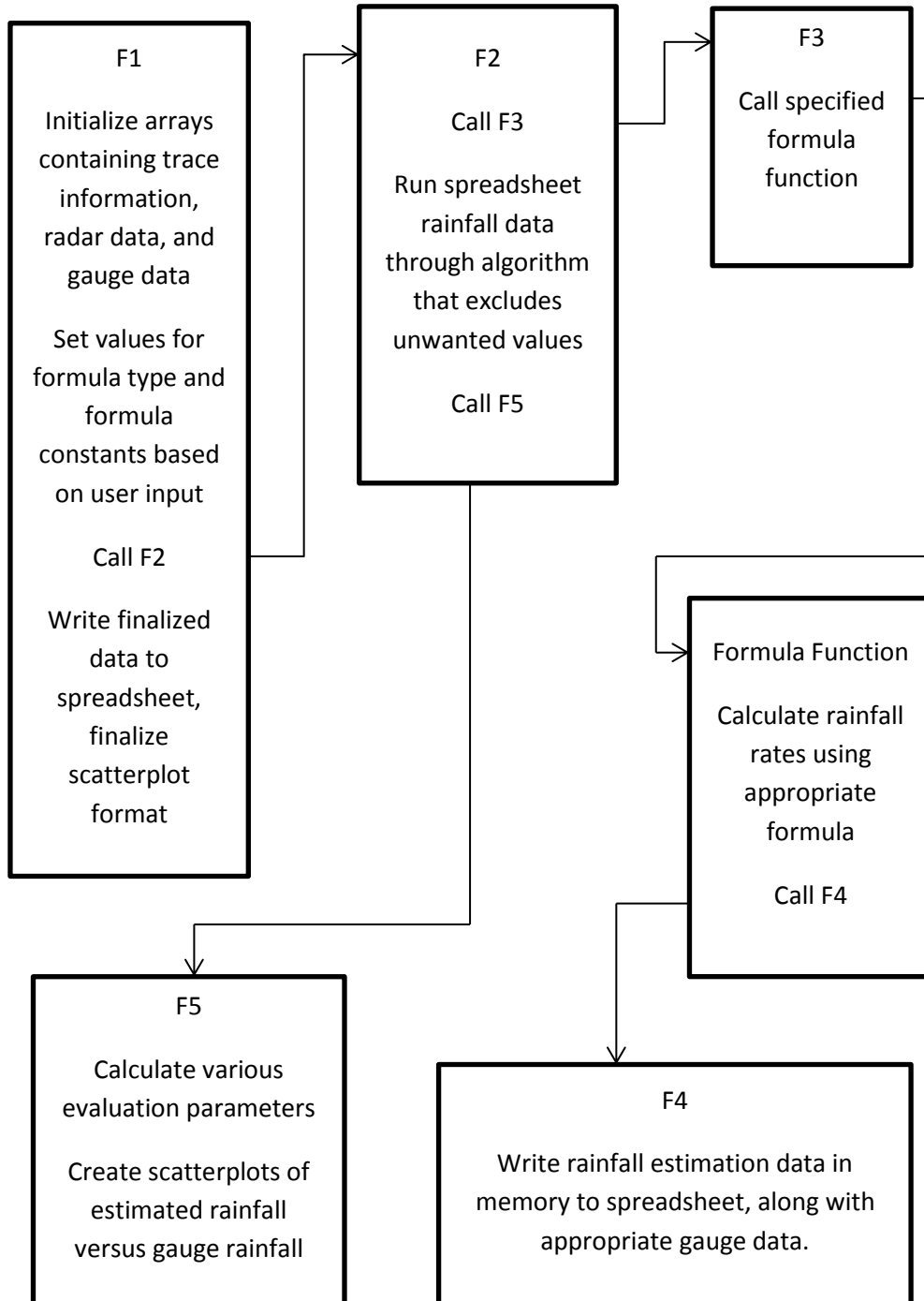
```
End If

End Function
```


Figure B.1. Program Flowchart. The F1, F2, F3, F4, F5, and Formula Function headers are labels denoting the different routines within the program.

Appendix C. Trace Information

C.1 Trace VBA Script

The tracing of raindrops was done through another VBA script. The following code is applicable for the drift and evaporation trace technique. Appropriate modifications were made to this script when the other trace techniques were calculated.

```
Variables are declared at the beginning.

Sub drift()
Dim xinit As Integer, yinit As Integer, xstore As Integer, ystore As
Integer, slat As Double, slon As Double, sh As Double, var1 As
Double, var2 As Double, var3 As Double, var4 As Double
Dim da(1 To 60, 1 To 16) As Double, ia(1 To 35, 1 To 5, 1 To 13, 1
To 8, 1 To 9) As Double, a(0 To 15) As Integer
Dim dd As Double, time As Double, time2 As Double, time3 As Double,
lat As Double, lon As Double, height As Double, pressure As Double,
us As Double, vs As Double, tv As Double
Dim temp As Double, vtemp As Double, index As Integer, index2 As
Integer, bvtemp As Double, avtemp As Double, timestart As Double
Dim var5 As Double, var6 As Double, var7 As Double, var8 As Double,
bheight As Double, aheight As Double
Dim ll As Integer, eradius As Double, Pi As Double, timestep As
Double, virtualt As Double, mint As Double, maxt As Double, xstore2
As Integer, totaln As Integer, index3 As Integer, index4 As Integer
Dim se(1 To 9) As Double, sname As String, xshift As Integer, xc As
Integer, yc As Integer, xd As Double, yd As Double, rh As Double,
uwnd As Double, vwnd As Double, initialtime As Double
Dim terminalv As Double, aird As Double
Dim lon2 As Double, lat2 As Double, h2 As Double, l2 As Integer, u2
As Double, v2 As Double, rh2 As Double, aheight2 As Double, bheight2
As Double, bvtemp2 As Double, avtemp2 As Double, pressure2 As Double
Dim virtualt2 As Double, dm2 As Double, terminalv2 As Double, dd2 As
Double, temp2 As Double
Dim timestart2 As Double, timeend As Double, index5 As Double,
index6 As Double, index7 As Double, index8 As Double, index9 As
Double

Values for pi and the earth's radius are set.

Pi = 3.14159265358979
eradius = 6371000
```

```
The array a() contains the number of hours of model data stored for
each particular event on the spreadsheet.

a(0) = 27
a(1) = 11

The se() array contains the elevation of the 9 sites in meters.

se(1) = 225.63
se(2) = 213.759
se(3) = 195.775
se(4) = 186.844
se(5) = 171.9
se(6) = 268.847
se(7) = 186.23
se(8) = 251.804
se(9) = 235.004
xinit = 141
yinit = 9

timestep determines how often calculations are made for each
raindrop.

timestep = 1

xstore2 = 117

Application.DisplayStatusBar = True

index3 is the identification # of the event in question.

For index3 = 0 To 1

sname = index3
Sheets(sname).Activate

The range of minimum and maximum time steps are calculated in the
next few lines. The minimum (mint) and maximum (maxt) are based on
the time stamps of the first and last radar images.

totaln = Sheets(sname).Cells(7, xstore2 + 1).Value
mint = 12 * Sheets(sname).Cells(9, xstore2 + 9).Value
maxt = 12 * Sheets(sname).Cells(8 + totaln, xstore2 + 9).Value

mint = Application.WorksheetFunction.Ceiling(mint, 1)
maxt = Application.WorksheetFunction.Floor(maxt, 1)
initialtime = Sheets(sname).Cells(8, 140).Value



The following "for loops" lift model data stored in the spreadsheet
into the program's memory.
```

```
For index5 = 1 To a(index3)
For index6 = 1 To 5
For index7 = 1 To 13
For index8 = 1 To 8
For index9 = 1 To 9

ia(index5, index6, index7, index8, index9) =
Sheets(sname).Cells(yinit + (index5 - 1) * 10 + (9 - index9), xinit
+ 130 * (index6 - 1) + 10 * (index7 - 1) + index8 - 1).Value


Next
Next
Next
Next
Next


xstore = 141
ystore = 400
Sheets(sname).Activate
```

index4 is the # of the site for which calculations are performed.

```
For index4 = 1 To 9

slat = Sheets("Sheet2").Cells(4 + index4, 2).Value
slon = Sheets("Sheet2").Cells(4 + index4, 3).Value
ystore = 400


sh = se(index4)
```

index2 is the time of landing for the raindrops being calculated.
Each subsequent value for index2 corresponds to a time five minutes
later than the previous.

```
For index2 = mint To maxt
```

The following two lines assure that the user can tell the progress
of the program's calculations.

```
DoEvents
Application.StatusBar = "Date: " & index3 & "  " & "Site: " & index4
& _
"Time: " & index2
```

ll (standing for lower level) is reset to a value of 1 and timestart
is defined as the time in hours passed since the beginning of the
event. time2 represents the hourly time preceding timestart, while
time3 represents the time elapsed between time2 and timestart.

```
ll = 1
timestart = CDbl(index2) / 12
time2 = Application.WorksheetFunction.Floor(timestart, 1)
time3 = timestart - time2
```

da() (standing for drop array) is the array containing all raindrop information. The function "findinfo" takes various drop parameters and calculates other information about the motion and environment of the drop based on the input given. The following lines of code initialize values for the da() array.

```
For index = 1 To 60
da(index, 1) = 0.1 * index
da(index, 2) = timestart
da(index, 3) = slat
da(index, 4) = slon
da(index, 5) = sh
da(index, 13) = 1

Call findinfo(da(index, 1), sh, slat, slon, time2, time3,
CInt(da(index, 13)), da(index, 7), da(index, 8), da(index, 16),
da(index, 15), initialtime, aheight, bheight, bvtemp, avtemp,
da(index, 6), virtualt, da(index, 14), da(index, 9), ia())
'MsgBox da(index, 14)


da(index, 10) = 0
da(index, 11) = 0

If index = 1 Then
Sheets(sname).Cells(ystore + index, xstore - 1).Value = da(index, 2)
End If

Next

Do While (da(1, 10) <> 1)

For index = 1 To 60
If da(index, 5) < 2168.905 Then

time = da(index, 2) - timestep / 3600
da(index, 2) = time
time2 = Application.WorksheetFunction.Floor(timestart, 1)

If time >= 0 Then


time3 = time - time2
```

Predicted (one second in the past) drop parameters based off linear extrapolations are calculated.

```
lon2 = da(index, 4) - timestep * da(index, 7) / (Sin((90 - lat) /
180 * Pi) * eradius * 2 * Pi) * 360
lat2 = da(index, 3) - timestep * da(index, 8) / (2 * Pi * eradius) *
360
h2 = da(index, 5) + timestep * da(index, 9)
l2 = da(index, 13)
var1 = 4 / 3 * 3.14159265358979 * (da(index, 1) / 2000) ^ 3 * 1000 +
da(index, 14) * timestep

dd2 = ((var1 * 3 / 4 / 3.14159265358979 / 1000) ^ (1 / 3)) * 2000

Call findinfo(dd2, h2, lat2, lon2, time2, time3, CInt(l2), u2, v2,
rh2, temp2, initialtime, aheight2, bheight2, bvtemp2, avtemp2,
pressure2, virtualt2, dm2, terminalv2, ia())
```

The predicted (one second in the past) drop motion and evaporation
rates are averaged with current values; these averages are used for
a second estimation.

```
da(index, 3) = da(index, 3) - timestep * ((da(index, 8) + v2) / 2) /
(2 * Pi * eradius) * 360
da(index, 4) = da(index, 4) - timestep * ((da(index, 7) + u2) / 2) /
(Sin((90 - lat) / 180 * Pi) * eradius * 2 * Pi) * 360
da(index, 5) = da(index, 5) + timestep * (da(index, 9) + terminalv2)
/ 2

var1 = 4 / 3 * 3.14159265358979 * (da(index, 1) / 2000) ^ 3 * 1000 +
timestep * (da(index, 14) + dm2) / 2
da(index, 1) = ((var1 * 3 / 4 / 3.14159265358979 / 1000) ^ (1 / 3))
* 2000

Call findinfo(da(index, 1), da(index, 5), da(index, 3), da(index,
4), time2, time3, CInt(da(index, 13)), da(index, 7), da(index, 8),
da(index, 16), da(index, 15), initialtime, aheight, bheight, bvtemp,
avtemp, da(index, 6), virtualt, da(index, 14), da(index, 9), ia())
```

If the height of a drop is found to be greater than 2 km above the
radar, the calculations are stopped.

```
If da(index, 5) > 2168.905 Then
da(index, 10) = 1
End If

Else
da(index, 11) = -1
da(index, 10) = 1
da(index, 2) = -1
End If

End If

Next

Loop
```

Several drop parameters describing its position and properties are
written to the spreadsheet.

```
For index = 1 To 60

Sheets(sname).Cells(ystore + index, xstore).Value = da(index, 2)
Sheets(sname).Cells(ystore + index, xstore + 1).Value = da(index, 1)
Sheets(sname).Cells(ystore + index, xstore + 2).Value = da(index, 3)
Sheets(sname).Cells(ystore + index, xstore + 3).Value = da(index, 4)
Sheets(sname).Cells(ystore + index, xstore + 4).Value = da(index,
15)

Next

ystore = ystore + 61

Next

xstore = xstore + 6

Next
Next

End Sub
```

C.2 findinfo Script

The findinfo function was used by the trace program to obtain information about the raindrop in question. The following lines of code describe the findinfo function. Within this function are two more functions called evc() and termvel(). The termvel function determines at what speed the raindrop is falling, while the evc function calculates the evaporation rate. The processes for both of these calculations are described in Chapter 2. The equation used to calculate absolute humidity was obtained from a 1977 NASA Technical Note (Parish and Putnam 1977). The diffusivity of water vapor in air and the kinematic viscosity of air were obtained from a technical report released by researchers from the University of Wisconsin in 1980 (Tracy et al. 1980).

```
Function findinfo(dd As Double, height As Double, lat As Double,
lon As Double, time2 As Double, time3 As Double, ByRef ll As
Integer, ByRef uwnd As Double, ByRef vwnd As Double, ByRef rh As
Double, ByRef temp As Double, initialtime As Double, ByRef
aheight As Double, ByRef bheight As Double _

, ByRef avtemp As Double, ByRef bvtemp As Double, ByRef pressure
As Double, ByRef virtualt As Double, ByRef dm As Double, ByRef
terminalv As Double, ByRef ia() As Double)


Dim var1 As Double, var2 As Double, var3 As Double, var4 As
Double, var5 As Double, var6 As Double, var7 As Double, var8 As
Double, var9 As Double, var10 As Double

Dim index As Integer, hour As Integer

Dim mint As Double, maxt As Double, meant As Double, bl As
Double, tl As Double, zd As Double

Dim yd As Double, xd As Double, xc As Integer, yc As Integer,
aird As Double
```

The following lines of code are designed to establish the location of the point in question relative to the model data grid.

```
hour = CInt(time2) - CInt(initialtime)


var5 = Application.WorksheetFunction.Floor(lat, 0.1)


yd = 10 * (lat - var5)



var6 = Application.WorksheetFunction.Floor(lon, 0.1)

xd = 10 * (lon - var6)


var7 = CInt((var5 - 38.6) / 0.1)

var8 = CInt((var6 + 92.7) / 0.1)


xc = CInt(var8) + 1

yc = CInt(var7) + 1


If var8 < 0 Then


xc = 1

xd = 0
```

```
ElseIf var8 > 6 Then


xc = 7

xd = 1


End If


If var7 < 0 Then


yc = 1

yd = 0


ElseIf var7 > 7 Then


yc = 8

yd = 1


End If
```

ll stands for "lower level". This section of code establishes which pressure layer in the atmosphere the point in question lies within. The interpolate2 function uses time and location data to find a value interpolated from the model data.

```
For index = ll To 13

var10 = var9

var9 = interpolate2(1, index, hour, yd, xd, time3, 0, yc, xc,
ia())
```

```
If height < var9 Then

ll = index

aheight = var9

bheight = var10

zd = (height - bheight) / (aheight - bheight)

Exit For

End If


Next

bl = 1025 - ll * 25

tl = 1025 - (ll + 1) * 25


bvtemp = virtualtemp(bl, interpolate2(2, ll, hour, yd, xd, time3,
0, yc, xc, ia())), interpolate2(3, ll, hour, yd, xd, time3, 0, yc,
xc, ia()))

avtemp = virtualtemp(tl, interpolate2(2, ll + 1, hour, yd, xd,
time3, 0, yc, xc, ia()), interpolate2(3, ll + 1, hour, yd, xd,
time3, 0, yc, xc, ia()))
```

The pressure at the point in question is found using the
hypsometric equation.

```
var1 = aheight - bheight

var2 = avtemp - bvtemp


var3 = var1 / 287.058 * 9.8 / Log(bl / tl)

mint = var3 - var2 / 2

maxt = var3 + var2 / 2
```

```
meant = (maxt + (maxt - (maxt - mint) * (height - bheight) /
var1)) / 2

pressure = bl / Exp((height - bheight) * 9.8 / 287.058 / meant)

temp = interpolate2(2, ll, hour, yd, xd, time3, zd, yc, xc, ia())

rh = interpolate2(3, ll, hour, yd, xd, time3, zd, yc, xc, ia())

If rh > 100 Then

rh = 100

End If

virtualt = virtualtemp(pressure, temp, rh)

uwnd = interpolate2(4, ll, hour, yd, xd, time3, (bl - pressure) /
(bl - tl), yc, xc, ia())

vwnd = interpolate2(5, ll, hour, yd, xd, time3, (bl - pressure) /
(bl - tl), yc, xc, ia())
```

terminalv is the calculated terminal velocity, while dm is the
change in mass per second of the drop due to evaporation.

```
terminalv = termvel(pressure, virtualt, dd)

dm = evc(rh, temp, pressure, dd, terminalv, virtualt)



End Function
```